Targeting mitochondria: Novel concepts for mechanisms underlying therapeutic effects of *Cimicifuga racemosa* and *Petasites hybridus* extracts

Dissertation

zur

Erlangung des Doktorgrads

der Naturwissenschaften

(Dr. rer. nat.)

dem

Fachbereich Pharmazie der

Philipps Universität Marburg

vorgelegt von

Malena Rabenau

aus **Gießen**

Marburg/Lahn 2019

Erstgutachter: **Prof. Dr. Carsten Culmsee**

Zweitgutachter: **Prof. Dr. Veronika Butterweck**

Eingereicht am **31.10.19**

Tag der mündlichen Prüfung am **19.12.19**

Hochschulkennziffer: 1180

Erklärung

Ich versichere, dass ich meine Dissertation mit dem Titel

"Targeting mitochondria:
Novel concepts for mechanisms underlying therapeutic effects of
Cimicifuga racemosa and *Petasites hybridus* extracts"

selbständig ohne unerlaubte Hilfe angefertigt und mich dabei keiner anderen als der von mir ausdrücklich bezeichneten Quellen bedient habe. Alle vollständig oder sinngemäß übernommenen Zitate sind als solche gekennzeichnet.

Die Dissertation wurde in der jetzigen oder einer ähnlichen Form noch bei keiner anderen Hochschule anlässlich eines Promotionsgesuchs eingereicht und hat noch keinen sonstigen Prüfungszwecken gedient.

Marburg, den 31.10.2019

.....

(Malena Rabenau)

Table of contents

1. Introduction

1.1. *Cimicifuga racemosa* rhizome extract

1.1.1. Cimicifuga racemosa

Cimicifuga racemosa extracts (L.) Nutt. (synonym for Actaea racemosa L., black cohosh) obtained from the rootstock are commonly used to treat menopausal complaints. *Cimicifuga racemosa* belongs to the buttercup family (Ranunculaceae) and is native to the Eastern part of the United States and Canada. In traditional Chinese medicine and in folk medicine it has been used against a wide range of symptoms for example, against headache [1].

Figure 1. *Cimicifuga racemosa*

Pictures of Cimicifuga racemosa at the cultivation site in Uttwill in Switzerland (Vitaplant AG, photographs by Malena Rabenau).

In Europe, *Cimicifuga racemosa* gained importance in the last decades; it is monographed for treatment of climacteric symptoms by the German Commission E since 1989, the WHO since 2002 and the ESCOP since 2012. Moreover, the HMPC granted *Cimicifuga racemosa* extracts with well-established use status [2,3]. Several clinical studies support the effective treatment of *Cimicifuga racemosa* extracts against menopausal complaints, which was summarized in a recent meta-analysis comparing *Cimicifuga racemosa* to placebo [4]. In this meta-analysis, a statistical difference of $p<0.0001$ in favor of *Cimicifuga racemosa* extracts was found. In the HMPC monograph, three different herbal preparations are listed: two ethanolic, and one isopropanolic dry extract [2]. Ze 450 is an ethanolic (60%, v/v) *Cimicifuga racemosa* dry extract that was

produced by a standardized procedure and this extract was exclusively investigated in this study.

The extract from the rhizome of *Cimicifuga racemosa* contains many different components. It consists of triterpene glycosides [5–7], mainly xylosides, like actein, 23-epi-26-deoxyactein and cimiracemoside C [8,9], besides phenolic acids, predominantly derivatives of hydroxycinnamic acid [10], including caffeic, ferulic and cimicfugic acid [7], and flavonoids [11] are represented. Moreover, it is suggested that mostly the phenolic compounds, especially ferulic, isoferulic and caffeic acid mediate antioxidant effects [12,13]. It is important to point out that, according to current knowledge, the rootstock does not contain phytoestrogens. In earlier studies the isoflavone and phytoestrogen formononetin was related to effects mediated by *Cimicifuga racemosa* extract [14], however, in more recent studies, formononetin was not detected [15–17].

1.1.2. Therapeutic use and mechanism of action

Ze 450 is approved for the treatment of peri-menopausal complaints in many European countries. Climacteric symptoms include sweating, insomnia, mood disorders, headache, vaginal dryness, and most frequently hot flushes [18,19]. It is well known that during menopausal transition estrogen depletion or fluctuation of estrogen level lead to alterations in CNS gene expression, neurotransmitter synthesis, and to an impairment of hypothalamic neuronal activity, including mitochondrial dysfunction and an imbalanced redox homeostasis (Figure 2) [20]. Those alterations promote inflammatory processes and oxidative stress [21]. The mentioned changes may largely contribute to the development of hut flushes via narrowing of the thermoregulatory set point [22]. In line with the general view of menopausal complaints being caused by hormonal dysregulation, hormone replacement therapy (HRT) is mainly used to treat menopausal complaints [21], but it is limited due to adverse side effects, like headache, uterine bleeding and enhanced risks for venous thromboembolic disease, breast cancer, stroke, and coronary artery disease [23,24]. Besides, the need for alternative treatment strategies is supported by the wish of women suffering from menopausal symptoms for hormone-free treatments [25,26]. Therefore, *Cimicifuga racemosa* extracts are an effective [4,27,28] and safe alternative [29] with a good tolerability and no known interactions [2]. Additionally, menopausal women with osteoporosis [30–34], metabolic disturbances [35,36] and myeloma [37] may benefit from *Cimicifuga racemosa* treatment.

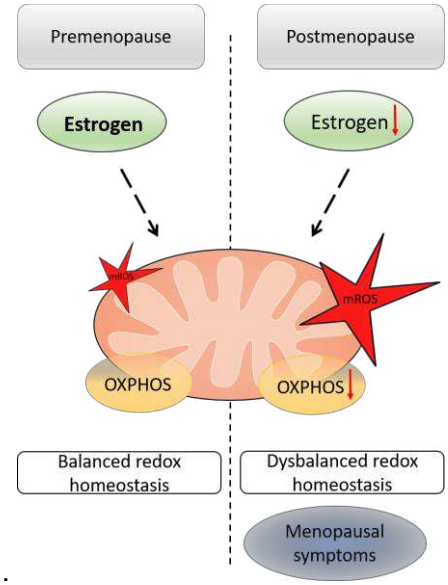

Figure 2. Scheme of estrogen-mediated effects in pre- and post-menopause

Estrogen mediates protective effects on metabolism. In premenopausal women, physiological estrogen levels contribute to a balanced brain redox homeostasis with normal activity of ETC (electron transport chain). Depletion of estrogen in the postmenopause leads to a decrease of mitochondrial respiration and an increase in ROS formation and consequently a dysbalanced redox homeostasis, which may contribute to climacteric complaints, like hot flushes (OXPHOS: oxidative phosphorylation, mROS: mitochondrial ROS).

Besides estrogen depletion mediated processes, mounting evidence suggests additional effects, such as increased oxidative stress, which may contribute to the development of metabolic disorders that do not respond to HRT [38,39].

Until now, very little is known about the exact mechanism of action of *Cimicifuga racemosa* extracts. *In vitro,* it was demonstrated that *Cimicifuga racemosa* extract binds to serotonergic receptors (5HT(1A), 5-HT(1D), and 5-HT(7)), and regulates signal transduction as a partial agonist [40,41]. This regulation might be responsible for the effective reduction of hot flushes since 5 HT(1A) and 5 HT(7) receptors are present in the hypothalamus, and they are involved in thermoregulation [42]. Moreover, another study identified Nω-methylserotonin as a serotonergic component of rhizomes of black cohosh [41]. *In vivo,* in ovariectomized rats, serving as a model of post-menopause, it was demonstrated that *Cimicifuga racemosa* extract reduced hot flushes [43], weight gain and serum triglycerides [36], which are indicators for beneficial metabolic effects.

Besides this, it was found that components of the *Cimicifuga racemosa* extract passed the blood-brain-barrier and were involved in thermoregulation in ovariectomized rats [44]. Moreover, black cohosh mediates neurobiological effects, for example, it increased the μ opioid receptor binding potential in brain regions involved in emotional and cognitive function in postmenopausal women [45].

Recent studies further revealed that *Cimicifuga racemosa* extract rather exerted anti-estrogenic than estrogenic effects, since black cohosh did not impact hormone level in a study with peri- and postmenopausal women [46].

Furthermore, *Cimicifuga racemosa* extract exerted anti-estrogenic effects in breast cancer cells *in vitro* [47] and can be used in patients with uterine myoma [37], endometrial cancer [33] and breast cancer treated with tamoxifen [48]. *Cimicifuga racemosa* extract has shown to be beneficial in some types of cancer, as it showed a reduced risk for recurrence of breast cancer [49] and endometrial cancer [33]. Moreover, *Cimicifuga racemosa* extract rather mediated protective effects against breast cancer [50].

Recent *in vitro* studies revealed that AMP-activated kinase A (AMPK) was activated by *Cimicifuga racemosa* extract and ameliorated metabolic disorders in *ob/ob* mice and ovariectomized rats, indicating that effects of black cohosh extract on the bioenergetic metabolism may significantly contribute to therapeutic effects against menopausal complaints [35,36]. In contrast to metformin, Ze 450 mediated beneficial effects on cumulative weight gain and decreased average daily food and water intake in the mentioned study [35]. Additionally, Ze 450 improved HOMA-IR index as an indicator of insulin resistance [35].

These recently emerging results highlight a potential role of Ze 450 on the energy metabolism *in vitro* and *in vivo*, proposing a novel therapeutic concept in the treatment of menopausal complaints that focuses on the metabolism rather than estrogen replacement. In a retrospective study, women treated with HRT or *Cimicifuga racemosa* were compared. In this study, body weight, metabolic serum parameters (lipids, glucose, insulin, HOMA-IR) and menopausal symptoms were assessed. In line with previous findings, *Cimicifuga racemosa* extract improved climacteric complaints. Notably, women treated with HRT or *Cimicifuga racemosa* extract did not gain weight, which points out beneficial effects of *Cimicifuga racemosa* extract on energy metabolism [52], since menopausal women accumulate risks for metabolic disease, including a significant weight gain [53]. In the current study, effects of Ze 450 on cellular metabolism were of particular interest with a special focus on mitochondria, since they are key organelles regulating cellular energy metabolism and thermoregulation.

1.2. Model systems of oxidative stress

1.2.1. Ferroptosis/Oxytosis

Oxidative stress plays a key role in the pathogenesis and progression of many metabolic, immunological and neurological diseases [54–57]. In this context, research was conducted in the field of oxidative stress-mediated cell death. Besides apoptosis, caspase-independent forms of cell death, like oxytosis or ferroptosis [58–60] contribute to the mentioned diseases. Well-established *in vitro* model systems of oxidative cell toxicity were used to study cellular and mitochondrial contribution to oxidative damage. HT22 cells lack expression of NMDA receptors and, consequently, glutamate-induced cell death is not mediated through glutamate-induced excitotoxicity through rapid calcium influx (Chapter 1.2.2.). Inhibition of the xCT (cysteine/glutamate antiporter) by erastin or glutamate provokes cellular depletion of glutathione, thereby disrupting the glutathione peroxidase 4 (GPX4) redox homeostasis [60]. GPX4 is an antioxidant enzyme, which catalyzes the detoxification of lipid-hydroperoxides [61]. 1S, 3R-RSL-3 (RSL-3) is capable to induce oxidative cell death by covalent binding and inactivation of GPX4. Either erastin or glutamate, as well as RSL-3 exposure, lead to massive ROS formation via lipid-peroxidation due to 12/15 lipoxygenases and subsequent mitochondrial impairments in neuronal and non-neuronal cells [59,62]. Loss of mitochondrial membrane potential, depletion of ATP generation via oxidative phosphorylation, enhanced mitochondrial fission [63] and mitochondrial ROS formation [64] mark the so-called “point of no return”, meaning that cells with massively impaired mitochondria cannot survive (Figure 3) [65].

Upon mitochondrial outer membrane permeabilization, AIF is released and translocates to the nucleus [66], triggering DNA fragmentation and subsequent induction of cell death [67].

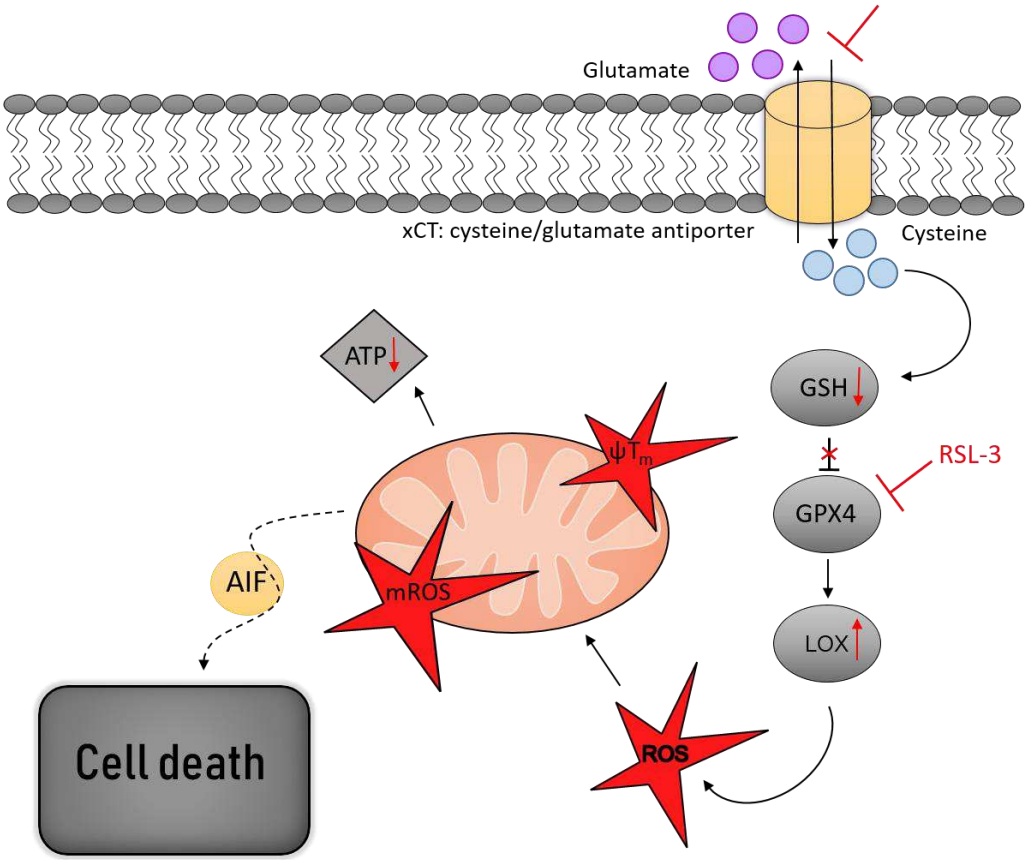

Figure 3. Oxytosis/Ferroptosis

The xCT transporter mediates the exchange of cysteine and intracellular glutamate across the plasma membrane. Milimolar concentrations of glutamate and micromolar concentrations of erastin inhibit the xCT antiporter reducing the intracellular cysteine required for the synthesis of glutathione (GSH). Depletion of GSH, in turn, reduces the activity of GPX4 (glutathione peroxidase 4) resulting in activation of 12/15 lipoxygenases (LOX) and ROS formation. Increase in ROS production mediates mitochondrial impairment and apoptosis-inducing factor (AIF) translocation from the mitochondria to the nucleus leading to DNA fragmentation and subsequently cell death (mROS: mitochondrial ROS; ψT_m: mitochondrial membrane potential).

1.2.2. Excitotoxicity

Glutamate is an important neurotransmitter and signaling molecule, which is involved in neuronal plasticity and learning [68]. The neurotransmitter is primarily located intracellularly but can reach concentrations in a 10 µM range during synaptic transmission. In physiological conditions, voltage-dependent NMDA receptors are blocked by Mg^{2+}, but after stimulation by glutamate, depolarization of the post-synaptic membrane removes the Mg^{2+} blockage and allows for Ca^{2+} influx [68,69]. However, excessive glutamatergic signaling followed by massive Ca^{2+} influx and disruption of the Ca^{2+} homeostasis causes excitotoxic cellular damage, which has been linked to a variety of neurodegenerative diseases, for example, stroke and traumatic brain injury [70]. In excitotoxicity, calcium dysregulation due to post-synaptic activation of glutamate

receptors (AMPAR, NMDAR, and metabotropic glutamate receptors) [69] triggers neuronal cell death (Figure 4). In particular, NMDAR mediated calcium and sodium influx contribute to a further increase in intracellular calcium levels [71] accompanied by dysregulation of the calcium extrusion via the sodium-calcium exchanger [72]. Upon excitotoxic signaling mitochondrial uptake of calcium leads to massive mitochondrial ROS formation, loss of mitochondrial membrane potential by opening of the mitochondrial permeability transition pore, thereby resulting in neuronal cell death [73,74].

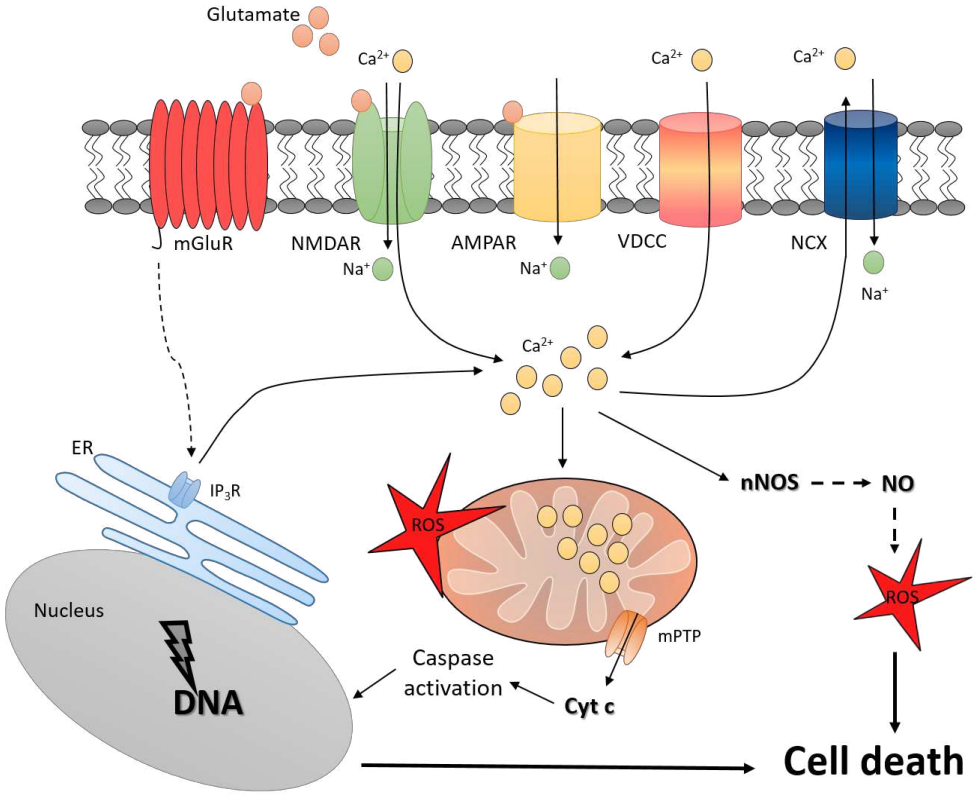

Figure 4. Excitotoxicity

Illustration of excitotoxic cell death in neurons. NMDAR: N-methyl-D-aspartate receptor; mGluR: metabotropic glutamate receptor, AMPAR: α-amino-3-hydroxy-5-methyl-4-isoxazolepropionic acid receptor; IP_3R: inositol trisphosphate receptor ;VDCC: voltage-dependent calcium channels; NCX: sodium-calcium exchanger; $Na^{+:}$ sodium, Ca^{2+}: calcium; ROS: reactive oxygen species; nNOS: neuronal nitric oxide synthase; NO: nitric oxide; mPTP: mitochondrial permeability transition pore; Cyt c, cytochrome c; DNA: deoxyribonucleic acid; ER: endoplasmic reticulum.

1.3. Cellular energy metabolism

Mitochondria are considered as crucial organelles in energy metabolism since mammalian cells primarily rely on energy supply via oxidative phosphorylation. Besides this, ATP production is provided by the degradation of nutrients via anaerobic glycolysis (Figure 5) [75]. Under certain physiological and pathophysiological conditions, the importance of glycolytic metabolism increases [75].

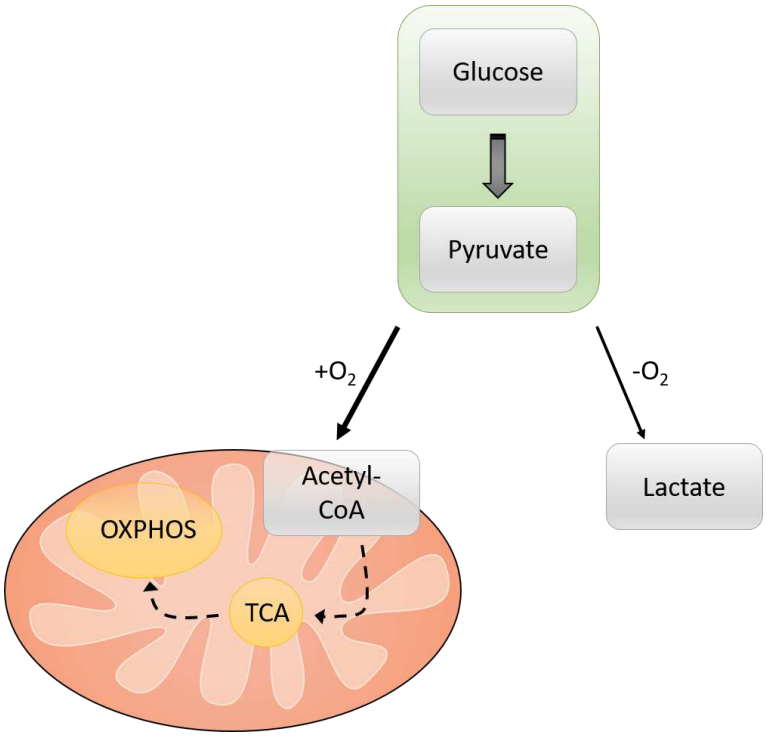

Figure 5. Main pathways of energy supply

Glucose is metabolized to pyruvate via the glycolytic pathway. Under aerobic conditions (sufficient oxygen supply), ATP is supplied by mitochondria due to oxidative phosphorylation (OXPHOS). Under anaerobic conditions, pyruvate is metabolized to lactate by recycling NAD^+ for glycolysis. Normally, the main energy demand is covered by mitochondrial use of acetyl-CoA via the tricarboxylic acid cycle (TCA) and following oxidative phosphorylation (OXPHOS).

Oxidative phosphorylation

Mitochondria are critical organelles for maintaining cellular energy homeostasis. In the tricarboxylic cycle, NADH is produced, which is essential for oxidative phosphorylation and ATP production. Five different mitochondrial complexes (I-V) are involved in energy production, by generating an electron and pH gradient along the inner mitochondrial membrane (Figure 6). Finally, complex V uses the energy provided by the proton electrochemical gradient to synthesize ATP from ADP in the mitochondrial matrix.

Mitochondria are considered as a major source of ROS upon electron leakage as a side product of oxidative phosphorylation [76]. Mitochondrial ROS are important mediators of cellular and mitochondrial damage and mitochondrial ROS production is often elevated under certain pathologic conditions, including oxidative stress [65]. Hence, protecting mitochondria has been proposed as a promising therapeutic strategy in the treatment of a variety of diseases, including metabolic diseases related to oxidative stress.

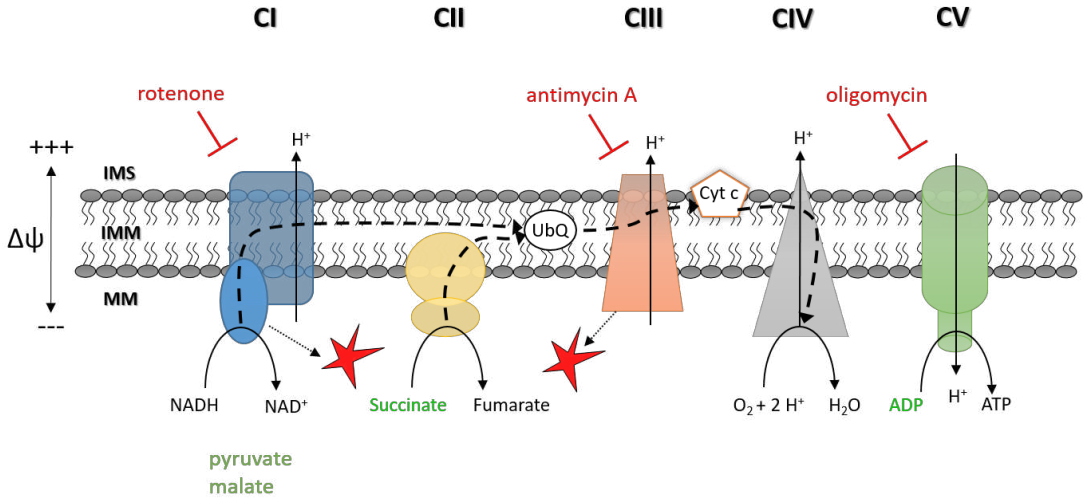

Figure 6. Scheme of the electron transport chain (ETC)

Oxidative phosphorylation is driven by a proton (black line) and an electron (dashed black line, indicates transport of electrons) gradient: NADH dehydrogenase (CI) uses NADH for electron entry and proton supply for the pH gradient. Succinate is metabolized by CII to fumarate; thereby electrons from CI and CII reactions were transferred to Ubiquinone (UbQ). Next, electrons were transferred from reduced ubiquinone to cytochrome c (Cyt c) via CIII. CIV transfers an electron from cytochrome c to a dioxygen molecule, which is converted to water. Moreover, complex IV increases the electrochemical potential by transferring protons to the IMS. Subsequently, ATP is produced by complex V driven from the pH and electron gradient. Inhibitors of the ETC are represented in red: rotenone inhibits CI, antimycin A inhibits CIII and oligomycin inhibits CV. Pyruvate and malate are involved in CI activity by supply of NADH, succinate is a substrate for CII (IMS: intermembrane space, IMM: inner mitochondrial membrane, MM: mitochondrial matrix, UbQ: Ubiquinone, Cyt c: cytochrome c).

Anaerobic glycolysis

In cases of low oxygen supply, glycolytic pyruvate is metabolized to lactate by lactate-dehydrogenase restoring NAD^+, this metabolic pathway is named anaerobic glycolysis, but glycolysis takes place in the presence or absence of oxygen. Under anaerobic conditions, pyruvate is metabolized to lactate (Figure 5), while during aerobic conditions it is metabolized to acetyl-CoA and used in the TCA cycle and following OXPHOS (Figure 5). In cancer or fast proliferating cells, pyruvate is preferentially metabolized to lactate independent of the presence or absence of oxygen, and this phenomenon is called the Warburg effect or aerobic glycolysis (Figure 7) [75,77].

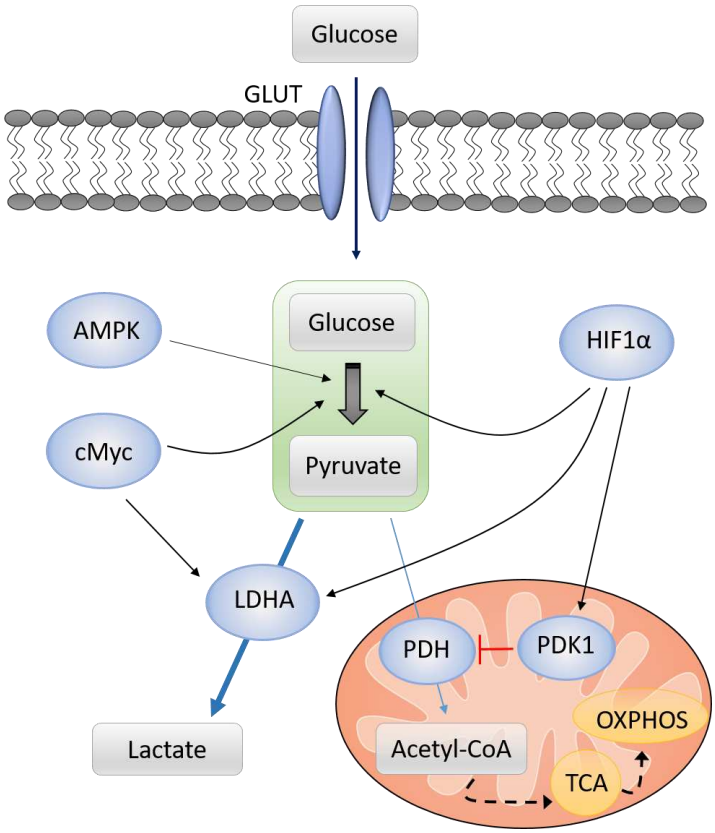

Figure 7. Molecular signaling pathways promoting the Warburg effect

Metabolic reprogramming in cancer cells is promoted by enhanced glycolysis. AMPK, cMyc, and HIF1α are key players in cellular energy regulation contributing to this bioenergetic shift. The mentioned regulators (AMPK, cMyc, and HIF1α) enhance glycolytic gene expression. cMyc and HIF1α increase LDHA expression and LDHA activity, leading to preferred metabolism of pyruvate to lactate and limited influx of pyruvate in mitochondrial energy production. HIF1α enhances the activity of PDK1 and following inhibition of PDH, resulting in decreased OXPHOS (GLUT: glucose transporters, TCA: tricarboxylic acid cycle, OXPHOS: oxidative phosphorylation, AMPK: AMP-activated protein kinase HIF1α: hypoxia-inducible factor α, PDH: pyruvate dehydrogenase, PDK1: pyruvate dehydrogenase kinase 1).

Since aerobic glycolysis is less effective in energy production compared to oxidative phosphorylation, larger amounts of glucose are required to fulfill the energy demand of fast proliferating cells. Much research was done investigating the mechanism beyond the altered energy supply in tumor cells. For instance, glucose transporters [78] and hexokinase [79,80] expression were enhanced to support glycolysis. Besides this, the Warburg effect is regulated by the hypoxia-inducible factor (HIF), cMyc and AMP-activated protein kinase (AMPK)–liver kinase B1 (LKB1) pathways [82], amongst others (Figure 7). Initially, cMyc was described as an oncogene, but further acts as a global transcriptional regulator affecting metabolism, mitochondrial function and cell growth in physiological conditions [83]. Intracellular signaling differentiating between oncogene and physiological pathways is the topic of current research. Besides, it has been demonstrated that cMyc regulates many glycolytic genes involved in the Warburg effect

[84] and, moreover, cMyc overexpression has been shown to be linked with Ark5 (AMPK related kinase 5), an upstream regulator of AMPK, which is involved in maintaining energy homeostasis [85]. Additionally, HIF1α is overexpressed in many human tumors and moreover, loss of function mutations were found in tumor suppressor genes like VHL (von Hippel-Lindau tumor suppressor gene), suggesting an essential role in cancer progression and tumor growth [86]. In this context suppression of HIF1 decreased mitochondrial respiration and enhanced glycolysis by involving pyruvate dehydrogenase kinase 1 [87]. The exact relationship of intracellular signaling pathways leading to a metabolic shift towards glycolysis remains to be elucidated, but metabolic reprogramming might play a role in diseases related to oxidative stress by reducing mitochondrial ROS mediated damage.

In the context of cellular energy supply, it was a major interest to elucidate the effects of Ze 450 on mitochondrial metabolism and molecular signaling, which might contribute to the previously observed metabolic changes *in vitro*, *in vivo*, and in patients [35,36,52].

1.4. Caenorhabditis elegans

Caenorhabditis elegans is a nematode, which is free-living [88] and inhabits in soil surrounded by microorganisms [89]. Before reaching adulthood, four larval stages (L1-L4) have been passed, the termination of each stage is marked by a molt [88]. It is a self-fertilizing hermaphroditic animal, with a length of 1 mm, which produces about 300 progenies every 3.5 days [88]. Besides the hermaphrodites, there are a few males, which are smaller and behave differently [90,91]. There is an alternative larval stage, which is entered under certain stress conditions, like high population density or restricted food intake [92]. In this stage, the larvae are able to remain for months [92].

Caenorhabditis elegans is an emerging model system to study neuronal development, behavior, and longevity. The neuronal system of *C. elegans* is well-studied and less complex than the mammalian nervous system. The nervous system of *C.elegans* consists of 302 neurons classified into 118 different neuronal classes, which share neuronal morphology and connectivity but differ in their position [88]. Moreover, it is known that the genome of *C. elegans* and humans have many features in common since a lot of the genes have a counterpart between the species [93].

In general, there are at least three classes of genes, which are involved in the regulation of lifespan: *eat* genes, *clk* genes and genes regulating dauer formation, for example *daf* [94,95]. For example, caloric restriction prolonged lifespan by affecting *eat* genes [95,96]. Moreover, it is known that mutations in *clk*-1-3 and *gro*-1 affect aging, but are further involved in plenty of other functions. Besides this, it was discovered that mitochondrial hydroxylase is encoded by *clk*-1, which is involved in the regulation of redox homeostasis; *clk*-2 encodes for a telomere length controlling protein and an enzyme that modifies tRNAs is encoded by *gro*-1 [97]. However, very little is known about the mechanisms leading to elongated lifespan [94]. The third group of genes is involved in the regulation of the larvae stage [94] and they merge in the same intracellular signaling pathway, involving *DAF*-2, which is an insulin receptor-like transmembrane tyrosine kinase [98], and *DAF*-16 that is a forkhead transcription factor and necessary for lifespan extension [99]. Further correlative data suggests that *daf*-2 mutants are more resilient to oxidative stress, thereby promoting the prolongation of lifespan [100].

Besides this, it has been shown that many genes which are involved in thermoregulation further promoted the extension of lifespan [101]. Additionally, the response to heat stress is preserved across different species [102] making the heat shock test in *C. elegans* a valuable tool to analyze lifespan under stress conditions because it involves hsf-1 [102]. During the heat shock thermosensory neurons (AFDs) sense and guide, heat mediated

signaling leading among other things to protein miss folding [103]. Thereby, activating heat shock response via IGF/ILS signaling pathway and *hsf*-1 and *daf*-16 involvement [104], leading to transcription of target genes, like SOD and HSP, for cytoprotection. During heat shock this regulatory mechanism cannot compensate for cellular damage, leading to a shortening of lifespan [102,105,106].

Taking use of the reduced lifespan due to heat shock, i.e. at 37 degrees Celsius, effects on long term survival are accessible in *C. elegans* in shorter time periods (~15 hours) compared to the real-time setting (~30 days).

Further, paraquat (PQ), a known herbicide, is used to induce oxidative stress, also in *C elegans*. It induces superoxides [107], which are mainly produced by mitochondria and lead, for example, to disruption of protein homeostasis and DNA damage [106,108]. This stress response might be detrimental for the nematode, depending on the dose, as low concentrations of PQ extended lifespan of *C. elegans* [109]. Paraquat-induced oxidative stress response is used to study protective mechanisms affecting mitochondria in *C. elegans*.

Caenorhabditis elegans is fed on bacteria, therefore it is essential for them to differentiate between food and pathogens [89]. For this reason, they have an excellent olfactory sense [89], which implies specialized chemosensory neurons to detect a wide range of odorants, including, for example, aromatic compounds [110,111], and they respond in a regulated manner to sensory stimuli [88]. This characteristic feature of *C. elegans* is used to assess chemotactic behavior and thereby neuronal function.

In this context, *C. elegans* is an excellent model system to gain new insights into the mechanism of longevity and aging and further studying mitochondrial involvement in the mentioned processes.

1.5. *Petasites hybridus* extract (Ze 339)

Petasites hybridus has been used to treat a variety of diseases, including gastrointestinal disorders [112] and migraine [113,114]. *Petasites hybridus* is also known as common butterbur, it belongs to the sunflower family (*Asteraceae*) and is spread over the northern hemisphere [115]. Mostly the leaves and the rhizomes of *Petasites hybridus* are used for medicinal purposes [116]. Multitudes of effects are described, but extracts of the rhizome are known to act spasmolytic and analgetic, while extracts of the leaves were reported to be inflammatory and anti-allergic [116].

Ze 339 is a standardized CO_2 extract, which is used to treat seasonal allergic rhinitis with a dosage of 16-24 mg petasin per day [117,118]. Efficacy and safety were proven in a prospective, randomized, double-blind, placebo-controlled study with 168 patients [117]. Petasin, isopetasin and neopetasin are sesquiterpenes, which are considered to mediate anti-allergic effects due to inhibition of inflammatory signaling molecules [119]. Besides the petasines, there are a variety of different components described, including pyrrolizidine alkaloids (PA) [120]. For Ze 339 PA-reduced plant species were selectively grown and a purification procedure was performed to ensure minimal PA content [115,120]. Moreover, in a highly sensitive UPLC TOF MS method PA were not detectable in Ze 339 within 29 different batches [120]. Besides Ze 339, seasonal allergic rhinitis can be treated with antihistamines, corticosteroids, decongestants, cromones, and immunotherapy [121–123].

The pharmacological mode of action of Ze 339 is not fully understood. So far, it is known from *in vitro* experiments that leukotriene (LT) synthesis [124,125] and the binding to histamine 1 receptors are blocked [126]. Moreover, Ze 339 and petasin demonstrated inhibitory effects on PAF- and C5a-induced increases in intracellular calcium concentrations [124]. Recent findings revealed that Ze 339 was effective in acute viral rather than bacterial infections [119] in primary human nasal epithelial cells (HNECs cells). In the same cell type, it was shown that neutrophil chemotaxis was reduced and this effect was mechanistically linked to reduced cytokine-induced STAT (signal transducer and activator of transcription) signaling [119]. Upon cytokine (IL-4, IFNγ, IL-6) release and binding to cytokine receptor 1 or 2, janus kinases (JAK) initiate autophosphorylation and subsequent recruitment of STATs [127]. STAT transcription factors are phosphorylated by JAK and then enter the nucleus as homo- or heterodimers to interact with target gene promotors. In the case of allergic rhinitis, pro-inflammatory gene products, like chemokines are expressed [128].

Since Ze 339 is a CO_2 extract it is mainly composed of lipophilic components, like terpenoids, lipids and glycolipids [129], which can interact with membranes and lower bioavailability. Further, the authors propose that the hydrophobic components interfere with the assembly of the JAK/STAT complex and thereby reducing pro-inflammatory responses [129].

In patients, it was found that Ze 339 reduced local IL-8 and LTB-4 production leading to symptom relief of allergic rhinitis [130]. Furthermore, nasal obstruction was recovered faster in patients treated with Ze 339 compared to desloratadine [130]. Moreover, in another study, Ze 339 was used and compared to cetirizine in patients with seasonal allergic rhinitis and mediated comparable effects by avoiding sedative side-effects [131].

Immunological diseases, including allergic rhinitis, have been shown to be associated with ROS formation [132]. Besides this pathophysiological role, ROS generated by mitochondria and via NADPH oxidase mediate functions as signaling molecules [133] maintaining a proper immune response via IL-1β, TNFα and IFNγ [134]. The principle of hormesis describes a specific regulation depending on the concentration of a hazardous compound or exposure to stress, for example of ROS and also phytochemicals [135]. Mechanistically hormesis is defined as an adaptive metabolic regulation to modulate stress responses [134,136,137]. Additionally, it has been shown that especially mild mitochondrial ROS formation mediates beneficial health effects (Figure 8), which is called mitohormesis [138,139]. In the context of the treatment of seasonal allergic rhinitis hormetic modulation might contribute to symptom relief, as low levels of ROS restore a healthy immune system with adequate but not overshooting reactivity to an allergen [134].

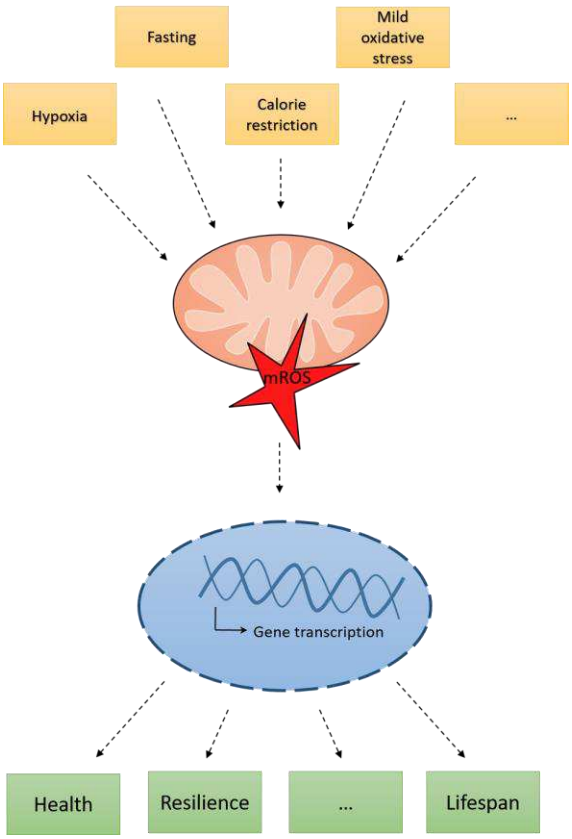

Figure 8. Scheme of mitohormesis

Mild mitochondrial ROS formation is triggered by various factors for example caloric restriction, fasting, mild oxidative stress, and others, thereby, involving a multitude of cellular pathways like AMPK or mTOR mediated signaling. Hereby, mitochondrial ROS function as signaling molecules affecting downstream transcriptional regulators like FoxOs or NRF2 leading to adaptive gene expression and beneficial effects on health, lifespan and promoting stress and mitochondrial resilience.

2. Aims and Objectives

The major aims of the study were to reveal novel insights into the mechanisms of action of *Cimicifuga racemosa* and *Petasites hybridus* extracts emphasizing new therapeutic concepts supported by a deeper understanding of their molecular targets.

The first part of the study focuses on the effects of the *Cimicifuga racemosa* extract Ze 450 on mitochondria as a major target in different model systems (cultured neuronal and liver cells, isolated mitochondria, and *C. elegans*). *Cimicifuga racemosa* extracts are commonly used to treat menopausal symptoms, such as hot flushes and night sweating. More recently, *in vitro* and *in vivo* studies suggested metabolic effects of *Cimicifuga racemosa* extract Ze 450 on AMPK signaling and enhanced insulin sensitivity in *ob/ob* mice, respectively. In addition, a retrospective clinical study revealed beneficial effects of *Cimicifuga racemosa* extract on weight gain in postmenopausal women, overall suggesting metabolic regulation as a major underlying mechanism of Ze 450. In line with this, one major aim of this study was to elucidate molecular effects of Ze 450 with a particular focus on mitochondria, since disturbances in energy metabolism are closely linked to menopausal complaints and metabolic disorders. Thus, investigating the effects of Ze 450 on metabolic regulation in hippocampal, hypothalamic and cortical neurons, as well as in liver cells shall reveal novel insights into the mechanism of action of *Cimicifuga racemosa* extracts and provide evidence for a new mechanistic concept explaining the relief of menopausal symptoms. Moreover, liver cells were used to address the ongoing discussion about *Cimicifuga racemosa* extracts causing hepatotoxicity. In this regard, Ze 450 was exposed to HepG2 and H4IIE cells to investigate potential cytotoxic effects.

Menopausal transition is a physiological phase, which is generally considered as a consequence of estrogen depletion. In addition to estrogen decline, age-related risk factors, such as accumulating reactive oxygen species (ROS), may contribute to menopausal alterations and associated diseases, such as diabetes mellitus type II or osteoporosis. In particular, accumulating oxidative stress may affect mitochondria and, thereby, energy homeostasis and metabolic changes, which occur during menopause and the mentioned associated diseases. In the present study, model systems of oxidative stress were applied to mimic processes of accelerated ROS formation contributing to climacteric complaints and age-related diseases and evaluate potential protective effects of Ze 450.

Alterations of cellular (e.g. cell death, lipid-peroxidation) and mitochondrial parameters (mitochondrial ROS formation, mitochondrial membrane potential) were assessed in

neuronal and liver cells under basal conditions and after induction of oxidative stress. Further, effects of Ze 450 on mitochondrial respiration and the rate of glycolysis were investigated, since cellular energy metabolism was found to be altered in menopausal transition but also in metabolic disorders, like diabetes mellitus type II.

In addition, functional analysis of isolated mitochondria addressed the question of whether Ze 450 directly impacts mitochondrial respiratory chain complexes. Furthermore, mechanistic regulations were assessed by analyzing protein and mRNA levels of key metabolic regulators, like mTOR and HIF1α. To gain further insights into Ze 450 mediated effects on energy metabolism, glucose uptake into cells was investigated for a comprehensive understanding of the effects of Ze 450 on glucose metabolism.

Further, isolated components (actein, 23-epi-26-deoxyactein and cimiracemoside C) and specific sub-fractions (EtOAc-, BuOH- and Aq. fraction) were investigated to elucidate which components of the extract contributed to the major effects of Ze 450.

Finally, the effects of Ze 450 were tested on a whole organism in *Caenorhabditis elegans.* In this model system, Ze 450 mediated effects on longevity and aging were studied *in vivo*. For that purpose, Ze 450 was tested in a lifespan analysis, a heat stress application and a real-time setup using *C. elegans*. Moreover, potential protective effects of Ze 450 in *C. elegans* were investigated upon mitochondrial impairment provoked by paraquat-induced oxidative stress.

In the second part of the thesis Ze 339, a *Petasites hybridus* leaf extract was investigated. Ze 339 is used to treat seasonal allergic rhinitis but there is little known about the molecular mechanism of *Petasites hybridus* extracts. Mitochondrial ROS have been shown to contribute to the pathogenesis of immunological diseases, but in addition, depending on the concentration, ROS mediate beneficial effects by modulation of metabolic adaptation processes. In this regard, it was of major interest to gain new insights into the mechanism of action of Ze 339 with a particular focus on mitochondria, since they are the major source of ROS and play a crucial role in cellular energy homeostasis. Further, metabolic regulations of Ze 339 in a model system of erastin-induced oxidative damage shall enable its potential protective effects in neuronal cells.

3. Materials and Methods

3.1. Cell culture

HT22 cells were generated from a glutamate sensitive sub-clone of HT-4 cells by David Schubert (Cellular Neurobiology Laboratory, Salk Institute for Biological Studies, La Jolla, California, USA). Originally, HT4 cells were derived from primary hippocampal neurons and immortalized with a temperature-sensitive SV40 T-antigen [140,141]. HT22 and mHypo-CLU190 cells (Cedarlane®, Cellutions Biosystems Inc., Canada) were grown in Dulbecco's modified Eagle medium (DMEM, Capricorn Scientific GmbH, Germany) supplemented with 10% heat-inactivated fetal calf serum (Merck KGaA, Germany), 100 units/mL penicillin (Merck KGaA, Germany), 100 µg/mL streptomycin (Merck KGaA, Germany), and 2 mM glutamine (Capricorn Scientific GmbH, Germany). To induce cell death, glutamate (Merck KGaA, Germany) or erastin (Calbiochem®, Germany) was added to the medium for the indicated amount of time (8-16 h). Neuronal cells were split twice a week in a ratio of 1:10 -1:20. HepG2 (ATCC®™ HB-8065™) cells were grown in Eagle´s minimum essential medium (EMEM, Merck KGaA, Germany) supplemented with 10% heat-inactivated fetal calf serum, 100 U/mL penicillin, 100 mg/mL streptomycin. 1S, 3R-RSL-3, which was kindly provided by Prof. Diederich (University of Marburg, Germany), was added to induce oxidative cell death in HepG2 cells. H4IIE cells (ATCC®™ CRL-1548, batch: 59997514) were kindly provided by Max Zeller Söhne AG, Switzerland. H4IIE cells were grown in EMEM supplemented with 10% heat-inactivated fetal calf serum, 100 U/mL penicillin, 100 mg/mL streptomycin. Liver cells were split twice a week in a ratio of 1:5-1:10. Splitting of cells was performed as follows: growth medium was replaced by 1x PBS following replacement by 0.05%/0.02% trypsin/EDTA (Merck KGaA, Germany). After detachment of the cells growth medium (containing FCS) was used to stop trypsinization. Cells were centrifuged for 3 min at 1000 x rpm and the cell pellet was re-suspended in fresh medium. The amount of cell suspension was adjusted to the size of the cultured flask. For determination of the cell number, a counting chamber was used (BLAUBRAND®, Brand GmbH, Germany). After dilution to the desired cell number, cells were seeded in appropriate plates. For standard cultivation, liver and neuronal cell lines were kept in 75 cm^2 flasks (T75) in a standard unified incubator (HERAcell®, KOBE, Germany) at 37°C and 5% CO_2.

Cell culture plates for primary neurons were incubated with 5% PEI (polyethyleneimine) for 4 h at 37°C, subsequently washed with sterile water and dried for 30 min under UV light exposure. Primary cortical neurons were prepared from embryonic mouse brains

(E16-18 from wild type C57BL/6 mice, Charles River, Germany). Dissected cortices were kept in HBSS (Hank´s balanced salt solution) on ice and rapidly processed as follows: Isolated cortices were trypsinized in HBSS containing 1 mg/mL trypsin for 15 min at 37°C. Next, DNase was added for 30 seconds and the cortices were washed with HBSS and then mixed with HBSS containing 2 mg/mL trypsin inhibitor (Merck KGaA, Germany) for 2 minutes at room temperature. Followed by a washing step with HBSS and trituration with a 1 mL pipet tip. The triturated cells were centrifuged at 2,000 rpm for 5 min at RT (room temperature) and the supernatant was removed. The neurons were cultured in neurobasal medium (NB, ThermoFisher Scientific, Germany) supplemented with 2 % (v/v) B-27 (Invitrogen, USA). Dissociated neurons were seeded with 50,000 cells per well onto PEI coated 96 well plates. Cultures were grown in NB medium supplemented with 1.2 mM L-glutamine, 2% B-27 supplement, 100 U/mL penicillin and 100 mg/mL streptomycin. On day four in culture, 10% fresh medium was added and on day seven in culture half of the medium was replaced. Treatment with Ze 450 and glutamate (20 µM) was carried out on day nine to ten in culture. The NMDA receptor antagonist, MK-801 (Merck KGaA, Germany) was added at a concentration of 10 µM. Compounds were diluted in EBSS and incubated for the indicated time.

Primary cortical rat neurons (kindly provided by Prof. Schratt, BPC Marburg, Germany) were plated on PEI coated 96 well plates with 20,000 cells/well and handled as described for the primary mouse neurons.

3.2. Materials, solutions, and chemicals

3.2.1. *Cimicifuga racemosa* extract (Ze 450)

The ethanolic (60% v/v) *Cimicifuga racemosa* dry extract Ze 450 was manufactured of dried roots and rhizomes and obtained from Max Zeller Söhne AG (Switzerland, batch: 151033). The content of triterpene glycosides was 6.4%. Ze 450 was dissolved in 60% ethanol (v/v) (Carl Roth GmbH, Germany) and filtered with a 0.22 µm Whatman Puradisc™ sterile filter. Ze 450 conforms to the herbal preparation B, which was granted well-established use in the 2010 Community herbal monograph on *Cimicifuga racemosa* by the HMPC. For the characterization of the extract, the HPLC fingerprint of Ze 450 (batch: 151033) was determined as reported previously [142].

Fractionation of Ze 450 was performed at Max Zeller Söhne AG in Switzerland by Samuel Hasler. Ze 450 (10.0 g) was re-suspended in 100 mL H_2O and subsequently

extracted with ethyl acetate (EtOAc, 4 ×100 mL) and butanol (BuOH, 4 ×100 mL) as described previously [143]. The EtOAc-, BuOH-, and aqueous fractions were concentrated in vacuo to yield the EtOAc soluble fraction (1.94 g, 19.3% (m/m)), the BuOH soluble fraction (0.94 g, 9.39% (m/m)) as well as the remaining aqueous (Aq.) fraction (7.32 g, 72.9% (m/m)).

The dried fractions were solubilized in 60% ethanol (v/v) and further diluted to equivalent potent Ze 450 concentrations. 70 µg/mL of the Aq. fraction, 10 µg/mL of the EtOAc fraction and 5 µg/mL of the BuOH fraction correspond to 100 µg/mL total Ze 450 extract.

3.2.2. *Petasites hybridus* extract (Ze 339)

The subcritical carbon dioxide (CO_2) *Petasites hybridus* leaf extract (Ze 339, batch: 140155) was provided by Max Zeller Söhne AG, Switzerland. Appropriate stock dilutions were made with DMSO in glass vials fresh on the day of the experiment.

3.2.3. Materials

Materials and equipment were used as listed in Table 1

Table 1. Materials and equipment

T75 flasks	Greiner, Germany
0.2, 0.5, 1.5 and 2 mL Eppendorf tubes	Sarstedt, Germany
0.22 µm Whatman Puradisc™ sterile filter	Whatman, Germany
1, 5, 10 mL syringes	Braun, Germany
15 and 50 mL tubes	Greiner, Germany
24-well plates	Greiner, Germany
4 mL glass vial	KOBE, Germany
6-well plates	Greiner, Germany
96-well plates	Greiner, Germany
96-well plates (white) for ATP	Greiner, Germany
96-well plates for BCA	Roche, Applied Science, Germany
Cell homogenizer	Isobiotec, Germany
Cell scraper	Sarstedt, Germany
Cell Strainer 100 µm Nylon	Life Sciences, USA

ChemiDoc XRS system	Bio-Rad Laboratories, USA
Counting chamber	BLAUBRAND®, Brand GmbH, Germany
EL_x808 Ultra Microplate Reader	Bio-Tek, Germany
FluoStar OPTIMA	BMG Labtech, Germany
Gas-tight glass syringe	Sulpeco, Germany
Guava Easy Cyte 6-2 L system	Merck Millipore, Germany
Heraeus FRESCO17	ThermoFisher Scientific, Germany
HERAcell®	KOBE, Germany
Leica DMI6000	Leica, Germany
NanoPhotometer™	Implen, Germany
Nalgene Rapid-Flow Bottle-Top Filter 0.2 µm filter	ThermoFisher Scientific, Germany
Neoject® Cannulae 20 G	Dispomed® WITT oHG; Germany
Omnifix®-FLuer Solo 1 mL	Braun, Germany
Pipette tips	Gilson, USA Greiner, Germany
PVDF membrane	Roche Diagnostics, Germany
Rotilab sealing film	Greiner Bio-One, Germany
Seahorse XFe96 Flux Pak	Agilent Technologies, USA
Sterican Cannulae 18 G	Braun, Germany
T175 flasks	Greiner, Germany
Whatman puradisc™	Sarstedt, Germany
xCELLigence system Real-Time Cell Analyzer RTCA-MP	ACEA Bioscience, Inc., USA
E plate 96	ACEA Bioscience, Inc., USA
XF Extracellular Flux Analyzer	Agilent Technologies, USA
XF96-well microplates and cartridges	Agilent Technologies, USA
µ slide 8 well	Ibidi GmbH, Germany

3.2.4. Solutions

Table 2. Phosphate buffered saline (PBS), pH 7.4

NaCl	9 g
Na_2HPO_4	0.527 g
KH_2PO_4	0.144 g
HCl (0.1 M)	q.s. for pH 7.4
Aqua demin.	up to 1 L

Table 3. Standard Trypsin/EDTA solution (TE)

Trypsin 7,500 U/mg	100 mg
Ethylene diamine-tetra-acetic acid (EDTA)	40 mg
1x PBS	up to 200 mL

Table 4. Hank´s balanced salt solution (HBSS), pH 7.2

10x HBSS	50 mL
Pen/Strep 1%(v/v)	1.2 g
KH_2PO_4	5 mL
Aqua demin.	up to 500 mL

Table 5. Polyethylenimine 5% (PEI)

Boric acid	3.1 g
Borax	9.0 g
PEI 5%	1 mL
Aqua demin.	up to 800 mL

Table 6. 0.5 M Ethylenediaminetetraacetic acid (EDTA) pH 8.0

EDTA (x 2 H_2O)	242 mg
NaOH	20 g
Bidest. H_2O	1000 mL

3.2.5. Chemicals and Kits

All standard chemical reagents commercially available were purchased from Merck KgaA (Germany) or Roth (Germany), in case otherwise stated. For the preparation of buffers and solution, ultrapure water (SG Ultra Clear UV plus pure water system, VWR, Germany) was used. Sterilization for aseptic preparation of solutions was achieved by using a steam autoclave (Systec V-40, Systec GmbH, Germany) or sterile filtration (0.22 µm Whatman Puradisc™ sterile filter, Sarstedt, Germany).

The kits (Table 7) were used according to manufacturer´s protocol, unless otherwise stated.

Table 7. Kits

Annexin-V-FITC Detection Kit	Promokine, Germany
BODIPY (581/591 C11)	Invitrogen, Germany
GSH Assay Kit	Cayman Chemical, USA
InviTrap Spin Universal RNA Mini Kit	Stratec Biomedical, Germany
MitoPT™ TMRE Kit	Immunochemistry Technologies, Germany
MitoSOX™	Invitrogen, Germany
Pierce BCA Kit	ThermoFisher Scientific, Germany
SuperScript III One-Step RT-PCR System with Platinum® Taq	Invitrogen, Germany
ViaLight™ ATP Plus-Kit	Lonza, Switzerland

Substances were purchased like listed in table 8.

Table 8. Substances

1,3,5-Tris(4-hydroxyphenyl)-4-propyl-1H-pyrazole (PPT)	Merck KgaA, Germany
17β-estradiol	Merck KgaA, Germany
2,2-diphenyl-1-picrylhydrazyl (DPPH)	Cayman Chemical, USA
23-epi-26-Deoxyactein (deoxyactein)	PhytoLab GmbH & Co.KG, Germany
4-Hydroxytamoxifen (4-OH-Tamoxifen)	Merck KgaA, Germany
6-(hydroxy-2,5,7,8-tetramethylchroman-2-carboxylic acid) (Trolox)	Merck KgaA, Germany

Actein	PhytoLab GmbH & Co.KG, Germany
Agarose	Merck KgaA, Germany
Cimigenol-3-alpha-L-arabinosid (cimiracemoside C)	PhytoLab GmbH & Co.KG, Germany
Diarylpropionitrile (DPN)	Merck KgaA, Germany
Metformin hydrochloride (metformin)	Cayman Chemical, USA
Phalloidin555	Thermo Fisher Scientific, Germany
Rhodamine 123 (R123)	Thermo Fisher Scientific, Germany
SYTOX™ green	Life Technologies, Germany
2-deoxy-2-[(7-nitro-2,1,3-benzoxadiazol-4-yl)amino]-D-glucose (2-NBDG)	Cayman Chemical, USA

3.3. Mitochondrial isolation

Spraque Dawley rats were kept at the Institute of Psychology, Marburg (AG Schwarting/ Wöhr, MR20/35 Nr.19/2014) and then transferred to the Institute of Pharmacology and Clinical Pharmacy (Marburg, Germany). Mitochondria were isolated immediately after dissection of the prefrontal cortex and liver. The following isolation steps were all carried out on ice. For cortical tissue ~ 50 mg and for liver tissue ~ 20 mg was minced with a scalpel in 1 mL of isolation buffer (Table 9). Cortical tissue was homogenized via 10 times trituration with a 20 G Neoject needle and strained through a 100 µm cell strainer (Life Science, USA). The cortical and liver suspension was filled in a gas-tight glass syringe (Supelco, Germany). Afterwards, a pump controlled cell homogenizer (Isobiotec, Germany) with a constant pump flow rate (700 µL/min) was used according to existing protocols with minor modifications [144,145]. The system was primed with 1 mL mitochondrial isolation buffer before usage. Using the cell homogenizer, the cortical suspension was pumped three times with a clearance of 10 µm and the liver suspension once through a clearance of 18 µm. Next, the system was rinsed with 1 mL isolation buffer to collect the total homogenate. Followed by centrifugation at 800 x g for 10 min at 4°C (Heraeus, FRESCO17, ThermoFisher Scientific, Germany). The supernatant was transferred to a new 1.5 mL tube and centrifuged at 9,000 g for 10 min at 4°C. The resulting pellet represents the crude mitochondrial fraction. After resuspension in ~1 mL of mitochondrial isolation buffer (MSHE, Table 10) a BCA assay for protein determination using the Pierce BCA Protein Assay Kit (ThermoFisher Scientific, Germany) was performed. Protein concentration was calculated via linear regression with a BSA standard based on mitochondrial isolation buffer.

Table 9. Isolation buffer

Sucrose	300 mM
TES	5 mM
EGTA	200 µM
DTT	1 mM

Table 10. Mitochondrial isolation buffer (MSHE, pH 7.2)

Sucrose	70 mM
Mannitol	210 mM
HEPES	5 mM
EGTA	1 mM
BSA	0.5%

3.4. MTT assay

Metabolic activity as an indicator of cell viability was quantified using the MTT assay [59,146]. Viable and metabolically active cells convert 3-(4,5-dimethylthiazol-2-yl)-2,5-diphenyltetrazolium bromide (MTT, Merck KGaA, Germany), which was added at a concentration of 2.5 mg/mL (cell lines) or 5 mg/mL (primary neurons) for 1 hour at 37°C to the culture medium, into purple formazan. Next, the supernatant was removed and the plate with the attached cells was frozen at -80°C for at least 1 h. Absorbance was measured at 570 nm versus 630 nm with a plate reader (FluoStar, BMG Labtech, Germany) after dissolving in 70 µL/well DMSO via shaking for 1 h at 37°C (Carl Roth GmbH, Germany).

3.5. ATP assay

ATP levels were detected using the ViaLight™ plus Kit (Lonza, USA) according to the manufacturer's protocol. Approximately, twenty-four hours post-seeding in 96-well plates, cells were exposed to the indicated treatment. At the indicated time points after treatment (8, 16, 24 h), cells were transferred into a white 96 well plate and ATP levels

were analyzed by luminescence detection with FluoStar OPTIMA (BMG Labtech, Germany).

3.6. DPPH assay

For determination of the radical scavenging activity via the DPPH assay samples were prepared in 75% ethanol. 90 µL of 150 µM DPPH and 10 µL of the sample were incubated for 30 min in a 96 well plate in the dark. Absorbance was measured at 517 nm with a plate reader (SPARK 20M, TECAN, Germany). Radical scavenging activity was calculated using the following formula: $(A_0-A_1)/(A_0) \times 100$

3.7. FACS measurements

The microcapillary Guava Easy Cyte 6-2 L system (Merck Millipore, Germany) was used for flow cytometry measurements. HT22, mHypo, HepG2, H4IIE cells were seeded in a 24-well format and treated 24-32 hours post-seeding for the indicated treatment time. Data was collected from at least three replicates per treatment condition and 5,000 cells per sample. The GuavaSoft Software package was used for analysis.

3.6.1. Cell death (Annexin V/PI)

For seeding 24 well plates were used. Neuronal cell lines were seeded at a density of 40,000 cells per well and liver cell lines were seeded at a density of 50,000 cells per well. Cell death of HT22, mHypo, HepG2 and H4IIE cells exposed to the indicated treatment and inducer of oxidative stress was detected using the Annexin-V-FITC/PI Detection Kit (PromoCell, Germany) followed by fluorescence-activated cell scanning (FACS, guava easyCyte, Merck KGaA, Germany). Annexin-V-FITC was excited at 488 nm and emission was detected through a 525 ± 30 nm bandpass filter. Propidium iodide was excited at 488 nm, fluorescence emission was detected using a 690 ± 50 nm bandpass filter. Data were collected from at least 5’000 cells with at least three replicates per condition.

3.6.2. Lipid-peroxidation (BODIPY™)

For determination of lipid-peroxidation 24 well plates were used. Neuronal cell lines were seeded at a density of 50,000 cells per well and HepG2 cells were seeded at a density of 60,000 cells per well. After the indicated treatments, HT22, mHypo and HepG2 cells were stained with BODIPY™ 581/591 C11 (Invitrogen, USA) for 1 h (37°C, 4.5% CO_2) and harvested for FACS analysis. Lipid-peroxidation was analyzed by recording green (excitation: 525nm/30) and red (emission: 690nm/50) fluorescence with 488 nm excitation wavelength of at least 5'000 cells of at least three replicates per condition. Upon oxidation of BODIPY, lipid-peroxidation was analyzed by recording a shift from red to green fluorescence.

3.6.3. Mitochondrial ROS formation (MitoSOX™)

For seeding 24 well plates were used. Neuronal cell lines were seeded at a density of 40,000 cells per well and liver cell lines were seeded at a density of 50,000 cells per well. 15 µg of mitochondrial protein was used per treatment condition for the experiments with isolated mitochondria. MitoSOX™ red (Invitrogen, USA) is selectively targeted to the mitochondria, where it is oxidized by superoxides exhibiting red fluorescence. For detection of mitochondrial ROS formation, MitoSOX™ red was applied for 30 min at 37°C and cells were harvested for FACS analysis. For analysis of isolated mitochondria MitoSOX™ red was added to 15 µg/ 500 µL mitochondrial suspension and incubated on ice for 30 min. Increasing red fluorescence correlates with the formation of mitochondrial ROS and was detected by FACS analysis (excitation 488 nm, emission 690/50 nm) as described previously [147]. Data were collected from at least 5'000 cells and three replicates per condition.

3.6.4. Mitochondrial membrane potential (TMRE™)

For seeding 24 well plates were used. Neuronal cell lines were seeded at a density of 40,000 cells per well and HepG2 cells were seeded at a density of 50,000 cells per well. After the indicated treatment, cells were stained with TMRE™ (0.4 nM for 30 min at 37°C, MitoPT ΔΨm Kit, Immunochemistry Technologies, USA) and harvested for TMRE fluorescence measurement via FACS analysis. Upon loss of the mitochondrial membrane integrity and, thus, membrane potential, loss of TMRE fluorescence was

detected by FACS analysis (excitation 488 nm, emission 690/50 nm) [147]. Data were collected from at least 5’000 cells and three wells per condition.

3.6.5. Glucose uptake (2-NBDG)

2-NBDG (2-deoxy-2-[(7-nitro-2,1,3-benzoxadiazol-4-yl)amino]-D-glucose) (Table 8) (excitation: 475 nm emission: 550 nm) was used to assess glucose uptake via flow cytometry according to published protocols with minor modifications [148]. In brief, HT22 cells were treated with Ze 450 and metformin for 16 h and with insulin for 30 min. Afterwards, cells were washed three times with DMEM (D5030, Merck KgaA, Germany) without glucose and FCS. 10 µM 2-NBDG was added and incubated 1 h protected from light at 37°C and 5% CO_2. After the incubation, cells were harvested via trypsinization and centrifugation including a washing step. Trypsinization was stopped using medium containing 10% FCS. Next, samples were collected in 1.5 mL tubes on ice, stained with propidium iodide for detection of dead cells and measured within 30 min by using 525 ± 30 nm bandpass filter to detect 2-NBDG fluorescence intensity and a 690 ± 50 nm bandpass filter to detect dead cells. Data were collected from at least 5’000 cells with at least three replicates per condition.

3.8. Impedance measurement

Cell proliferation was analyzed in real-time by measuring electrical impedance via the xCELLigence system Real-Time Cell Analyzer [149]. First, the background of the 96-well E plate is determined with pure culture medium. Afterwards, cells were seeded at 6,000 HT22 cells/well. Impedance is measured via gold electrodes on the bottom of the wells due to changes in electrical impedance and visualized as changes in cell index. After adding the treatment cell proliferation was monitored for 16- 24 h. Impedance is increasing by attached and proliferating cells, whereas the detachment of dying cells leads to a decrease in electrical impedance. Cell index was normalized to 1.0 before treatment was added for data analysis and comparability between treatment groups. Data are presented as mean ± SD.

3.9. Glutathione assay

To determine GSH (glutathione) levels, HT22 cells seeded in 6-well plates (180,000 cells/well). After treatment with Ze 450 and erastin for the indicated amount of time two to three wells per condition were harvested by scratching and rinsing with PBS on ice, followed by centrifugation at 1,000 rpm for three minutes. After a washing step with PBS and another centrifugation, the cell pellet was frozen and stored at -80°C. GSH measurements were performed using the Glutathione Assay Kit (Cayman Chemical Company, USA) following manufacturer's protocol. Therefore, the cells were thawed on ice, resuspended in 100 µL MES-buffer (Table 11), and homogenized by sonification. Insoluble fragments were removed by centrifugation at 10,000×g for 15 min at 4°C. 80 µL of metaphosphoric acid (MPA,1.25 M) was added to 80 µL of the supernatant. The remaining part of the supernatant was used for protein determination via BCA assay. After incubation for 5 min, the mixture was centrifuged at 17,000×g for 10 min at 4°C. To increase the pH, 100 µL of the supernatant was mixed with a 4 M solution of triethanolamine. After transferal of 50 µL of each sample and a GSH standard into a 96-well plate, 150 µL of assay cocktail provided MES-buffer, co-factor mixture (NADP+ and glucose-6-phosphate), enzyme mixture (glutathione reductase and glucose-6-phosphate dehydrogenase) and Ellman's reagent (DTNB; (5,5-dithio-bis-(2-nitrobenzoic acid)) was added. Absorbance was measured at 405 nm after 30 min of incubation at RT using the ELx808 Ultra Microplate Reader (Bio-Tek, Germany). Total GSH amount was determined via standard curve calculation and normalized to protein content. Data are displayed as percent GSH of control.

Table 11. MES buffer (pH 6.0)

M 2-(N-mopholino)ethanesulphonic acid (MES)	0.4 M
Phosphate	0.1 M
EDTA	2 mM

3.10. Microscopy

3.9.1. Mitochondrial morphology

MitoTracker® Deep Red FM (Invitrogen, Germany, 200 nM) was used to visualize changes in mitochondrial morphology. HT22 cells were seeded in 8-well ibidi slides (Ibidi GmbH, Germany) with 14,000 cells per well and treated with Ze 450 and erastin or glutamate. After 16 h of treatment 0.2 µM MitoTracker® Deep Red was added to cells and incubated for 30 min at 37°C. Cells were fixed with 4% formaldehyde for 20 min at RT. Mitochondrial morphology was analyzed by categorizing cells as previously described with minor modifications [63]. Category I mitochondria were organized in a tubular network, category II mitochondria were fragmented but equally distributed throughout the cytosol, whereas category III mitochondria were fully fragmented and surrounding the nucleus. At least 500 cells per condition were counted without knowledge of treatment history. Images were acquired using a Leica DMI6000 (fluorescence microscope at 63x magnification, Leica Microsystems, Germany).

3.9.2. Glucose uptake via confocal microscopy

HT22 cells were seeded at 14,000 cells per well in 8-well ibidi slides (Ibidi GmbH, Germany) and grown for about 30-33 hours. Then, cells were treated with 100 µg/mL Ze 450 for 16 h. Afterwards, cells were washed three times with DMEM without glucose. 10 µM 2-NBDG was added to half of the samples, the remaining wells were not stained and used later on for background measurements. After incubation for 1 h protected from light at 37°C and 5% CO_2 cells were washed two times with cold PBS and fixed with 4% formaldehyde for 20 min at RT. Samples were stained with 4',6-diamidino-2-phenylindol (DAPI,1:1000 in PBS) and phalloidin555 (Thermo Fisher Scientific, Germany; 1:400) for 10 min at RT. Images were obtained using an LSM 700 confocal microscope with a 63x, 1.4 NA oil objective (Zeiss, Germany). Sections of approximately 200 µm in width and length were chosen with an average number of 20 cells per section. Fluorescent microscopy pictures of the cells were captured with the following laser settings: 405 nm for DAPI, 488 nm for 2-NBDG and 555 nm for phalloidin-Alexa555. Two out of six Z-stacks (center planes; best DAPI fluorescence) were processed to maximum intensity projections using FIJI (National Institute of Health, USA). For quantification, brightness and contrast of each channel were adjusted to equal histogram settings. Phalloidin555 signal was used to select ROIs surrounding the cell groups (to avoid background errors)

and 2-NBDG fluorescence intensity was measured for corresponding areas. Values were normalized to corresponding background values within the individual experiments.

3.11. Seahorse

3.10.1. Cellular analysis of mitochondrial respiration and glycolysis

To assess oxygen consumption rate (OCR) and extracellular acidification rate (ECAR) as measures of mitochondrial respiration and glycolysis, respectively, simultaneous real-time measurements were performed using the XF Extracellular Flux Analyzer (Agilent Technologies, USA) as previously described [59]. Briefly, HT22 and HepG2 cells were plated in XF96-well microplates (6'000/10,000 cells per well, Seahorse Bioscience) without seeding into the corner wells (background determination) and treated with the indicated compounds or extracts. After 16 h of treatment, the growth medium was replaced by ~180 µl of assay medium (containing 143 mM NaCl, 4.5 g/l glucose, 2 mM glutamine, 1 mM pyruvate, pH 7.35) and cells were incubated at 37°C for 60 min. Three to six baseline measurements were recorded before adding the compounds. Oligomycin (ATP synthase inhibitor) (Merck KGaA, Germany) was injected into port A (20 µL) at a final concentration of 3 µM (HT22 cells) or 2 µM (HepG2 cells), FCCP (uncoupling agent) (22.5 µL into port B) (Merck KGaA, Germany) at a concentration of 0.5 µM (HT22 cells) or 0.8 µM (HepG2 cells), rotenone/antimycin A (complex I/III inhibitors) (25 µL into port C) (Merck KGaA, Germany) at a concentration of 100 nM and 1 µM (HT22 and HepG2 cells) and 2-deoxyglucose (Carl Roth GmbH, Germany) (glycolysis inhibitor) at a concentration of 50 mM (HT22 and HepG2 cells) (27.5 µL into port D), respectively. Three measurements were performed after the addition of each compound (4 min mixing followed by 3 min detection). Data analysis was performed using XFe Wave software and visualized using GraphPad Prism software.

3.10.2. Analysis of mitochondrial respiration of isolated mitochondria

Electron flow assay

Electron flow assay was used to analyze the activity of mitochondrial complex I measuring the OCR with a Seahorse XFe96 Analyzer. To this end, mitochondrial isolation was performed as described before (Chapter 3.3.). 10 µg of cortical or liver mitochondrial protein per well were resuspended in 25 µL/well of mitochondrial assay

solution (Table 12, MAS) supplemented with pyruvate (10 mM) and malate (2 mM). Subsequently, the plate was centrifuged at 2,000 x g for 20 min at 4°C (Heraeus Megafuge 40R, ThermoFisher Scientific, Germany) to ensure adherence of the mitochondria to the bottom. Afterwards, 155 µL/well MAS with 4 µM FCCP was added to the final volume of 180 µL/well. Rotenone, succinate and antimycin A were diluted in MAS without sucrose and mannitol, while ascorbate and TMPD was diluted in MAS containing sucrose and mannitol, and serially injected as follows: 2 µM rotenone (port A), 10 mM succinate (port B), 4 µM antimycin A (port C), 10 mM/100 µM ascorbate and TMPD (N1,N1,N1,N1-tetramethyl-1,4-phenylene diamine) (port D). For investigating complex IV driven respiration, 1.0 M ascorbate in H_2O (pH 7.2) and 10 mM TMPD in H_2O (pH 7.2) was mixed with an equimolar concentration (10 mM) ascorbate to ensure TMPD remains reduced. Up to three baseline measurements were recorded and up to three measurements were performed after each injection (3 min mixing followed by 3 min detection). Data analysis and visualization were performed using XFe Wave software and GraphPad Prism software displayed as point-to-point oxygen consumption rates.

Table 12. Mitochondrial assay solution (MAS, pH 7.2)

Sucrose	70 mM
Mannitol	220 mM
KH_2PO_4	10 mM
$MgCl_2$	5 mM
HEPES	2 mM
EGTA	1 mM
Fatty acid free BSA	0.2 % (w/v)

Coupling assay

The coupling assay was used to measure the activity of mitochondrial complex II and III recording the OCR with a Seahorse XFe96 Analyzer. The coupling assay was realized as previously described with minor modifications [150]. In brief, mitochondria were isolated like described before (Chapter 3.3.). 10 µg of cortical and 12 µg of liver mitochondrial protein per well were re-suspended in MAS (Table 12) with the addition of the complex II substrate succinate (10 mM) and the complex I inhibitor rotenone (2 µM). Subsequently, the plate was centrifuged at 2,000 xg for 20 minutes at 4°C (Heraeus Megafuge 40R, ThermoFisher Scientific, Germany) to ensure adherence of the mitochondria to the bottom of the well. Afterwards, 155 µL/well MAS was added to the

final volume of 180 µL/well. Modulators of the respiratory chain were diluted in MAS without sucrose and mannitol and serially injected as follows: 4 mM ADP (port A), 2.5 µg/mL oligomycin (port B), 4 µM FCCP (port C), 4 µM antimycin A (port D). Up to three baseline measurements were recorded and up to three measurements were performed after each injection (3 min mixing followed by 3 min detection). Data analysis and visualization was performed using XFe Wave software and GraphPad Prism software and displayed as point-to-point oxygen consumption rates.

3.12. Rhodamine measurement

Rhodamine measurement was used to assess mitochondrial membrane potential integrity. Therefore fluorescence quenching of rhodamine 123 (ThermoFisher Scientific, Darmstadt, Germany) was measured over 40 min as described previously [151]. Mitochondria were plated in a black 96-well plate with 75 µg mitochondrial protein per well and therefore diluted in a buffer containing 200 mM sucrose, 10 mM MOPS-Tris, 5 mM succinate, 1 mM Pi(H_3PO_4), 10 µM EGTA, and 2 µM rotenone (pH 7.3). Loss of mitochondrial membrane potential was induced by FCCP (500 nM), which was injected at the end of the measurement. Fluorescence (excitation: 485/12 nm, emission: 530/10 nm) was measured with FLUOstar OPTIMA plate reader.

3.13. Protein analysis

HT22 cells were seeded in 6-well plates at a density of 200,000 cells per well. After 24-32 h cells were treated for the indicated amount of time and harvested by scratching in lysis buffer (Table 13) at 4 °C. Liquid nitrogen was used to disrupt cell membranes; afterwards, the lysate was stored at -80 °C or thawed on ice and centrifuged for 15 min at 10,000 rpm at 4 °C. Protein lysate was used from the resulting supernatant and a BCA was performed according to the manufacturer's protocol for the determination of protein content. Therefore, 2.5 µL of the respective protein sample was mixed with 97.5 µL of BCA mix (1:50 reagent A: reagent B) and shaken at 60°C for 30 min. Absorbance was measured at 560 nm (FLUOstar OPTIMA, BMG Labtech, Germany) and the respective protein amount was calculated using a protein standard curve of bovine serum albumin (BSA).

40-80 µg protein in loading buffer (Table 22) was loaded on a 7.5-12.5% polyacrylamide gel (Table 19-21) and a 3.5% stacking gel was used (Table 18). Spectra Multicolor High

Range Protein Ladder or PageRuler Prestained Protein Ladder (ThermoFisher Scientific, Germany) were used as molecular weight (MW) marker and gel electrophoresis was performed at 60 V for ~30 min, and then switched to 110 V until separation in running buffer (Table 23). After electrophoresis, the proteins were transferred from the gel onto a PVDF membrane (Roche Diagnostics, Germany), which was previously activated by incubation in methanol for 2 min and then transferred in 1x transfer buffer (Table 24). Blotting was performed in a Mini-Trans-Blot Cell tank (Bio-Rad, Germany) for 105-150 min at 350 mA in ice-cold 1x transfer buffer. Afterwards, the membrane was transferred shortly into TBS (Table 25) followed by at least 1 hour incubation in blocking solution (5 % BSA in TBST or 5% milk in TBST, Table 26-28). Next, the primary antibody (Table 29) was incubated at 4°C overnight. Followed by 1 h incubation at room temperature and incubation with the corresponding peroxidase-labeled secondary antibodies (Table 30). Before and after the secondary antibody incubation three x 10 minutes washing steps with TBST (Table 26) were performed. The membrane was incubated with luminol based HRP-Juice Plus (PJK GmbH, Germany) for 2 minutes for protein detection. Visualization was realized with a ChemiDoc XRS system (Bio-Rad, Germany). For densitometric protein analysis, the Bio Rad Image Lab Software was used. For loading control, a housekeeping protein (Actin, GAPDH, Vinculin) was detected in the same way.

Table 13. Lysis buffer for protein analysis

D-Mannitol	0.25 M
Tris	0.05 M
EDTA	1 mM
EGTA	1 mM
100 mM DTT	1:100
Triton® X-100	1:100
PhosSTOP	1 tablet
Complete MiniProtease Inhibitor Cocktail	1 tablet
Bidest. H_2O	Ad 10 mL

Table 14. 1.5 M Tris pH 8.8

Tris-HCl	23.6 g
HCl	q.s.
Bidest. H_2O	ad 100 mL

Table 15. 0.5 M Tris pH 6.8

Tris-HCl	7.88 g
HCl	q.s.
Bidest. H_2O	ad 100 mL

Table 16. 10% sodium dodecyl sulfate (SDS)

SDS	1 g
Bidest. H_2O	ad 10 mL

Table 17. 10% ammonium persulfate (APS)

APS	1 g
Bidest. H_2O	ad 10 mL

Table 18. 3.5 % stacking gel

Acrylamide/bisacrylamide (37.5:1)	0.58 mL
10% SDS	0.05 mL
0.5 M Tris-HCl pH 6.8	1.2 mL
10% APS	0.03 mL
Tetramethylethylenediamine (TEMED)	0.008 mL
Bidest. H_2O	ad 5 mL

Table 19. 6% running gel

Acrylamide/bisacrylamide (37.5:1) 30%	2 mL
10% SDS	0.1 mL
1.5 M Tris-HCl pH 8.8	2.5 mL
10% APS	0.0625 mL
Tetramethylethylenediamine (TEMED)	0.0125 mL
Bidest. H_2O	ad 10 mL

Table 20. 10% running gel

Acrylamide/bisacrylamide (37.5:1) 30%	3.34 mL
10% SDS	0.1 mL
1.5 M Tris-HCl pH 8.8	2.5 mL
10% APS	0.0625 mL
Tetramethylethylenediamine (TEMED)	0.0125 mL
Bidest. H_2O	ad 10 mL

Table 21. 12.5% running gel

Acrylamide/bisacrylamide (37.5:1) 30%	4.17 mL
10% SDS	0.1 mL
1.5 M Tris-HCl pH 8.8	2.5 mL
10% APS	0.0625 mL
Tetramethylethylenediamine (TEMED)	0.0125 mL
Bidest. H_2O	ad 10 mL

Table 22. Loading buffer for protein analysis (5x SDS sample buffer)

1.5 M Tris-HCl pH 6.8	2 mL
Glycerol	5 mL
SDS	1 g
β-Mercaptoethanol	2.5 mL
1% Bromophenol blue	0.5 mL

Table 23. 10x running buffer for SDS PAGE (dilution 1:10 with H_2O)

Tris base	30 g
SDS	10 g
Glycine	144 g
Bidest. H_2O	ad 1000 mL

Table 24. 10x transfer buffer for blotting (dilution 1:10 with H_2O and 20% methanol)

Tris base	30 g
Glycine	144 g
HCl	q.s. (pH 8.3)
Bidest. H_2O	ad 1000 mL

Table 25. 10x TBS pH 7.5 (dilution 1:10 with H_2O)

NaCl	292 g
Tris base	24.2 g
HCl	q.s. (pH 7.5)
Bidest. H_2O	ad 1000 mL

Table 26. 1x TBST

10x TBS	100 mL
Tween® 20	0.05 mL
Bidest. H_2O	ad 1000 mL

Table 27. 5% Blocking milk

Skim milk powder	5 g
TBST	ad 100 mL

Table 28. 5% BSA

BSA	5 g
TBST	ad 100 mL

Antibodies were used as listed: ***Table 29. Primary antibodies***

Primary Antibody	Company	Host	Dilution
Akt	Cell signaling, USA	Rabbit	1:1000 in 5% milk
Catalase	Santa Cruz, USA	Mouse	1:1000 in 5% milk
cmyc	Cell signaling, USA	Rabbit	1:1000 in 5% milk
CuZnSOD	Santa Cruz, USA	Mouse	1:1000 in 5% milk
HIF1α	Cell signaling, USA	Rabbit	1:1000 in 5% milk
HXKII	Cell signaling, USA	Rabbit	1:1000 in 5% milk
LDHA	Cell signaling, USA	Rabbit	1:1000 in 5% milk
mitoProfile® OXPHOS	Abcam, USA	Mouse	1: 250 in 5% milk
MnSOD	Sigma Aldrich, USA	Rabbit	1:500 in 5% milk
mTOR	Cell signaling, USA	Rabbit	1:500 in 5% BSA
pAkt	Cell signaling, USA	Rabbit	1:1000 in 5% milk
PDK1	Enzo Life Science, USA	Rabbit	1:1000 in 5% milk
pmTOR	Cell signaling, USA	Rabbit	1:1000 in 5% milk
Actin	Novus Biologicals, USA	Mouse	1:2000 in 5% milk
GAPDH	Cell signaling, USA	Rabbit	1:50,000 in 5% milk
Vinculin	Sigma-Aldrich, Germany	Mouse	1:10,000 in 5% milk

Table 30. Secondary antibodies

Secondary Antibody	Company	Host	Dilution
HRP-anti-mouse	Vector Laboratories, Inc., USA	Mouse	1:2000 in 5% milk
HRP-anti-rabbit	Vector Laboratories, Inc., USA	Mouse	1.3000 in 5% milk

3.14. RNA analysis

Reverse transcription PCR was performed after isolation of mRNA. To this end, HT22 cells were plated into 6 well plates with 200,000 cells per well. After treatment, cells were harvested and RNA was isolated using the InviTrap Spin Universal RNA Mini Kit (Stratec Biomedical, Germany). RNA isolation was performed according to the manufacturer's protocol. Eluted RNA was placed on ice and directly used or stored at - 80°C until the day of analysis. RNA content was determined using the NanoPhotometer™ (Implen, Germany) an absorbance ratio (260/280 nm) of ~2.0 was accepted as pure RNA. Reverse transcription PCR (RT PCR)was performed (Table 33) using SuperScript III One-Step RT-PCR system with platinum Taq DNA polymerase (Thermo Fisher Scientific, Germany) and the following primer (Table 34).

Table 31. 10x Loading dye for agarose gel

Tris base	60.57 mg
40% Glycerol	20 mL
EDTA	186.2 mg
0.25% Orange G	125 mg
Bidest. H_2O	ad 50 mL

Table 32. 50x TAE

Tris base	242 mg
Acetic acid	57.1 mL
0.5 M EDTA pH 8.0	10 mL

Table 33. RT PCR

2x reaction buffer	12.5 µL
RNA sample	500 ng
Primer fwd.	0.5 µL
Primer rev.	0.5 µL
Superscript III enzyme	0.5 µL
Nuclease free water	ad 25 µL

Table 34. Primer

Primer	Sequence (5´to 3´)	Amplicon size
cmyc fwd.	GCTCGCCCAAATCCTGTACCTCGTCCGAT	237 bp
cmyc rev.	GAGATGAGCCCGACTCCGACCTCTT	
Glut1 fwd.	CAGTTCGGCTATAACACTGGTG	156 bp
Glut1 rev.	GCCCCCGACAGAGAAGATG	
Glut4 fwd.	GGACCGGATTCCATCCCAC	120 bp
Glut4 rev.	TCCCAACCATTGAGAAATGATGC	
Raptor fwd.	TCAAATTCCATCCCTTTACACC	217 bp
Raptor rev.	TCAGCAAAATTCTTCCAGACC	
GAPDH fwd.	CGTCTTCACCACCATGGAGAAGGC	399 bp
GAPDH rev.	AAGGCCATGCCAGTGAGCTTCCC	

mRNA was transcribed into DNA and then amplified using the following programs:

Table 35. cmyc

cmyc		cycles
55°C	30 min	
95°C	2 min	
95°C	45 sec	30
61°C	45 sec	
70°C	1 min	
70°C	5 min	
4°C	∞	

Table 36. Glut1

Glut1		cycles
55°C	30 min	
95°C	2 min	
95°C	30 sec	30
60°C	30 sec	
70°C	1 min	
70°C	10 min	
4°C	∞	

Table 37. Glut4

Glut4		**cycles**
55°C	30 min	
95°C	2 min	
95°C	30 sec	35
58°C	30 sec	
70°C	1 min	
70°C	10 min	
4°C	∞	

Table 38. Raptor

Raptor		**cycles**
55°C	30 min	
95°C	2 min	
95°C	45 sec	27
50.5°C	45 sec	
70°C	1 min	
70°C	10 min	
4°C	∞	

Table 39. GAPDH

GAPDH		**cycles**
55°C	30 min	
95°C	2 min	
95°C	30 sec	27
60°C	30 sec	
70°C	1 min	
70°C	10 min	
4°C	∞	

After amplification, the samples were loaded mixed with a 10x loading dye (Table 31) on a 1.5% agarose gel (Biozym Scientific GmbH, Germany) stained with ethidium bromide. Electrophoresis was performed at 80 V for 20-35 min in TAE buffer (Table 32). GeneRuler 100 bp Plus DNA Ladder (ThermoFisher Scientific, Germany) was used as

a size standard. For visualization of the resulting DNA bands, UV light of the ChemiDoc XRS system (Bio-Rad, Germany) was used.

3.15. Caenorhabditis elegans

The experimental procedures including *C. elegans* were conducted in collaboration with the group of Gunter Eckert at the Institute of Nutritional Sciences, Justus-Liebig University Giessen (Giessen, Germany). Benjamin Dilberger performed the cultivation and the experimental procedures with *C. elegans*.

3.15.1. Nematode and bacterial strain

C. elegans wild-type strain N2 was obtained from the *Caenorhabditis elegans* Genetics Center (University of Minnesota, MN, US). Nematodes were maintained on nematode growth medium (NGM) agar plates seeded with E. coli OP50 at 20°C according to standard protocols [152]. For all experiments, synchronous populations were generated through a standard bleaching protocol [153]

Preparation of NGM agar plates

3 g NaCl, 2.5 g Bactopeptone (Difco) and 17 g Bacto-agar (Difco) were dissolved in 975 mL distilled water. After autoclaving, 1 mL cholesterol in ethanol (5 mg/mL), 1 mL 1 M $CaCl_2$, 1 mL 1 M $MgSO_4$, and 25 mL 1 M potassium phosphate buffer (pH 6.0) (108.3 g KH_2PO4, 35.6 g K_2HPO_4, H_2O to 1 L) are added in order.

3.15.2. Cultivation and treatment

Synchronous larvae were washed twice in M9 buffer (6 g Na_2HPO_4, 3 g KH_2PO_4, 5 g NaCl and 0.2 g $MgSO_4$ x 7 H_2O per L), counted and adjusted to 10 larvae per 10 µL. Nematodes were cultivated in cell culture flasks (Sarstedt, Germany) or OP50 spread NGM plates. OP50-NGM was added as a standardized food source with a volume 4.4-fold of the larvae containing M9 solution used. L1 larvae were maintained under shaking at 20°C reaching adulthood within 3 days.

After reaching young adulthood, 48 h prior to the experiment, nematodes were treated with Ze 450 dissolved in EtOH 1% and metformin or paraquat (5 mM) dissolved in M9. Standard OP50, M9, and EtOH 1% served as controls.

3.15.3. Lifespan assay

To determine the lifespan of the nematodes at 20°C a modified protocol from Amrit et. al. was applied [154] and synchronized larvae, obtained from egg preparation as stated above, were raised on NGM agar plates spread with standard OP50 E. coli culture. After completing the L4 larval stage 40 healthy animals per group were transferred to fresh NGM E. coli containing plates with a sterilized platinum wire. Effectors were incorporated into the OP50 culture with the concentration as needed. Nematodes were transferred to new plates every two days to distinguish between offspring until egg-laying stopped. In line with the separation from eggs and larvae, nematodes were checked for vital signs using a hot platinum wire held next to the animal´s heads. Worms showing no reaction to the heat stimulus were considered dead. The lifespan curves were statistically compared using the log-rank test.

3.15.4. Heat-shock survival assay

Approximately 10 nematodes were raised per well in a 96-well microplate as mentioned above. After 48 h of incubation with effectors, time till death was determined using a microplate thermo-tolerance assay [155]. In brief, nematodes were washed off the wells with M9-buffer into 15 mL tubes followed by three additional washing steps. Each well of a black 384-well low-volume microtiter plate (Greiner Bio-One, Germany) was prefilled with 6.5 µL M9-buffer/Tween® 20 (1% v/v). Subsequently, one nematode was immersed in 1 µL M9 buffer under a stereomicroscope (Breukhoven Microscope Systems, Netherlands). A volume of 7.5 µL SYTOX™ green (final concentration 1 µM; Life Technologies, Germany), which penetrates only into cells with compromised plasma membrane and gets fluorescent after binding to DNA, was added for fluorescent detection. To prevent water evaporation, the plates were sealed with a Rotilab sealing film (Greiner Bio-One, Germany). Heat shock (37°C) was applied and fluorescence measured with a ClarioStar plate reader (BMG, Germany) every 30 min over the course of 17 hours. The excitation wavelength was set at 485 nm and the emission was detected at 538 nm.

3.15.5. Chemotaxis assay

Chemotaxis was assessed using a previously published method [156]. Briefly, agar plates were divided into four quadrants. Sodium azide (0.5 M) was mixed in same parts with ethanol (95%) as control, or diacetyl (0.5%) as attractant. 2 µL of either control or attractant solution was added to the center of two opposite quadrants with the same distance to the middle of the plate. Nematodes were washed and separated from larvae as stated above and a number of approximately 150 animals placed in the center of the plates. After 1 h each quadrant was counted and a chemotaxis index calculated ((number of attractant – number of control) / number total).

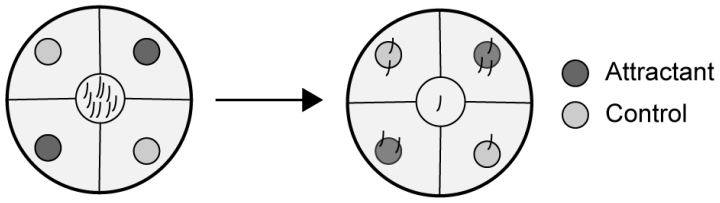

Figure 9. Chemotaxis assay

Principle of the chemotaxis assay

3.16. Statistical analysis

For statistical analysis of two treatment groups, the unpaired t-test was used. Statistical comparison between more than two treatment groups was performed by analysis of variance (two-way ANOVA) followed by Scheffé's post hoc test and a p-value < 0.05 was considered to be statistically significant. Calculations were executed with Winstat standard statistical software (R. Fitch Software, Germany) and data visualization was performed using GraphPad Prism software (GraphPad Software, USA).

For statistical analysis of the survival curves, the log-rank test (Mantel-Cox test) was employed compared to the corresponding control. A p-value lower than 0.05 was considered to be a significant difference between two survival curves (***p<0.001; **p<0.01; *p<0.05).

For statistical analysis of the chemotaxis assay, one-way ANOVA with post hoc Turkey HSD test was used. A p-value lower than 0.05 was considered to be a significant difference between two survival curves (***p<0.001; **p<0.01; *p<0.05).

4. Results

4.1. Effects of Ze 450 on neuronal cells

4.1.1. Ze 450 prevents neuronal cell death in model systems of oxidative stress

In order to study the impact of Ze 450 on neuronal cells, metabolic activity and cell death were investigated. The HT22 cells were treated with Ze 450 (1-200 µg/mL) for 16 h and oxidative stress was induced via co-treatment with erastin. Ze 450 reduced metabolic activity in a concentration-dependent manner under control conditions to ~60% at concentrations of 100-200 µg/mL but also significantly prevented erastin-mediated decrease of metabolic activity at these concentrations (Figure 10A). Analyzing cell death via Annexin V and PI staining revealed that Ze 450 did not affect cell viability under control conditions, but significantly protected erastin-induced cellular damage at concentrations of 50-200 µg/mL (Figure 10B). In neuronal mHypo cells, metabolic activity was not affected in the controls (Figure 10C), but similar protective effects of Ze 450 were observed in the co-treatment with erastin resulting in a protection of metabolic activity as well as cell death (Figure 10C, D).

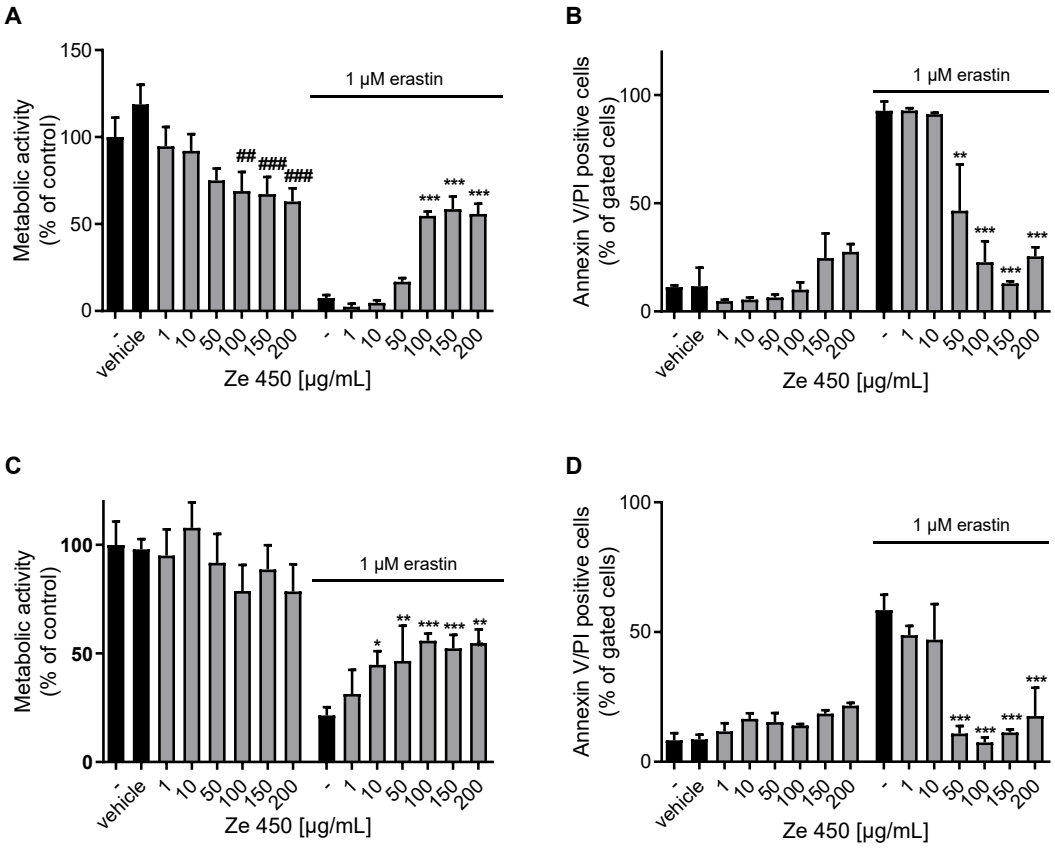

Figure 10. Effects of Ze 450 on cell viability in neuronal HT22 and mHypo cells

A: *MTT assay was performed after 16 h of treatment with Ze 450 and erastin in HT22 cells. Eight replicate wells per condition are displayed as mean + SD. The absorbance under control conditions is set as 100%.* ***B:*** *Cell death was assessed by flow cytometry using Annexin V and PI staining after 16 h of treatment in HT22 cells. The bar graph shows one representative experiment with three replicates per sample (mean + SD; 5,000 cells per replicate).* ***C:*** *Metabolic activity was evaluated in erastin-challenged mHypo cells by measuring MTT formazan absorbance (1 µM, 16 h). Eight replicate wells per condition are displayed as mean + SD. The absorbance under control conditions is set as 100%.* ***D****: Annexin V and PI measurement of mHypo cells treated with Ze 450 and erastin for 16 h. The bar graph shows one representative experiment with three replicates per sample (mean + SD; 5,000 cells per replicate).* ***A-D:*** ****p<0.001; **p<0.01, *p<0.05 compared to erastin-treated control; ###p<0.001, ##p<0.01, #p<0.05 compared to untreated control (ANOVA, Scheffé's test).*

Further, Ze 450 was analyzed in paradigms of oxytosis in HT22 cells. Consistently, the same effects were observed after 16 h of treatment with Ze 450 and glutamate investigating metabolic activity and cell death (Figure 11A, B).

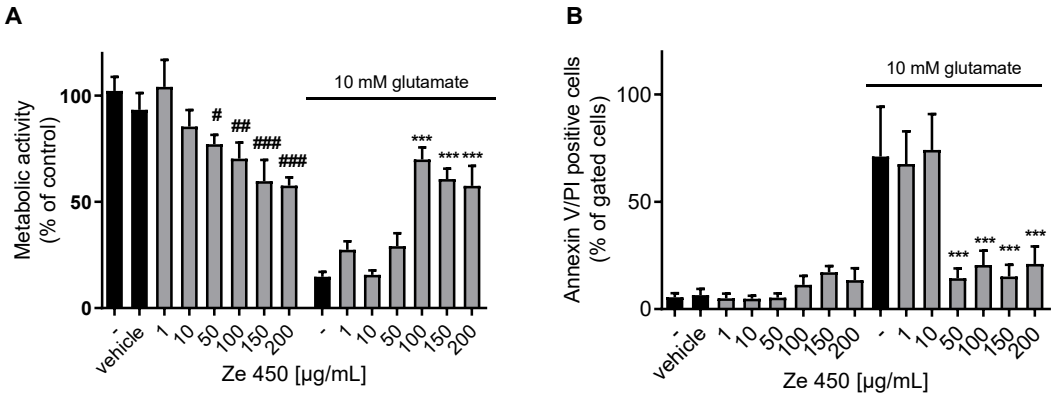

Figure 11. Effects of Ze 450 in paradigms of oxytosis

A: *Metabolic activity was evaluated in glutamate-challenged HT22 cells by measuring MTT formazan absorbance (10 mM, 16 h). Eight replicate wells per condition are displayed as mean + SD. The absorbance under control conditions is set as 100%.* ***B:*** *Cell death was assessed by flow cytometry using Annexin V and PI after 16 h of treatment in HT22 cells. The bar graph shows one representative experiment with three replicates per sample (mean + SD; 5,000 cells per replicate).* ***A, B:*** ****p<0.001 compared to glutamate-treated control; ###p<0.001, ##p<0.01, #p<0.05 compared to untreated control (ANOVA, Scheffé's test).*

Besides the concentration-dependent protection against oxidative stress, Ze 450 was also effective in post-treatment paradigms. The cells were incubated with either erastin or glutamate and Ze 450 was added afterwards at the indicated time points. Ze 450 provided protection even when added up to 6 hours after onset of erastin or glutamate challenge (Figure 12A, B). Interestingly, 100 µg/mL of Ze 450 was protective even 10 h after glutamate exposure (Figure 12B)

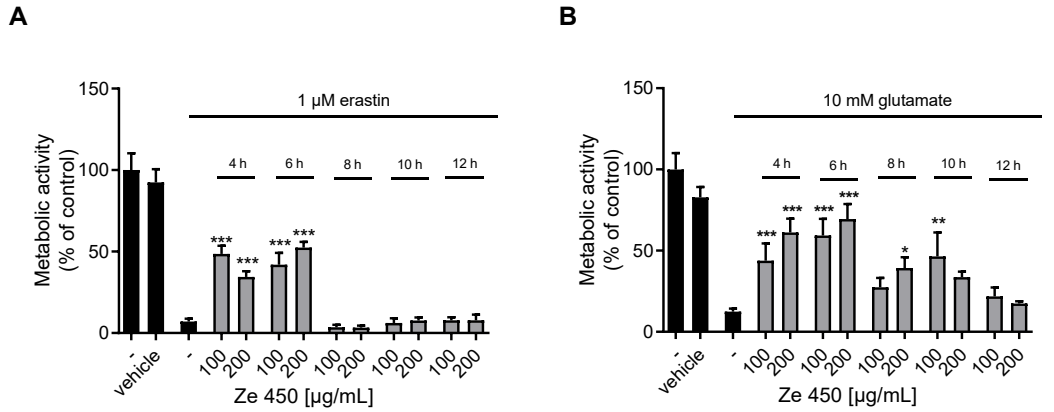

Figure 12. Ze 450 post-treatment

A+B: *Metabolic activity was evaluated in erastin or glutamate-challenged HT22 cells by measuring MTT formazan absorbance (1 µM/10 mM, total incubation of 16 h, pre-treatment with erastin or glutamate 4-12 h). Eight replicate wells per condition are displayed as mean + SD. The absorbance under control conditions is set as 100% (***p<0.001; **p<0.01; *p<0.05 compared to erastin/glutamate-treated control; ANOVA, Scheffé's test).*

In addition, the effects of Ze 450 on glutamate-mediated excitotoxicity were assessed in primary cortical rat and mouse neurons via MTT assay. Ze 450 protected against excitotoxicity in primary cortical rat and mouse neurons after early and late time points (Figure 13A-D). 50 µg/mL Ze 450 was able to protect against glutamate-mediated (20 µM, 8 h, 24 h, 48 h) reduction of metabolic activity in primary cortical neurons. Besides, ATP levels were investigated in primary cortical mouse neurons. Glutamate-mediated ATP depletion was prevented by 50 µg/mL of Ze 450, while basal ATP levels were not affected by Ze 450 (Figure 13E).

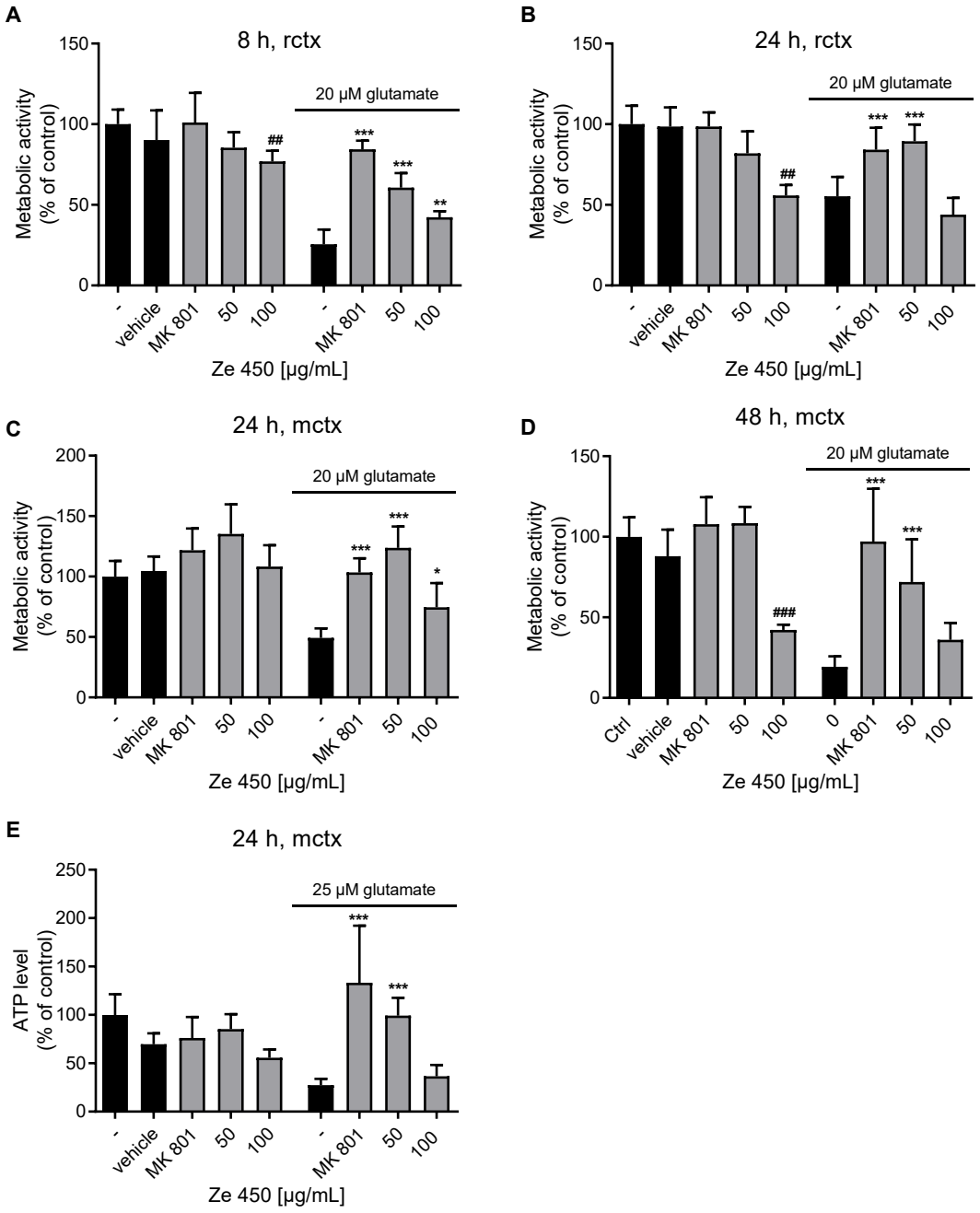

Figure 13. Effects of Ze 450 on primary cortical neurons

A-D: *Metabolic activity was evaluated in glutamate-challenged primary cortical cells (**A+B**: rat, **C+D**: mouse) by measuring MTT formazan absorbance (20 µM, timepoint as indicated). Six-eight replicate wells per condition are displayed as mean + SD. The absorbance under control conditions is set as 100%.* ***E:*** *ATP levels were assessed using a luciferase-based assay in glutamate-exposed (20 µM) primary cortical mouse neurons. Values from eight replicate wells per condition are displayed as mean + SD. The luminescence under control conditions is set as 100%.* ***A-E:*** *##p<0.01, ###p<0.001 compared to untreated control; *p<0.05, **p<0.01, ***p<0.001 compared to glutamate treated primary cortical cells; ANOVA Scheffé's test (rctx: rat cortical neurons; mctx: mouse cortical neurons).*

Further, real-time impedance measurements showed that proliferation of HT22 cells was reduced at Ze 450 concentrations greater than 100 µg/mL compared to the control condition (Figure 14A). These real-time measurements revealed that 10 and 50 µg/mL of Ze 450 conducted to a transient protection against erastin-toxicity, while at concentrations higher than 100 µg/mL, Ze 450 mediated a permanent protective effect (Figure 14B). These results were confirmed in mHypo cells (Figure 14C, D) and in paradigms of oxytosis in HT22 cells (Figure 14E). The impairment of proliferation was reversible after the withdrawal of Ze 450 (Figure 14F).

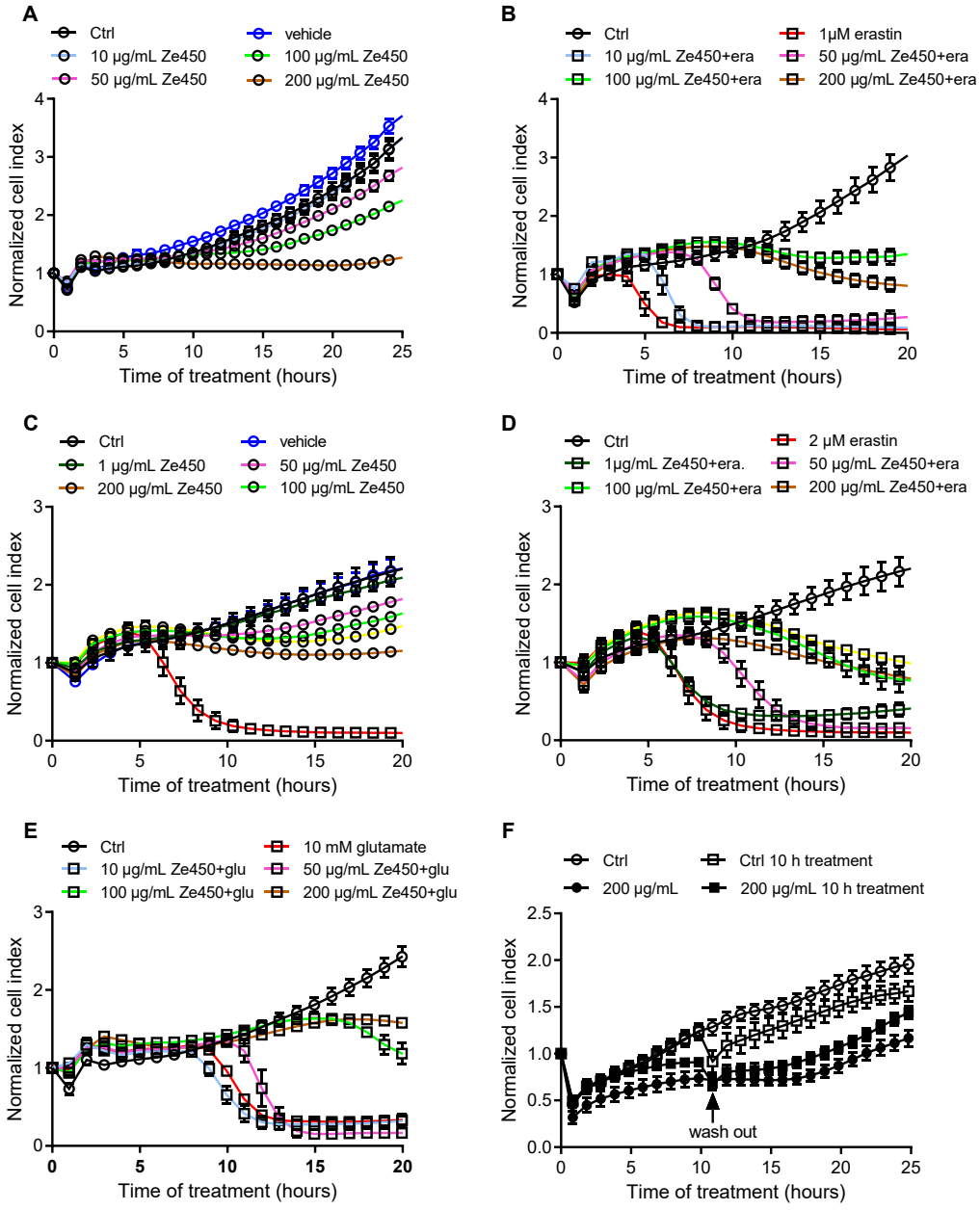

Figure 14. Influence of Ze 450 on proliferation in HT22 and mHypo cells

xCELLigence measurements were conducted after the indicated treatment was added. ***A, B, E, F:*** *HT22 cells.* ***C, D****: mHypo cells. Data are displayed as mean ± SD (n=5-8/treatment condition).*

Moreover, the mammalian target of rapamycin (mTOR) was investigated at protein and mRNA levels, as it is a crucial regulator of cell growth [157]. 100 µg/mL Ze 450 reduced mTOR protein level in HT22 cells after 16 h of treatment (Figure 15A, B). The phosphorylation level of mTOR was not affected by Ze 450 (Figure 15C, D). Consequently, reduced mTOR protein levels might contribute to the decreased proliferation of Ze 450 treated cells.

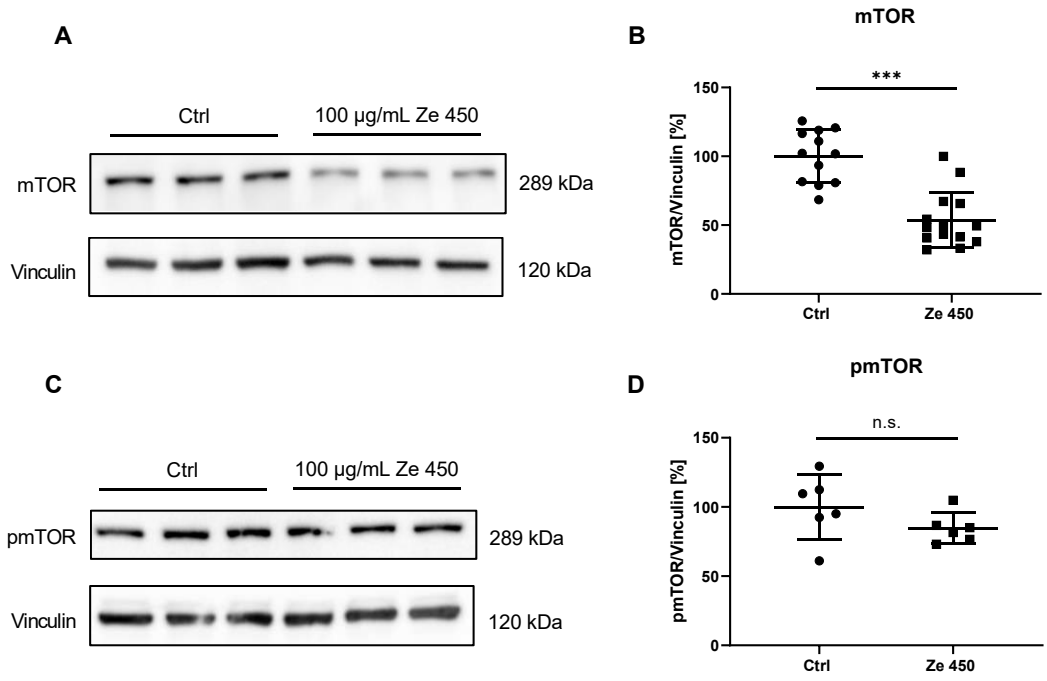

Figure 15. mTOR and pmTOR Western Blot

A: *The representative Western Blot shows a decrease of mTOR protein levels after 16 h of Ze 450 treatment (100 µg/mL) in HT22 cells.* ***B:*** *Quantification of Western Blot as optical density compared to vinculin as loading control (n=12-14 per treatment condition; ***p<0.001 compared to control, unpaired t-test).* ***C:*** *The representative Western Blot shows comparable protein levels of pmTOR in Ze 450 treated (100 µg/mL, 16 h) and control HT22 cells.* ***D:*** *Quantification of Western Blot as optical density compared to vinculin as loading control (n=6/treatment condition).*

Raptor is the regulatory subunit of mTORC1 complex, which is necessary for mTOR activation and downstream signaling [158]. The mRNA analysis of Raptor revealed that Raptor mRNA levels of HT22 cells treated with Ze 450 were not altered (Figure 16A, B).

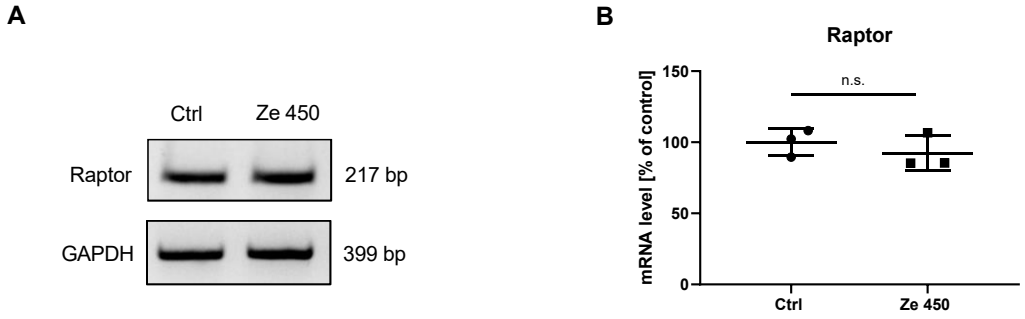

Figure 16. Raptor mRNA level upon 16 h of Ze 450 treatment

A: *Raptor mRNA levels were analyzed after 16 h of treatment with 100 µg/mL Ze 450.* ***B:*** *Quantification of Raptor mRNA levels normalized to GAPDH (n=3/treatment condition, unpaired t-test).*

4.1.2. Ze 450 preserves glutathione level and protects against mitochondrial fragmentation

Oxidative stress-mediated cell death, including oxytosis and ferroptosis, has been linked to depleted glutathione levels, leading to cellular and mitochondrial ROS formation and finally cell death. Ze 450 did not affect glutathione levels and did not rescue erastin-mediated glutathione depletion in HT22 cells (Figure 17A).

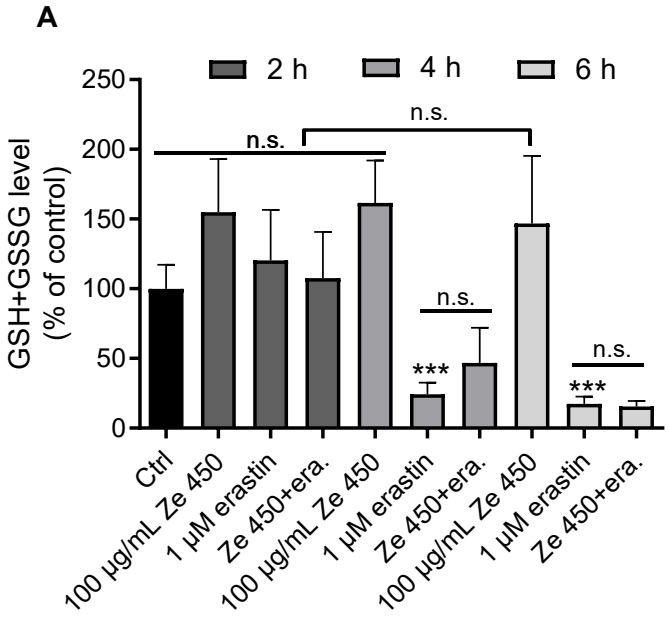

Figure 17. Effects of Ze 450 on glutathione level in HT22 cells

A: *Measurement of cellular glutathione levels depicts a rapid decrease of GSH after 4 h of erastin exposure, which was not restored by Ze 450 (n=5-7/treatment condition). Data are shown as mean + SD (***p<0.001 compared to untreated control; ANOVA, Scheffé's test).*

Further, mitochondrial morphology was analyzed. Mitochondrial shape was evaluated by classifying mitochondria as previously described [64]. Oxidative stress-induced neuronal cell death is accompanied by mitochondrial fragmentation, whereas under standard culture conditions mitochondria build a tubular network throughout the cytosol [64]. Cytotoxicity induced by erastin and glutamate was associated with massive fragmentation of mitochondria and accumulation of the organelles around the nucleus (Figure 18). There was no difference observed between category I-III mitochondria of control and Ze 450 treated cells. In line with this, Ze 450 did not cause mitochondrial fragmentation under standard culture conditions, and the cells showed similar mitochondrial morphology as the control cells (Figure 18). Furthermore, concentrations greater than 50 µg/ml of Ze 450 prevented mitochondrial fragmentation despite erastin or glutamate treatment (Figure18).

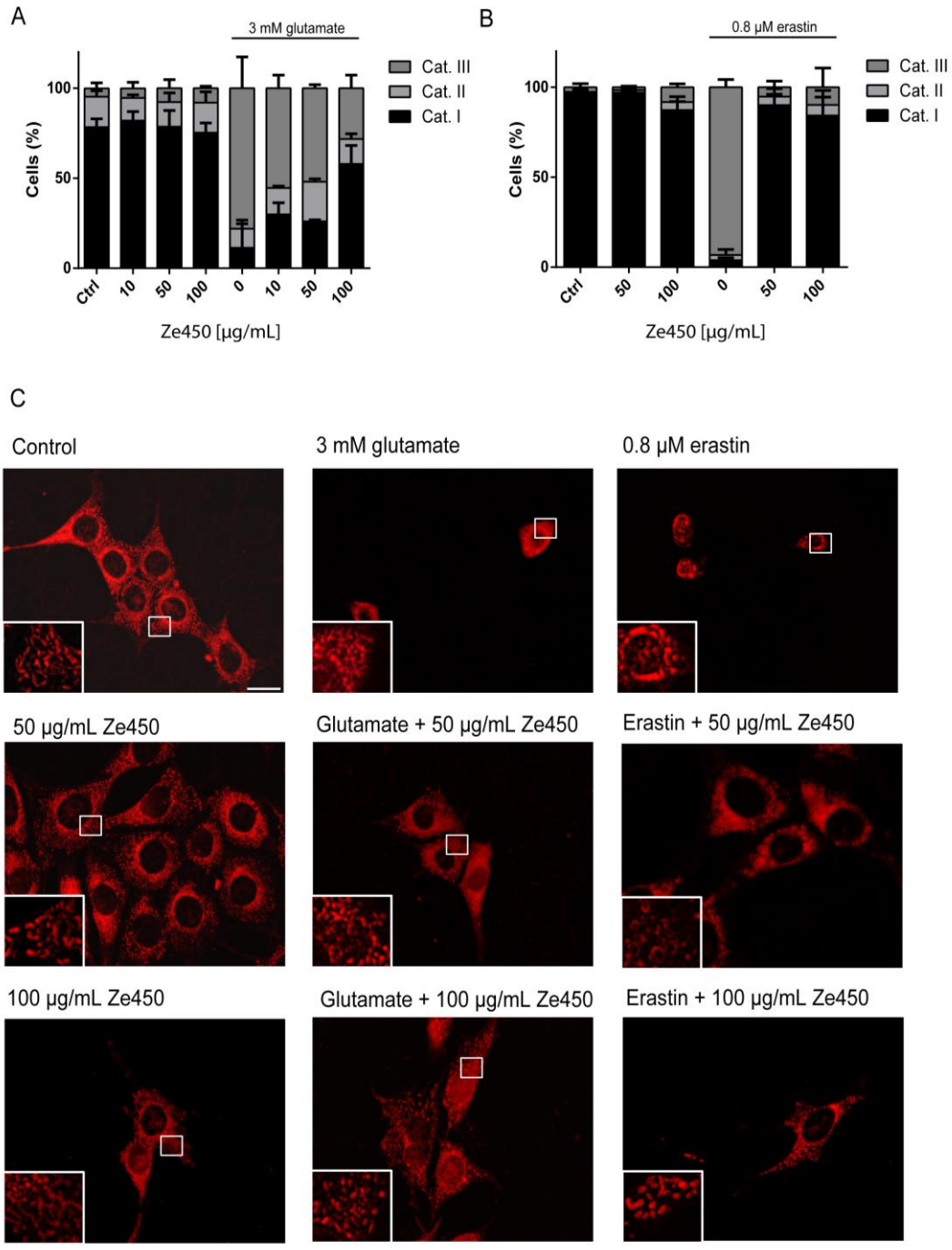

Figure 18. Mitochondrial morphology

A+B: *Quantification of mitochondrial morphology in HT22 cells exposed to Ze 450 and erastin (0.8 µM, 16 h) or glutamate (3 mM, 16 h). Mean values were pooled from three independent experiments, where mitochondrial morphology was determined from at least 500 cells per condition without knowledge of treatment history. All data are given as mean + SD. There were no changes within category II mitochondria in any of the treatment conditions.* ***A:*** *Glutamate exposure led to an increase in category III mitochondria, which was prevented upon 100 µg/mL of Ze 450 ($p<0.001$ compared to glutamate control, ANOVA Scheffé´s test).* ***B:*** *Erastin exposure led to an increase in category III mitochondria, which was prevented by concentrations greater than 50 µg/mL of Ze 450 ($p<0.001$ compared to erastin control, ANOVA Scheffé´s test).* ***C:*** *Representative epifluorescence images were acquired with a fluorescence microscope (DMI6000, Leica, Germany; using 63×1.4 NA oil immersion objective; scale bar 20 µm).*

4.2. Metabolic effects of Ze 450

4.2.1. Ze 450 protects mitochondria from oxidative damage

As demonstrated in the previous chapter, Ze 450 affected metabolic activity and proliferation (4.2.), leading to the question of whether mitochondria are involved in the mechanism of action and if Ze 450 is capable to reduce oxidative damage induced by erastin or glutamate at the level of mitochondria. Therefore, lipid-peroxidation was investigated, since this is an early event in the model system of glutamate- and erastin-induced oxidative cell death. Cellular ROS formation, through increased activity of 12/15 lipoxygenases was investigated using C11-BODIPY FACS analysis at 8 h and 16 h of treatment in HT22 and mHypo cells (Figure 19). Ze 450 did not increase cellular ROS formation but abolished erastin-mediated increase in lipid-peroxidation at concentrations higher than 50 µg/mL as detected at both time points in HT22 cells (Figure 19A, B). The same effect was observed in HT22 cells challenged with glutamate (Figure 19C). Consistently, these results were confirmed in mHypo cells (Figure 19D).

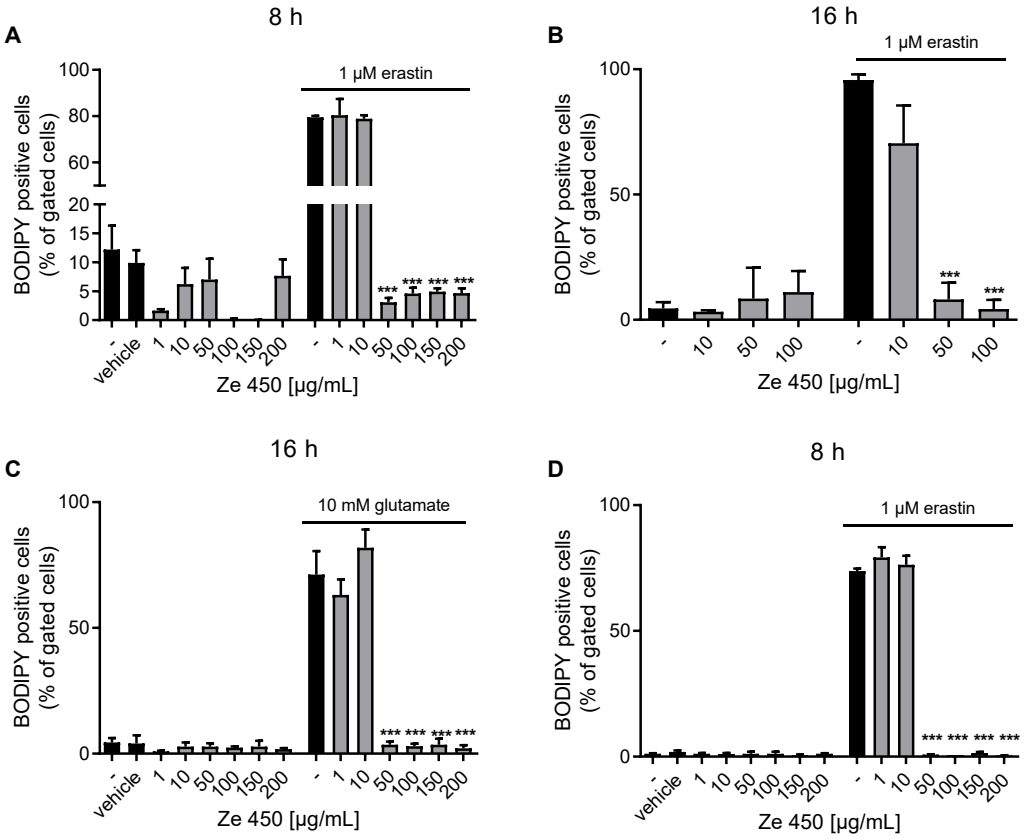

Figure 19. Effects of Ze 450 on lipid-peroxidation

*Lipid-peroxidation was assessed by flow cytometry using BODIPY™ after the indicated times of treatment. Each bar graph diagram shows one representative experiment with three replicates per sample (mean + SD; 5,000 cells per replicate; ***p<0.001 compared to glutamate- or erastin-treated control; ANOVA, Scheffé's test).* ***A-C:*** *HT22 cells;* ***D:*** *mHypo cells*

The influence of Ze 450 on ATP levels was further analyzed to gain insights into mitochondrial involvement in the neuroprotective effects of Ze 450 (Figure 20). In mHypo and HT22 cells, Ze 450 reduced cellular ATP levels to ~70% upon concentrations greater than 150 µg/mL under standard culture conditions (Figure 20). After erastin-exposure, ATP depletion was partly prevented by concentrations greater than 100 µg/mL in HT22 cells and by 50-150 µg/mL of Ze 450 in mHypo cells (Figure 20A, C). This was confirmed in HT22 cells challenged with glutamate (Figure 20B).

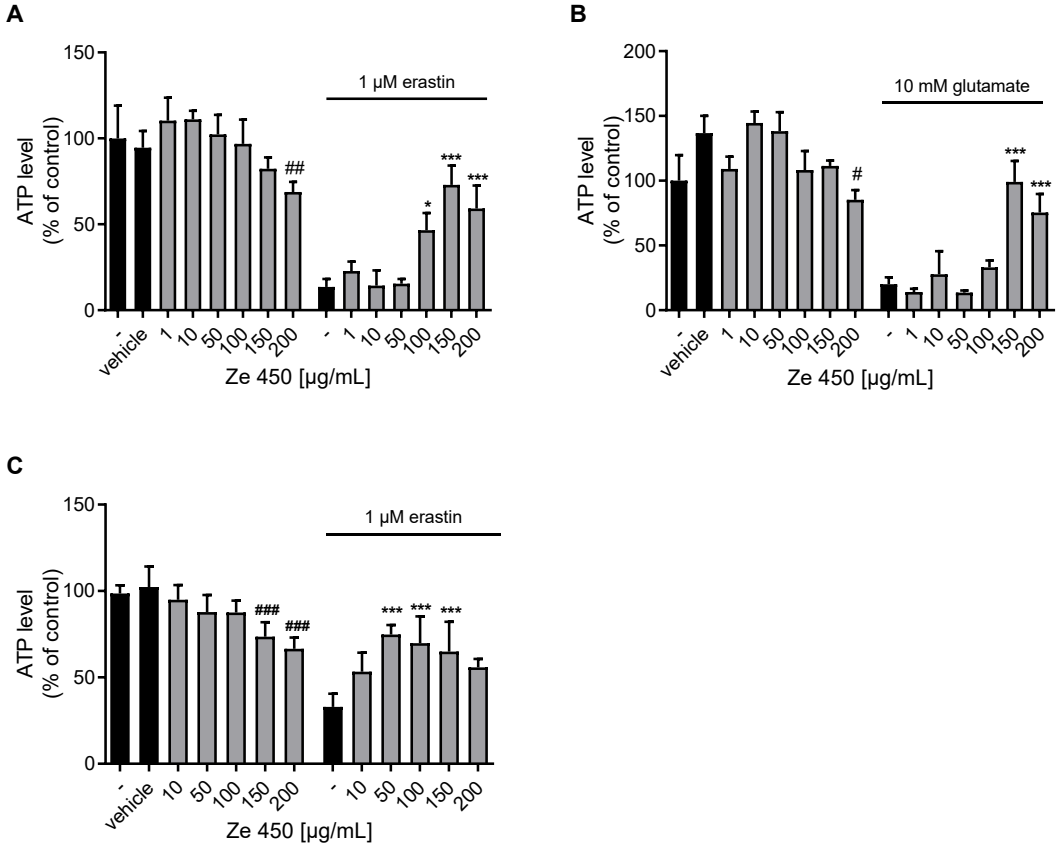

Figure 20. Effects of Ze 450 on ATP levels

*ATP levels were determined using a luciferase-based assay after 16 h of treatment. Values from five-eight replicate wells per condition are displayed as mean + SD. The luminescence under control conditions is set as 100% (***p<0.001; **p<0.01; *p<0.05 compared to glutamate-/erastin-treated control, ###p<0.001; ##p<0.01; #p<0.05 compared to untreated control; ANOVA, Scheffé's test).* ***A+B:*** *HT22 cells,* ***C:*** *mHypo cells*

Mitochondrial ROS are important mediators of cellular stress, and mitochondrial dysfunction is associated with increased mitochondrial ROS formation and associated pathways of oxidative cell death. Mitochondrial ROS formation was investigated using MitoSOX™ red staining and FACS analysis in HT22 and mHypo cells 16 hours after treatment. In both neuronal cell lines, Ze 450 did not affect mitochondrial ROS accumulation at basal conditions (Figure 21A-C). In contrast, erastin- and glutamate-induced increase in mitochondrial ROS formation was prevented by concentrations greater than 50 µg/mL of Ze 450 (Figure 21A-C). This effect was also observed in a post-treatment paradigm when Ze 450 was applied 1 h after onset of erastin or glutamate exposure (Figure 21D, E).

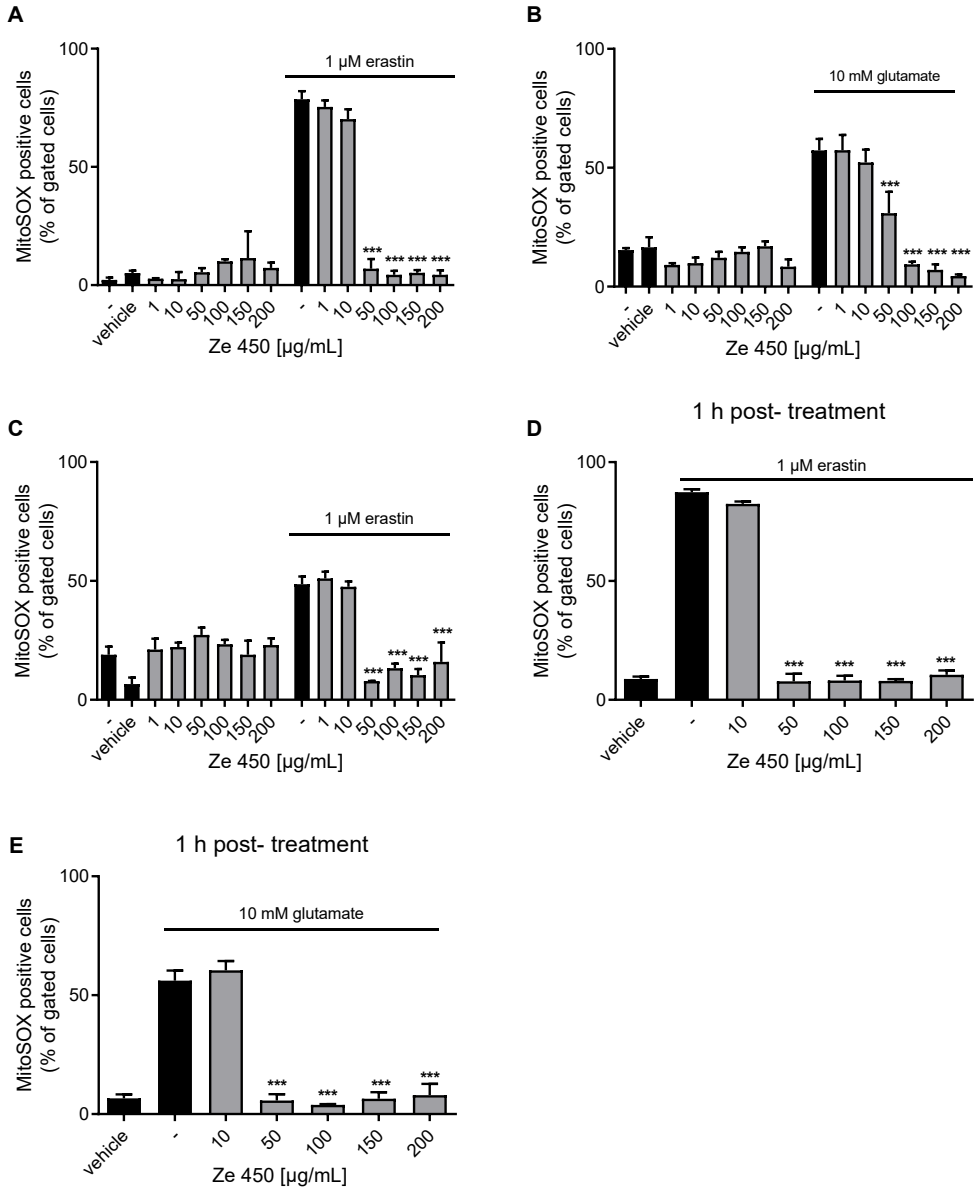

Figure 21. Effects of Ze 450 on mitochondrial ROS formation

*Mitochondrial ROS formation was assessed by flow cytometry using MitoSOX™ after 16 h of treatment. The bar graph shows one representative experiment with three replicates per sample (mean + SD; 5,000 cells per replicate, ***p<0.001; **p<0.01; *p<0.05 compared to erastin or glutamate treated control; ANOVA, Scheffé's test).* ***A, B, D, E:*** *HT22 cells;* ***C:*** *mHypo cells;* ***D, E:*** *HT22 cells were stressed with either erastin or glutamate 1 h before Ze 450 co-treatment.*

Next, mitochondrial membrane potential was analyzed after 16 h of treatment in HT22 and mHypo cells using TMRE™. Mitochondrial membrane potential was not affected by Ze 450 in both neuronal cell lines under standard culture conditions (Figure 22A-C), but loss of mitochondrial membrane potential due to erastin or glutamate exposure was prevented by concentrations greater than 50 µg/mL of Ze 450 (Figure 22A-C).

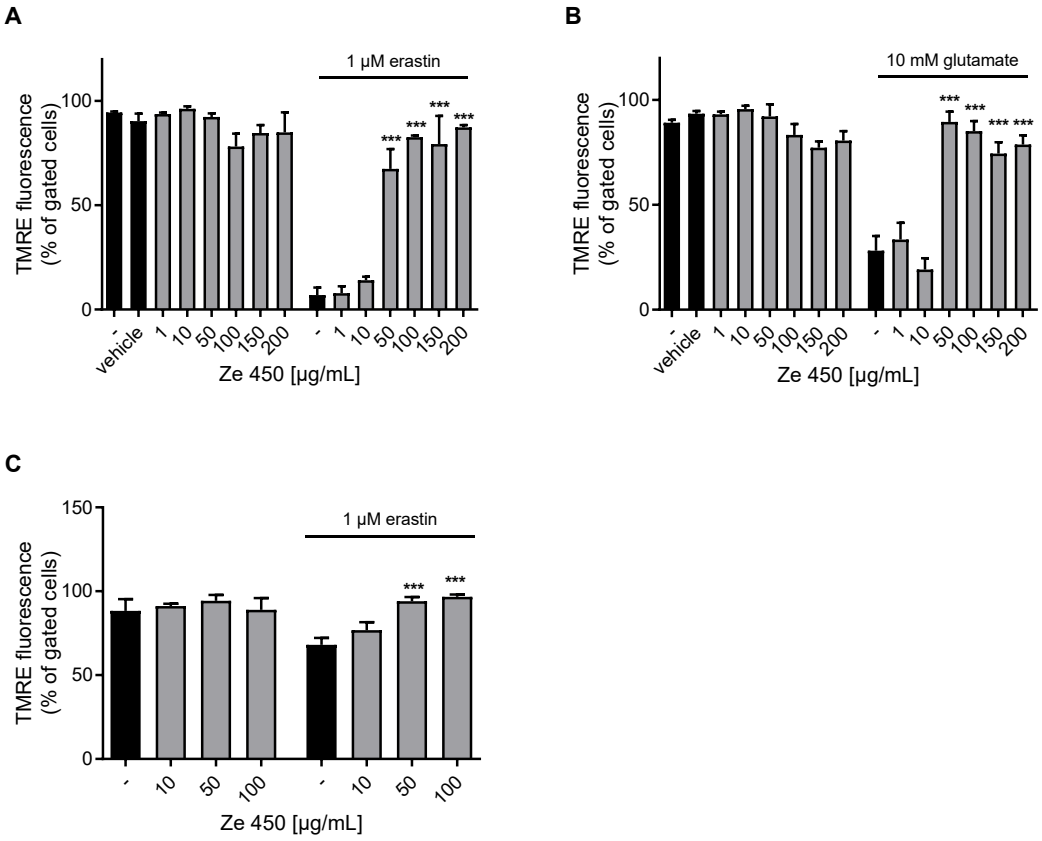

Figure 22. Effects of Ze 450 on mitochondrial membrane potential

*Mitochondrial membrane potential was assessed via flow cytometry analysis with TMRE™ staining after 16 h of erastin or glutamate treatment. Each bar chart depicts one representative experiment with three replicates per sample (mean + SD; 5,000 cells per replicate, ***p<0.001 compared to erastin- or glutamate- treated control; ANOVA, Scheffé's test).* ***A-B:*** *HT22 cells;* ***C:*** *mHypo cells*

Overall, Ze 450 demonstrated strong protective effects at the level of mitochondria in the applied model systems of erastin- and glutamate-induced oxidative stress in both neuronal cell lines. Further, Ze 450 prevented glutamate-mediated excitotoxicity in primary cortical neurons.

4.2.2. Ze 450 provokes a glycolytic shift under oxidative stress conditions

Mitochondria are crucial organelles responsible for the energy metabolism and energy supply for the whole cell and play a decisive role in regulated oxidative cell death, especially in neurons as described before in chapter 1.3. To gain further insights into potential metabolic effects such as alterations of mitochondrial respiration and metabolic status of cells exposed to Ze 450, oxygen consumption rate (OCR) and extracellular acidification rate (ECAR) were investigated using the Agilent Seahorse XF96 system for detection of oxidative phosphorylation and glycolysis, respectively. These functional metabolic parameters are essential for further elucidating the mechanism of action of Ze 450 at the level of mitochondria. Figure 23A shows that Ze 450 reduced the OCR compared to control cells in a concentration-dependent manner; especially the basal and maximal respiration after FCCP injection were affected. Intriguingly, oxidative stress-mediated reduction of mitochondrial respiration after erastin exposure was not rescued by Ze 450 (Figure 23B). While cells performed less mitochondrial respiration, an enhanced glycolysis rate compared to control cells was detected. Furthermore, 100 µg/mL of Ze 450 increased the ECAR compared to control cells (Figure 23C). Consistently, Ze 450 compensated the erastin-mediated reduction of ECAR in a concentration-dependent manner (Figure 23D), thereby preserving the energy production of the cell. Interestingly, the response after oligomycin injection (port A) was much steeper in control cells compared to cells treated with 100 µg/mL Ze 450 and erastin (Figure 23D). Oligomycin inhibits the ATP synthase of the respiratory chain, and consequently, leading to an increase of the ECAR. Ze 450 induced a shift towards glycolysis and following the increase in glycolysis stimulated by oligomycin was not as prominent as in corresponding control conditions.

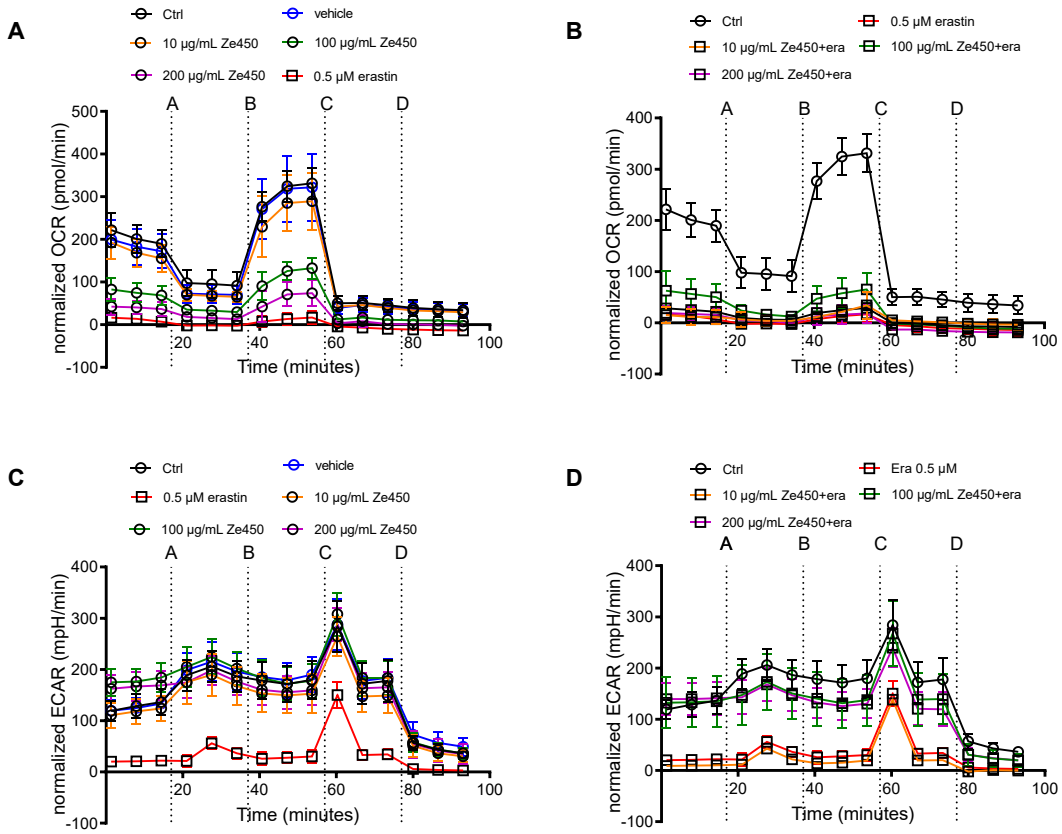

Figure 23. Effects of Ze 450 on energy metabolism

Data of one representative experiment is depicted showing OCR and ECAR under basal and oxidative stress conditions. ***A, B:*** *After 16 h of treatment with Ze 450* ***(A)*** *and challenged with 0.5 µM erastin* ***(B)****, the oxygen consumption rate (OCR) of HT22 was analyzed with a Seahorse XFe96 Analyzer. Data of 5-12 replicate wells per condition are given as mean ± SD.* ***C, D****: After 16 h of treatment with Ze 450* ***(C)*** *and challenged with 0.5 µM erastin* ***(D)*** *the extracellular acidification rate (ECAR) was determined with a Seahorse XFe96 Analyzer. Data of 4-12 replicate wells per condition are given as mean ± SD (port A: oligomycin; port B: FCCP; port C: rotenone and antimycin A; port D: 2-deoxyglucose).*

Overall, Ze 450 reduced OCR in a concentration-dependent manner under basal conditions (Figure 24A), and attenuated erastin-mediated reduction of the ECAR (Figure 24B), thereby preventing mitochondrial ROS formation, deletion of mitochondrial membrane potential and preserving ATP levels.

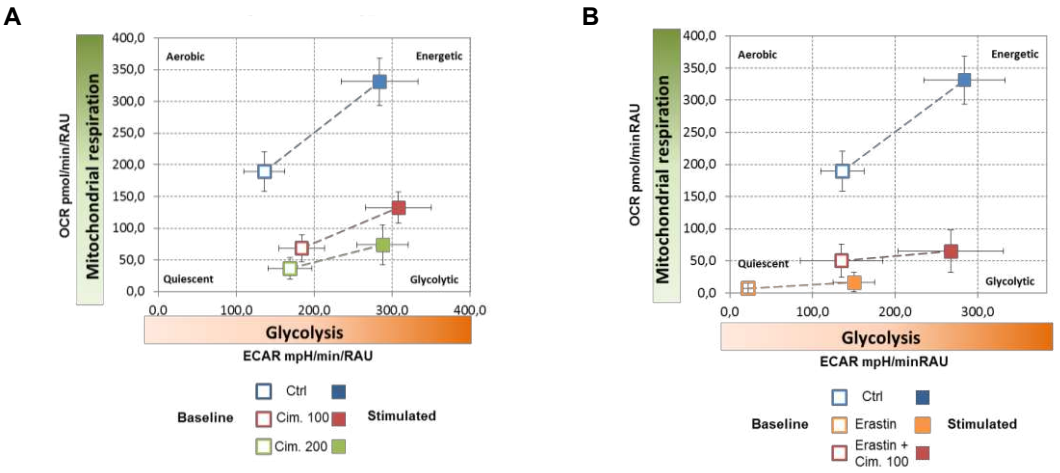

Figure 24. Energetic phenotype

*The cell energy phenotype is depicted as the OCR blotted against the ECAR under basal **(A)** and oxidative stress conditions **(B)**. Baseline phenotype after 16 h of treatment is depicted with an open square representing the OCR and ECAR of HT22 cells at starting conditions. Stressed phenotype is depicted with a filled square representing the energy phenotype demand under FCCP treatment (induced energy demand, uncoupling agent), (Cim. 100: 100 µg/mL Ze 450; Cim. 200: 200 µg/mL Ze 450).*

Furthermore, protein levels of the mitochondrial respiratory chain complexes were assessed to reveal insights into translational regulation by Ze 450 (Figure 25A). While mitochondrial respiratory chain function is reduced upon Ze 450 treatment, there was no impact on the level of protein of all five mitochondrial respiratory chain complexes detectable (Figure 25B-F).

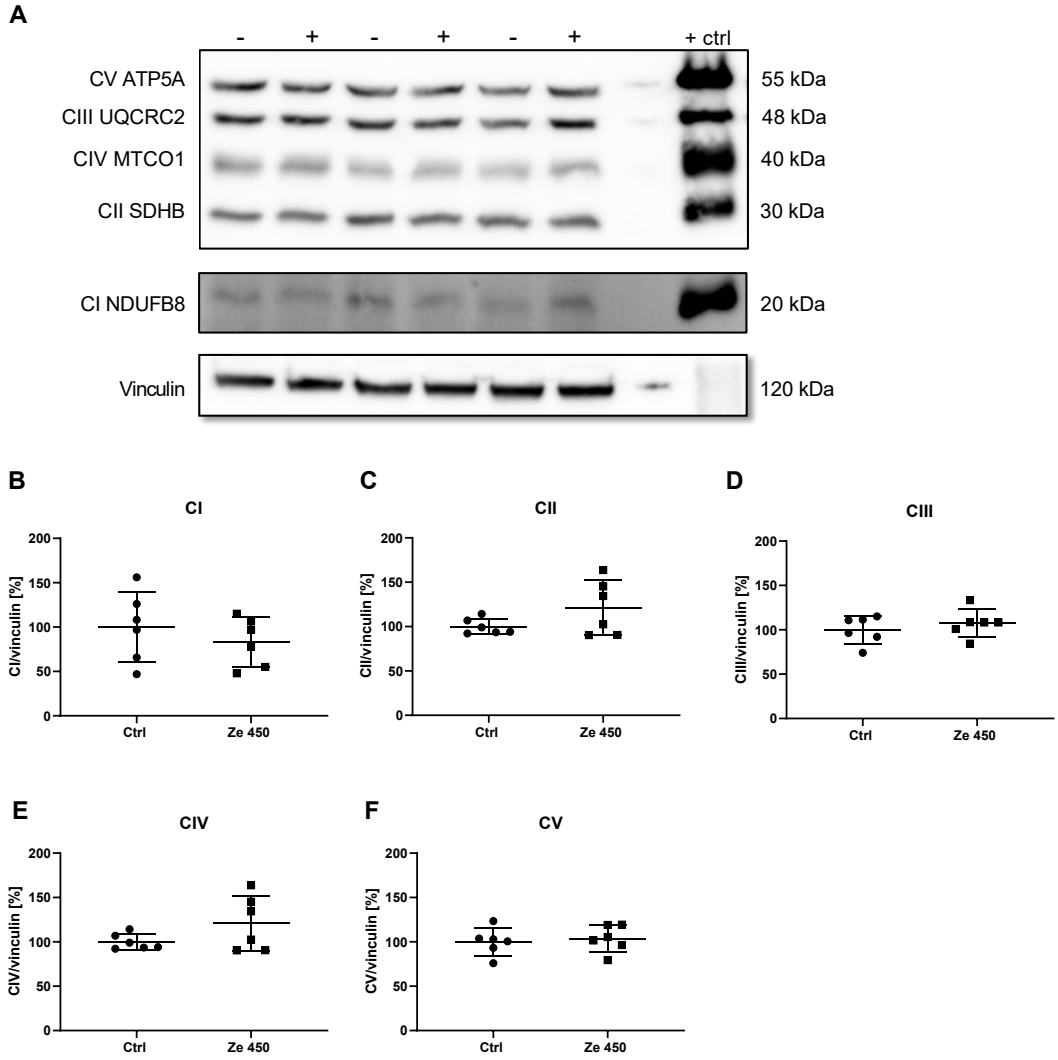

Figure 25. Protein levels of the five electron transport chain complexes

*Relative protein levels of the five electron transport chain complexes (CI-CV) were assessed in HT22 cells treated with 100 µg/mL Ze 450 for 16 h compared to untreated control (- control, + Ze 450). Rat cortical mitochondria served as a positive control (+ ctrl). Figure **A** depicts a representative immunoblot. Figures **B-F** show the densitometric quantification of the individual complexes (CI-CV). The values are normalized to vinculin as a housekeeping protein. Data is presented as percent of control (mean ± SD, n=6).*

Ze 450 exerted potent effects at the level of mitochondria indicating a strong influence on metabolism. However, the question remained, whether this metabolic shift is important for protection against oxidative damage. Therefore, Ze 450 was combined with the glycolysis inhibitor 2-deoxyglucose and erastin and investigated via Annexin V and PI flow cytometry analysis (Figure 26A). Erastin-induced cell death was prevented by Ze 450, but the addition of 2-DG led to a loss of the protective effect. To further analyze the mechanism of action, Ze 450 was compared to the known antioxidant Trolox. While the metabolic shift is a prerequisite for Ze 450 mediated protection against oxidative

damage, in contrast, the antioxidant Trolox still mediated protection against erastin-induced toxicity in the presence of 2-DG (Figure 26A). Moreover, *Cimicifuga racemosa* plant extracts, such as Ze 450 contain many components including antioxidants, for example, ferulic acid. However, the content of ferulic acid is less than 0.2% in this batch of Ze 450, and therefore, most likely not the major component contributing to the observed protective effects. In order to study the antioxidant properties of Ze 450, the radical scavenging activity of Ze 450 was analyzed using the DPPH assay (Figure 26B). Indeed, Ze 450 showed only moderate antioxidant properties compared to Trolox but as demonstrated in figure 26A this antioxidant capacity was unlikely contributing to the observed protective effects of Ze 450.

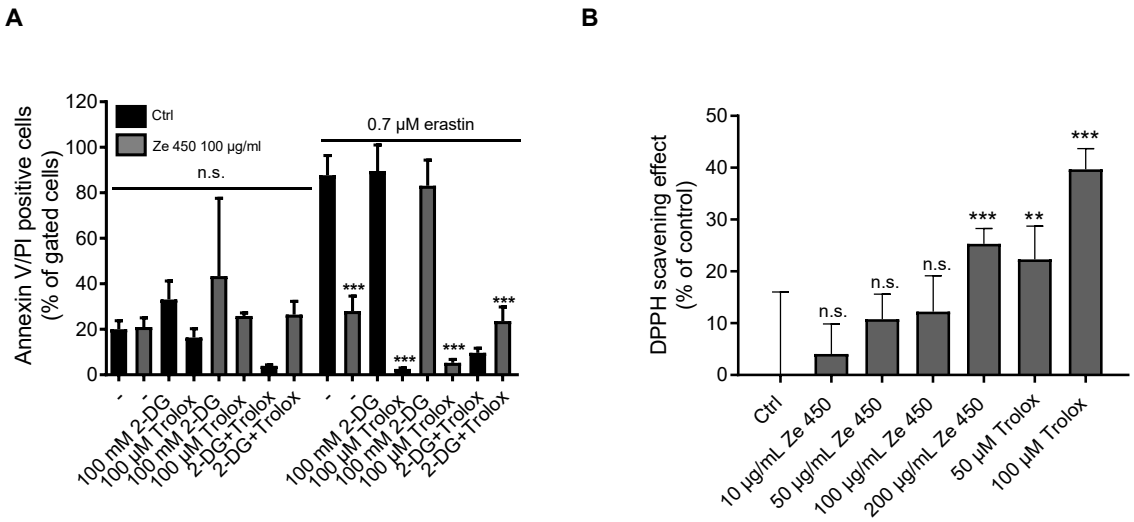

Figure 26. Ze 450 mediated effects in comparison to Trolox

A: *Cell death was assessed by flow cytometry using Annexin V and PI after 16 h of treatment in HT22 cells. The bar graph shows one representative experiment with three replicates per sample (mean + SD; 5,000 cells per replicate; ***p<0.001 compared to erastin treated control; ANOVA Scheffé´s test).* ***B:*** *DPPH radical scavenging activity was determined at 517 nm (***p<0.001, **p<0.01 compared to control; ANOVA Scheffé´s test).*

Additionally, the protein level of key antioxidant enzymes (Catalase, MnSOD and CuZnSOD) were analyzed (Figure 27A-F). None of the mentioned proteins of the cellular antioxidant defense were upregulated upon 16 h of Ze 450 treatment (Figure 27A-F).

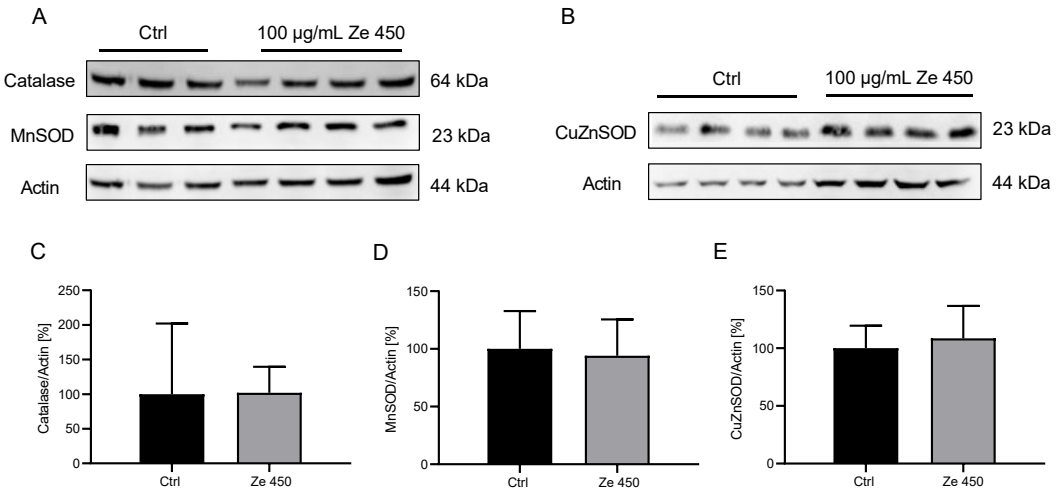

Figure 27. Protein levels of antioxidant enzymes

A, B: *Representative Immunoblots showed no changes in protein levels after 16 h of Ze 450 treatment (100 µg/mL) in HT22 cells.* ***C-E:*** *Quantification of Western Blot as optical density compared to actin as loading control (n=3-4/treatment condition).*

4.2.3. Ze 450 influences the functionality of mitochondrial respiratory chain complexes

Isolated mitochondria were used to elucidate, whether Ze 450 directly targeted mitochondria. For that purpose, mitochondrial respiration was investigated using the coupling assay, with rotenone as an inhibitor for complex I and succinate as substrate for complex II driven respiration. Rat cortical mitochondria were incubated with Ze 450 on ice for 30-60 minutes (Figure 28A, B). After 30 min, the respiration profile under control conditions and in Ze 450 treated mitochondria did not differ (Figure 28A), whereas, after 60 min incubation, Ze 450 mediated a concentration-dependent reduction of oxygen consumption rate (after injection of ADP) and complex II functionality upon FCCP stimuli (Injection C, Figure 28B). Rhodamine 123 measurement was performed as a quality control of isolated mitochondria to test the integrity of the mitochondrial membrane. Control mitochondria and Ze 450 treated mitochondria showed similar quenching of the Rhodamine 123 fluorescence (Figure 28C).

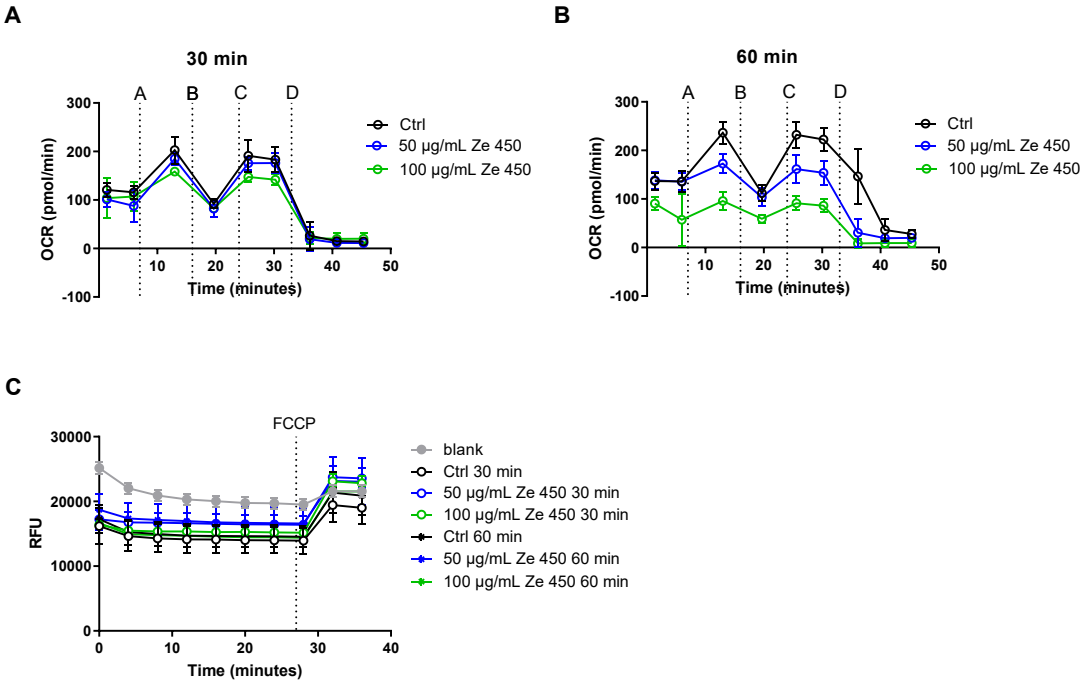

Figure 28. Ze 450 affects mitochondrial complex II and III functionality

A, B: *OCR was analyzed after 30 and 60 min of incubation with Ze 450 (50 and 100 µg/mL). ADP (port A), oligomycin (port B), FCCP (port C) and antimycin A (port D) were injected, successively. Rotenone was initially present and hence respiration is being driven by complex II-IV activity.* ***C:*** *Rhodamine 123 is positively charged and accumulated within the mitochondria. Fluorescence quenching was monitored until FCCP was injected.*

In order to sequentially study the electron flow through different complexes of the electron transport chain, the coupling assay was used. Basal respiration served as an indicator for complex I activity as pyruvate and malate were initially present to deliver NADH as a substrate for mitochondrial complex I. Ze 450 affected pyruvate and malate driven respiration in a time-dependent manner (Figure 29A), but did not completely inhibited complex I activity, since the injection of rotenone (port A, Figure 29A) further reduced mitochondrial respiration. Injection of FCCP (port B, Figure 26A) led to an increase in OCR, showing that the electron transport chain is function properly.

A

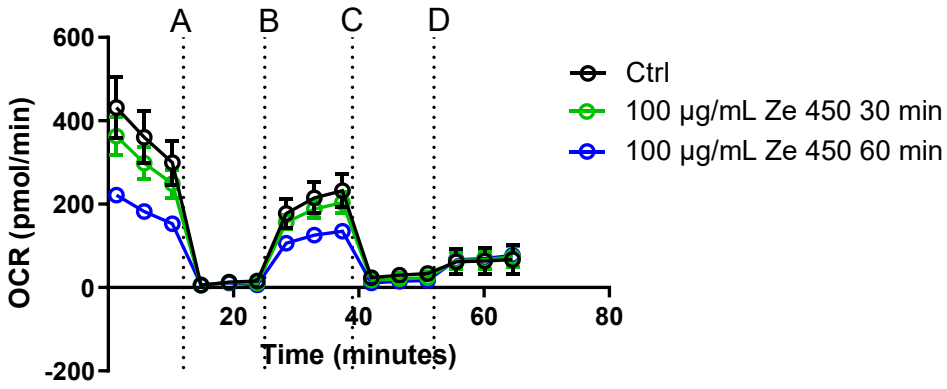

Figure 29. Ze 450 affects mitochondrial complex I functionality

A: *OCR was analyzed after 30 and 60 min of incubation with Ze 450 (50 and 100 µg/mL). Rotenone (port A), FCCP (port B), antimycin A (port C) and ascorbate with TMPD (port D) were injected successively. Pyruvate and malate were initially present and hence respiration is being driven by complex I.*

Taken together, the findings of the coupling and electron transport chain assay demonstrated that Ze 450 affected mitochondrial respiration by mild inhibition of complex I-III activities.

Mitochondrial ROS produced by the electron transport chain are majorly contributing to oxidative damage and further function as signaling molecules [134]. Thus, investigating mitochondrial ROS formation of isolated mitochondria treated with Ze 450, allowed for the conclusion that Ze 450 did not induce superoxide formation (Figure 30A, B) after an acute incubation time of 60 minutes, whereas antimycin A served as a positive control.

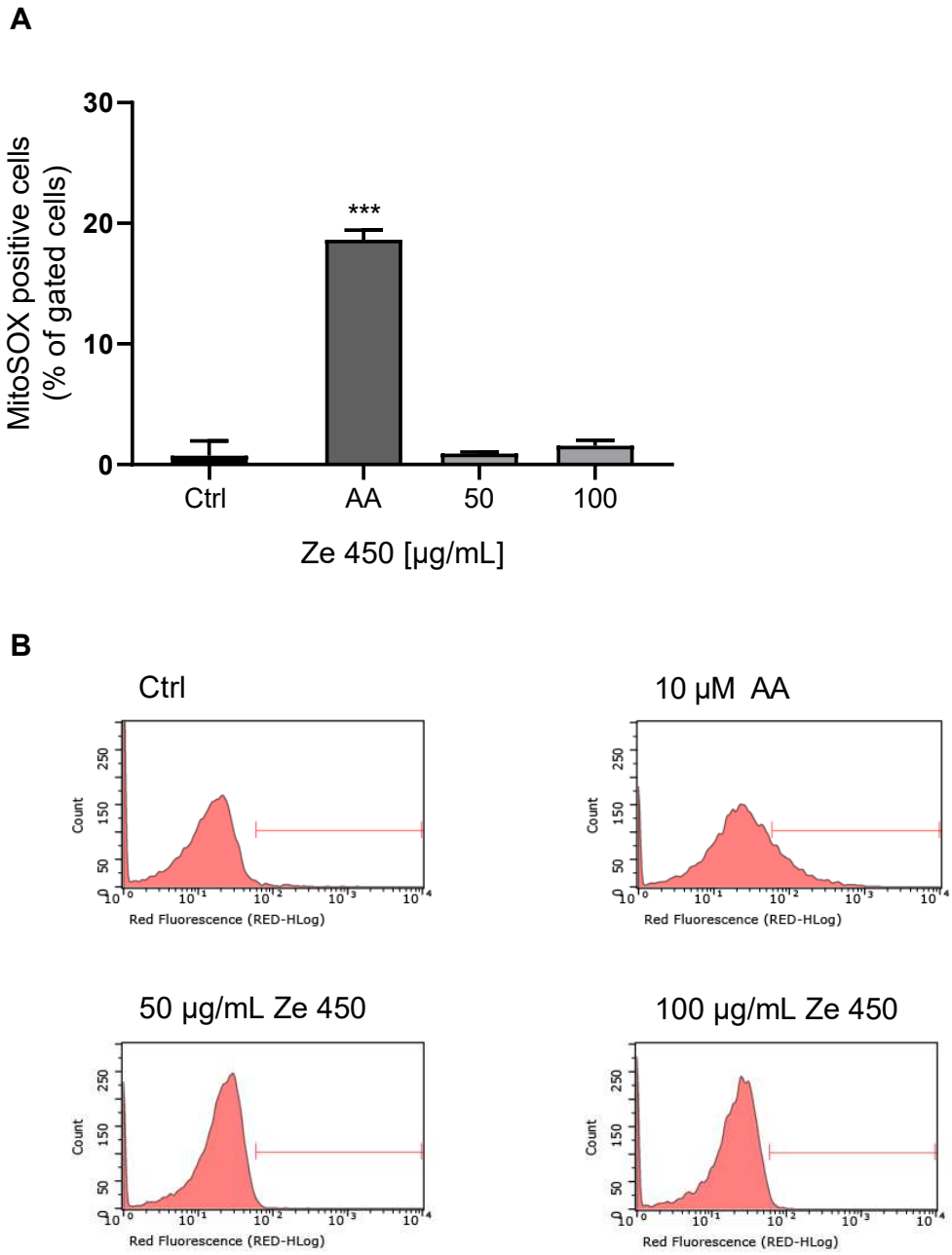

Figure 30. Ze 450 did not induce mitochondrial ROS formation

A-B: *Mitochondrial ROS formation of cortical mitochondria was assessed with MitoSOX™ red staining and flow cytometry. Mitochondrial superoxide levels were not altered upon Ze 450 treatment (60 minutes). 10 µM antimycin A (AA) was incubated for 30 min and served as a positive control.* ***A:*** *Representative data is shown as mean +SD of three replicates per treatment condition (5,000 events per condition, ***p<0.001 compared to untreated control mitochondria; ANOVA, Scheffé´s test).* ***B:*** *Representative flow cytometry histograms.*

Overall, the experiments on ETC functionality and mitochondrial ROS formation with isolated cortical mitochondria confirmed that Ze 450 modulates oxidative phosphorylation by weakly inhibiting mitochondrial respiration complexes and thereby lower oxidative damage most likely by reducing mitochondrial ROS formation.

4.2.4. Metabolic regulation upon Ze 450 treatment in neurons

Hypoxia-inducible factor α (HIF1α) is a transcriptional regulator, known to be majorly involved as a key regulator in response to hypoxia [159]. The alpha subunit of HIF is responsive to low oxygen concentrations and then activates genes involved in angiogenesis [160], glucose metabolism, proliferation, and many more [161].

In order to study the involvement of HIF1α in the metabolic changes upon Ze 450 treatment, Western Blot analysis was performed (Figure 31A). Ze 450 regulated HIF1α protein levels in a time-dependent manner.

A

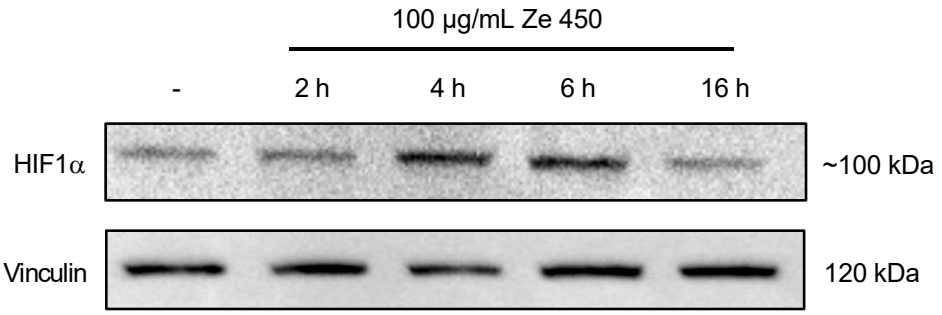

Figure 31. Time-dependent Western Blot analysis of HIF1α protein level

A: *The depicted Western Blot shows an initial increase of HIF1α protein levels and subsequent decrease after 16 h of Ze 450 treatment (100 µg/mL) in HT22 cells.*

The initially increased HIF1α protein levels were further studied within 3 hours of treatment with 100 µg/mL Ze 450 (Figure 32A, B). Indeed, the HIF1α upregulation was confirmed as depicted in the representative immunoblot (Figure 32A) and the quantification (Figure 32B). In contrast, HIF1α protein level was decreased after 16 h of Ze 450 treatment (Figures 31A and 32C).

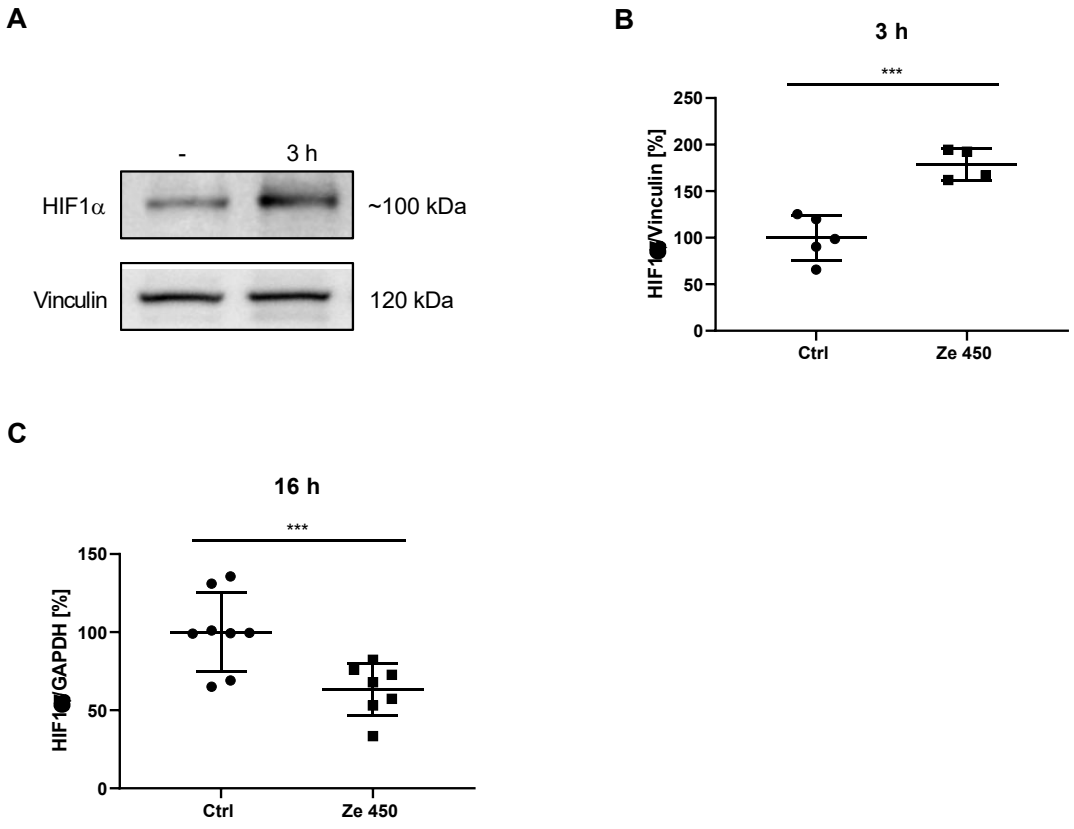

Figure 32. Western Blot analysis of HIF1α protein level after 3 and 16 h of Ze 450 treatment

A: *Representative Western Blot showed an initial increase of HIF1α protein level after 3 h of Ze 450 treatment (100 µg/mL) in HT22 cells.* ***B:*** *Quantification of Western Blot as optical density compared to vinculin as loading control (n=4-5/treatment condition; ***p<0.001; unpaired t-test).* ***C:*** *Quantification of Western Blot revealed decreased HIF1α protein level after 16 h of Ze 450 treatment (100 µg/mL) in HT22 cells, depicted as optical density compared to GAPDH as loading control (n=7-8/treatment condition; ***p<0.001; unpaired t-test).*

Besides HIF1α, cMyc is known to be involved in promoting and regulating glycolysis. It was initially described as an oncogene involved in tumor progression and invasiveness, but it also promotes important physiological functions, including energy metabolism [83]. In this study, it was of great interest to analyze, whether cMyc contributed to the observed metabolic shift towards glycolysis induced by Ze 450 [162].

Therefore, cMyc protein levels were investigated after 3 and 16 h upon Ze 450 treatment (Figure 33). Initially, there was no change detected, but after 16 h of Ze 450 treatment, cMyc protein levels were significantly upregulated (Figure 33).

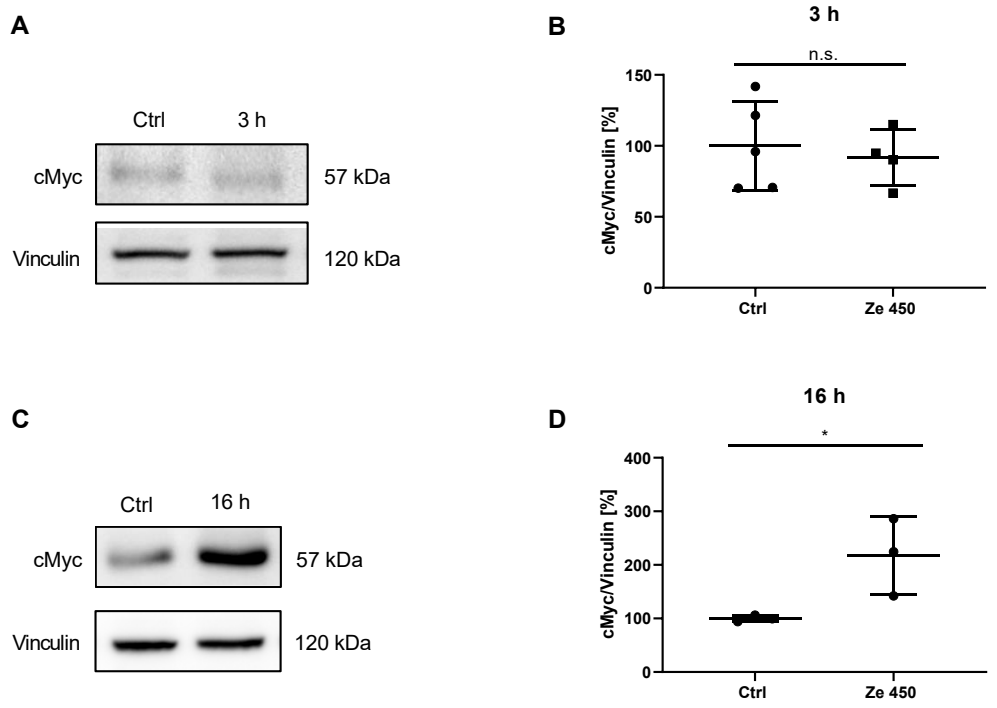

Figure 33. Western Blot analysis of cMyc upon Ze 450 treatment

A: *Representative Western Blot of cMyc protein levels after 3 h of Ze 450 treatment (100 µg/mL) in HT22 cells.* ***B:*** *Quantification of Western Blot as optical density compared to vinculin as loading control (n=4-5/treatment condition, unpaired t-test).* ***C:*** *Representative Western Blot of cMyc protein levels after 16 h of Ze 450 treatment (100 µg/mL) in HT22 cells.* ***D:*** *Quantification of Western Blot revealed decreased cMyc protein levels after 16 h of Ze 450 treatment (100 µg/mL) in HT22 cells, depicted as optical density compared to vinculin as loading control (n=3/treatment condition; *p<0.05; unpaired t-test).*

In contrast to the regulation of cMyc at the protein level, there was no change detected after 16 h of Ze 450 incubation at the mRNA level (Figure 34A, B).

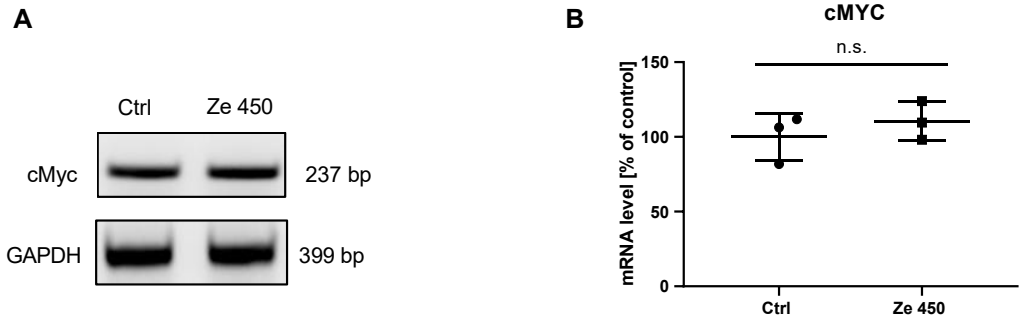

Figure 34. Analysis of cMYC mRNA levels after 16 h of treatment with Ze 450

A: *cMyc mRNA level was analyzed after 16 h of treatment with 100 µg/mL Ze 450.* ***B:*** *Quantification of cMyc mRNA levels normalized to GAPDH (n=3/treatment condition, unpaired t-test).*

Since both, HIF1α and cMyc are known to activate key enzymes involved in energy metabolism [83,87], protein levels of hexokinase II (HXKII), pyruvate dehydrogenase kinase 1 (PDK1) and lactate dehydrogenase A (LDHA) were investigated after 16 h of treatment with Ze 450 (Figure 35). While the protein levels of HXKII and PDK1 were upregulated, there was no change detectable for LDHA (Figure 35).

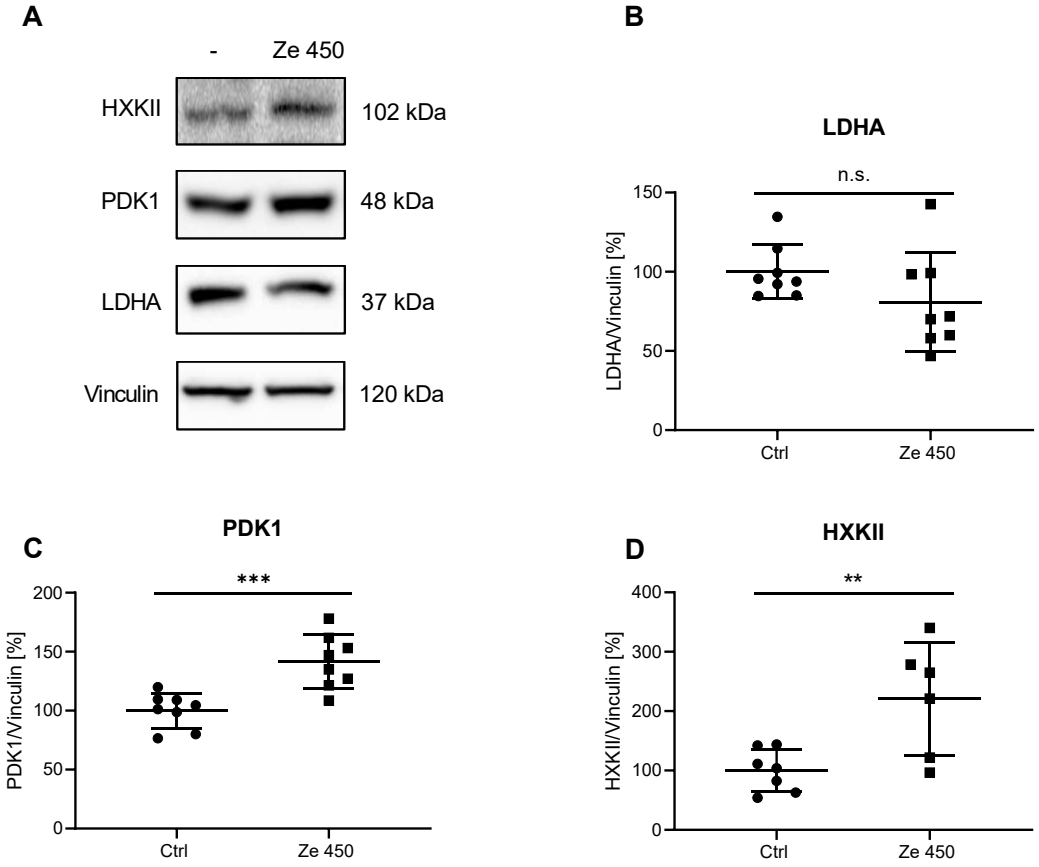

Figure 35. Western Blot analysis of HXKII, PDK1, and LDHA after Ze 450 treatment

A: *Representative Western Blot of LDHA, PDK1, and HXKII protein levels after 16 h of Ze 450 treatment (100 µg/mL) in HT22 cells.* ***B-D:*** *Quantification of Western Blot as optical density compared to vinculin as loading control (n=8/treatment condition, ***p<0.001; **p<0.01, unpaired t-test).*

4.2.5. Ze 450 enhances glucose uptake

Generally, there are two types of glucose transporters; sodium-independent (GLUTs) and sodium-dependent ones (for example SGLTs) [163]. They further differ in their regulation: GLUT 1-3 are constitutively expressed at the cell membrane, while GLUT 4 is translocated to the membrane upon specific stimuli (e.g. insulin). These are important

glucose transporting proteins, controlling the glycolytic flux. Here, glucose uptake into cells was measured using a fluorescent-labeled analog of glucose, 2- NBDG [148]. 2-NBDG can not be fully used in glycolysis and thus accumulates intracellularly after uptake into the cell. Glucose and 2-NBDG enter the cell via glucose transporters according to the Michalis-Menten-kinetics [164]. Compared to glucose, 2-NBDG transport is slower and less sufficient. The effects of Ze 450 on glucose uptake were studied using flow cytometry (Figure 36) and confocal microscopy (Figure 37). Compared to control conditions, Ze 450 mediated enhanced glucose uptake (Figure 36A, B), and this effect was not affected by any auto-fluorescence (Figure 36 B). Notably, neither metformin nor insulin led to a detectable increase in glucose uptake. For Ze 450, it was demonstrated that there is a mild initial increase after 2-6 hours of treatment (Figure 36C), which further increased after 14 h of treatment (Figure 36D).

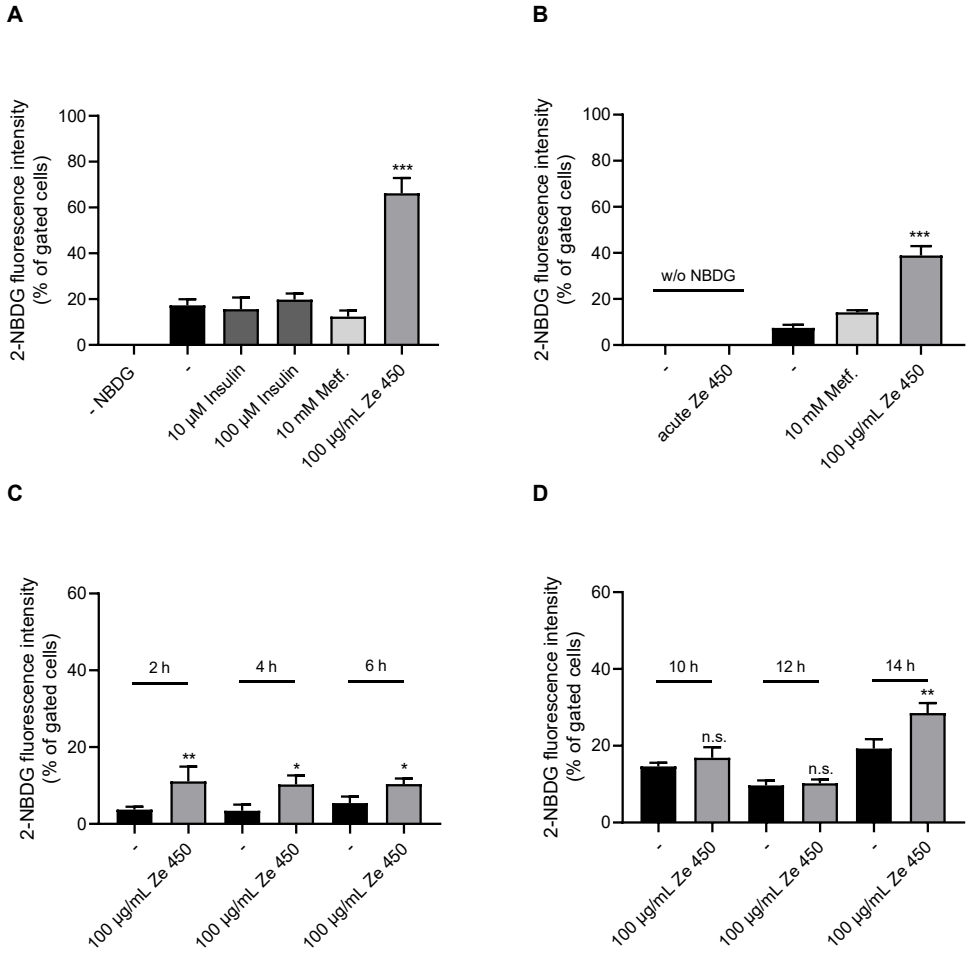

Figure 36. Glucose uptake measured with 2-NBDG via flow cytometry analysis

A-D: *Flow cytometry analysis with 2-NBDG of HT22 cells treated with Ze 450.* ***A:*** *The negative control without 2-NBDG staining did not show an increase in fluorescence intensity.* ***B:*** *Auto-fluorescence of Ze 450 was excluded. Acute treatment without 2-NBDG staining did not show enhanced fluorescence intensity.* ***C-D:*** *Time-dependent effects of Ze 450 on glucose uptake were analyzed (n=3/treatment condition; ***p<0.001, **p<0.01, *p<0.05 compared to untreated control; ANOVA, Scheffé´s test).*

Furthermore, glucose uptake was investigated using confocal microscopy (Figure 37). After 16 h of treatment with Ze 450 enhanced glucose uptake was confirmed by an increase in fluorescence intensity of 2-NBDG (Figure 37D).

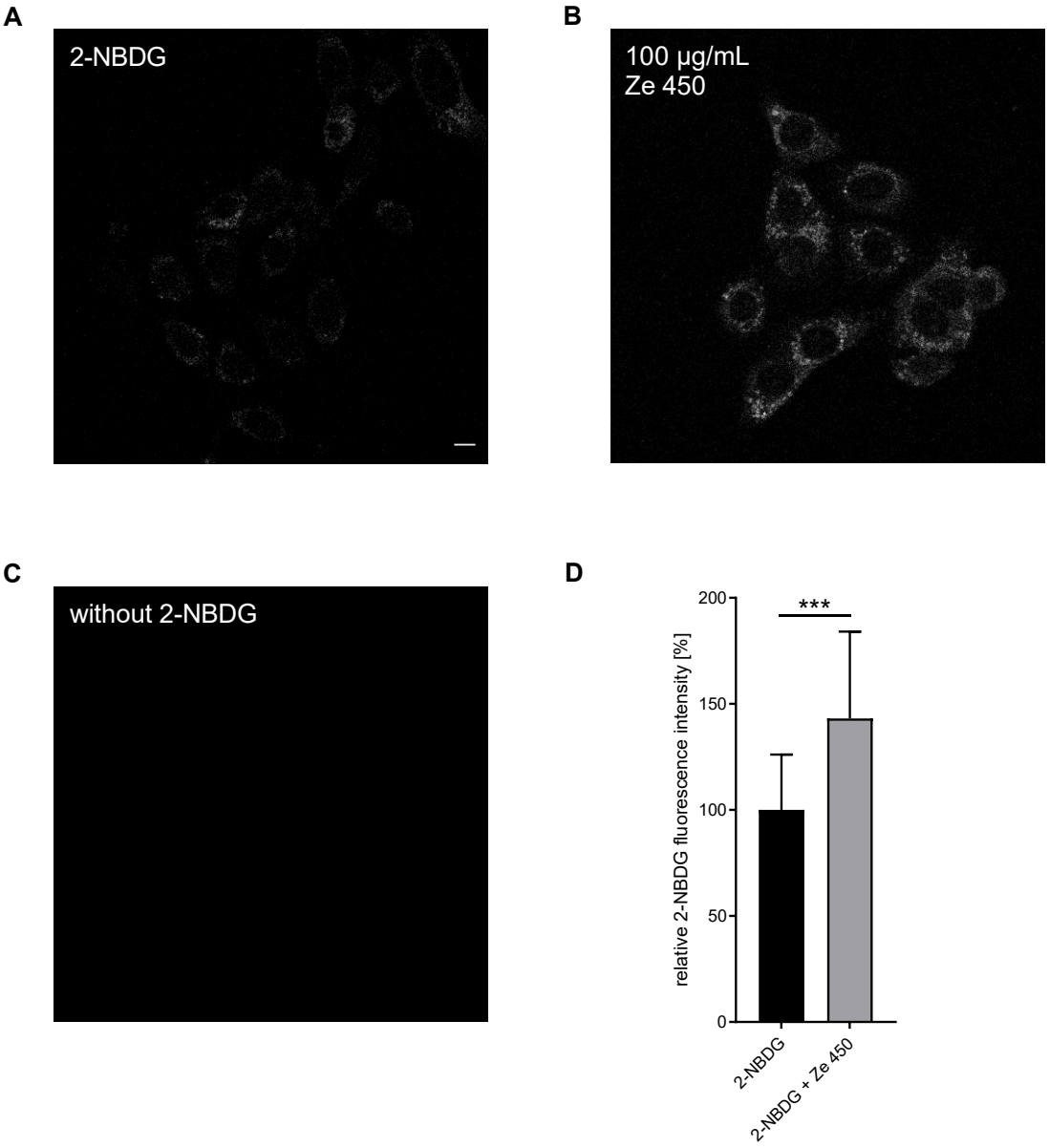

Figure 37. Ze 450 led to an increase of glucose uptake in HT22 cells

A+B**: Confocal images of 2-NBDG staining **A:** 2-NBDG control cells, scale bar 10 µm. **B:** 100 µg/mL Ze 450 for 16 h and 2-NBDG staining. **C:** Representative confocal background image, 100 µg/mL Ze 450 for 16 h without 2-NBDG staining. **D:** Quantification depicts data of four independent experiments with n=20 per treatment condition (p<0.001, unpaired t-test).*

Moreover, mRNA expression of glucose transporter 1 and 4 (SLC2A1 and 4) were analyzed to confirm expression in HT22 cells (Figure 38).

Besides this 100 µg/mL of Ze 450 increased SLC2A4 expression levels compared to control, while the expression of SLC2A1 was not affected.

Consequently, it can be concluded that Ze 450 promoted the increase of SLC2A4 expression levels, thereby supporting glucose uptake and glycolysis. In contrast to SLC2A1, the regulation of SLC2A4 is inducible, which indicated a specific effect of Ze 450 on the glucose transport system.

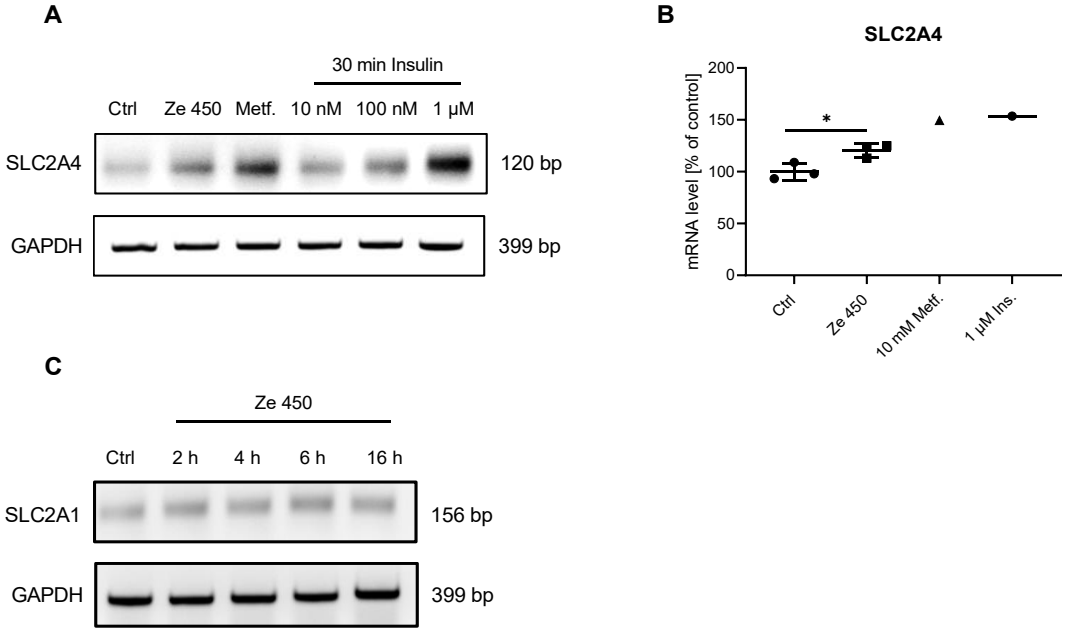

Figure 38. mRNA analysis of SLC2A1 and 4

A: *SLC2A4 mRNA levels were analyzed after 16 h of treatment with 100 µg/mL Ze 450 and 10 mM metformin in HT22 cells. Insulin was exposed for 30 min. Ze 450, metformin and insulin increased optical density compared to GAPDH control.* ***B:*** *Quantification of SLC2A4 mRNA levels normalized to GAPDH (n=3/treatment condition, unpaired t-test).* ***C:*** *SLC2A1 mRNA levels were analyzed after the indicated time of treatment with 100 µg/mL Ze 450 compared to GAPDH.*

SLC2A4 is known to be induced upon insulin stimulus leading to the transfer of vesicular GLUT4 to the plasma membrane enhancing glucose uptake. To gain insights into insulin signaling and compare this to Ze 450-mediated effects, Akt protein levels and according phosphorylation states were investigated. Figure 39A demonstrates that insulin increased phospho Akt levels, while basal Akt protein levels were not altered (Figure 39A). These results suggested proper insulin signaling in HT22 cells. Consequently, the question remained, why insulin did not increase 2-NBDG uptake. In comparison to insulin, Ze 450 rather decreased phospho Akt protein levels, while Akt level remained stable. These effects led to the conclusion, that Ze 450 mediated signaling affected

glucose uptake in an insulin-independent manner, while effects of insulin were restricted to Akt phosphorylation, while GLUT4-mediated glucose uptake was not stimulated by insulin in HT22 cells.

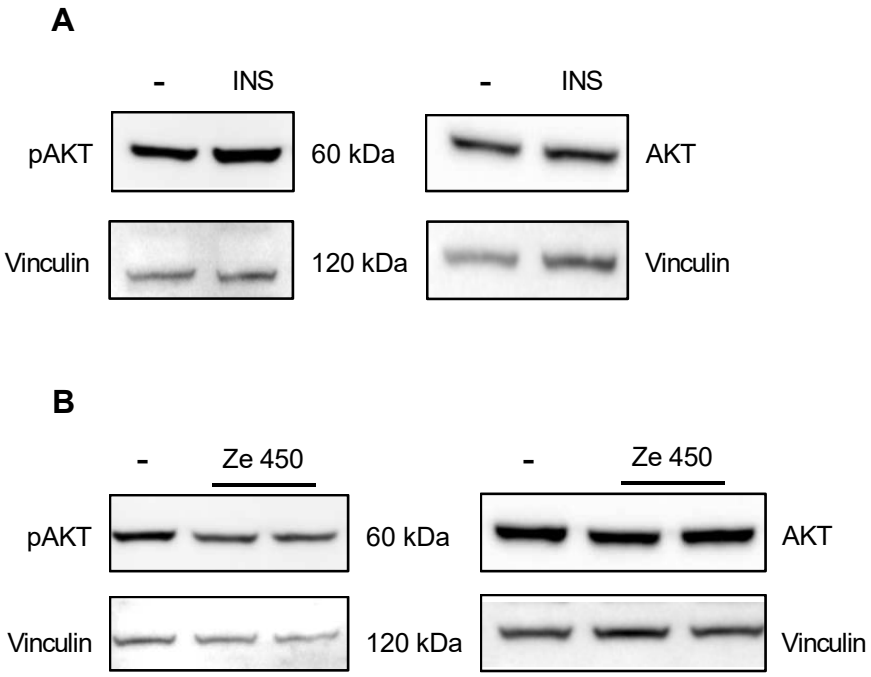

Figure 39. Western Blot analysis of phospho Akt and Akt protein levels

A: *Representative Western Blots of pAkt and Akt protein levels after 30 min of 1 µM insulin (INS) treatment in HT22 cells.* ***B:*** *Representative Western Blots of pAkt and Akt protein level after 16 h of treatment with 100 µg/mL Ze 450 in HT22 cells.*

4.2.6. Effects of isolated components and sub-fractions of Ze 450 on cell metabolism

Ze 450 is a plant extract consisting of many different components. In the literature triterpene glycosides, for example, actein, 23-epi-26-deoxyactein and cimiracemoside C have been described as active ingredients [5]; besides this group, Ze 450 further contains flavonoids [11] and multiple phenolic acids. In order to study the effects of the isolated components (actein, 23-epi-26-deoxyactein and cimiracemoside C) HT22 cells were co-treated with glutamate and the triterpene glycosides (Figure 40A-C). Routine analysis of this batch of Ze 450 (performed at Max Zeller Söhne AG, Switzerland) revealed that total amount of triterpene glycosides was 6.4%, thereof 1.08% actein, 0.94% deoxyactein and 0.52% cimiracemoside C. Hence, 1,6 µM actein, 1.42 µM deoxyactein and 0.848 µM cimiracemoside C correspond to 100 µg/mL Ze 450. Notably, none of these concentrations did show comparable effects to Ze 450. Actein reduced

metabolic activity upon concentrations greater than 20 µM but protected glutamate-mediated reduction of metabolic activity in a concentration range that is not reached in corresponding amounts of Ze 450 (Figure 40A). Similar effects on metabolic activity were obtained from deoxyactein (Figure 40B) and cimiracemoside C (Figure 40C).

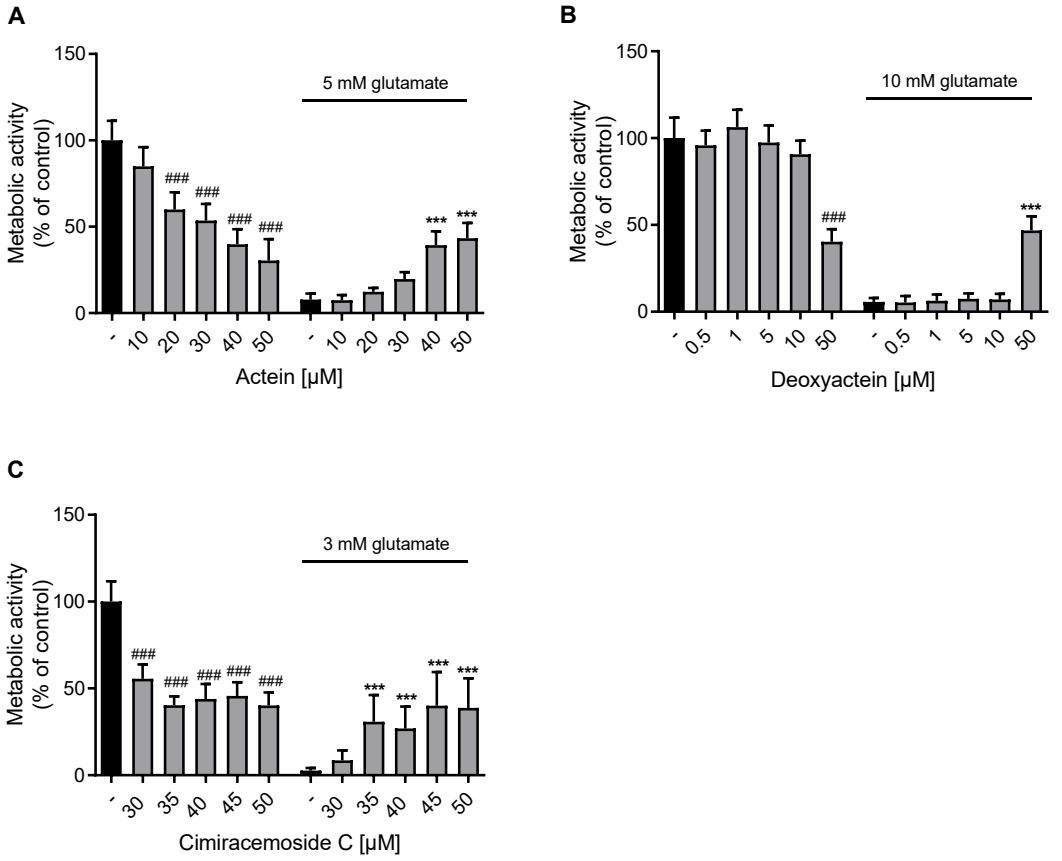

Figure 40. Effects of actein, 23-epi-26-deoxyactein and cimiracemoside C on metabolic activity

A-C: *Metabolic activity was evaluated in glutamate-challenged HT22 cells by measuring MTT formazan absorbance (3-10 mM, 16 h). Eight replicate wells per condition are displayed as mean + SD. The absorbance under control conditions is set as 100% (***p<0.001, **p<0.01, *p<0.05 compared to glutamate-treated control; ###p<0.001, ##p<0.01, #p<0.05 compared to untreated control; ANOVA, Scheffé's test).*

The isolated components did not exert comparable effects like Ze 450, and this may be attributed to two reasons: one is the need for a combination of the different triterpene glycosides, or second only insufficient concentrations of the individual components were reached intracellularly. To answer the first assumption the triterpene glycosides were combined and metabolic activity was investigated (Figure 41A). The combination of 6 µM of each triterpene-glycoside mediated comparable effects like 100 µg/mL of Ze 450. Notably, equivalent concentrations corresponding to 100 µg/mL of Ze 450 were exceeded by the use of 6 µM triterpene-glycosides by a multiple.

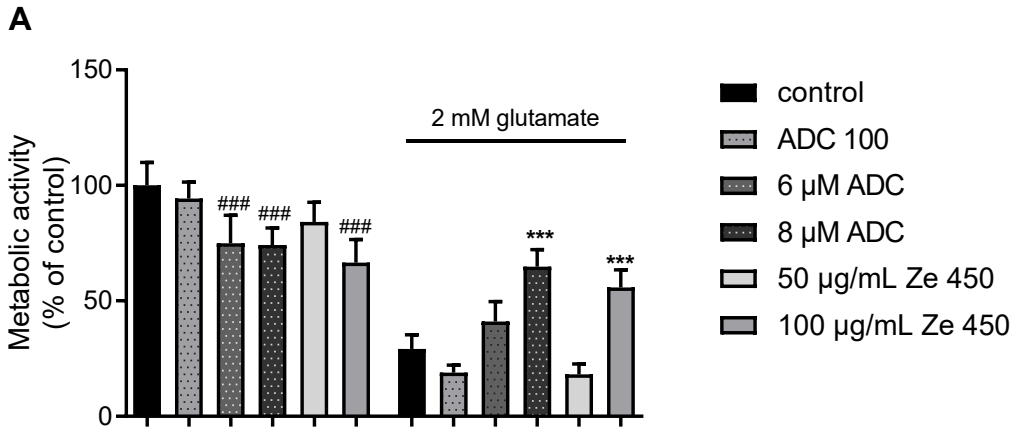

Figure 41. Metabolic activity of combined triterpene glycosides

A: *Metabolic activity was evaluated in glutamate-challenged HT22 cells by measuring MTT formazan absorbance (2 mM, 16 h). Eight replicate wells per condition are displayed as mean + SD. The absorbance under control conditions is set as 100% (***p<0.001; compared to glutamate-treated control; ###p<0.001 compared to untreated control; ANOVA, Scheffé's test). Different concentrations of the triterpene glycosides were tested in combination: ADC 100: 1.6 µM actein, 1.42 µM deoxyactein and 0.838 µM cimiracemoside C (corresponds to 100 µg/mL Ze 450); 6 µM ADC: 6 µM of each; 8 µM ADC: 8 µM of each*

To gain further insights into which components are relevant for the mechanism of protection and metabolic regulation of Ze 450 different solvents were used to obtain sub-fractions of Ze 450. Three sub-fractions resulted: ethyl acetate fraction (EtOAc), buthanolic fraction (BuOH) and water fraction (Aq.).

10 µg/mL EtOAc, 5 µg/mL BuOH and 70 µg/mL Aq. fraction were present in 100 µg/mL of total Ze 450.

Metabolic activity was reduced at concentrations greater than 20 µg/mL of the EtOAc fraction (Figure 42A). Erastin-mediated reduction in metabolic activity was prevented by high concentrations of EtOAc and BuOH fraction, but not by the Aq. fraction (Figure 42A).

Besides Ze 450, the EtOAc fraction mediated protection against erastin-induced oxidative cell death (Figure 42B). Regarding cell proliferation 20 µg/mL of the EtOAc fraction showed similar effects compared to 100 µg/mL Ze 450 (Figure 42C, D). Moreover, this fraction remained to be the most promising compared to Ze 450, since erastin-mediated lipid-peroxidation and mitochondrial ROS were partly prevented (Figure 42E, F).

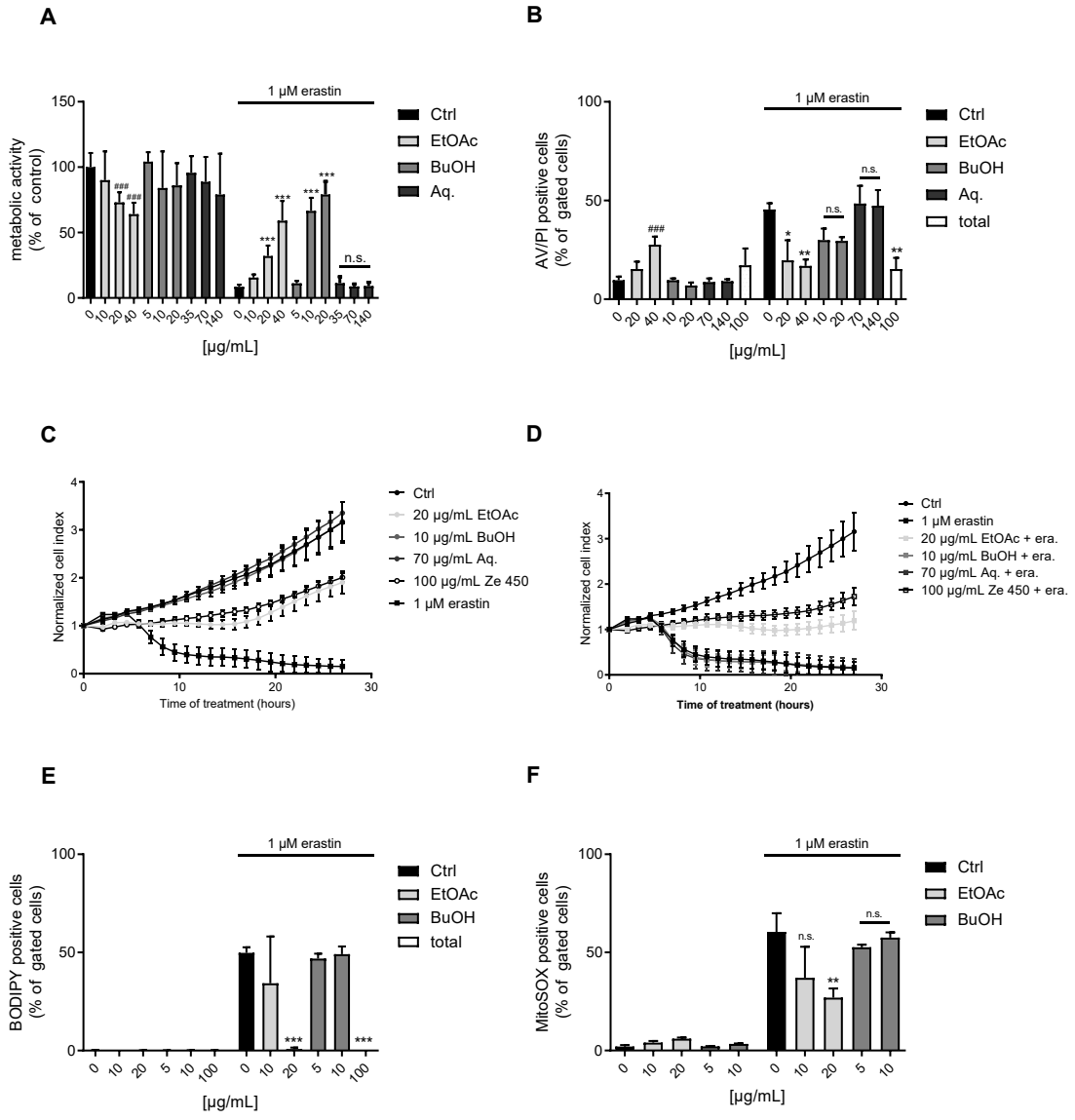

Figure 42. Cellular and mitochondrial effects of sub-fractions of Ze 450 on HT22 cells

A: *Metabolic activity was evaluated in erastin-challenged HT22 cells by measuring MTT formazan absorbance (1 µM, 16 h). Eight replicate wells per condition are displayed as mean + SD. The absorbance under control conditions is set as 100%.* ***B:*** *Cell death was assessed by flow cytometry using Annexin V and PI after 16 h of treatment in HT22 cells.* ***C:*** *Lipid-peroxidation was assessed by flow cytometry using BODIPY™ after 16 h of treatment.* ***D:*** *Mitochondrial ROS formation was investigated by flow cytometry using MitoSOX™ after 16 h of treatment.* ***A-D:*** *The bar graph shows one representative experiment with three replicates per sample (mean + SD; 5,000 cells per replicate; ***p<0.001, **p<0.01, *p<0.05 compared to erastin-treated control; ###p<0.001 compared to untreated control; ANOVA, Scheffé's test).*

Ze 450 demonstrated strong effects on mitochondrial respiration. Similar effects on OCR were observed with 20 µg/mL of EtOAc fraction, while 70 µg/mL of the Aq. fraction enhanced mitochondrial respiration after FCCP injection (Figure 43A). None of the tested fractions rescued erastin-mediated reduction of OCR (Figure 43B). Under basal conditions, EtOAc and BuOH fraction had comparable rates of glycolysis, but their

oligomycin response was more pronounced than it was the case for Ze 450 treated cells and further erastin-mediated reduction of ECAR was not rescued by any sub-fraction, but by Ze 450 (Figure 43C, D).

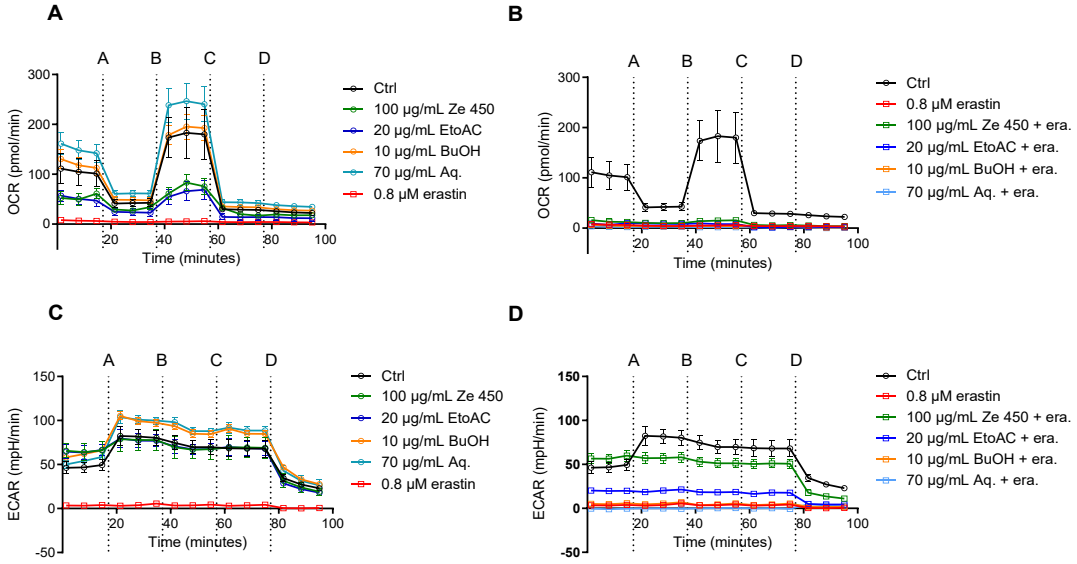

Figure 43. Effects of sub-fractions on OCR and ECAR of HT22 cells

A-D: *Data of a representative experiment is depicted, showing OCR and ECAR under basal and oxidative stress conditions.* ***A, B****: After 16 h of treatment* ***(A)*** *and challenged with 0.8 µM erastin* ***(B)****, the oxygen consumption rate (OCR) of HT22 was analyzed with a Seahorse XFe96 Analyzer. Data of 4-6 replicate wells per condition are given as mean ± SD.* ***C, D:*** *After 16 h of treatment* ***(C)*** *and challenged with 0.8 µM erastin* ***(D)*** *the extracellular acidification rate (ECAR) was determined with a Seahorse XFe96 Analyzer. Data of 4-6 replicate wells per condition are given as mean ± SD (Injections: port A: oligomycin; port B: FCCP; port C: rotenone and antimycin A; port D: 2-deoxyglucose).*

Taken together, EtOAc was identified as the most promising fraction with similar effects comparable to Ze 450, but none of the tested fractions was capable to be as effective as Ze 450. As triterpene glycosides were enriched in EtOAc fraction they most likely contribute to the mechanism of action of Ze 450, but not exclusively. Since, Ze 450 is a plant extract with a variety of components the complex and robust metabolic effects might be caused by an interplay of the compounds, thus making it difficult to highlight just one group or even one component as the leading active ingredient.

4.3. Effects of Ze 450 on neuronal cells in comparison to metformin

Metformin is considered as the state of the art in the treatment of patients with diabetes mellitus type II [165]. In a recent study, Ze 450 was compared to metformin in an *ob/ob* mouse model [35]. It was found, that Ze 450 exerted anti-diabetic effects, as it led to a reduction in body weight and further improved insulin sensitivity and glucose tolerance in male, diabetic mice. In the present study, metformin was compared to Ze 450 in neuronal cells to elucidate similarities or differences in their mechanism of action and response to oxidative stress.

Millimolar concentrations of metformin did not influence metabolic activity (Figure 44A). Erastin-meditated reduction of metabolic activity was prevented by 50 mM metformin in a similar fashion like 100 µg/mL of Ze 450 (Figure 44A). In addition, metformin-mediated protection against erastin-induced oxidative cell death in a concentration-dependent manner (Figure 44B).

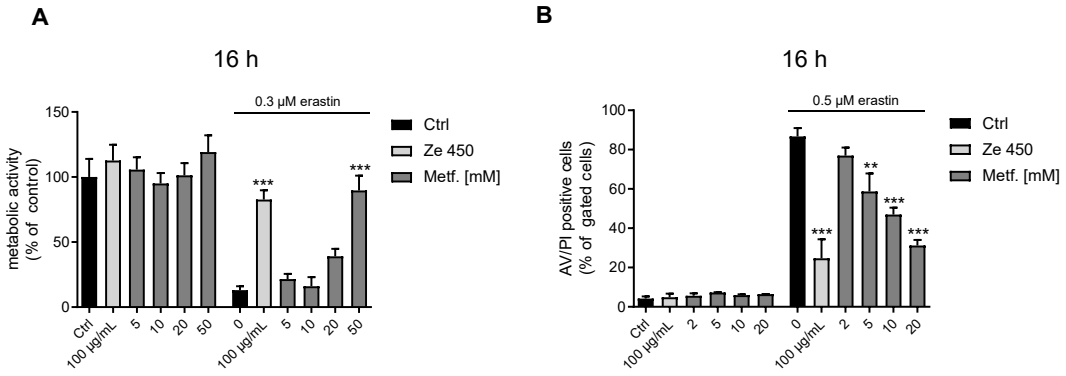

Figure 44. Metformin protects HT22 cells against oxidative damage

A: *Metabolic activity was evaluated in erastin-challenged HT22 cells by measuring MTT formazan absorbance (0.3 µM, 16 h). Eight replicate wells per condition are displayed as mean + SD. The absorbance under control conditions is set as 100%.* ***B:*** *Cell death was assessed by flow cytometry using Annexin V and PI after 16 h of treatment in HT22 cells. The bar graph shows one representative experiment with three replicates per sample (mean + SD; 5,000 cells per replicate).* ***A, B:*** ****p<0.001, **p<0.01 compared to erastin treated control (ANOVA, Scheffé´s test).*

Whether metformin has similar effects as Ze 450 on cell proliferation was assessed using the xCELLigence system (Figure 45A, B). Metformin affected proliferation at a concentration of 50 mM in a comparable manner as 100 µg/mL of Ze 450 (Figure 45A), and erastin-mediated reduction in proliferation was partly prevented by 50 mM metformin (Figure 45B).

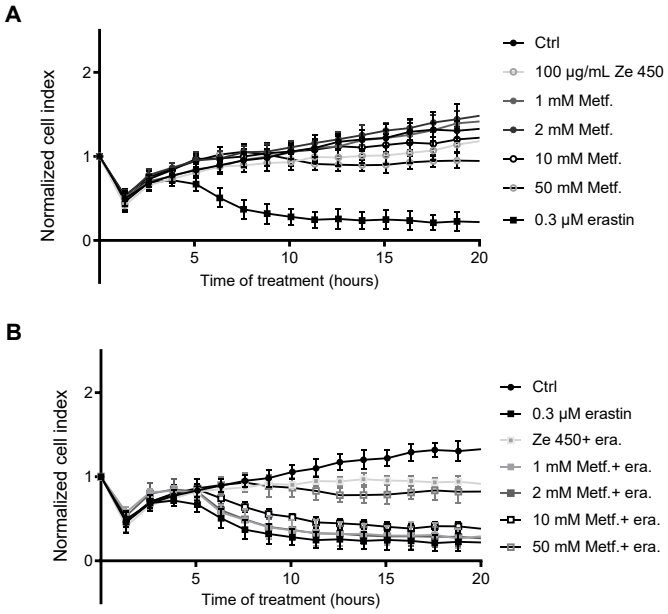

Figure 45. Effects of metformin on proliferation

xCELLigence measurements were conducted after the indicated treatment was added. ***A:*** *HT22 cells were treated with Ze 450 or metformin.* ***B:*** *HT22 cells were co-treated with either Ze 450 or metformin and 0.3 µM erastin (n=5-8/treatment condition). Data are displayed as mean ± SD.*

Next, lipid-peroxidation and mitochondrial parameters (mitochondrial ROS formation, mitochondrial membrane potential, and ATP levels) were investigated. Most prominently was the complete rescue of erastin-mediated lipid-peroxidation by Ze 450 (Figure 46A). After 8 hours of treatment, this effect was less pronounced with metformin (Figure 46A). In addition, mitochondrial ROS formation was assessed and erastin-induced superoxides were reduced upon concentrations greater than 2 mM metformin (Figure 46B). Moreover, metformin prevented erastin-mediated loss of mitochondrial membrane potential in a concentration-dependent manner (Figure 46C). Interestingly, metformin led to ATP depletion, while 100 µg/mL of Ze 450 did not affect ATP levels (Figure 46D). Erastin-induced drop of ATP levels were completely prevented by 100 µg/mL Ze 450, whereas metformin merely preserved ATP levels under these conditions of cellular stress (Figure 46D).

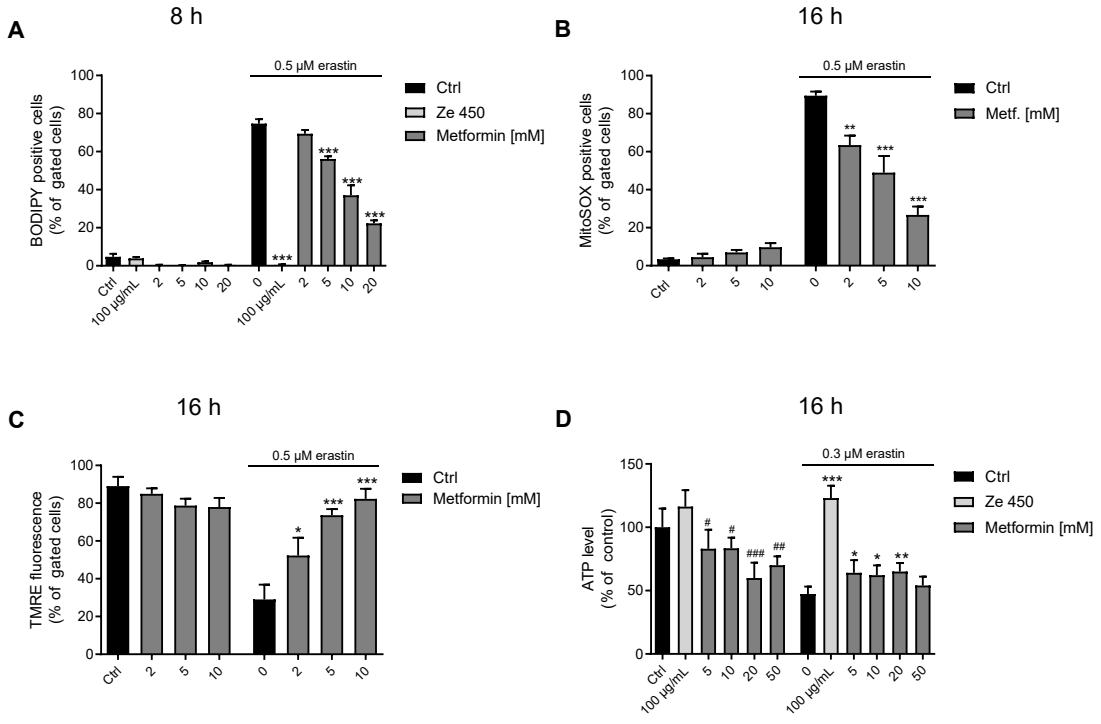

Figure 46. Effects of metformin on lipid-peroxidation and mitochondrial parameters

A: *Lipid-peroxidation was assessed by flow cytometry using BODIPY™ after 8 h. The bar graph shows one representative experiment with three replicates per sample.* ***B:*** *Mitochondrial ROS formation was measured by flow cytometry using MitoSOX™ after 16 h of treatment. The bar graph shows one representative experiment with three replicates per treatment.* ***C:*** *Mitochondrial membrane potential was assessed via flow cytometric analysis with TMRE™ staining after 16 h of erastin treatment. Each bar chart depicts one representative experiment with three replicates per sample* ***D:*** *ATP levels were determined using a luciferase-based assay after 16 h of treatment. Values from five-eight replicate wells per condition are displayed as mean + SD. The luminescence under control conditions is set as 100%.* ***A-D:*** ****p<0.001, **p<0.01, *p<0.05 compared to erastin-treated control; ###p<0.001, ##p<0.01, #p<0.05 compared to untreated control (ANOVA, Scheffé's test).*

In order to evaluate the effects of metformin on the energy supply of HT22 neuronal cells, mitochondrial respiration and the rate of glycolysis were assessed using the Seahorse system (Figure 47A-D). Metformin reduced OCR in a concentration-dependent manner comparable to Ze 450 (Figure 47A) and erastin-mediated reduction of mitochondrial respiration was neither rescued by metformin nor Ze 450 (Figure 47B). Focusing on the ECAR, metformin showed an enhanced basal rate of glycolysis, which was more pronounced than the effect obtained with Ze 450 (Figure 47C), but however, metformin-mediated rescue of the ECAR was less pronounced compared to Ze 450 (Figure 47D). This might explain that Ze 450 was capable to fully rescue erastin-mediated ATP depletion and metformin did not, because ATP production was less compensated by glycolysis in the metformin-treated cells compared to Ze 450 treatment.

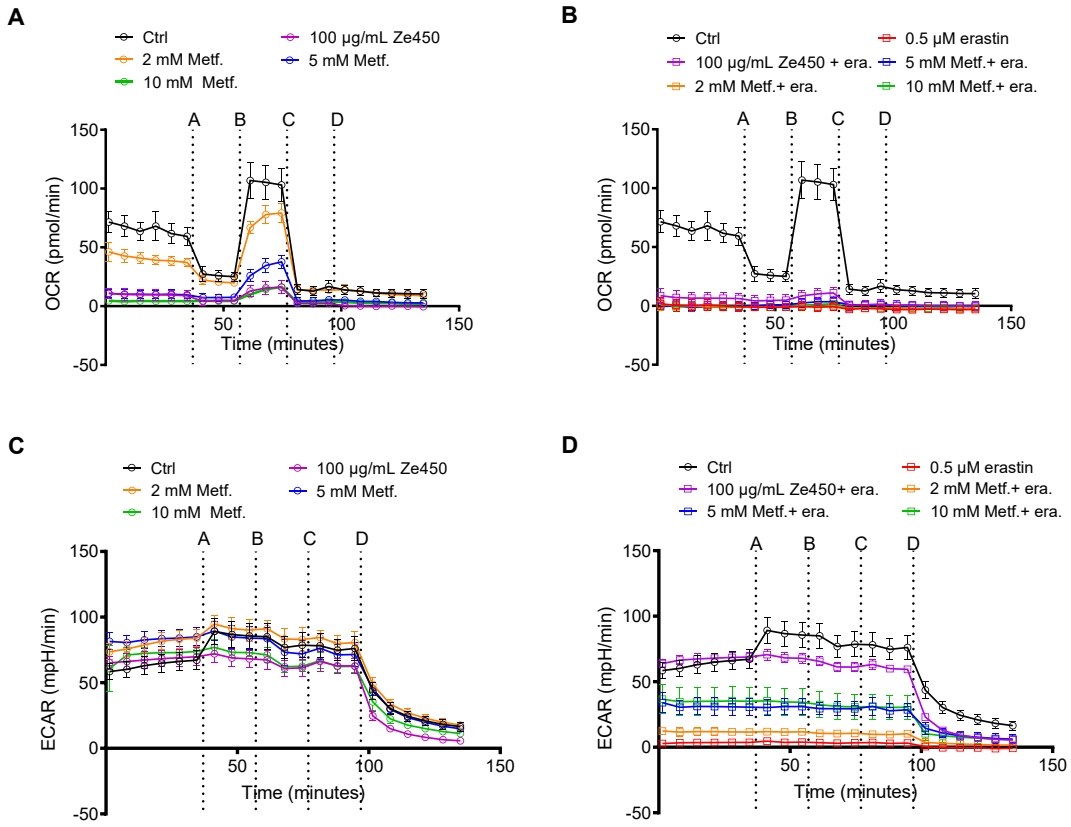

Figure 47. Metformin mediated effects on OCR and ECAR

Data of a representative experiment is depicted, showing OCR and ECAR under basal and oxidative stress conditions. ***A, B:*** *After 16 h of treatment with Ze 450 and metformin* ***(A)*** *and challenged with 0.5 µM erastin* ***(B)****, the oxygen consumption rate (OCR) of HT22 was analyzed with a Seahorse XFe96 Analyzer. Data of 5-8 replicate wells per condition are given as mean ± SD.* ***C, D:*** *After 16 h of treatment with Ze 450 and metformin* ***(C)*** *and challenged with 0.5 µM erastin* ***(D)*** *the extracellular acidification rate (ECAR) was determined with a Seahorse XFe96 Analyzer. Data of 5-8 replicate wells per condition are given as mean ± SD (port A: oligomycin; port B: FCCP; port C: rotenone and antimycin A; port D: 2-deoxyglucose).*

Overall, metformin and Ze 450 mediated similar effects on HT22 cells, but in this study, some main differences were identified. Surprisingly, Ze 450 mediated effects on glycolysis, ATP levels and according cytoprotection were more pronounced and potent compared to metformin in the model system of erastin-mediated oxidative stress.

4.4. Effects of Ze 450 in comparison to estrogen receptor signaling

In previous years, the mechanism of action of *Cimicifuga racemosa* rhizoma extracts had been attributed to an estrogen-like effect, but more recently, this was rebutted [46,166–168]. Moreover, researchers found out, that *Cimicifuga racemosa* extracts were rather anti-estrogenic than exerting hormone-like effects [166,169,170]. Nevertheless, in this study, Ze 450 was compared to 17β-estradiol, estrogen receptor agonists (DPN, PPT), and a selective estrogen receptor modulator (4-OH-Tamoxifen) to gain new insights in this previously proposed mechanism of action.

In order to evaluate the effects of 17β-estradiol on HT22 neuronal cells, metabolic activity was determined. A wide concentration range was tested. Notably, just nanomolar or low micromolar concentrations were considered to mediate hormonal effects, whereas higher micromolar concentrations of 17β-estradiol were described to exhibit anti-oxidant effects [171–173].

At concentrations greater than 100 µM, 17β-estradiol reduced metabolic activity (Figure 48A). Erastin-mediated reduction of metabolic activity was prevented upon 50 µM 17β-estradiol (Figure 48A). Moreover, protection against erastin-induced cytotoxicity was analyzed using the Annexin V/PI assay; here, 17β-estradiol preserved cell viability at 50 µM (Figure 48B, C), while nanomolar concentrations did not demonstrate any protective effect (Figure 48B). At the level of lipid-peroxidation, the results were largely confirmed (Figure 48D). These experiments suggested that protective effects by 17β-estradiol were mediated through its antioxidant effects at high concentration, thereby also supporting the conclusion that estrogen-like effects were not involved in the mechanism of action of Ze 450.

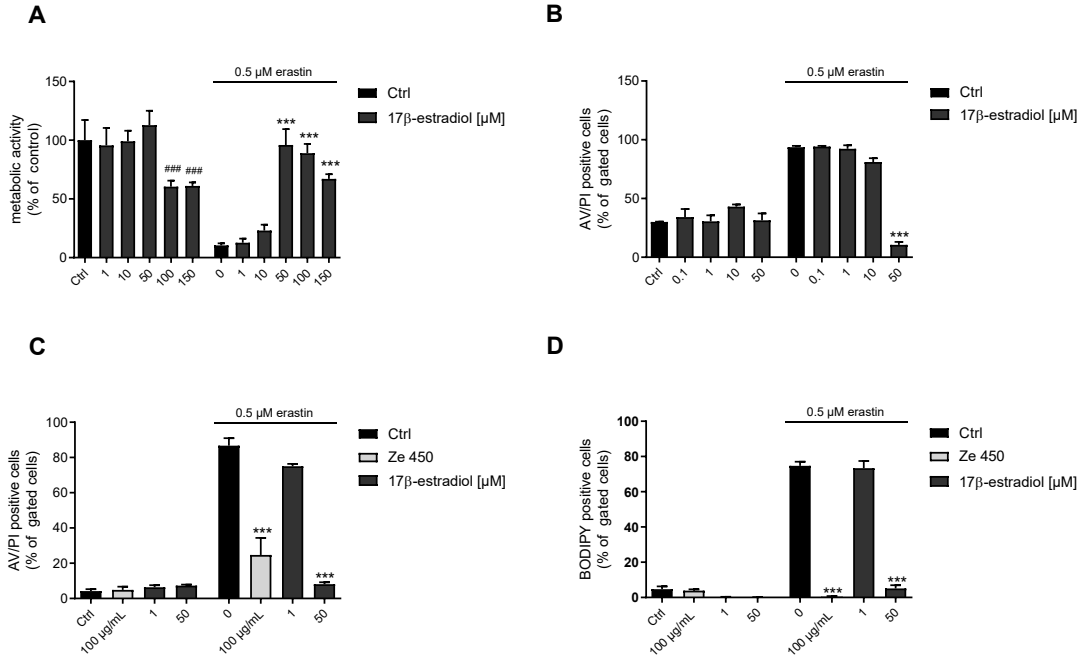

Figure 48. Effects of 17β-estradiol on HT22 cells

A: *Metabolic activity was evaluated in erastin-challenged HT22 cells by measuring MTT formazan absorbance (0.5 µM, 16 h). Eight replicate wells per condition are displayed as mean + SD. The absorbance under control conditions is set as 100%.* ***B, C:*** *Cell death was assessed by flow cytometry using Annexin V and PI staining after 16 h of treatment in HT22 cells. The bar graph shows one representative experiment with three replicates per sample (mean + SD; 5,000 cells per replicate).* ***D:*** *Lipid-peroxidation was assessed by flow cytometry using BODIPY™ after 8 h. The bar graph shows one representative experiment with three replicates per sample (***p<0.001, **p<0.01 compared to erastin-treated control; ###p<0.001 compared to untreated control; ANOVA, Scheffé´s test).*

In particularly, mitochondrial function was analyzed with special regard on the energy phenotype of cells treated with 17β-estradiol in comparison to Ze 450 treatment (Figure 49A-D). Opposite to Ze 450, 1 µM of 17β-estradiol led to an increase in mitochondrial respiration (Figure 49A). 50 µM of 17β-estradiol acted in a similar fashion like Ze 450 as it decreased OCR (Figure 49A). In contrast to Ze 450, erastin-mediated reduction of OCR was partly prevented by 50 µM 17β-estradiol (Figure 49B). Regarding the basal rate of glycolysis, there was no difference observed between 17β-estradiol-treated and control conditions (Figure 49C). The reduction of the ECAR mediated by erastin was partly prevented by 50 µM 17β-estradiol and Ze 450 (Figure 49D).

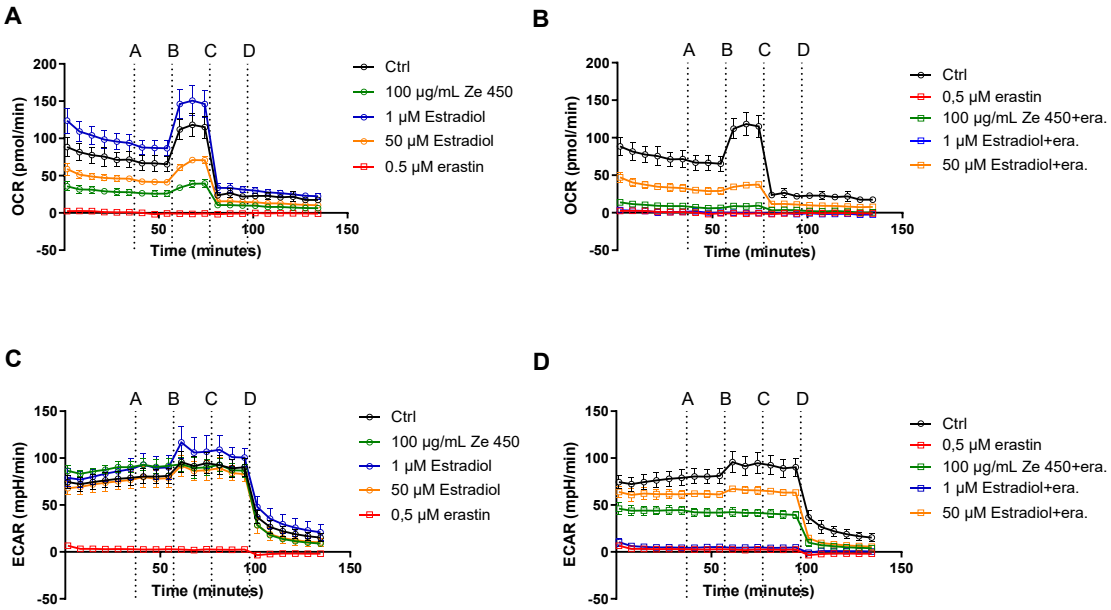

Figure 49. Effects of 17β-estradiol on energy metabolism

Data of a representative experiment is depicted, showing OCR and ECAR under basal and oxidative stress conditions. ***A, B:*** *After 16 h of treatment with Ze 450 and 17β-estradiol* ***(A)*** *and challenged with 0.5 µM erastin* ***(B)****, the oxygen consumption rate (OCR) of HT22 was analyzed with a Seahorse XFe96 Analyzer. Data of 5-8 replicate wells per condition are given as mean ± SD.* ***C, D****: After 16 h of treatment with Ze 450 and 17β-estradiol* ***(C)*** *and challenged with 0.5 µM erastin* ***(D)*** *the extracellular acidification rate (ECAR) was determined with a Seahorse XFe96 Analyzer. Data of 5-8 replicate wells per condition are given as mean ± SD (port A: oligomycin; port B: FCCP; port C: rotenone and antimycin A; port D: 2-deoxyglucose).*

Moreover, the estrogen receptor agonists (DPN and PPT) were used to investigate selective estrogen-mediated signaling in comparison to Ze 450. Estrogen binds to two different isoforms of the estrogen receptor (ER) alpha and beta. ERα can be found, for example, in the mammary gland, male reproductive organs, bone and brain, and ERβ is localized in pulmonary epithelial cells, uterus and also in the brain. DPN preferentially binds to ERβ and PPT is binding to ERα.

Both agonists did not affect metabolic activity and did not prevent erastin-mediated oxidative damage, which was assessed via the MTT assay (Figure 50A, B).

Furthermore, combined treatment of the ER agonists together with 100 µg/mL of Ze 450 did not exceed Ze 450-mediated effects (Figure 50C).

In addition, 4-OH-Tamoxifen, the active metabolite of tamoxifen and a selective estrogen receptor modulator with tissue-specific agonistic and antagonistic effects, was tested. Tamoxifen is a known antagonist of ER in breast tissue and therefore used to treat breast cancer [174].

Here, the effects of 4-OH-Tamoxifen were compared to Ze 450 in neuronal cells exposed to oxidative stress. 50 µM 4-OH-Tamoxifen strongly reduced metabolic activity (Figure 50D), and in the erastin model of ferroptosis in HT22 cells, 10 µM 4-OH-Tamoxifen mediated protection against oxidative damage (Figure 50D). To further analyze synergistic or additive effects of Ze 450 with 4-OH-Tamoxifen, sub-protective concentrations of 4-OH-Tamoxifen (0.5 and 1 µM) were used (Figure 50E). In this study, no additional effects of 4-OH-Tamoxifen were detected on metabolic activity compared to Ze 450 alone (Figure 50E).

The MTT assay, however, does not differentiate between metabolic effects and cytotoxicity. Therefore, propidium iodide staining with subsequent flow cytometry analysis was used to investigate cell death (Figure 50F). In accordance with the previous findings, Ze 450 protected against erastin-mediated cytotoxicity, while there was no additive or synergistic effect observed, neither for ER agonists (DPN, PPT) nor for 4-OH-Tamoxifen (Figure 50F).

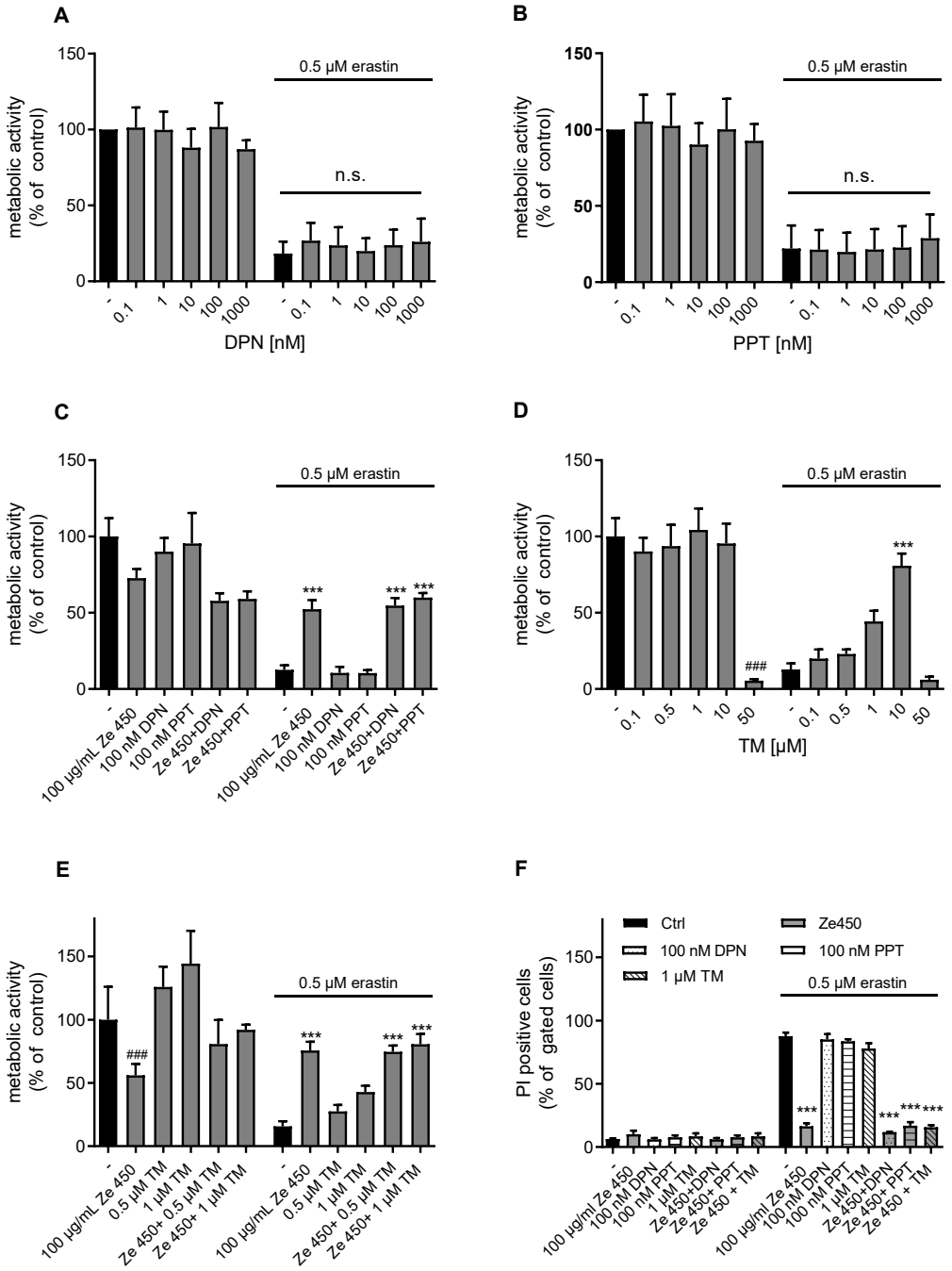

Figure 50. Effects of ER agonists and 4-OH-Tamoxifen on HT22 neuronal cells in comparison to Ze 450

A+B: *Metabolic activity was evaluated in erastin-challenged HT22 cells by measuring MTT formazan absorbance (0.3-0.5 µM, 16 h). Eight replicate wells per condition of four independent experiments are displayed as mean + SD. The absorbance under control conditions is set as 100%.* ***C-E:*** *Metabolic activity was evaluated in erastin-challenged HT22 cells by measuring MTT formazan absorbance (0.3-0.5 µM, 16 h). Eight replicate wells per condition of one representative experiment are displayed as mean + SD. The absorbance under control conditions is set as 100%.* ***A:*** *DPN;* ***B:*** *PPT,* ***C:*** *DPN, PPT combined with 100 µg/mL Ze 450;* ***D:*** *4-OH-Tamoxifen;* ***E:*** *4-OH-Tamoxifen combined with 100 µg/mL Ze 450.* ***F:*** *Cell death was assessed by flow cytometry using PI staining after 16 h of treatment (DPN, PPT, 4-OH-Tamoxifen, Ze 450) in HT22 cells. The bar graph shows one representative experiment with three replicates per sample (mean + SD; 5,000 cells per replicate).* ***A-F:*** ****p<0.001 compared to erastin treated control, ###p<0.001 compared to untreated control (ANOVA, Scheffé´s test).*

Overall, the mode of action of Ze 450 is most likely independent of estrogen-receptor-mediated signaling, since 17β-estradiol only provided protection at concentrations mediating antioxidant effects. In contrast, appropriate concentrations of 17β-estradiol and the ER agonists, as well as 4-OH Tamoxifen, did not exceed Ze 450 mediated effects on metabolic activity. Furthermore, no additive or synergistic effects of the tested ER-binding compounds were detected in HT22 neuronal cells.

4.5. Effects of Ze 450 on longevity

Caenorhabditis elegans has been widely used as a model organism to investigate the effects of pharmacological compounds, genetic approaches, and nutritional or other environmental factors on lifespan and is a suitable model organism to study behavior. In addition, heat shock is an established method to assess lifespan after a stress insult [102], which impedes transcriptional and translational processes of most proteins [105]. In this study, heat shock conditions were used as a screening tool to elucidate an optimal concentration range of Ze 450 for a long-term lifespan assay in the *C. elegans* model. It was found that Ze 450 affected the survival of *C. elegans* in a concentration-dependent manner under heat shock conditions (Figure 51A). From these initial results, 100 µg/mL of Ze 450 was considered as an appropriate concentration for an experiment investigating paraquat (PQ)-induced stress (Figure 51B). Paraquat led to a reduction of median survival from 11 h (vehicle) to 8 h. Ze 450 was capable to improve overall survival and improved median survival compared to PQ treated conditions in the heat shock assay (9.5 h; Figure 51B).

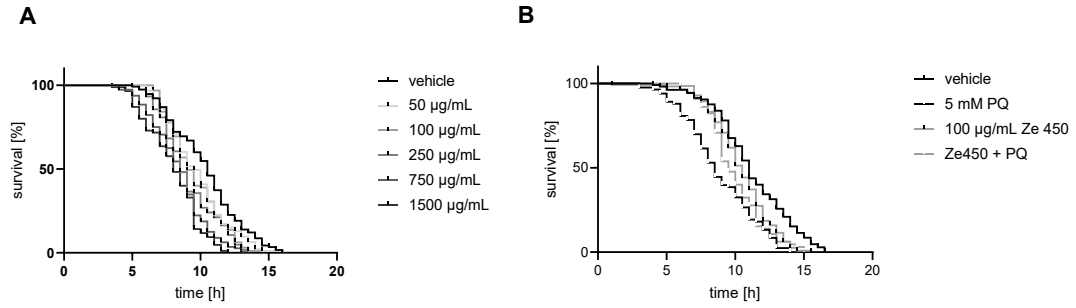

Figure 51. Effects of Ze 450 on C. elegans under heat shock and paraquat (PQ) treatment

A: *Effects of different concentrations of Ze 450 in a heat stress model system in C. elegans. 50-250 µg/mL Ze 450 did not affect lifespan, while worms treated with 750 or 1500 µg/mL showed a decrease in lifespan (*p<0.05, n= 85-115).* ***B:*** *Effects of 100 µg/mL Ze 450 in a model system of paraquat (PQ) induced oxidative stress in C. elegans (n=65-113, ***p<0.001 PQ compared to vehicle, *p<0.05 Ze 450 + PQ compared to PQ).*

As metformin is known to prolong lifespan [175,176] and as it acts in a similar fashion on mitochondrial metabolism like Ze 450 in HT22 cells it was used as a control substance. In line with previous investigations for effects of Ze 450, the heat stress survival assay was used to test for an effective concentration range of metformin (Figure 52A). The results showed that 50 and 100 mM metformin decreased survival of *C. elegans*, while 25 mM led to an increase in survival compared to vehicle control (Figure 52A). In the paraquat-induced stress model system, 25 mM metformin demonstrated an

improvement of survival in paraquat challenged nematodes compared to PQ treated control condition (Figure 52B).

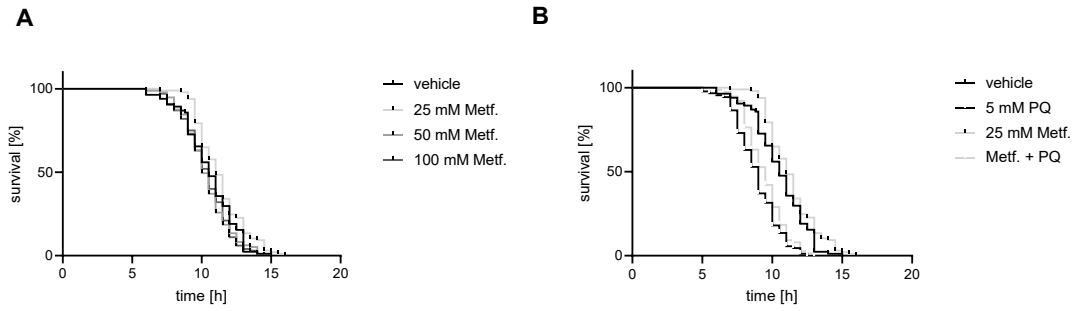

Figure 52. Effects of metformin on C. elegans under heat shock and PQ treatment

A: *Effects of metformin (25-100 mM) in a heat stress model system in C. elegans. 25 mM metformin improved lifespan (*p<0.05 compared to M9 vehicle control), while treatment with ≥50 mM metformin did not affect lifespan (n=75-97).* ***B:*** *Effects of 25 mM metformin in a model system of paraquat (PQ) induced oxidative stress in C. elegans (n=76-97, ***p<0.001 PQ compared to M9 vehicle, *p<0.05 25 mM metformin +PQ compared to PQ).*

Next, a real-time assay without further stress conditions was performed to elucidate the influence of Ze 450 and metformin on the life cycle of worms. There was no difference observed regarding overall and median survival between the control conditions (Figure 53A), therefore, OP50 was used as a standard feeding control; M9 was the vehicle for metformin and 1% ethanol for Ze 450. In contrast to the heat shock survival assay, 100 µg/mL Ze 450 prolonged the overall survival in the real-time setting (Figure 53B). The Ze 450 extract improved the median survival (24 days) compared to vehicle control (20 days) (Figure 53B). Metformin (25 mM) improved the overall survival rate compared to the vehicle control (Figure 53C), but not the median survival rate (22 days for both, M9 and 25 mM metformin). In conclusion, Ze 450 was more effective on both parameters overall survival and median survival rates than the approved drug metformin in this setting.

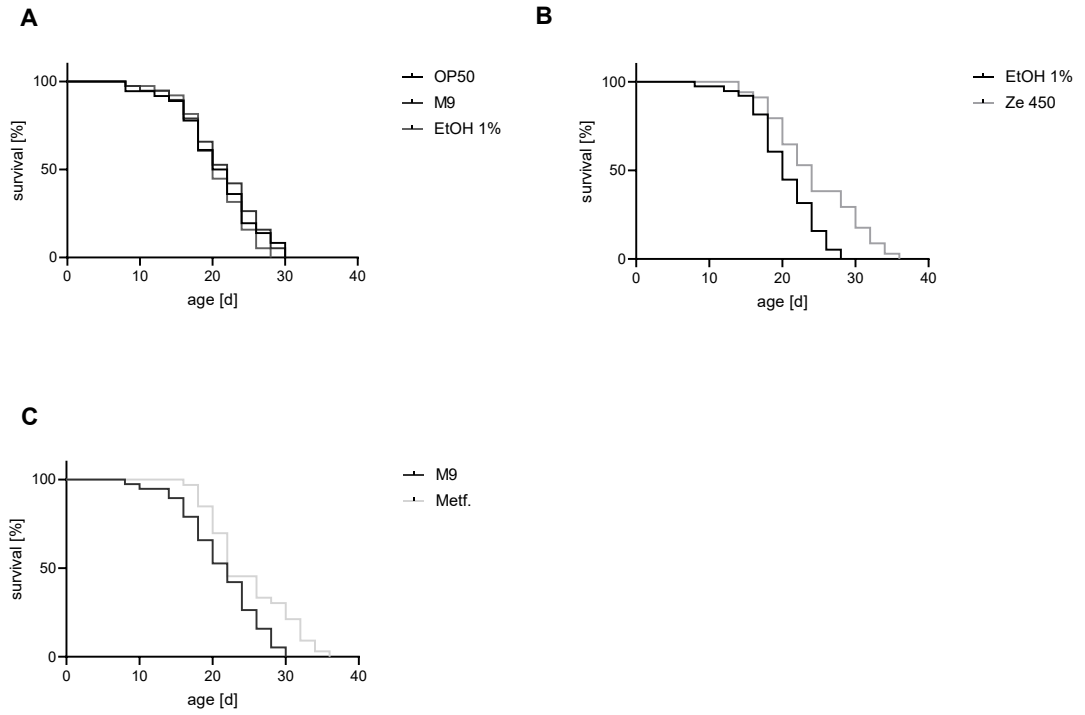

Figure 53. Lifespan analysis

A-C: *Lifespan was analyzed using 40 healthy animals for each group. Control conditions (OP50, M9 and EtOH) showed comparable lifespan, while 100 µg/mL Ze 450 (***p<0.001) and 25 mM metformin (**p<0.01) improved lifespan compared to vehicle control (1% EtOH, M9).*

C. elegans have a pronounced sensory and olfactory system since this is essential for their survival. It has been shown that *C. elegans* respond in a regulated manner to certain sensory stimuli [88], thus making the nematodes suitable to study for chemotactic behavior in response to olfactory sensing as an indicator for neuronal function [156]. The chemotactic index was improved in both, Ze 450 (100 µg/mL) and metformin (25 mM) treated conditions (Figure 54A).

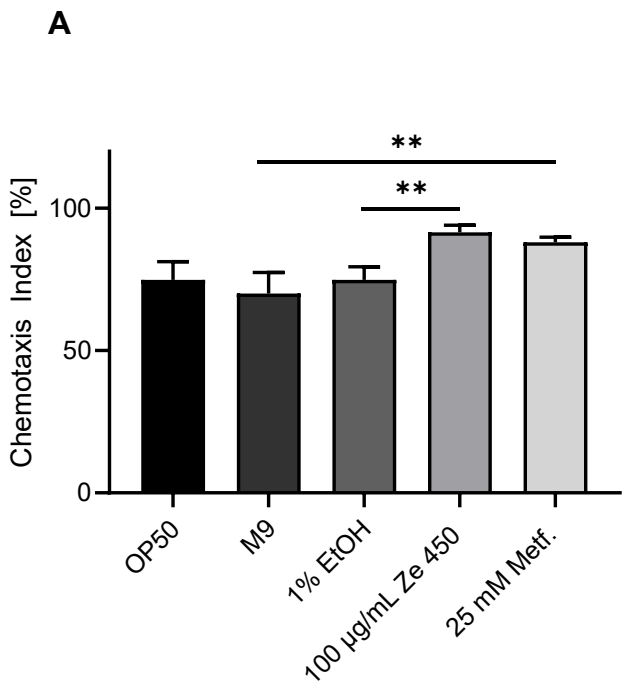

Figure 54. Chemotactic behavior of C. elegans treated with Ze 450 and metformin

A: *Chemotaxis was assessed using four replicates of each condition using 100-200 worms per plate. Chemotaxis index was calculated as followed: ((number of attractant – number of control) / number total).*

Taken together, the findings in *C. elegans* demonstrated that Ze 450 improved lifespan and chemotactic behavior, i.e. neuronal functions suggesting that Ze 450 mediates beneficial effects on the level of a whole organism.

4.6. Effects of Ze 450 on liver cells

In the context of drug metabolism research focuses on the liver since this organ is responsible for the majority of metabolic processes. For this purpose, Ze 450 was exposed to liver cells and metabolic parameters including cellular energy supply were analyzed. Moreover, the human hepatoma cell line HepG2 was used as it is a common system for toxicological studies to address the ongoing discussion about plant extracts causing hepatotoxicity [177]. In this study, aspects of cytotoxicity and mitochondrial involvement in response to oxidative stress were investigated. Since erastin treatment only exerted minor toxicity in the hepatoma cells, the GPX4 inhibitor, RSL-3, was applied in this liver cell line to directly induce ferroptotic oxidative stress. RSL-3 [178] acts downstream of the cysteine/glutamate antiporter and directly blocks the GPX4 independent of glutathione depletion, thereby leading to lipid-peroxidation and to ferroptosis-associated comparable cell death signaling pathway such as erastin treatment (Figure 3). Figure 55A shows that Ze 450 did not induce cell death at concentrations up to 200 µg/mL. The toxic effects were exerted at very high concentrations above the therapeutic range relevant for the treatment of postmenopausal complaints (Figure 55A). Moreover, at concentrations higher than 50 µg/mL Ze 450 protected against RSL-3-mediated cytotoxicity (Figure 55B).

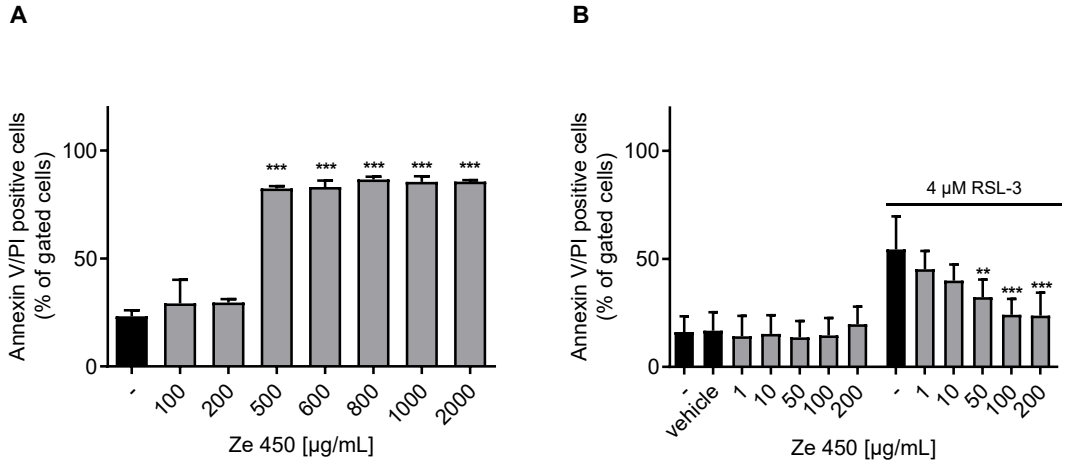

Figure 55. Effects of Ze 450 on cell viability in HepG2 cells

A: *Cell death was assessed by flow cytometry using Annexin V and PI after 16 h of treatment in HepG2 cells. The bar graph shows a representative experiment with three replicates per sample (mean + SD; 5,000 cells per replicate, ***p<0.001 compared to untreated control; ANOVA, Scheffé´s test).* ***B:*** *Cell death was assessed by flow cytometry using Annexin V and PI after 16 h of treatment in HepG2 cells. The bar graph shows consolidated data from three independent experiments with each three replicates per sample (mean + SD; 5,000 cells per replicate, ***p<0.001 compared to RSL-3 treated control; ANOVA, Scheffé´s test).*

As detected previously in the neuronal cell lines, Ze 450 affected mitochondrial function by inducing a bioenergetic shift from mitochondrial respiration towards glycolysis that mediated protection of mitochondrial integrity and reduced mitochondrial ROS formation. Therefore, investigating the effects of Ze 450 on mitochondrial parameters on human HepG2 cells was of major interest. Analyzing lipid ROS levels using C11-BODIPY staining and FACS analysis revealed that Ze 450 did not affect lipid-peroxidation after 8 h and 16 h under basal conditions (Figure 56A). In contrast, RSL-3-induced lipid-peroxidation was abolished by concentrations greater than 1 µg/mL of Ze 450 after 8 hours of treatment. At the later time point (16 h) 100 µg/mL of Ze 450 prevented oxidative stress-mediated increase in lipid-peroxidation. In the model system of HepG2 cells, Ze 450 attenuated RSL-3-mediated mitochondrial ROS formation, while Ze 450 alone did not induce an increase in mitochondrial ROS levels (Figure 56C). Moreover, mitochondrial membrane potential was not affected by Ze 450, while the RSL-3-induced loss of mitochondrial membrane potential was prevented by concentrations of Ze 450 greater than 10 µg/mL (Figure 56D). ATP levels remained unaltered by Ze 450 at concentrations up to 200 µg/mL, while RSL-3-mediated ATP depletion was rescued by Ze 450 at concentrations higher than 100 µg/mL (Figure 56E).

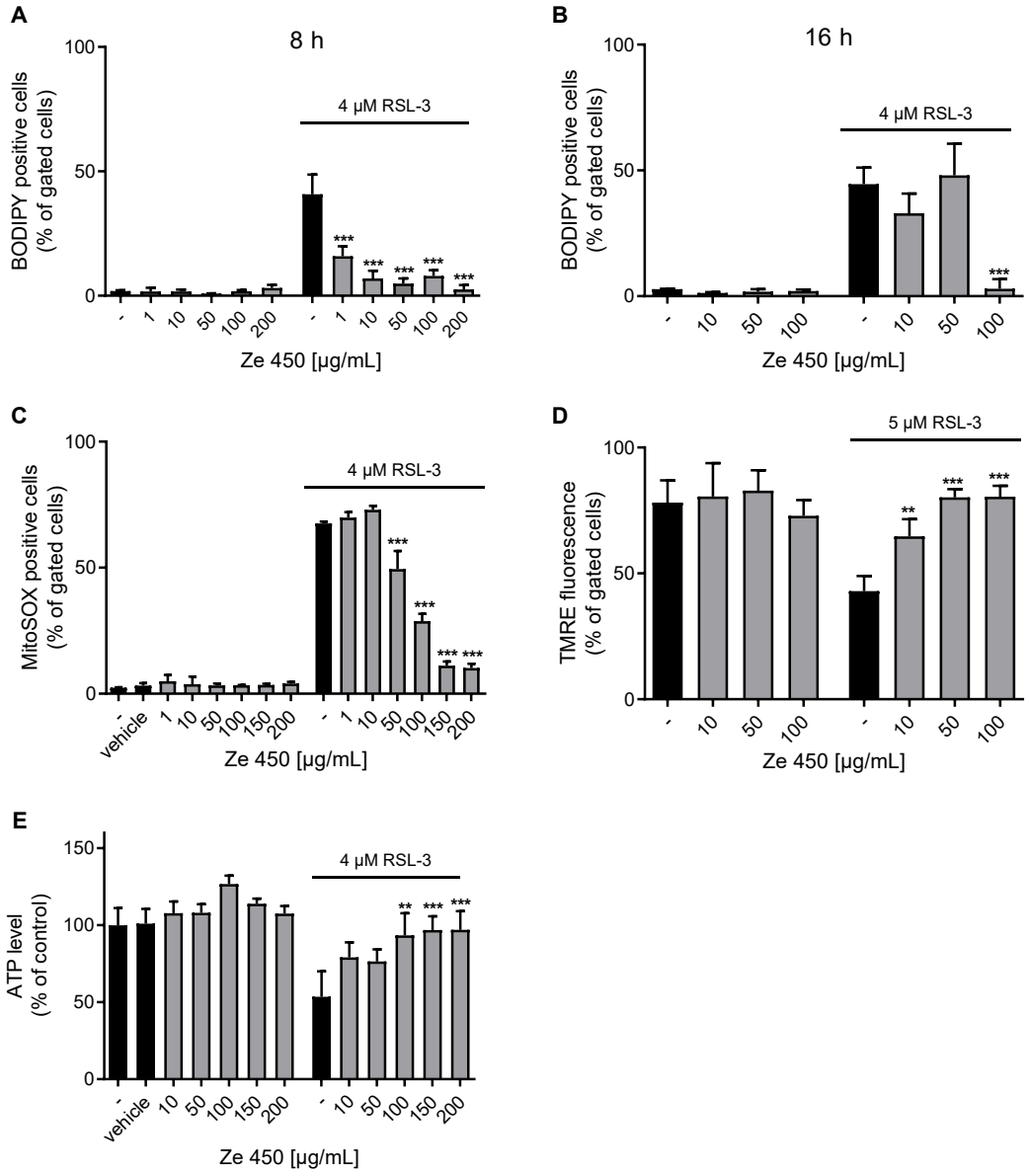

Figure 56. Effects of Ze 450 on lipid-peroxidation and mitochondrial parameters in HepG2 cells

A, B*: Lipid-peroxidation was assessed by flow cytometry using BODIPY™ after 8 and 16 h. The bar graph shows one representative experiment with three replicates per sample.* ***C:*** *Mitochondrial ROS formation was measured by flow cytometry using MitoSOX™ after 16 h of treatment. The bar graph shows one representative experiment with three replicates per treatment.* ***D:*** *Mitochondrial membrane potential was assessed via flow cytometric analysis with TMRE™ staining after 16 h of RSL-3 treatment. Each bar chart depicts one representative experiment with three replicates per sample* ***E:*** *ATP levels were determined using a luciferase-based assay after 16 h of treatment. Values from five-eight replicate wells per condition are displayed as mean + SD. The luminescence under control conditions is set as 100%.* ***A-E:*** ****p<0.001, **p<0.01, *p<0.05 compared to erastin-treated control, ###p<0.001, ##p<0.01, #p<0.05 compared to untreated control (ANOVA, Scheffé's test).*

For detailed analysis of mitochondrial respiration and glycolysis, OCR and ECAR were assessed using the Seahorse system. Consistent with the previous results obtained in models of erastin and glutamate-induced oxidative stress in neuronal cells, Ze 450 reduced OCR in a concentration-dependent manner in the liver cells (Figure 57A) and did not affect the reduction of mitochondrial respiration mediated by RSL-3 (Figure 57B). At the level of glycolysis, Ze 450 acted in a comparable manner like control cells (Figure 57C). Nevertheless, Ze 450 prevented RSL-3-mediated reduction of ECAR (Figure 57D).

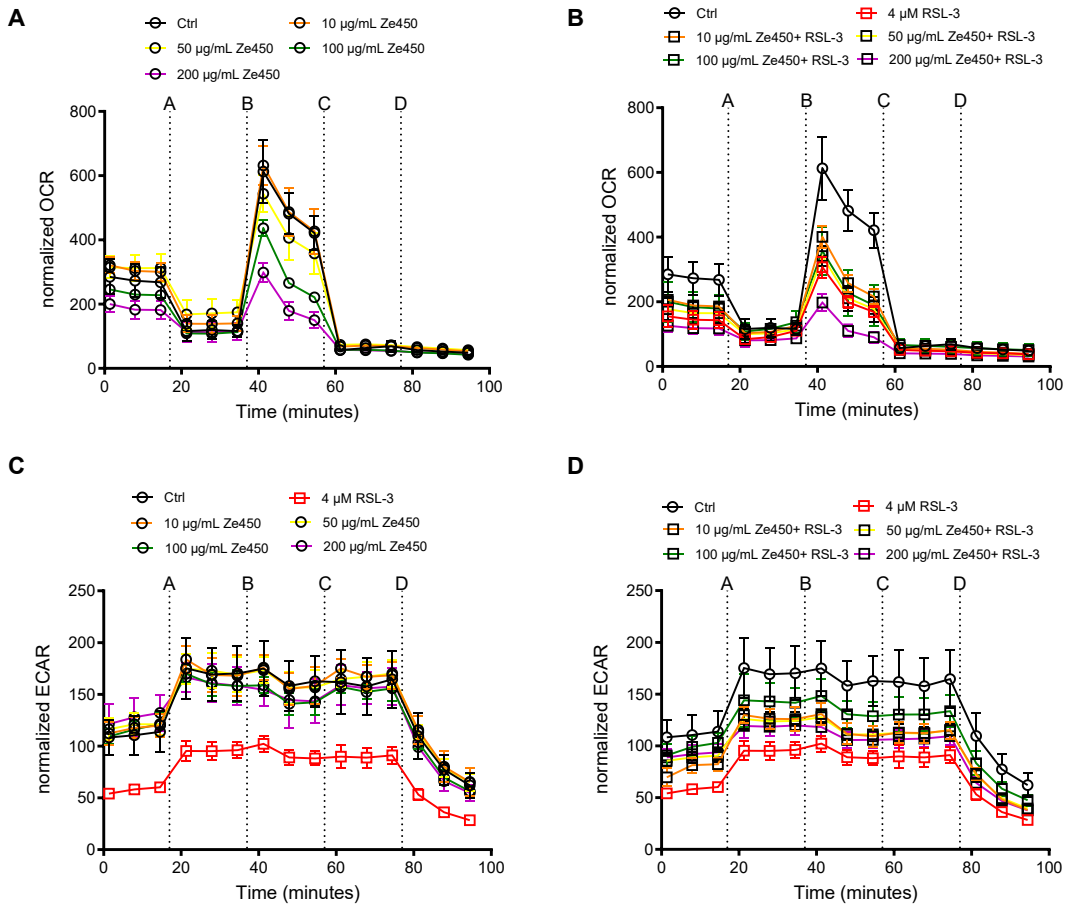

Figure 57. Ze 450 mediated effects on OCR and ECAR in HepG2 liver cells

Data of a representative experiment is depicted, showing OCR and ECAR under basal and oxidative stress conditions. ***A, B:*** *After 16 h of treatment with Ze 450* ***(A)*** *and challenged with 4 µM RSL-3* ***(B)****, the oxygen consumption rate (OCR) of HepG2 cells was analyzed with a Seahorse XFe96 Analyzer. Data of 5-8 replicate wells per condition are given as mean ± SD.* ***C, D****: After 16 h of treatment with Ze 450* ***(C)*** *and challenged with 4 µM RSL-3* ***(D)*** *the extracellular acidification rate (ECAR) was determined with a Seahorse XFe96 Analyzer. Data of 5-8 replicate wells per condition are given as mean ± SD (port A: oligomycin; port B: FCCP; port C: rotenone and antimycin A; port D: 2-deoxyglucose).*

HepG2 cells were derived from human heptoma, but they do not express all cytochrome P enzymes, which are important for drug metabolism. Because of this lack of metabolic activity in the HepG2 cells, H4IIE cells were used, in addition. H4IIE cells are derived

from rat hepatoma and an established model system for studies of cytochrome P450 enzyme activity and induction [179,180].

Consistent with the previous results (Chapter 4.1.), the H4IIE cells demonstrated in response to Ze 450 a slight reduction of metabolic activity in response to Ze 450 in the MTT assay (Figure 58A). In contrast to HepG2 cells, erastin treatment led to sufficient oxidative damage and was used for the experiments in H4IIE cells as oxidative stressor. Erastin-mediated reduction of metabolic activity was prevented at concentrations of Ze 450 higher than 50 µg/mL (Figure 58A). Under basal conditions, Ze 450 alone did not exert any cytotoxic effect in the tested concentration range (Figure 58B). The AnnexinV/PI assay confirmed that erastin-induced cytotoxicity was prevented by concentrations higher than 50 µg/mL of Ze 450 (Figure 58B). Moreover, mitochondrial ROS formation was investigated (Figure 58C), also confirming the protective effects of Ze 450 obtained in HepG2 cells and neuronal cell lines. Overall, these results showed that Ze 450 did not exert toxic effects on the liver cells but rather protected these from the oxidative challenge, indicating that Ze 450 mediates protective effects in a variety of different cell types.

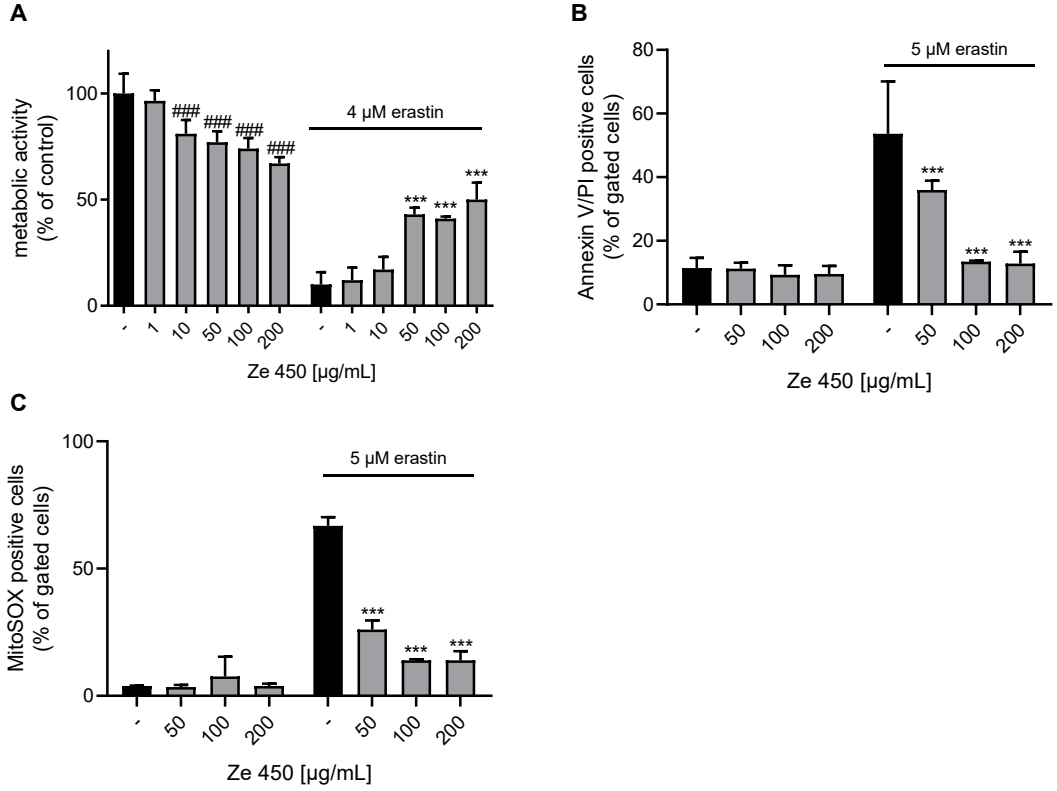

Figure 58. Effects of Ze 450 an H4IIE cells

A: *Metabolic activity was evaluated in erastin-challenged H4IIE cells by measuring MTT formazan absorbance (4 µM, 16 h). Eight replicate wells per condition are displayed as mean + SD. The absorbance under control conditions is set as 100%.* ***B:*** *Cell death was assessed by flow cytometry using Annexin V and PI after 16 h of treatment in H4IIE cells. The bar graph shows one representative experiment with three replicates per sample (mean + SD; 5,000 cells per replicate).* ***C:*** *Mitochondrial ROS formation was measured by flow cytometry using MitoSOX™ after 16 h of treatment. The bar graph shows a representative experiment with three replicates per treatment.* ***A-C:*** ****p<0.001 compared to erastin-treated control, ###p<0.001 compared to untreated control (ANOVA, Scheffé's test).*

To further analyze direct effects on liver mitochondria, the organelles were isolated from rat liver for functional investigations using the coupling and the electron flow assay.

Isolated liver mitochondria were exposed to 100 µg/mL Ze 450 in the presence of rotenone and succinate. Notably, initial OCR of control and treated mitochondria was low, in turn, there was no statistical difference observed between the different pretreatment paradigms (Figure 59A). After injection of FCCP (port C) Ze 450 treatment demonstrated a less pronounced increase in OCR compared to control mitochondria.

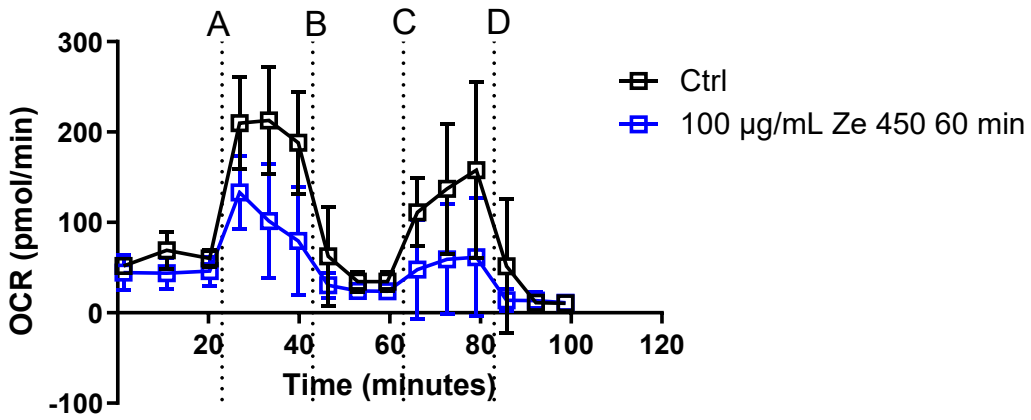

Figure 59. Effects of Ze 450 on isolated liver mitochondria (coupling assay)

A: *OCR was analyzed after 30 and 60 min of incubation with Ze 450 (100 µg/mL). ADP, oligomycin, FCCP and antimycin A were injected successively. Rotenone was initially present and hence respiration is being driven by complex II-IV activity.*

Moreover, complex I functionality of liver mitochondria treated with Ze 450 was analyzed. While 50 µg/mL of Ze 450 did not impact electron flow, 100 µg/mL of Ze 450 slightly reduced OCR after FCCP injection, but the effect was not statistically significant (Figure 60A).

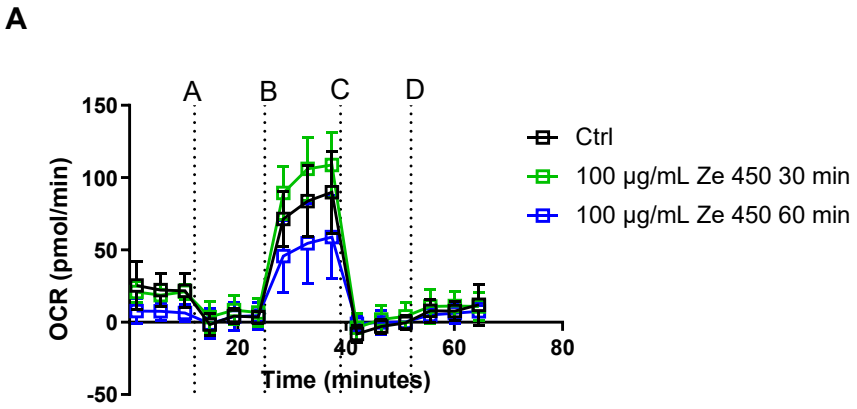

Figure 60. Ze 450 affects mitochondrial complex I functionality

***A, B**: OCR was analyzed after 60 min of incubation with Ze 450 (100 µg/mL). Rotenone, FCCP, antimycin A and ascorbate with TMPD were injected successively. Pyruvate and malate were initially present and hence respiration is being driven by complex I.*

Taken together, the results in liver cells and isolated liver mitochondria supported the previous findings in neurons, suggesting that Ze 450 impaired mitochondrial respiration in a direct manner, thereby reducing mitochondrial ROS formation and mediating protection against oxidative damage.

4.7. Effects of Ze 339 on neuronal cells

4.7.1. Effects of Ze 339 on cell viability and proliferation

In order to study the influence of Ze 339 on neuronal cells, cell death was analyzed to determine a non-toxic concentration range of Ze 339 (Figure 61A). Ze 339 induced cell death at concentrations of 100 µg/mL (Figure 61A), consequently, 50 µg/mL of Ze 339 was set as the highest concentration tested in the following experiments. Furthermore, erastin-mediated cell death was prevented by 10 and 50 µg/mL Ze 339 detected with Annexin V and propidium iodide (Figure 61A). Metabolic activity was reduced by 1 µg/mL of Ze 339 compared to the controls (Figure 61B), and in the same concentration range, metabolic activity was preserved after erastin exposure (Figure 61B). Reduced metabolic activity upon Ze 339 suggested an influence of the extract on cell metabolism, these finding was supported by impaired proliferation measured with the xCELLigence system. Ze 339 reduced proliferation in a concentration-dependent manner (Figure 61C). Interestingly, erastin-mediated reduction in cell index was not compensated by Ze 339 (Figure 61C).

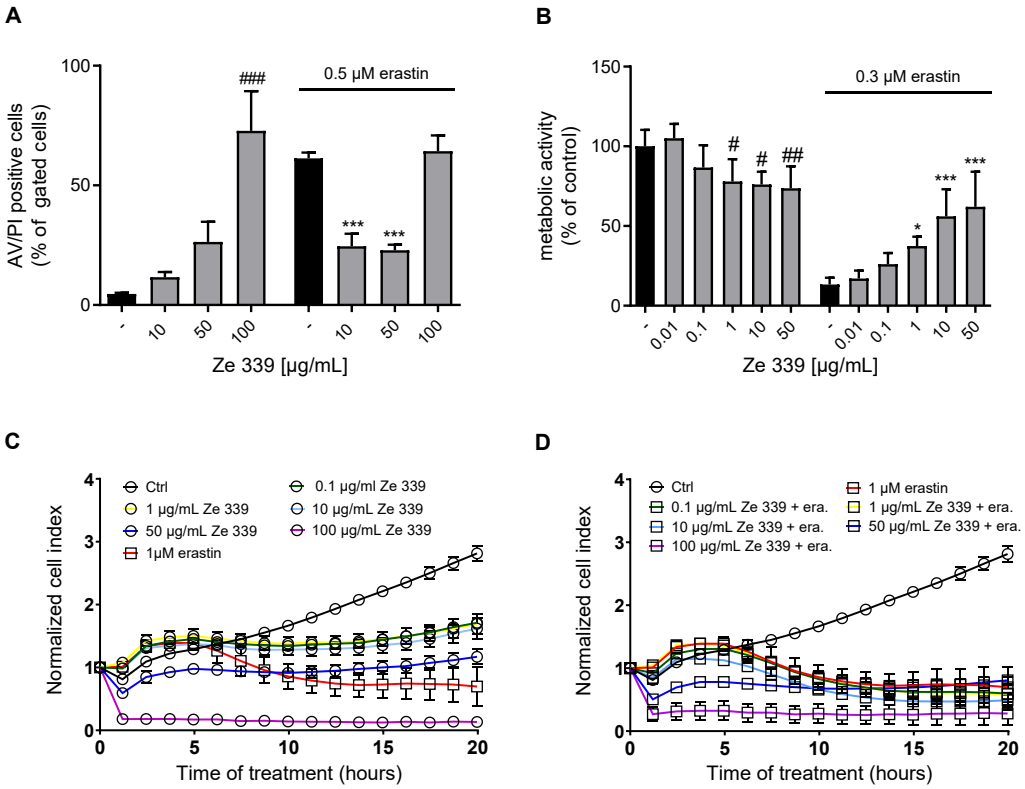

Figure 61. Effects of Ze 339 on cell viability and proliferation

A: *Cell death was assessed by flow cytometry using Annexin V and PI staining after 16 h of treatment in HT22 cells. The bar graph shows one representative experiment with three replicates per sample (mean + SD; 5,000 cells per replicate).* ***B:*** *MTT assay was performed after 16 h of treatment with Ze 339 and erastin in HT22 cells. Eight replicate wells per condition are displayed as mean + SD. The absorbance under control conditions is set as 100 %.* ***A-B:*** ****p<0.001, *p<0.05 compared to erastin-treated control; ##p<0.01, #p<0.05 compared to untreated control (ANOVA, Scheffé's test)* ***C-D:*** *xCELLigence measurements were conducted after the indicated treatment was added (n=4-6/treatment condition). Data are displayed as mean ± SD.*

4.7.2. Effects of Ze 339 on mitochondrial function and bioenergetics

Next, lipid-peroxidation was assessed to analyze soluble ROS formation. After 8 h of exposure Ze 339 induced an increase in green fluorescence detecting oxidized lipids (Figure 62B), which was statistically significant at 50 µg/mL Ze 339 (Figure 62A). Nevertheless, the even more pronounced erastin-mediated lipid-peroxidation was attenuated with 1-50 µg/mL of Ze 339 at this time point of incubation (Figure 62C, D).

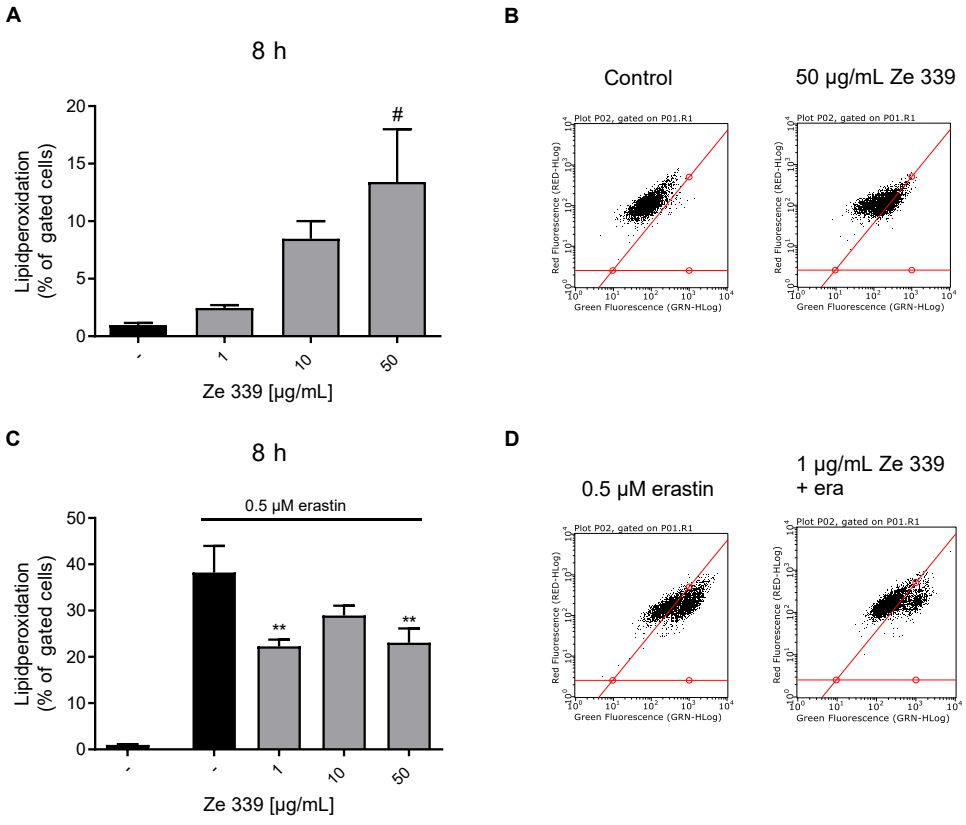

Figure 62. Impact of Ze 339 on lipid-peroxidation

*Lipid-peroxidation was assessed by flow cytometry using BODIPY™ after the indicated time of treatment. The bar graph shows one representative experiment with three replicates per sample (mean + SD; 5,000 cells per replicate; **p<0.01 compared to erastin-treated control; #p<0.05 compared to untreated control; ANOVA, Scheffé's test).* ***A, C:*** *Quantification* ***B, D:*** *representative flow cytometry histograms*

To gain insights, whether Ze 339 induced superoxide generation by mitochondria, mitochondrial ROS formation was investigated after 8 h of treatment. At concentrations greater than 10 µg/mL of Ze 339 an increase in red fluorescence detected under basal incubation conditions (Figure 63A, B). However, the erastin-mediated mitochondrial ROS formation was partly prevented with 1 µg/mL of Ze 339 at this time point. Notably, 10 and 50 µg/mL of Ze 339 were not effective against oxidative stress-mediated damage after 8 h of treatment.

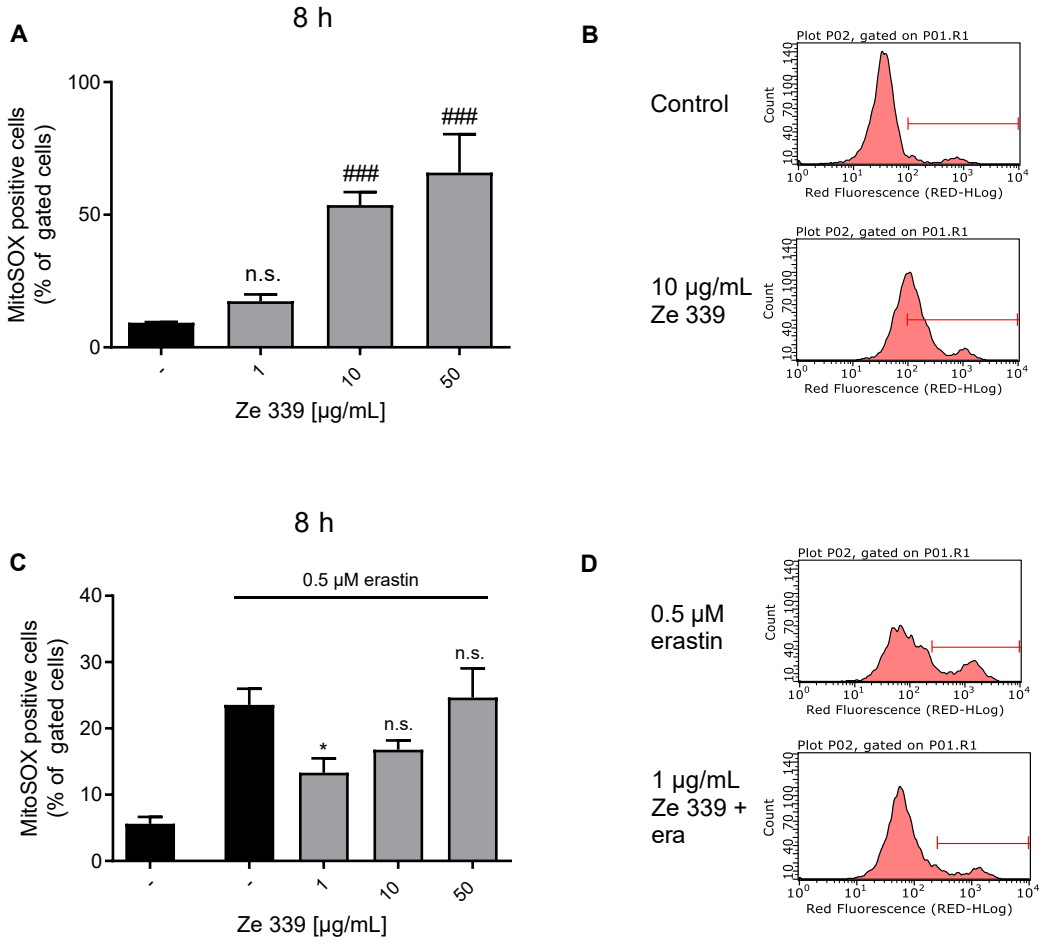

Figure 63. Effects of Ze 339 on mitochondrial ROS formation after 8 h of treatment

*Mitochondrial ROS formation was assessed by flow cytometry using MitoSOX™ after 8 h of treatment. The bar graph shows one representative experiment with three replicates per sample (mean + SD; 5,000 cells per replicate, *p<0.05 compared to erastin treated control; ###p<0.001 compared to untreated control; ANOVA, Scheffé's test).* ***A, C:*** *Quantification* ***B, D:*** *representative flow cytometry histograms, two different gates were used to differentiate between smaller* ***(B)*** *and greater changes* ***(D)****.*

The basal effect of Ze 339 on mitochondrial ROS formation was at a similar level after 16 h of incubation (Figure 64A, B), while erastin-mediated induction of superoxides was more pronounced after 16 h compared to the 8 h treatment. In turn, also 10 and 50 µg/mL

of Ze 339 protected against erastin-induced mitochondrial ROS formation at 16 hours of incubation (Figure 64C, D).

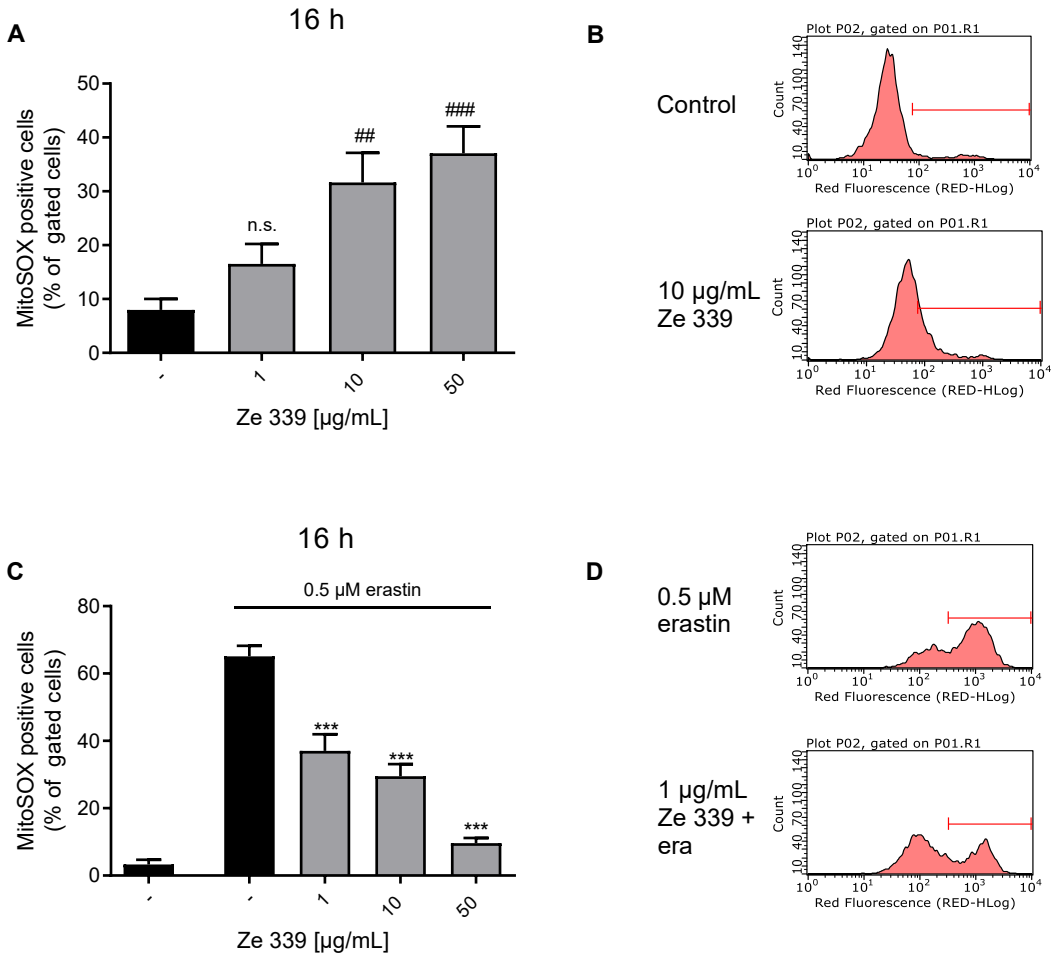

Figure 64. Effects of Ze 339 on mitochondrial ROS formation after 16 h of treatment

*Mitochondrial ROS formation was assessed by flow cytometry using MitoSOX™ after 16 h of treatment. The bar graph shows a representative experiment with three replicates per sample (mean + SD; 5,000 cells per replicate, ***p<0.001 compared to erastin treated control; ###p<0.001, ##p<0.01 compared to untreated control; ANOVA, Scheffé's test).* ***A, C:*** *Quantification* ***B, D:*** *representative flow cytometry histograms, two different gates were used to differentiate between smaller* ***(B)*** *and greater changes* ***(D).***

Furthermore, ATP levels were investigated to analyze energy supply. Ze 339 led to a decrease of basal ATP levels, while further erastin-mediated ATP depletion was attenuated in a concentration-dependent manner (Figure 65A). In addition, the integrity of the mitochondrial membrane potential was assessed (Figure 65B). While erastin-mediated loss of mitochondrial membrane potential was protected at concentrations of Ze 339 greater than 10 µg/mL, there was no effect of Ze 339 on mitochondrial membrane potential under basal conditions (Figure 65B).

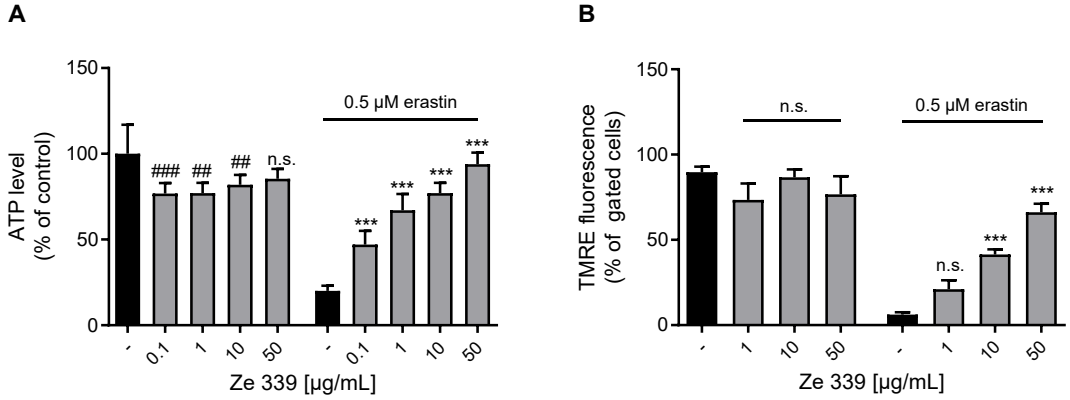

Figure 65. Effects of Ze 339 on ATP levels and on mitochondrial membrane potential

A: *ATP levels were determined using a luciferase-based assay after 16 h of treatment. Values from five-eight replicate wells per condition are displayed as mean + SD. The luminescence under control conditions is set as 100%.* ***B:*** *Mitochondrial membrane potential was assessed via flow cytometric analysis with TMRE™ staining after 16 h of erastin treatment. Each bar chart depicts one representative experiment with three replicates per sample.* ***A-B:*** *mean + SD; 5,000 cells per replicate, ***p<0.001 compared to erastin- treated control (ANOVA, Scheffé's test).*

In line with the previous findings, Ze 339 reduced mitochondrial respiration in a concentration-dependent manner as detected in OCR measurements using the Seahorse system (Figure 66A). In addition, erastin-mediated reduction of OCR was not prevented by Ze 339 (Figure 66B). HT22 cells treated with Ze 339 led to an increase in ECAR, which was the most pronounced with 10 µg/mL Ze 339 (Figure 66C). Erastin-mediated reduction of ECAR was less distinct, but 10 and 20 µg/mL Ze 339 preserved ECAR under oxidative challenge (Figure 66D). Moreover, upon oligomycin injection, the increase in ECAR in Ze 339 treated samples was not as steep as in the control condition, suggesting that the pre-incubation of the cells with Ze 339 already stimulated glycolysis.

Taken together, Ze 339 demonstrated strong effects on metabolism in neuronal HT22 cells and further protected against oxidative damage mediated by erastin, while ROS formation was promoted, suggesting that ROS contribute to Ze 339 mediated molecular signaling.

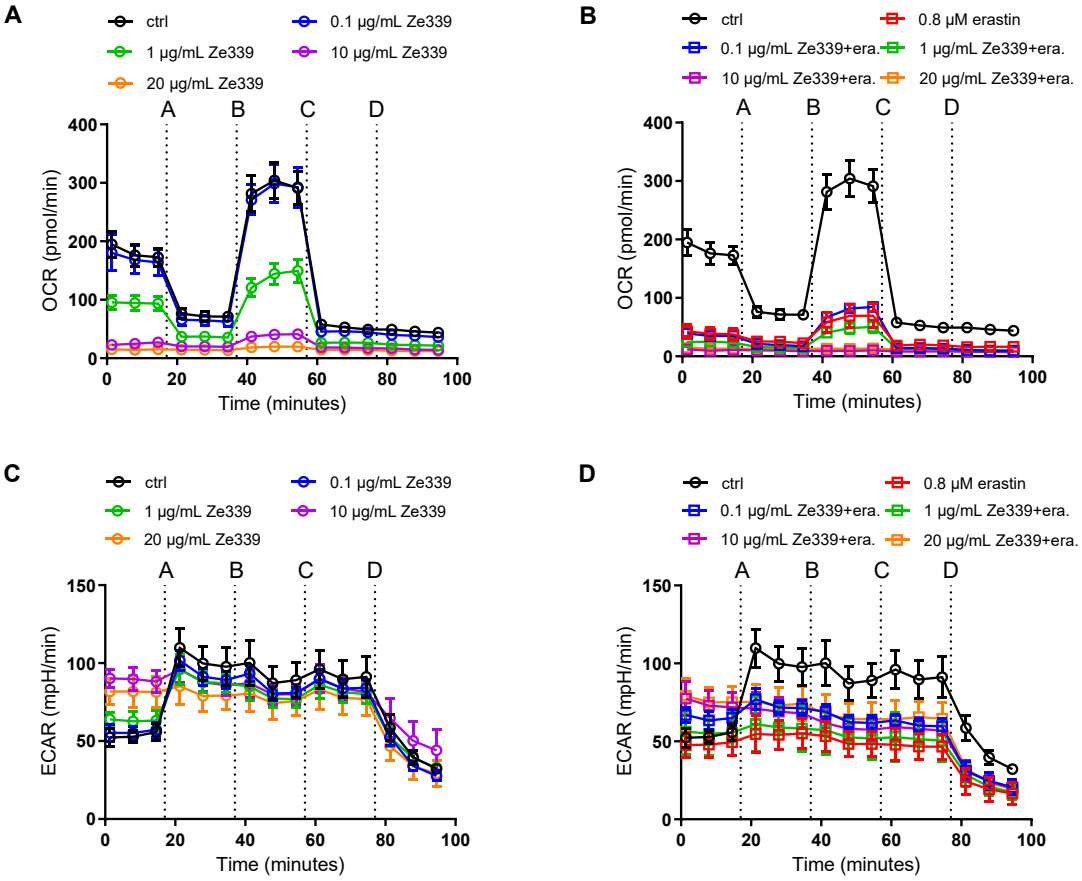

Figure 66. The impact of Ze 339 on mitochondrial respiration and the rate of glycolysis

Data of a representative experiment is depicted, showing OCR and ECAR under basal and oxidative stress conditions. ***A, B:*** *After 16 h of treatment with Ze 339* ***(A)*** *and challenged with 0.8 µM erastin* ***(B)****, the oxygen consumption rate (OCR) of HT22 was analyzed with a Seahorse XFe96 Analyzer. Data of 5-12 replicate wells per condition are given as mean ± SD.* ***C, D:*** *After 16 h of treatment with Ze 339* ***(C)*** *and challenged with 0.8 µM erastin* ***(D)*** *the extracellular acidification rate (ECAR) was determined with a Seahorse XFe96 Analyzer. Data of 4-12 replicate wells per condition are given as mean ± SD (port A: oligomycin; port B: FCCP; port C: rotenone and antimycin A; port D: 2-deoxyglucose).*

5. Discussion

5.1. Impact of Ze 450 on metabolism

Cimicifuga racemosa extracts are well established in the treatment of menopausal symptoms, such as hot flushes and night sweating, but the exact mechanism of action is still elusive. Menopausal transition is considered as a physiological process, which ends one year after the final menstruation. Besides estrogen depletion, age-related metabolic changes (for example the increase in body weight) occur during this phase, leading to the accumulation of risk factors for metabolic diseases, like diabetes mellitus type II or osteoporosis. Recent studies demonstrated that Ze 450 promoted advantageous metabolic changes including a reduction in body weight and improved glucose metabolism in a mouse model of diabetes [35] and attenuated weight gain in menopausal women [52]. Based on these results, it was hypothesized that Ze 450 mediated its therapeutic effects through alterations of metabolic regulation and independent of estrogen receptor stimulation. In this context, a novel concept of menopausal transition emerged, suggesting that climacteric complaints and weight gain in menopause are largely caused by metabolic changes. Therefore, it was of great interest to investigate basal effects of Ze 450 on metabolism in neuronal cells and its impact on cellular resilience under conditions of oxidative stress as a model of age-related alterations. In fact, it was found that Ze 450 modulated cellular energy supply, thereby protecting from oxidative damage.

5.1.1. Ze 450 induces metabolic changes by mild mitochondrial inhibition

Mitochondria are the powerhouses of the cell. In this context, respiratory chain activity and oxidative phosphorylation are important in meeting the cellular energy demand, as they are responsible for the majority of energy supply, while, anaerobic glycolysis plays a minor role in ATP production under physiological conditions [75]. Ze 450 demonstrated strong effects on energy supply at the level of mitochondria. Surprisingly, Ze 450 mediated a concentration-dependent reduction of the OCR, which corresponds to mitochondrial respiration, but in contrast, only concentrations greater than 150 µg/mL reduced ATP levels in HT22 cells (Figure 20). Further, Ze 450 did not rescue the erastin-mediated decrease of OCR (Figures 23A, B and 24A), while erastin-mediated ATP depletion was prevented by Ze 450 (Figure 20). Concomitantly, cells treated with 100 µg/mL of Ze 450 showed an increase in ECAR suggesting that the energy supply was switched from oxidative phosphorylation to anaerobic glycolysis in cells exposed to Ze 450 (Figures 23C, B and 24B). Notably, the response to oligomycin in Ze 450-treated cells was not as pronounced as in control conditions assuming that Ze 450 treatment provoked maximal glycolytic flux (Figure 23C). Besides this, erastin-mediated reduction of glycolysis was prevented by Ze 450 (Figures 23D and 24B). From these results, it was concluded that mitochondrial protection and cell survival after oxidative stress was attributed to the metabolic switch from mitochondrial respiration to glycolysis. In fact, inhibition of glycolysis by 2-DG abolished the protection against oxidative stress (Figure 26A) supporting, the proposed link between the bioenergetic shift induced by Ze 450 and the observed protective effects. In order to specify the mode of action of Ze 450 on the ETC complexes, isolated mitochondria were used to investigate mitochondrial complex functionality. It was observed, that Ze 450 decreased the activity of CI-III in a time and concentration-dependent manner (Figures 28 and 29). These findings support the hypothesis that Ze 450 modulates mitochondrial respiration by inhibiting respiratory chain complexes and thereby reducing mitochondrial ROS formation, which is regarded as the underlying protective mechanism.

ROS production as a side product of OXPHOS can occur in forward and reverse direction of the electron flow. Through normal electron flow, CI and CII mainly produced mitochondrial ROS, but if the Coenzyme Q pool is over-reduced, reversed electron flow is promoted, leading to an increased ROS production by CI. The exact mechanisms leading to reverse electron flow are still not known, but it has been proposed that it occurs when CV is inactive [138,181]. To maintain a high mitochondrial membrane potential, CV transfers protons in the opposite direction into the IMS by consuming ATP, leading to enhanced ROS production by CI. Moreover, it has been shown that blockage of CI by

rotenone at low concentrations prevents reversed electron flow to CI and following ROS production [182,183], thereby mediating beneficial effects. On the other hand, at high concentrations, rotenone potentiates ROS production by interfering with the flavin-binding site of CI [183,184]. Besides this, slightly enhanced ROS production by reverse electron flow was suggested to contribute to mitohormesis and thereby leading, for example, to lifespan extension in *C. elegans* [138]. The reduction of OCR by Ze 450 in neuronal cells and in isolated mitochondria found in this study suggests an inhibitory effect of Ze 450 on mitochondrial respiration, which is most likely involved in beneficial cellular effects, such as protection against oxidative damage. For example, it was detected here that Ze 450 directly inhibited mitochondrial respiratory chain activity (Figures 28 and 29), but in contrast to rotenone [184], Ze 450 neither induced mitochondrial ROS formation in neuronal nor liver cells, nor in isolated mitochondria (Figures 21, 56 and 30). Consequently, it is assumed that Ze 450 interferes with the ubiquinone-binding site but not with the flavin-binding site of CI, since rotenone exposure on isolated mitochondria led to a further decrease of mitochondrial respiration (29) and increased mitochondrial ROS formation [184]. Most intriguingly, the protective effects of Ze 450 at the level of mitochondria and on cell viability were attributed to a bioenergetic shift from oxidative phosphorylation to anaerobic glycolysis, in particular under conditions of oxidative stress.

5.1.2. Ze 450 promotes metabolic reprogramming

Moreover, other mechanisms are known for enhancing the rate of anaerobic glycolysis, like activation of AMPK [35], which is a master regulator of cellular energy homeostasis. In addition, a previous study demonstrated that AMPK is activated by Ze 450 in HepaRG cells [35]. Therefore, AMPK might be one target of Ze 450, which provides a potential mechanistic link between mitochondrial parameters and cellular responses to oxidative stress.

Furthermore, AMPK has been identified as a key player in promoting aerobic glycolysis [75]. In this regard, the major proteins involved in the Warburg effect (Figure 7) were analyzed to gain further insights into the mechanism of action of Ze 450 (Figure 67).

In particular, HIF1α and cMyc have been identified as crucial regulators of key glycolytic enzymes, like HXKII. In HT22 cells, Ze 450 mediated time-dependent effects on HIF1α protein level. Initially, an increase in HIF1α was detected (Figure 32) promoting glycolytic gene expression [185], which was confirmed by an increase in HXK II protein level (Figure 35A, D). Interestingly, HIF1α protein levels dropped after 16 h of Ze 450 treatment, while a concomitant increase in cMyc protein levels was observed at these late time points (Figure 33C, D).

One main difference between HIF and cMyc signaling on metabolic regulation is that HIF blocks the entry of pyruvate into the TCA cycle by enhanced activity of PDK1, which inhibits PDH mediated transformation of pyruvate to acetyl-CoA, and, as a consequence, mitochondrial respiration is decreased (Figure 67) [186,187]. In line with this, the PDK1 protein levels were increased (Figure 35C) and the OCR decreased (Figure 23A) upon Ze 450 treatment in the current study. HIF has been demonstrated to alter COX4 subunits in response to hypoxia in mammalian cells and thereby reducing toxic levels of ROS production by restoring the electron transfer to O_2 resulting in H_2O formation [188] and thereby reducing superoxide formation by CI and CIII [188]. In this context, the limitation of ROS formation is an essential HIF-mediated metabolic adaption [188,189], which might contribute to the observed protective effect by Ze 450.

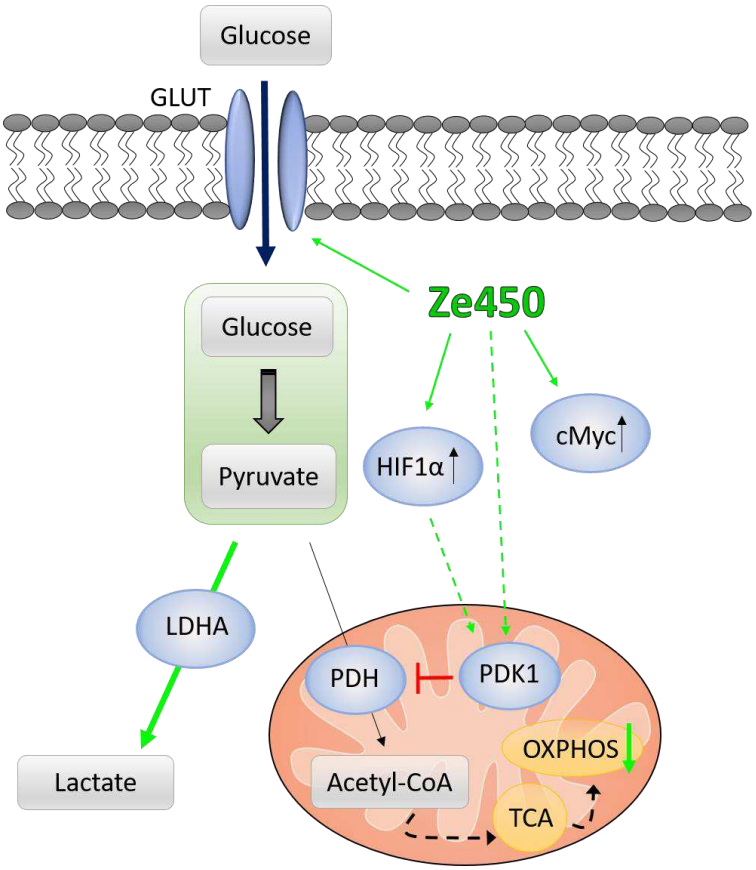

Figure 67. Metabolic reprogramming mediated by Ze 450

Ze 450 increased HIF1α and cMyc protein levels, and following glycolytic gene expression (for example HXKII) was upregulated. Moreover, protein levels of pyruvate dehydrogenase kinase 1 (PDK1) were increased upon Ze 450 treatment, leading to decreased oxygen consumption rate (OXPHOS). Moreover Ze 450 promoted the expression of glucose transporter 4 (GLUT) and increased glucose uptake. Ze 450 mediated these metabolic changes supporting the enhanced glycolytic energy supply.

Besides the enhanced expression of key glycolytic enzymes, cMyc is further involved in growth regulation. For this purpose mitochondrial respiration and the production of biosynthetic substrates are crucial to support cMyc-mediated increases in proliferation [189]. In the present study, this is not the case since mitochondrial respiration and mTOR protein levels are reduced by Ze 450 (Figure 23A and 15A, B), suggesting that the initial enhancement of glycolytic energy metabolism was largely mediated by HIF1α.

In this context, the increase in cMyc protein levels after 16 hours may support the glycolytic shift rather than promoting cMyc-mediated oncogene signaling (enhanced proliferation), suggesting a predominant metabolic regulation by cMyc that is independent of the regulation of enhanced cell proliferation. In line with this, Ze 450 reduced proliferation in different cell lines (Chapter 4.1.1.), highlighting major differences to cMyc-driven tumorigenesis, which relays on mTORC1 activation promoting oncogene

signaling [190]. These findings distinguish Ze 450 mediated adaptive regulations on cell metabolism from cMyc-dependent signaling in proliferating cancer cells.

In this regard, the effects of Ze 450 on cellular metabolism were of particular interest in this study. Indeed, it was demonstrated that Ze 450 mediated concentration-dependent effects on metabolic activity in neuronal and liver cells, but did not induce cell death (Chapter 4.1. and 4.6.), suggesting a significant influence of the extract on metabolism. Furthermore, Ze 450 reduced proliferation in a time- and concentration-dependent manner (Figure 14), but this effect on cell growth was reversible after withdrawal of Ze 450 (Figure 14F). Thus, assuming regulatory effects at the protein level, the mammalian target of rapamycin (mTOR) was of major interest in further investigations on the mechanism of action. So far, two protein complexes have been identified with mTOR as a main component, mTORC1 and mTORC2 [191], which are involved in many essential processes of the cell, for example, cell growth, proliferation, energy metabolism, and protein synthesis [192]. Inhibition of mTOR is well known to initiate autophagy by ULK1 activation leading to beneficial health effects, for example, lifespan extension [193]. Whether Ze 450 modulates autophagy or the autophagic flux is a matter of current research. However, the exact downstream signaling involved in mTOR-mediated cell proliferation is still elusive [191]. Ze 450 reduced total mTOR protein levels; while the expression levels of Raptor (regulatory subunit of mTORC1) was not affected. These findings led to the conclusion, that Ze 450 affected mTORC2-mediated signaling, leading to a reduced proliferation rate upon Ze 450 treatment (Figure 14A). It is known that upon growth factor stimulus mTORC2 is activated via Akt signaling leading to the activation of mTORC1 and, thereby, enhanced proliferation [191] In contrast, in this study phospho Akt protein levels were not increased upon Ze 450 treatment suggesting Akt-independent signaling of Ze 450. Moreover, recent findings revealed that both mTOR complexes were involved in the regulation of cell proliferation by regulating FoxO3 gene expression [191]. Whether Ze 450 enhances FoxO3 gene expression and thereby reduced proliferation was not addressed in this study but might have an impact on Ze 450 mediated metabolic effects.

Besides the impact on proliferation, it was demonstrated that upregulation of mTOR contributes to obesity and associated metabolic diseases. Overnutrition enhanced mTOR signaling, which led to alterations in energy metabolism and insulin resistance, and therefore, contributed to metabolic diseases, such as diabetes mellitus type II [194]. In a recent study, it was demonstrated that Ze 450 mediated anti-diabetic effects in an *ob/ob* mouse model, which was accompanied by enhanced AMPK activation, an upstream regulator of mTOR [35]. The present findings, in cultured neuronal cells supported this link suggesting that the observed metabolic effects of Ze 450 were

mediated via impaired mTOR signaling, thereby might involve modulation of autophagy and regulation via enhanced FoxO3 gene expression.

Besides the proposed metabolic regulation by Ze 450 via modulated mTOR signaling, enhanced expression of cMyc, HIF1α, HXKII, and PDK1 contributed in a time-dependent manner to an enhanced glycolytic energy supply upon Ze 450 exposure (Figure 67). Thus, leads to the hypothesis that Ze 450 modulates different molecular pathways, in which reduced proliferation lowers the energy demand of the cells and the above-mentioned proteins support glycolytic energy supply contributing to the described protective effect against oxidative damage (Chapter 4.2.1. and 5.1.4.). Since glycolytic energy supply is less sufficient than oxidative phosphorylation, the cells' demand for glucose is expanded. In this regard, functional analysis of glucose uptake via flow cytometry and confocal microscopy upon Ze 450 treatment was investigated (Figures 36 and 37). In fact, Ze 450 stimulated glucose uptake in a concentration- and time-dependent manner supporting the observed metabolic reprogramming with the supply of sufficient glucose to maintain cellular energy homeostasis (Figures 36 and 37). In this context, an increase of glucose uptake mediated by insulin was not observed (Figure 36A). However, functional insulin signaling was proven by an increase of pAkt protein level (Figure 39A), which was not detectable upon Ze 450 treatment, suggesting a metabolic regulation independent of insulin-mediated signaling.

In conclusion, it was demonstrated that Ze 450 mediated important metabolic changes at the level of mitochondria and affected important regulators of cellular energy supply, thus offering promising therapeutic potential in diseases related to impaired energy metabolism, like diabetes mellitus type II. Moreover, increased ROS formation is largely contributing to typical climacteric complaints, such as hot flushes, supporting the hypothesis that menopausal transition is a phase of accumulation of age-related risk factors and not exclusively relying on estrogen depletion. In this context, the direct effects of Ze 450 on mitochondrial respiration provide a novel mechanistic explanation for the relief of menopausal symptoms, like weight gain and hot flushes.

5.1.3. Effects of Ze 450 on hypothalamic neurons in the context of thermoregulation

As *Cimicifuga racemosa* extracts were used to treat menopausal complaints, like hot flushes and night sweating it was a major interest to gain insights into the effects of Ze 450 on neuronal cells from the hypothalamus, as this is the superordinate endocrine control center of metabolism and thermoregulation [22,195]. In this context, it was previously hypothesized that Ze 450 acts as a serotonergic agent and thereby reducing hot flushes [40–42]. Moreover, the hypothalamus has been discussed as a central regulator of mediating menopausal symptoms, such as hot flushes and associated metabolic impairments [196]. ARC neurons of the hypothalamus consist of “neurons of first-order”, which are the first neurons in contact with peripheral signals [197,198]. In this regard, metabolic changes occurring during menopause may directly affect energy homeostasis of the hypothalamus, since it was demonstrated that arcuate neurons are responsive to many peripheral signals, such as hormones like leptin [197]. The importance of the hypothalamus in metabolic regulation was demonstrated, for example, by lesions in this brain region, which induced obesity [199].

mHypo cells are hypothalamic neurons and a suitable *in vitro* system to study the impact of Ze 450 under oxidative stress conditions. Since the development of menopausal symptoms, like hot flushes and night sweating, is associated with an increase in reactive oxygen species, which contribute to the mentioned symptoms (Figure 2) [20,38,39]. Increased ROS formation dependent and independent of estrogen depletion has shown to trigger climacteric complaints [20] (Figure 2).

Ze 450 demonstrated protective effects on the level of mitochondria and cell death in a model system of erastin-induced oxidative damage (Chapter 4.1. and 4.2.1). Erastin-mediated mitochondrial ROS formation, lipid-peroxidation and loss of mitochondrial membrane potential was attenuated upon concentrations greater than 50 µg/mL of Ze 450 demonstrating that Ze 450 is capable to reduce ROS mediated signaling, thereby preventing oxidative damage. Hence, this provides a mechanistic link, for the beneficial effects of Ze 450 on menopausal symptoms [4], like night sweating and hot flushes, which are triggered by an imbalance in redox homeostasis especially in neuronal cells (Chapter 4.2.1 and Figure 2).

In conclusion, the experimental approaches in hypothalamic neurons demonstrated that Ze 450 is capable to reduce oxidative damage, especially mitochondrial ROS formation thus suggesting a mechanistic link for the reduction of hot flushes and night sweating. Implications of the energy metabolism in mHypo cells by Ze 450 were not assessed, but

might explain the metabolic regulation, by promoting glycolysis and thereby protecting from oxidative damage, as it was demonstrated in hippocampal HT22 cells.

5.1.4. Ze 450 protects against oxidative damage

Maintaining redox homeostasis is essential for crucial cell functions, as reactive oxygen species are important second messengers [134,200]. Besides this, many age-related neurodegenerative pathologies including Alzheimer´s and Parkinson´s disease, but also metabolic illnesses, like diabetes mellitus type II, hypertension and cancer share common pathomechanisms, involving enhanced ROS production and imbalanced redox homeostasis [54,182,201,202]. More specifically, enhanced free radical formation has been described as massively damaging to cells and organs, thereby significantly contributing to the mentioned diseases. Moreover, it was demonstrated that climacteric complaints, like hot flushes, were associated with an increase in reactive oxygen species, which contributed to the mentioned symptoms (Figure 2) [20,38,39]. Further, metabolic disturbances in redox homeostasis provide evidence that menopausal transition is rather an impairment involving energy metabolism than exclusively caused by estrogen depletion [20]. Thus, it was a major aim to evaluate the effects of Ze 450 under oxidative stress conditions with a particular focus on mitochondrial integrity and function, since they are the major source of reactive oxygen species and crucial for maintaining cellular energy homeostasis.

HT22 neuronal cells were established as a suitable model system to study oxidative stress. In these cells, oxidative cell death such as oxytosis or ferroptosis can be induced by glutamate or erastin, respectively (Figure 3) [59,203]. Ze 450 exerted protective effects in various cells in model systems of oxidative stress (Chapter 4.1.1) as summarized in Figure 68.

Oxidative stress-mediated lipid-peroxidation was abolished by concentrations higher than 50 µg/mL of Ze 450, while Ze 450 alone did not induce enhanced lipoxygenase 12/15 activity. Notably, this pronounced protective effect was present after 8 h, but also after 16 h of the oxidative challenge. This finding indicated that even the secondary ROS burst initiated through mitochondrial impairment was prevented by Ze 450. In turn, Ze 450 protected mitochondria from oxidative damage. Mitochondria are the powerhouses of the cell and they are key regulators in maintaining energy homeostasis. One major hallmark in neuronal cell death is massive mitochondrial impairment due to enhanced cellular and following mitochondrial ROS formation [55,202,204]. In fact, Ze 450 prevented oxidative stress-mediated mitochondrial ROS formation. Besides this, loss of mitochondrial membrane potential, ATP depletion and enhanced mitochondrial fragmentation mark mitochondrial damage and the so-called “point of no return” (Figure 3) [65].

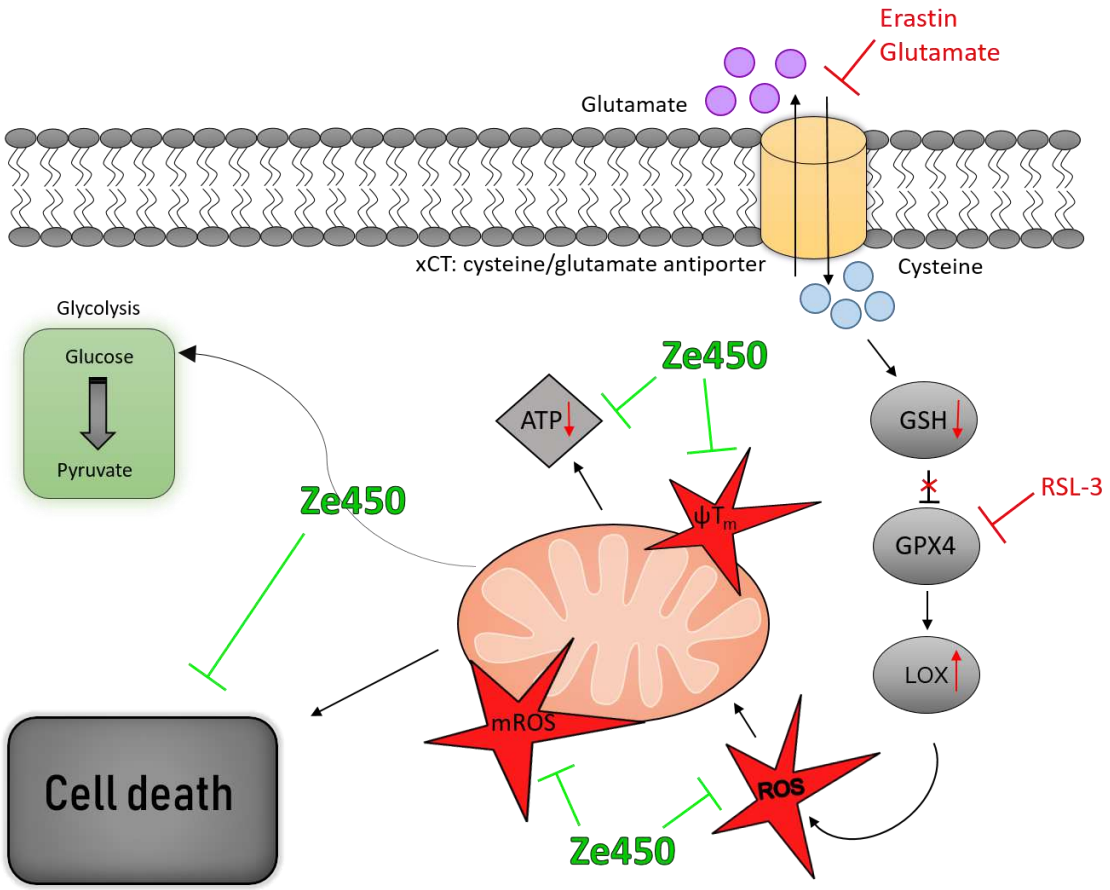

Figure 68. Scheme of Ze 450 mediated effects under oxidative challenge

Disruption of redox homeostasis by erastin, glutamate or RSL-3 led to mitochondrial impairment and subsequently cell death. Ze 450 mediated protection against erastin/glutamate or RSL-3 induced lipid-peroxidation, mitochondrial ROS formation, ATP depletion, and cell death by decreasing mitochondrial respiration and enhancing glycolysis to compensate energy supply of the cells.

Upon mitochondrial impairment, AIF is released and mediates neuronal cell death [67]. Thus, protecting mitochondria is an important strategy to prevent neuronal damage, since oxidative stress is closely linked to many neurodegenerative diseases, like stroke or Parkinson's disease and further metabolic diseases including diabetes mellitus type II and the development of menopausal symptoms [205]. The results of this study show that Ze 450 mediated a shift in energy metabolism towards glycolysis, as described before in chapter 4.2 and discussed in chapter 5.1.2. and 5.1.3., thereby protecting against erastin- and glutamate-mediated mitochondrial damage (Chapter 4.1.2 and 4.2). Consequently, cell viability was persevered by Ze 450 under oxidative stress conditions, which might provide new therapeutic options for other metabolic diseases, which are related to increased ROS formation and a disbalance in energy homeostasis.

5.1.5. Ze 450 and metformin share protective effects against oxidative damage in neuronal cells

Besides the effective treatment of menopausal complaints, it was suggested that Ze 450 has further therapeutic potential. Since Ze 450 mediated antidiabetic effects in an *ob/ob* mouse model which were comparable to metformin [35], this study provided evidence for Ze 450 as a potential treatment option for metabolic diseases, like diabetes mellitus type II. Therefore, in the present study, it was a major interest to compare the mode of action of Ze 450 to metformin. Metformin is currently used to treat type II diabetes mellitus, but so far, the molecular mechanism of action is not fully understood. It is known that metformin lowers blood glucose levels and fasting insulin levels by reducing gastrointestinal and increasing peripheral glucose uptake [165,206]. At the cellular level, metformin acts as an ETC inhibitor and an AMPK activator [207], thereby it is interfering with several important cellular pathways involved in energy metabolism [208]. It has been demonstrated that activation of AMPK contributed to neuroprotective effects of metformin in H_2O_2-treated PC12 neuronal cells [209]. In this context, metformin is currently discussed as a potential anticancer, antiaging, neuroprotective and cardioprotective agent [165,206].

In this study, metformin and Ze 450 both protected against erastin-mediated cytotoxicity, mitochondrial ROS formation and loss of mitochondrial membrane potential (Chapter 4.3). However, metformin did not decrease metabolic activity in the tested concentration range in the MTT assay and was not as effective as Ze 450 in protecting against erastin-mediated lipid-peroxidation. Notably, proliferation was reduced in a similar manner, assuming an impairment in mTOR signaling, which was shown in this study for Ze 450 (Chapter 4.1) and was demonstrated for metformin earlier [165,210–212]. Furthermore, it is known, that metformin inhibits mitochondrial CI, thereby reducing ROS production by mitochondria [78,208]. In line with this, metformin reduced OCR in a concentration-dependent manner in the current study (Figure 47). Moreover, metabolic reprogramming by an energetic shift towards glycolysis was less pronounced in metformin treatment conditions compared to Ze 450 (Figure 47C). In accordance with this Ze 450 was more effective in the rescue of erastin-mediated ATP depletion compared to metformin, most likely because the promoted shift towards glycolysis was more pronounced under oxidative stress conditions (Figure 46D).

In this study, it was demonstrated that Ze 450 exerted metabolic effects in a similar fashion as metformin, but the Ze 450 mediated effects were more pronounced and the protective effects against oxidative damage were more potent. Therefore, it is of great

interest to further characterize the complex mechanism of action of Ze 450 and to evaluate its potential use as a treatment against diseases related to oxidative damage and metabolic impairments, like diabetes mellitus type II.

5.1.6. Ze 450 mediated effects are distinct from estrogen receptor-mediated signaling

Hormonal replacement therapy is an effective treatment option against menopausal complaints, like hot flushes or mood disorders [18,19]. However, the indication of HRT is limited by adverse side effects and contraindications, like coronary heart disease, stroke, and personal history of thromboembolic disease. In this context, the need for alternative treatment options was highly warranted. *Cimicifuga racemosa* extracts are hormone-free compositions and well-established for the treatment of climacteric complaints. Nevertheless, *Cimicifuga racemosa* extracts have been initially linked to mediate estrogenic effects, but this classification of the extracts as “phyto-estrogens” was revised. In fact, it was demonstrated that *Cimicifuga racemosa* extracts rather mediate anti-estrogenic than hormone-like effects [47]. Further, *Cimicifuga racemosa* extracts can be used in menopausal women with, for example, hormone-sensitive endometrial cancer [33]. In the current study, Ze 450 mediated effects were compared to estrogen-driven effects in neuronal cells in order to further evaluate a distinct or similar mode of action of the extract compared to estrogen receptor-mediated signaling activated by estrogens. 17β-estradiol is known to mediate hormonal and anti-oxidant effects in a concentration-dependent manner [173,213]. The results depicted in chapter 4.4 demonstrate that17β-estradiol protected against erastin-mediated damage, but this effect is most likely linked to its antioxidant activities as described before [171,172,213]. More intriguingly, mitochondrial respiration was slightly increased by 1 µM of 17β-estradiol compared to control conditions (Figure 49A), in contrast to Ze 450, which decreased OCR. In line with current research [20,214], the increase in OXPHOS by 17β-estradiol has shown beneficial effects on disturbed energy metabolism in the brain of menopausal women. The findings of this study clearly indicate a distinct mechanism of action of Ze 450, since OXPHOS was decreased by the extract as summarized in figure 69.

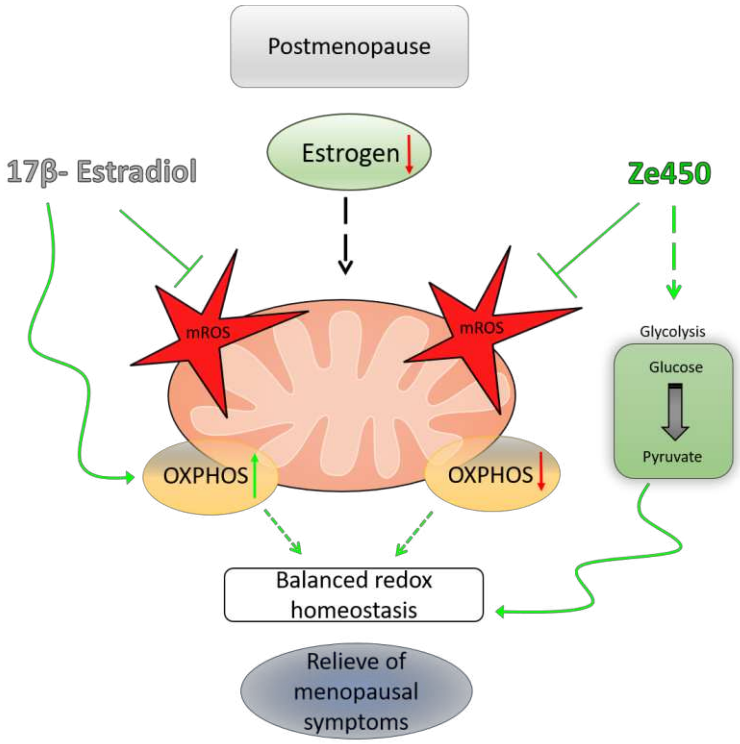

Figure 69. Effects of estradiol and Ze 450 on altered energy metabolism in postmenopause

17-β estradiol and Ze 450 mediate beneficial effects on brain energy metabolism during menopause by distinct mechanisms. Compensation of energy deficit during postmenopause is compensated by 17-β estradiol by an increase in mitochondrial respiration, while Ze 450 led to a metabolic reprogramming towards glycolysis (OXPHOS: oxidative phosphorylation, mROS: mitochondrial ROS).

Besides this, both ER agonists (PPT and DPN) did not affect HT22 cells under basal and oxidative stress conditions (Figure 50A, B), supporting the hypothesis that Ze 450 rather mediates a metabolic than an estrogen-like effect. Furthermore, the comparison to 4-OH-Tamoxifen did not show a synergistic or additive effect in combination with Ze 450. Tamoxifen has been studied in model systems of oxidative stress previously, and the reported neuroprotective effects were independent of estrogen receptor inhibition [215]. In line with this, in the present study 10 µM of 4-OH-Tamoxifen mediated protective effects against erastin-induced oxidative damage (Chapter 4.4).

Taken together, the results obtained in the present study confirmed that Ze 450 promoted effects were distinct from estrogen receptor-mediated signaling, underlining the importance of *Cimicifuga racemosa* extracts as hormone-free alternatives to HRT in the treatment of climacteric complaints.

5.1.7. Total Ze 450 is more effective than isolated components and sub-fractions

Cimicifuga racemosa extract contains many components, including antioxidants, like ferulic acid. In line with this, it was demonstrated earlier that the main antioxidant properties *of Cimicifuga racemosa* extracts from rhizomes were attributed to phenolic acids, for example, caffeic acid, ferulic acid and isoferulic acid [12]. The content of ferulic acid, however, is less than 0.2 % in this batch of Ze 450 and, therefore, most likely not responsible for the observed protective effects. Further, Ze 450 demonstrated a strong influence on energy metabolism, and this metabolic regulation is important for the protection against oxidative damage (Chapter 4.2.1.).

In fact, the protective effect of Ze 450 against erastin-mediated toxicity was abolished by the glycolysis inhibitor 2-DG. In contrast, the antioxidant Trolox still mediated protection against erastin-induced toxicity in the presence of 2-DG (Figure 26A). These results demonstrated that the protective effects of antioxidants cannot be inhibited through interference with glycolysis, suggesting that protection by Ze 450 was mediated by metabolic mechanisms beyond the inherent antioxidant properties. In order to evaluate the upregulation of the key antioxidant enzymes, the protein levels of MnSOD, CuZnSOD, and Catalase were analyzed, since it is known that some antioxidants accelerate their direct radical scavenging potential through an increased expression of the mentioned enzymes for ROS detoxification [216,217]. Notably, the protein levels of the mentioned antioxidant enzymes were unaltered after incubation with the extract (Figure 27), supporting the conclusion that the antioxidant properties of Ze 450 were not substantially contributing to the observed protective effects in HT22 cells.

Ze 450 is a plant extract; therefore, there are besides the above-mentioned antioxidants many other components. So far, it is not possible to attribute all of the therapeutic effects of *Cimicifuga racemosa* extracts to either a single constituent or a class of components. Nevertheless, much research was done and triterpene glycosides [5–7] for example, actein, 23-epi-26-deoxyactein and cimiracemoside C [8,9]; phenolic acids, predominantly derivatives of hydroxycinnamic acid [10], including caffeic, ferulic and cimicfugic acid [7] and flavonoids [11] were represented in extracts of the rhizome. For example, a fraction containing triterpene glycosides [5] inhibited the growth of MCF7 human breast cancer cells and induced cell cycle arrest at the G1 phase. In line with this, it is known that the EtOAc fraction consists of major triterpene glycosides and this fraction showed reduced proliferation in HT22 neuronal cells, which was comparable to total Ze 450 (Figure 42C), in a reproducible and reliable way. In addition, 20 µg/mL of EtOAc

fraction reduced OCR but was not as effective as Ze 450 against erastin-mediated reduction of the ECAR (Figure 43D). Notably, the Aq. fraction, which consists of the phenolic acids, did not mediate protection against erastin-mediated damage. For the BuOH fraction, it was found that it had some similarities to the mode of action of total Ze 450, but especially at the level of mitochondria, the buthanolic fraction was not able to prevent erastin-mediated mitochondrial impairment. Interestingly, the isolated chemical triterpene glycosides did not mediate protection against oxidative damage in neuronal cells comparable to Ze 450, in a relevant concentration range. Moreover, the combination of different glycosides was only effective in concentrations higher than the concentrations in 100 µg/mL of total Ze 450 (Chapter 4.2.6.). The observed results suggest that neither sub-fractions nor single or combined components were as effective as total Ze 450 in the used model system of oxidative stress in HT22 cells.

Conclusively, in the current study, Ze 450 was described as a plant extract with a complex mode of action, which, so far, cannot be attributed to a single component or a specific group of ingredients.

5.1.8. Ze 450 protects liver cells from oxidative damage

Assessing cytotoxicity in liver cells was of particular interest in the present study since there is an ongoing debate whether *Cimicifuga* extracts may cause hepatotoxicity. There are reports in the literature that associated *Cimicifuga racemosa* extract to hepatic side effects in patients with possible yet unknown risk-factors [218–220]. Notably, none of the adverse liver effects was directly linked to Ze 450. Besides this, the causality in general, the exclusion of other causes and the consideration of the herbal constitution leading to the case reports, were criticized in the field [29,221]. Still, known liver damage is a contraindication for *Cimicifuga racemosa* preparations. At a very high dose (1000 mg/kg body weight) Ze 450 caused microvesicular steatosis in the liver of rats [222]. In this regard, the authors concluded that these high concentrations are very unlikely to be reached in humans treated with the recommended daily doses of 6.5-13 mg extract [222]. In the present study, two different liver cell lines were investigated and up to 200 µg/mL of Ze 450, cytotoxicity was not detected in either cell line (Figure 55B and 58B). In contrast, the results obtained in the cultured liver cells showed a pronounced protection against oxidative damage (Figure 55B and 58B) and further demonstrated that the concentrations leading to the enhanced cell death of liver cells (Figure 55A) are much greater (≥500 µg/mL) than the concentrations required for protective effects (50-200 µg/mL) (Figure 55B). In particular, in HepG2 liver cells, strong protective effects of Ze 450 on ATP depletion, lipid peroxidation, mitochondrial ROS formation and loss of mitochondrial membrane potential (Figure 56) were detected, which were consistent with the findings in neuronal cells.

Regarding these findings, it might be suggested that Ze 450 shows beneficial effects on diseases related to oxidative liver damage, rather than causing liver toxicity.

5.1.9. Ze 450 extends the overall survival of *Caenorhabditis elegans*

Moreover, it was of great interest to evaluate the effects of Ze 450 on a whole organism under basal and oxidative stress conditions.

Therefore, *Caenorhabditis elegans* served as a model organism to study the effects of Ze 450 on survival in a real-time setting and under oxidative stress conditions *in vivo*. In the present study, it was demonstrated that 100 µg/mL of Ze 450 was capable to prevent PQ-mediated shorting of survival (Figure 51B). As described before in chapter 5.1.5., metformin was used as a control since it is used to treat patients with diabetes mellitus type II [165] and discussed as a potential agent promoting longevity in *C. elegans* [175,176]. In the current study, the heat shock assay demonstrated similar findings for 25 mM metformin compared to 100 µg/mL of Ze 450 (Figure 52). Notably, 25 mM metformin enhanced survival in the heat stress resistance test, while 100 µg/mL of Ze 450 did not, highlighting mechanistical differences in the mode of action of Ze 450 compared to metformin. In the real-time setting Ze 450 enhanced median and overall survival compared to its vehicle control, while metformin did not improve median survival, but overall survival (Figure 53).

Metformin has been shown to improve survival of type II diabetic patients compared to healthy subjects [223]. In this context, the gut microbiota is of great interest since it was demonstrated that metformin mediated effects were regulated by interactions with the microbiota in *C. elegans* [224]. *C.elegans* is a good model to study drug microbiome interactions since *C. elegans* and humans share many gut microbes such as E. coli [225]. In a recent study, bacterial metabolites like agmatine were shown to mediate metformin related effects on longevity in *C. elegans* [224], which might explain the survival benefit in type II diabetic patients. A currently ongoing clinical trial (TAME, Targeting Aging with Metformin) is focusing on metformin mediated effects on aging and will give new insights into modulations of metformin beyond its impact on diabetes mellitus type II [223].

Regarding *Cimicifuga racemosa* extracts, it remains open which exact cellular mechanisms are involved in the prolongation of survival. Moreover, it was previously stated that several pathways and molecular mechanisms interact and contribute to longevity in *C. elegans* [100,226,227]. *daf-16* has been identified as a major regulator leading to lifespan extension [104,228], thereby involving a forkhead box O1 ortholog, which is regulated by the ortholog of Sirtuin 1 in *C. elegans* [229,230]. Additionally, AMPK was identified as another key player in longevity in *C. elegans* suggesting a link between lifespan extension and energy metabolism [227]. In *C. elegans* the AMP/ATP ratio increases upon aging. In this context, it was found that the AAK-2, which is the α subunit

of the *C. elegans* AMP-activated protein kinase, functions as an AMP sensor and modulates lifespan prolongation [227,231]. Metformin was shown to enhance lifespan in this study (Chapter 4.5) and previously [175,232]. Recently, it was demonstrated that activation of AMPK and inhibition of mTOR upon stimulation of the lysosomal pathway by metformin contribute to lifespan extension [232]. These mechanistical considerations might also account for Ze 450, but this needs to be confirmed in further experiments.

Furthermore, the improvement of the chemotactic behavior of *C. elegans* due to Ze 450 (Figure 54) implicates a potential effect on neuronal activity. Thus implying new mechanistical characteristics for Ze 450 involving the olfactory system of *C. elegans*.

The *in vivo* setting with *C. elegans* emphasizes that Ze 450 has beneficial effects on a whole organism and might contribute to healthy aging. Alongside, PQ mimics an oxidative stress insult, which led to mitochondrial impairment. Hereby, Ze 450 demonstrated protective effects, confirming the findings *in vitro*, that Ze 450 preserved mitochondrial function and integrity. Moreover, the results in *C. elegans* demonstrate that Ze 450 mediated advantageous effects in the paraquat model system of oxidative stress, which suggests a mode of protection involving mitochondria. These findings led to the conclusion that Ze 450 has a strong impact at the level of mitochondria, which was demonstrated in neuronal and liver cells, as well as in isolated mitochondria and in *C. elegans*.

5.2. Effects of Ze 339 on neuronal cells

Petasites hybridus leaf extract is used to treat seasonal allergic rhinitis but the exact mechanism of action is not fully understood so far. Therefore, *Petasites hybridus* leaf extract, Ze 339 was investigated in regard to specify its mechanism of action and assess its potential protective effects against oxidative damage in HT22 neuronal cells, since inflammatory diseases like allergic respiratory diseases are often accompanied with an increase in reactive oxygen species [233,234].

In this study, the model system of ferroptosis was used to induce oxidative stress in a well-established *in vitro* system of immortalized neuronal cells [59] as described in chapter 1.2.1. Interestingly, 50 µg/mL of Ze 339 enhanced lipid-peroxidation after 8 hours of treatment, while mitochondrial ROS formation was induced upon 10 µg/mL Ze 339 (Figures 62 and 63). Annexin V/PI FACS measurement confirmed that this metabolic regulation was not accompanied by enhanced cytotoxicity (Figure 61A). These results demonstrated that Ze 339 induced mild oxidative stress via ROS formation (Figure 70), but was not harmful in these concentrations. Taken together, these results demonstrated that Ze 339 induced mitochondrial ROS formation and enhanced 12/15 lipoxygenase activity in a concentration- and time-dependent manner.

In line with this, it is known that mild oxidative stress mediates protection due to pre-conditioning effects [235], and therefore, is relevant for aging and promotes disease resistance [137,236]. Whether Ze 339 mediates its anti-allergic and anti-inflammatory effects via (mito-) hormetic processes needs to be further investigated. In this context, it was demonstrated that besides an increase in (mitochondrial) ROS formation, autophagic processes were suggested to contribute to beneficial hormetic cytoprotection [235,237]. In this regard, it would be interesting to evaluate the effects of Ze 339 on autophagy, since it is known that mild mitochondrial or cellular stress induces (mito-) hormetic processes [238], which are accompanied by various molecular mechanisms involving, for example, unfolded protein response (UPR), but also impacts mito- and autophagy [239,240].

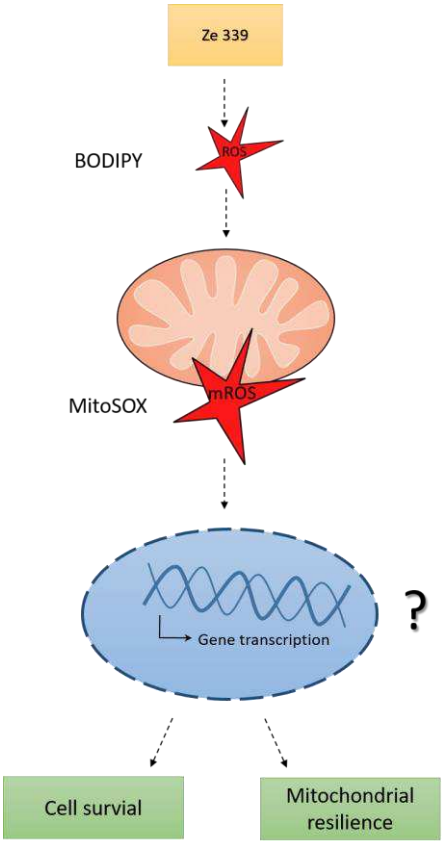

Figure 70. Proposed mechanism of action of Ze 339

Ze 339 led to a mild increase in lipid-peroxidation and subsequent mitochondrial ROS formation. Mitohormetic adaptations might contribute to Ze 339-mediated protection against oxidative damage by enhancing mitochondrial resilience.

Furthermore, in the current study, it was investigated if Ze 339 protects neuronal cells against oxidative stress-mediated cytotoxicity and mitochondrial impairment since an imbalance in redox homeostasis is linked to many diseases, including inflammatory diseases, like allergic respiratory disease [233].

In fact, it was found that Ze 339 mediates protection against erastin-mediated cytotoxicity in neuronal cells. Moreover, Ze 339 slightly induced lipid-peroxidation and mitochondrial ROS formation, but alongside abolished erastin-mediated oxidative insult (Figure 62-64). Hence, Ze 339 protected mitochondria from oxidative damage by preserving mitochondrial membrane potential (Figure 65B).

Further, Ze 339 decreased ATP production compared to control conditions, which might be explained by a reduced mitochondrial respiration rate (Figures 65A and 66A). Notably, erastin-mediated ATP depletion was rescued by Ze 339 (Figure 65A). Analyzing mitochondrial respiration and glycolysis, upon 1 µg/mL Ze 339 the OCR was decreased but ECAR was maintained to ensure proper energy supply of the cells. Hereby, it would be of great interest to analyze energy supply at an early stage and therefore answer the

question, whether enhanced mitochondrial ROS formation is accompanied by an increase in mitochondrial respiration and hence superoxide production.

Moreover, it was shown that Ze 339 acts via inhibition of STAT activation [119], leading to reduced transcription of cytokines and inflammatory effects. The authors proposed that Ze 339 acts upstream of STAT since cytokine-induced nuclear translocation was reduced for STAT 1, 3 and 6, suggesting interference with the assembly of the JAK/STAT complex. Whether STAT inhibition is essential for Ze 339 mediated protection in neuronal cells needs to be investigated in future studies more in detail.

So far, it might be hypothesized that Ze 339 exerts multiple effects contributing to symptom relief of allergic rhinitis including reduced inflammatory responsiveness. Further (mito-) hormetic adaptions might mediate pre-conditioning effects supporting, for example, the endogenous antioxidant defense system, which protects against disturbances in redox homeostasis, but until now the exact mechanism of action remains to be clarified. In the current study, it was demonstrated that *Petasites hybridus* extract, Ze 339 reduced proliferation in a concentration-dependent manner, while cell viability until 50 µg/mL of Ze 339 was unaffected. Moreover, Ze 339 prevented lipid-peroxidation, mitochondrial ROS formation, loss of mitochondrial membrane potential and cell death in a model system of oxidative cell death. These effects might support the treatment of seasonal allergic rhinitis and likely in many other respiratory diseases with increased ROS formation. Further, Ze 339 might provide mitochondrial resilience via mild (mitochondrial) ROS formation at low concentrations and thereby promoting beneficial adaptions.

6. Summary

The *Cimicifuga racemosa* extract Ze 450 is produced by a standardized procedure and well-established in the treatment of menopausal complaints; however, the underlying mechanism of action has not been clarified. In a recent study, Ze 450 mediated beneficial effects on glucose tolerance, insulin sensitivity and weight gain in diabetic *ob/ob* mice and on weight gain in a clinical study investigating therapeutic effects of Ze 450 on climacteric symptoms in menopausal women. Therefore, it was of great interest to study the effects of Ze 450 on cell metabolism in more detail. To address this issue, Ze 450 was exposed to neuronal and liver cells alone, and in model systems of oxidative stress, since an imbalance in redox homeostasis was shown to be crucially involved in the pathogenesis of many age-related diseases, including, for example, diabetes mellitus type II, and further provides a molecular link towards menopause. In this context, a new concept of menopause is hypothesized, implying age-related metabolic disturbances rather than exclusively focusing on estrogen depletion.

This study revealed that Ze 450 mediated remarkable effects on metabolism by reducing metabolic activity and the rate of cell proliferation in various cell types. Furthermore, it was demonstrated that Ze 450 provided protection against erastin- and glutamate-mediated oxidative cytotoxicity in neuronal and liver cells. Notably, the findings on liver cells clearly demonstrated, that Ze 450 is rather protective than causing hepatotoxicity. Additionally, Ze 450 preserved mitochondrial integrity and function, while under oxidative challenge, Ze 450 prevented mitochondrial impairments by protecting against erastin- and glutamate-mediated lipid-peroxidation, mitochondrial ROS formation, loss of mitochondrial membrane potential and ATP depletion. Ze 450 exerted beneficial effects by directly inhibiting mitochondrial respiration and, thereby, reducing mitochondrial superoxide production. Moreover, Ze 450 preserved the energy supply of the cell by metabolic reprogramming towards glycolysis. In this context, it was demonstrated that a regulation of HIF1α and cMyc most likely contributed to the metabolic shift by enhancing the protein expression of key glycolytic enzymes. Further, it was demonstrated that Ze 450 enhanced glucose uptake to maintain cellular energy homeostasis by promoting glycolysis. These results demonstrated that Ze 450 affects energy metabolism by direct inhibition of mitochondrial respiration and metabolic reprogramming towards glycolysis, supporting a novel therapeutic concept describing Ze 450 as a metabolic regulator.

Ze 450 is a plant extract, which consists of many different components. In former studies, triterpene glycosides were identified as active ingredients, but in neuronal cells, the isolated components (actein, 23-epi-26-deoxyactein, cimiracemoside C) were not able

to mediate effects comparable to Ze 450. Nevertheless, sub-fractions of Ze 450 were investigated and the EtOAc fraction turned out to act in a similar manner like Ze 450, but the effective concentrations were higher than contained in 100 µg/mL of Ze 450.

Besides triterpene glycosides, Ze 450 also contains phenolic acids that mediate antioxidant effects. Indeed, Ze 450 showed moderate antioxidant properties compared to Trolox but this antioxidant effect is not mainly contributing to the observed protection by Ze 450.

Taken together, Ze 450 offers promising therapeutic potential in diseases involving mitochondrial damage and increased ROS formation and provides first evidence for a novel mechanism of action involving metabolic reprogramming, which highlights a new perspective on menopausal transition.

Besides Ze 450, a special extract of *Petasites hybridus* was investigated in the model systems of ferroptosis. Ze 339 is a CO_2 extract obtained from leaves of *Petasites hybridus* and is used to treat seasonal allergic rhinitis. In this study, Ze 339 was investigated in order to specify its mechanism of action and assess its potential protective effects against oxidative damage in HT22 neuronal cells. Ze 339 induced mild ROS formation produced by lipid-peroxidation and by mitochondria but did not impair cell viability at concentrations up to 50 µg/mL of Ze 339. In the context of mitohormesis, Ze 339 might provide protection against mitochondrial impairment by a mild increase in ROS. Moreover, Ze 339 protected against erastin- mediated cytotoxicity and mitochondrial impairment in HT22 neuronal cells. In conclusion, it is hypothesized that Ze 339 provides mitochondrial resilience by a mild increase in ROS formation leading to beneficial metabolic adaptions or responses to allergens. In this study, it was demonstrated that (mito-) hormetic regulation processes might contribute to symptom relief of allergic rhinitis.

7. Zusammenfassung

Cimicifuga racemosa Extrakte, wie Ze 450 werden zur Behandlung von Wechseljahresbeschwerden eingesetzt. Der zugrundeliegende Wirkmechanismus ist jedoch nicht bekannt. In einem diabetischen Mausmodell wurde gezeigt, dass Ze 450 die Glucosetoleranz, Insulinsensitivität und Gewichtszunahme günstig beeinflusste. Die positiven Effekte auf das Körpergewicht wurden in einer retrospektiven klinischen Studie mit Frauen in der Menopause bestätigt. Die Menopause markiert die Zeit bis 12 Monate nach dem Ausbleiben der letzten Regelblutung und wird durch schwankende oder abfallende Östrogenspiegel eingeleitet. Die Akkumulation reaktiver Sauerstoffspezies ist maßgeblich an altersbedingten Erkrankungen, wie Diabetes mellitus Typ II, ebenso wie an der Entstehung typischer menopausaler Beschwerden beteiligt. In diesem Zusammenhang wurde postuliert, dass die Menopause nicht nur auf den Östrogenabfall, sondern vielmehr auf metabolische Veränderungen zurückzuführen ist, die zur Entstehung altersbedingter Erkrankungen mit beitragen.

Diesbezüglich war die Untersuchung der Auswirkungen von Ze 450 auf den Zellstoffwechsel von großem Interesse. Daher wurden basale und potentiell protektive Effekte von Ze 450 in Modelsystemen des oxidativen Stresses untersucht, um den Einfluss von Ze 450 auf ein Ungleichgewicht der Redox-Homöostase zu untersuchen. Eine Beeinflussung des zellulären und mitochondrialen Metabolismus durch Ze 450 wurde insbesondere durch eine vermindert mitochondriale Respiration und eine reduzierte Proliferationsrate gezeigt. Weiterhin schützte Ze 450 vor Erastin- und Glutamat-vermittelter Zytotoxizität in Neuronen und Leberzellen und induzierte in den relevanten Konzentrationsbereich keine Zellschädigung in den verwendeten Zelllinien. Darüber hinaus wurden in dieser Studie Einflüsse von Ze 450 auf mitochondriale Parameter untersucht, da diese Zellorganellen maßgeblich die Energiebereitstellung und die Thermoregulation steuern. Ze 450 schützte die Mitochondrien vor oxidativen Schäden und bewahrte so die Integrität der Mitochondrienmembran und die Funktion der Organellen. Ze 450 schützte vor Erastin- und Glutamat-vermittelter Lipidperoxidation, mitochondrialer ROS-Bildung, Verlust des mitochondrialen Membranpotenzials und dem Abfall der zellulären ATP Spiegel. Darüber hinaus verminderte Ze 450 die mitochondriale Atmung durch eine direkte Hemmung der Atmungskettenkomplexe. Der protektive Effekt von Ze 450 gegen die oxidativen Schädigung ist durch eine Verschiebung des Energiemetabolismus in Richtung Glykolyse begründet. Weiterhin tragen HIF1α und cMyc maßgeblich zur metabolischen Verschiebung bei, indem die Proteinexpression wichtiger glykolytischer Enzyme

hochreguliert wurde. Weiterhin erhöhte Ze 450 die Glukoseaufnahme in den Zellen und gewährleistete so die Energieversorgung über die verstärkte Glykolyse. Diese Erkenntnisse zeigen einen völlig neuen Wirkmechanismus von Ze 450 auf, wobei Ze 450 als Regulator den Energiehaushalt vorteilhaft beeinflusst und so neben der effektiven Behandlung klimakterischer Beschwerden eine neue Sichtweise auf altersbedingte Erkrankungen eröffnet.

Des Weiteren wurde die Frage nach den wirksamen Bestandteilen in Cimicifuga racemosa Extrakten adressiert. In früheren Studien wurden Triterpenglykoside als an der Wirkung beteiligte Stoffgruppe identifiziert, aber in den HT22 Zellen konnten Actein, 23-Epi-26-Desoxyactein und Cimiracemosid C keine mit Ze 450 vergleichbaren Effekte vermitteln. Weiterhin wurden Subfraktionen von Ze 450 untersucht. Die EtOAc-Fraktion zeigte vergleichbare Effekte wie Ze 450, jedoch lagen die effektiven Konzentrationen höher als in korrespondierenden Konzentrationen des Gesamtextrakts. Ze 450 enthält neben Triterpenglykosiden auch Phenolsäuren, die antioxidative Effekte vermitteln. Tatsächlich zeigte Ze 450 im Vergleich zu Trolox moderate Eigenschaften als Radikalfänger, diese antioxidativen Effekten von Ze 450 tragen jedoch nicht hauptsächlich zum protektiven Mechanismus durch Ze 450 bei.

Ze 450 zeigt großes Potential zur Behandlung von Erkrankungen, bei denen oxidative Schädigungen an der Pathophysiologie entscheidend mit beteiligt sind. Darüber hinaus wurde erstmalig ein neues Wirkprinzip herausgestellt, dass die metabolische Umprogrammierung und den damit verbundenen Schutz der Mitochondrien als zentralen Wirkmechanismus von Ze 450 hervorhebt.

Neben Ze 450 wurde Ze 339, ein CO_2-Extrakt aus Blättern von *Petasites hybridus* untersucht. Dieser wird zur Behandlung der saisonalen allergischen Rhinitis eingesetzt. Ziel dieser Studie war es den Wirkmechanismus von Ze 339 zu untersuchen und mögliche protektive Effekte gegen oxidative Schäden in HT22 neuronalen Zellen zu bewerten. Ze 339 induzierte eine milde Superoxidproduktion, beeinträchtigte aber die Zelllebensfähigkeit mit Konzentrationen bis zu 50 µg/mL von nicht. Im Rahmen der Theorie der Mitohormesis könnte Ze 339 durch einen leichten Anstieg der reaktiven Sauerstoffspezies vor mitochondrialer Beeinträchtigung schützen. Darüber hinaus schützte Ze 339 vor Erastin-vermittelter Zytotoxizität und mitochondrialen Schäden in HT22 neuronalen Zellen. Aus dieser Studie ergibt sich zusammenfassend die Hypothese, dass Ze 339 die Widerstandskraft der Mitochondrien durch moderate Superoxidinduktion stärkt und diese im Kontext der (mito-) hormetischen Regulation zu vorteilhaften Effekten, wie der Symptomlinderung bei der saisonalen allergischen Rhinitis beitragen können.

Abbreviations

2-DG	2-deoxyglucose
2-NBDG	2-(N-(7-Nitrobenz-2-oxa-1,3-diazol-4-yl)amino)-2-deoxyglucose
AD	Alzheimers disease
ADP	Adeonsinediphosphate
AFDs	Amphid neurons with finger-like ciliated endings
AIF	Apoptosis-inducing factor
AMPK	AMP-activated protein kinase
AMR	ATP monitoring reagent
ANOVA	Analysis of variance
ATP	Adenosinetriphosphate
ARC	Arcuate nucleus
BID	Bcl-2 interacting domain death antagonist
BODIPY	4,4-difluoro-5-(4-phenyl-1,3-butadienyl)-4-bora-3a,4a-diaza-s-indacene-3-undecanoic acid
bp	Base pairs
BSA	Bovine serum albumin
C. elegans	*Caenorhabditis elegans*
C5a	Complement component 5a
Ca^{2+}	Calcium
CI, II, III, IV, V	Mitochondrial complex I, II, III, IV, V
Cl^-	Chloride
CLSM	Confocal laser scanning microscopy
CNS	Central nervous system
CO_2	Carbon dioxide
COX	Cyclooxygenase
Cyt c	Cytochrome c
DAPI	4',6-Diamidino-2-phenylindole
DMEM	Dulbecco's Modified Eagle Medium
DMSO	Dimethyl sulfoxide
DNA	Desoxyribonucleic acid
DNase	Deoxyribonuclease
DPN	Diarylpropionitrile

DTT	DL-Dithiothreitol
e.g.	Exempli gratia
EBSS	Earle's balanced salt solution
ECAR	Extracellular acidification rate
EDTA	Ethylenediamine-tetra-acetic acid
EGTA	Ethylene glycol-bis(2-aminoethylether)-N,N,N',N'- tetraacetic acid
EMA	European Medicines Agency
ER	Estrogen receptor
ETC	Electron transport chain
FACS	Fluorescence-activated cell scanning
FBS	Fetal bovine serum
FCCP	Carbonyl cyanide-4-(trifluoromethoxy) phenylhydrazone
FCS	Fetal calf serum
FoxOs	Forkhead Transcription Factors
fwd.	forward
GAPDH	Glyceraldehyde-3-phosphatedehydrogenase
GLUT	Glucose transporter
GPX4	Glutathione peroxidase 4
GSH	Glutathione
h	Hour
H_2O_2	Hydrogen peroxide
HBSS	Hank´s balanced salt solution
HCl	Hydrogen chloride
HEPES	4-(2-hydroxyethyl)-1-piperazineethanesulfonic acid
HIF	Hypoxia-inducible factor
HMPC	Committee on Herbal Medicinal Products
HPLC	High performance liquid chromatography
HRP	Horseradish peroxidase
HSP	Heat shock protein
HXKII	Hexokinase II
IFN	Interferon
IGF	Insulin-like growth factor

IL	Interleukin
IL-8	Interleukin 8
JAKs	Janus kinases
IMM	Inner mitochondrial membrane
IMS	Mitochondrial intermembrane space
kDa	Kilo Dalton
L.	Carl von Linné
LDHA	Lactate dehydrogenase A
LKB1	Liver kinase B1
LOX	Lipoxygenase
LT	Leukotriene
LTB4	Leukotriene B4
mctx	Mouse cortical neurons
min	Minute
mL	Milliliter
mM	Millimolar
MM	Mitochondrial matrix
MOM	Mitochondrial outer membrane
MOMP	Mitochondrial outer membrane potential
mPTP	Mitochondrial permeability transition pore
mtDNA	Mitochondrial DNA
mTOR	Mammalian target of rapamycin
mTORC1	Mammalian target of rapamycin complex 1
mTORC2	Mammalian target of rapamycin complex 2
MTT	3-(4,5-Dimethylthiazol-2-yl)-2,5-diphenyltetrazolium bromide
n.s.	Not significant
NAC	N-acetyl-L-cysteine
NADH	Nicotinamide adenine dinucleotide
NADPH	Nicotinamide adenine dinucleotide phosphate
NaOH	Sodium hydroxide
nM	Nanomolar
nm	Nanometer
NMDA	N-methyl-D-aspartic acid

NMDAR	N-methyl-D-aspartic acid receptor
Nrf2	Nuclear factor erythroid 2- related factor 2
Nutt.	Thomas Nuttal
OCR	Oxygen consumption rate
OXPHOS	Oxidative phosphorylation
PA	Pyrrolizidine alkaloids
PAF	Platelet-activating factor
PBS	Phosphate buffered saline
PCR	Polymerase chain reaction
PDK1	Pyruvate dehydrogenase kinase 1
PEG	Polyethylenglycole
PEI	Polyethylenimine
Pen/Strep	Penicillin + Streptomycin
pH	Potentia hydrogenii
PI	Propidium iodide
PI3K	Phosphoinositide 3 kinase
PPT	1,3,5-Tris(4-hydroxyphenyl)-4-propyl-1H-pyrazole
rctx	Rat cortical neurons
rev.	reverse
RNA	Ribonucleic acid
ROI	Region of interest
ROS	Reactive oxygen species
RT	Room temperature
RTCA	Real-time cell analysis
s	Second
SD	Standard deviation
SDS	Sodium dodecyl sulfate
SDS-PAGE	Sodium dodecyl sulfate polyacrylamide gel electrophoresis
SGLTs	Sodium-glucose linked transporter
SLC2A	Solute carrier family 2
SOD	Superoxide dismutase
STAT	Signal transducer and activator of transcription
TBS	Tris-buffered saline

TBST	Tris-buffered saline and Tween 20
TCA	Tricarboxylic acid cycle
TEMED	Tetramethylenethylendiamine
TMRE	Tetramethylrhodamin ethyl ester
U	Units
UbQ	Ubiquinone
UPLC TOF MS	Ultra performance liquid chromatography time of flight mass spectrometry
UV	Ultra-violet
V	Volt
WHO	World Health Organization
xCT	Glutamine-cystine antiporter
ΔΨm	Inner mitochondrial membrane potential

References

[1] Y. Guo, T. Yin, X. Wang, F. Zhang, G. Pan, H. Lv, X. Wang, J. Owoicho Orgah, Y. Zhu, H. Wu, Traditional uses, phytochemistry, pharmacology and toxicology of the genus Cimicifuga: A review, Journal of ethnopharmacology 209 (2017) 264–282.

[2] European Medicines Agency (EMA), Committee on Herbal Medicinal Products (HMPC), European Union herbal monograph on Cimicifuga racemosa (L.) Nutt., rhizoma (2018).

[3] European Medicines Agency (EMA), Committee on Herbal Medicinal Products (HMPC), Assessment report on Cimicifuga racemosa (L.) Nutt., rhizoma (2018).

[4] A.-M. Beer, R. Osmers, J. Schnitker, W. Bai, A.O. Mueck, H. Meden, Efficacy of black cohosh (Cimicifuga racemosa) medicines for treatment of menopausal symptoms - comments on major statements of the Cochrane Collaboration report 2012 "black cohosh (Cimicifuga spp.) for menopausal symptoms (review)", Gynecological endocrinology : the official journal of the International Society of Gynecological Endocrinology 29 (2013) 1022–1025.

[5] L.S. Einbond, M. Shimizu, D. Xiao, P. Nuntanakorn, J.T.E. Lim, M. Suzui, C. Seter, T. Pertel, E.J. Kennelly, F. Kronenberg, I.B. Weinstein, Growth inhibitory activity of extracts and purified components of black cohosh on human breast cancer cells, Breast cancer research and treatment 83 (2004) 221–231.

[6] Y. Shao, A. Harris, M. Wang, H. Zhang, G.A. Cordell, M. Bowman, E. Lemmo, Triterpene glycosides from Cimicifuga racemosa, Journal of natural products 63 (2000) 905–910.

[7] K. He, B. Zheng, C.H. Kim, L. Rogers, Q. Zheng, Direct analysis and identification of triterpene glycosides by LC/MS in black cohosh, Cimicifuga racemosa, and in several commercially available black cohosh products, Planta medica 66 (2000) 635–640.

[8] S.-N. Chen, W. Li, D.S. Fabricant, B.D. Santarsiero, A. Mesecar, J.F. Fitzloff, H.H.S. Fong, N.R. Farnsworth, Isolation, structure elucidation, and absolute configuration of 26-deoxyactein from Cimicifuga racemosa and clarification of nomenclature associated with 27-deoxyactein, Journal of natural products 65 (2002) 601–605.

[9] E. Bedir, I.A. Khan, Cimiracemoside a: A new cyclolanostanol xyloside from the rhizome of Cimicifuga racemosa, Chemical & pharmaceutical bulletin 48 (2000) 425–427.

[10] V. Werner, M. Petersen, A BAHD hydroxycinnamoyltransferase from Actaea racemosa catalyses the formation of fukinolic and cimicifugic acids, Planta (2019).

[11] D. Struck, M. Tegtmeier, G. Harnischfeger, Flavones in extracts of Cimicifuga racemosa, Planta medica 63 (1997) 289.

[12] X. Li, J. Lin, Y. Gao, W. Han, D. Chen, Antioxidant activity and mechanism of Rhizoma Cimicifugae, Chemistry Central journal 6 (2012) 140.

[13] R. Qin, Y. Zhao, Y. Zhao, W. Zhou, C. Lv, J. Lu, Polyphenolic compounds with antioxidant potential and neuro-protective effect from Cimicifuga dahurica (Turcz.) Maxim, Fitoterapia 115 (2016) 52–56.

[14] H. Jarry, G. Harnischfeger, Studies on the endocrine effects of the contents of Cimicifuga racemosa, Planta medica 51 (1985) 46–49.

[15] B. Avula, Y.-H. Wang, T.J. Smillie, I.A. Khan, Quantitative determination of triterpenoids and formononetin in rhizomes of black cohosh (Actaea racemosa) and dietary supplements by using UPLC-UV/ELS detection and identification by UPLC-MS, Planta medica 75 (2009) 381–386.

[16] B. Jiang, F. Kronenberg, M.J. Balick, E.J. Kennelly, Analysis of formononetin from black cohosh (Actaea racemosa), Phytomedicine : international journal of phytotherapy and phytopharmacology 13 (2006) 477–486.

[17] E.J. Kennelly, S. Baggett, P. Nuntanakorn, A.L. Ososki, S.A. Mori, J. Duke, M. Coleton, F. Kronenberg, Analysis of thirteen populations of black cohosh for formononetin, Phytomedicine : international journal of phytotherapy and phytopharmacology 9 (2002) 461–467.

[18] J.L. Bacon, The Menopausal Transition, Obstetrics and gynecology clinics of North America 44 (2017) 285–296.

[19] T.A. Takahashi, K.M. Johnson, Menopause, The Medical clinics of North America 99 (2015) 521–534.

[20] I. Lejri, A. Grimm, A. Eckert, Mitochondria, Estrogen and Female Brain Aging, Frontiers in aging neuroscience 10 (2018) 124.

[21] T.D. Shanafelt, D.L. Barton, A.A. Adjei, C.L. Loprinzi, Pathophysiology and treatment of hot flashes, Mayo Clinic proceedings 77 (2002) 1207–1218.

[22] R.R. Freedman, Pathophysiology and treatment of menopausal hot flashes, Seminars in reproductive medicine 23 (2005) 117–125.

[23] J.E. Rossouw, G.L. Anderson, R.L. Prentice, A.Z. LaCroix, C. Kooperberg, M.L. Stefanick, R.D. Jackson, S.A.A. Beresford, B.V. Howard, K.C. Johnson, J.M. Kotchen, J. Ockene, Risks and benefits of estrogen plus progestin in healthy postmenopausal women: principal results From the Women's Health Initiative randomized controlled trial, JAMA 288 (2002) 321–333.

[24] S. Hulley, C. Furberg, E. Barrett-Connor, J. Cauley, D. Grady, W. Haskell, R. Knopp, M. Lowery, S. Satterfield, H. Schrott, E. Vittinghoff, D. Hunninghake, Noncardiovascular disease outcomes during 6.8 years of hormone therapy: Heart and Estrogen/progestin Replacement Study follow-up (HERS II), JAMA 288 (2002) 58–66.

[25] Breast cancer and hormone-replacement therapy in the Million Women Study, The Lancet 362 (2003) 419–427.

[26] M.M. Regan, S.K. Emond, M.J. Attardo, R.A. Parker, S.L. Greenspan, Why do older women discontinue hormone replacement therapy?, Journal of women's health & gender-based medicine 10 (2001) 343–350.

[27] R.E. Nappi, B. Malavasi, B. Brundu, F. Facchinetti, Efficacy of Cimicifuga racemosa on climacteric complaints: a randomized study versus low-dose transdermal estradiol, Gynecological endocrinology : the official journal of the International Society of Gynecological Endocrinology 20 (2005) 30–35.

[28] R. Osmers, M. Friede, E. Liske, J. Schnitker, J. Freudenstein, H.-H. Henneicke-von Zepelin, Efficacy and safety of isopropanolic black cohosh extract for climacteric symptoms, Obstetrics and gynecology 105 (2005) 1074–1083.

[29] B. Naser, J. Schnitker, M.J. Minkin, S.G. de Arriba, K.-U. Nolte, R. Osmers, Suspected black cohosh hepatotoxicity: no evidence by meta-analysis of randomized controlled clinical trials for isopropanolic black cohosh extract, Menopause (New York, N.Y.) 18 (2011) 366–375.

[30] G. Cui, H. Leng, K. Wang, J. Wang, S. Zhu, J. Jia, X. Chen, W. Zhang, L. Qin, W. Bai, Effects of Remifemin Treatment on Bone Integrity and Remodeling in Rats with Ovariectomy-Induced Osteoporosis, PLoS ONE 8 (2013).

[31] D. Seidlova-Wuttke, G. Stecher, M. Kammann, J. Haunschild, N. Eder, V. Stahnke, J. Wessels, W. Wuttke, Osteoprotective effects of Cimicifuga racemosa and its triterpene-saponins are responsible for reduction of bone marrow fat, Phytomedicine : international journal of phytotherapy and phytopharmacology 19 (2012) 855–860.

[32] V. Viereck, C. Gründker, S.C. Friess, K.-H. Frosch, D. Raddatz, M. Schoppet, T. Nisslein, G. Emons, L.C. Hofbauer, Isopropanolic extract of black cohosh stimulates osteoprotegerin production by human osteoblasts, Journal of bone and mineral research : the official journal of the American Society for Bone and Mineral Research 20 (2005) 2036–2043.

[33] W. LI, N.-x. SUN, X. CHEN, D.-f. LANG, Z.-j. JIN, Cimicifuga racemosa for treatment of menopausal symptoms in patients with early endometrial cancer after operation, Academic Journal of Second Military Medical University 32 (2013) 562–564.

[34] M.A. García-Pérez, B. Pineda, C. Hermenegildo, J.J. Tarín, A. Cano, Isopropanolic Cimicifuga racemosa is favorable on bone markers but neutral on an osteoblastic cell line, Fertility and sterility 91 (2009) 1347–1350.

[35] C. Moser, S.P. Vickers, R. Brammer, S.C. Cheetham, J. Drewe, Antidiabetic effects of the Cimicifuga racemosa extract Ze 450 in vitro and in vivo in ob/ob mice, Phytomedicine : international journal of phytotherapy and phytopharmacology 21 (2014) 1382–1389.

[36] Y. Sun, Q. Yu, Q. Shen, W. Bai, J. Kang, Black Cohosh Ameliorates Metabolic Disorders in Female Ovariectomized Rats, Rejuvenation research 19 (2016) 204–214.

[37] S. Xi, E. Liske, S. Wang, J. Liu, Z. Zhang, L. Geng, L. Hu, C. Jiao, S. Zheng, H.-H.H.-v. Zepelin, W. Bai, Effect of Isopropanolic Cimicifuga racemosa Extract on Uterine Fibroids in Comparison with Tibolone among Patients of a Recent Randomized, Double Blind, Parallel-Controlled Study in Chinese Women with Menopausal Symptoms, Evidence-based complementary and alternative medicine : eCAM 2014 (2014).

[38] S.B. Doshi, A. Agarwal, The role of oxidative stress in menopause, Journal of mid-life health 4 (2013) 140–146.

[39] L.H. Sekhon, A. Agarwal, The Menopause and Oxidative Stress, in: A. Agarwal, N. Aziz, B. Rizk (Eds.), Studies on Women's Health, vol. 3, Humana Press, Totowa, NJ, 2013, pp. 181–203.

[40] J.E. Burdette, J. Liu, S.-N. Chen, D.S. Fabricant, C.E. Piersen, E.L. Barker, J.M. Pezzuto, A. Mesecar, R.B. van Breemen, N.R. Farnsworth, J.L. Bolton, Black cohosh acts as a mixed competitive ligand and partial agonist of the serotonin receptor, Journal of agricultural and food chemistry 51 (2003) 5661–5670.

[41] S.L. Powell, T. Gödecke, D. Nikolic, S.-N. Chen, S. Ahn, B. Dietz, N.R. Farnsworth, R.B. van Breemen, D.C. Lankin, G.F. Pauli, J.L. Bolton, In vitro serotonergic activity

of black cohosh and identification of N(omega)-methylserotonin as a potential active constituent, Journal of agricultural and food chemistry 56 (2008) 11718–11726.

[42] P.B. Hedlund, P.E. Danielson, E.A. Thomas, K. Slanina, M.J. Carson, J.G. Sutcliffe, No hypothermic response to serotonin in 5-HT7 receptor knockout mice, Proceedings of the National Academy of Sciences of the United States of America 100 (2003) 1375–1380.

[43] P. Kapur, W. Wuttke, D. Seidlova-Wuttke, The Cimicifuga racemosa special extract BNO 1055 prevents hot flashes in ovariectomized rats, Phytomedicine : international journal of phytotherapy and phytopharmacology 17 (2010) 890–894.

[44] Z. Hui, M. Xiaoyan, Y. Mukun, W. Ke, Y. Liyuan, Z. Sainan, J. Jing, Q. Lihua, B. Wenpei, Effects of black cohosh and estrogen on the hypothalamic nuclei of ovariectomized rats at different temperatures, Journal of ethnopharmacology 142 (2012) 769–775.

[45] N.E. Reame, J.L. Lukacs, V. Padmanabhan, A.D. Eyvazzadeh, Y.R. Smith, J.-K. Zubieta, Black cohosh has central opioid activity in postmenopausal women: evidence from naloxone blockade and positron emission tomography neuroimaging, Menopause (New York, N.Y.) 15 (2008) 832–840.

[46] E. Liske, W. Hänggi, H.-H. Henneicke-von Zepelin, N. Boblitz, P. Wüstenberg, V.W. Rahlfs, Physiological investigation of a unique extract of black cohosh (Cimicifugae racemosae rhizoma): a 6-month clinical study demonstrates no systemic estrogenic effect, Journal of women's health & gender-based medicine 11 (2002) 163–174.

[47] M. Crone, K. Hallman, V. Lloyd, M. Szmyd, B. Badamo, M. Morse, S. Dinda, The antiestrogenic effects of black cohosh on BRCA1 and steroid receptors in breast cancer cells, Breast cancer (Dove Medical Press) 11 (2019) 99–110.

[48] M. Rostock, J. Fischer, A. Mumm, U. Stammwitz, R. Saller, H.H. Bartsch, Black cohosh (Cimicifuga racemosa) in tamoxifen-treated breast cancer patients with climacteric complaints - a prospective observational study, Gynecological endocrinology : the official journal of the International Society of Gynecological Endocrinology 27 (2011) 844–848.

[49] H.H. Henneicke-von Zepelin, H. Meden, K. Kostev, D. Schröder-Bernhardi, U. Stammwitz, H. Becher, Isopropanolic black cohosh extract and recurrence-free survival after breast cancer, International journal of clinical pharmacology and therapeutics 45 (2007) 143–154.

[50] N. Obi, J. Chang-Claude, J. Berger, W. Braendle, T. Slanger, M. Schmidt, K. Steindorf, W. Ahrens, D. Flesch-Janys, The use of herbal preparations to alleviate

climacteric disorders and risk of postmenopausal breast cancer in a German case-control study, Cancer epidemiology, biomarkers & prevention : a publication of the American Association for Cancer Research, cosponsored by the American Society of Preventive Oncology 18 (2009) 2207–2213.

[51] A.L. Hirschberg, M. Edlund, G. Svane, E. Azavedo, L. Skoog, B. von Schoultz, An isopropanolic extract of black cohosh does not increase mammographic breast density or breast cell proliferation in postmenopausal women, Menopause (New York, N.Y.) 14 (2007) 89–96.

[52] P. Stute, L. Ost, L. Bütikofer, Effect of CIMicifuga racemosa on metaBOLIC parameters in women with menopausal symptoms – a retrospective cohort study (CIMBOLIC), in: Frauenheilkunde im Fokus: wissenschaftlich fundiert und der Qualität verpflichtet, Georg Thieme Verlag KG, 2018.

[53] H.N. Polotsky, A.J. Polotsky, Metabolic implications of menopause, Seminars in reproductive medicine 28 (2010) 426–434.

[54] C.E. Cross, B. Halliwell, E.T. Borish, W.A. Pryor, B.N. Ames, R.L. Saul, J.M. McCord, D. Harman, Oxygen radicals and human disease, Annals of internal medicine 107 (1987) 526–545.

[55] C. Culmsee, S. Landshamer, Molecular insights into mechanisms of the cell death program: role in the progression of neurodegenerative disorders, Current Alzheimer research 3 (2006) 269–283.

[56] K. Stadler, Oxidative stress in diabetes, Advances in experimental medicine and biology 771 (2012) 272–287.

[57] M. Celik, A. Tuncer, O.U. Soyer, C. Saçkesen, H. Tanju Besler, O. Kalayci, Oxidative stress in the airways of children with asthma and allergic rhinitis, Pediatric allergy and immunology : official publication of the European Society of Pediatric Allergy and Immunology 23 (2012) 556–561.

[58] W.S. Yang, B.R. Stockwell, Ferroptosis: Death by Lipid Peroxidation, Trends in Cell Biology 26 (2016) 165–176.

[59] S. Neitemeier, A. Jelinek, V. Laino, L. Hoffmann, I. Eisenbach, R. Eying, G.K. Ganjam, A.M. Dolga, S. Oppermann, C. Culmsee, BID links ferroptosis to mitochondrial cell death pathways, Redox biology 12 (2017) 558–570.

[60] S. Tan, D. Schubert, P. Maher, Oxytosis: A novel form of programmed cell death, Current topics in medicinal chemistry 1 (2001) 497–506.

[61] R. Brigelius-Flohé, M. Maiorino, Glutathione peroxidases, Biochimica et Biophysica Acta (BBA) - General Subjects 1830 (2013) 3289–3303.

[62] A. Jelinek, L. Heyder, M. Daude, M. Plessner, S. Krippner, R. Grosse, W.E. Diederich, C. Culmsee, Mitochondrial rescue prevents glutathione peroxidase-dependent ferroptosis, Free radical biology & medicine 117 (2018) 45–57.

[63] J. Grohm, S.-W. Kim, U. Mamrak, S. Tobaben, A. Cassidy-Stone, J. Nunnari, N. Plesnila, C. Culmsee, Inhibition of Drp1 provides neuroprotection in vitro and in vivo, Cell death and differentiation 19 (2012) 1446–1458.

[64] J. Grohm, N. Plesnila, C. Culmsee, Bid mediates fission, membrane permeabilization and peri-nuclear accumulation of mitochondria as a prerequisite for oxidative neuronal cell death, Brain, behavior, and immunity 24 (2010) 831–838.

[65] L. Galluzzi, K. Blomgren, G. Kroemer, Mitochondrial membrane permeabilization in neuronal injury, Nature reviews. Neuroscience 10 (2009) 481–494.

[66] E.C.C. Cheung, L. Melanson-Drapeau, S.P. Cregan, J.L. Vanderluit, K.L. Ferguson, W.C. McIntosh, D.S. Park, S.A.L. Bennett, R.S. Slack, Apoptosis-inducing factor is a key factor in neuronal cell death propagated by BAX-dependent and BAX-independent mechanisms, The Journal of neuroscience : the official journal of the Society for Neuroscience 25 (2005) 1324–1334.

[67] N. Doti, C. Reuther, P.L. Scognamiglio, A.M. Dolga, N. Plesnila, M. Ruvo, C. Culmsee, Inhibition of the AIF/CypA complex protects against intrinsic death pathways induced by oxidative stress, cddis 5 (2014) e993. https://www.nature.com/articles/cddis2013518.pdf.

[68] R. Wang, P.H. Reddy, Role of Glutamate and NMDA Receptors in Alzheimer's Disease, Journal of Alzheimer's disease : JAD 57 (2017) 1041–1048.

[69] A. Mehta, M. Prabhakar, P. Kumar, R. Deshmukh, P.L. Sharma, Excitotoxicity: bridge to various triggers in neurodegenerative disorders, European journal of pharmacology 698 (2013) 6–18.

[70] D.W. Choi, S.M. Rothman, The role of glutamate neurotoxicity in hypoxic-ischemic neuronal death, Annual review of neuroscience 13 (1990) 171–182.

[71] E. Berdichevsky, N. Riveros, S. Sánchez-Armáss, F. Orrego, Kainate, N-methylaspartate and other excitatory amino acids increase calcium influx into rat brain cortex cells in vitro, Neuroscience Letters 36 (1983) 75–80. http://www.sciencedirect.com/science/article/pii/0304394083904895.

[72] D. Bano, K.W. Young, C.J. Guerin, R. Lefeuvre, N.J. Rothwell, L. Naldini, R. Rizzuto, E. Carafoli, P. Nicotera, Cleavage of the plasma membrane Na+/Ca2+ exchanger in excitotoxicity, Cell 120 (2005) 275–285.

[73] D. Nicholls, Mitochondrial Dysfunction and Glutamate Excitotoxicity Studied in Primary Neuronal Cultures, CMM 4 (2004) 149–177.

[74] R.I. Stanika, N.B. Pivovarova, C.A. Brantner, C.A. Watts, C.A. Winters, S.B. Andrews, Coupling diverse routes of calcium entry to mitochondrial dysfunction and glutamate excitotoxicity, Proceedings of the National Academy of Sciences of the United States of America 106 (2009) 9854–9859.

[75] M.G. Vander Heiden, L.C. Cantley, C.B. Thompson, Understanding the Warburg Effect: The Metabolic Requirements of Cell Proliferation, Science (New York, N.Y.) 324 (2009) 1029–1033.

[76] M.P. Murphy, How mitochondria produce reactive oxygen species, The Biochemical journal 417 (2009) 1–13.

[77] O. WARBURG, On the origin of cancer cells, Science (New York, N.Y.) 123 (1956) 309–314.

[78] R.A. Medina, G.I. Owen, Glucose transporters: expression, regulation and cancer, Biological research 35 (2002) 9–26.

[79] R.A. Nakashima, M.G. Paggi, L.J. Scott, P.L. Pedersen, Purification and characterization of a bindable form of mitochondrial bound hexokinase from the highly glycolytic AS-30D rat hepatoma cell line, Cancer research 48 (1988) 913–919.

[80] A. Marín-Hernández, S. Rodríguez-Enríquez, P.A. Vital-González, F.L. Flores-Rodríguez, M. Macías-Silva, M. Sosa-Garrocho, R. Moreno-Sánchez, Determining and understanding the control of glycolysis in fast-growth tumor cells. Flux control by an over-expressed but strongly product-inhibited hexokinase, The FEBS journal 273 (2006) 1975–1988.

[81] L. BAGGETTO, Deviant energetic metabolism of glycolytic cancer cells, Biochimie 74 (1992) 959–974.

[82] R.A. Cairns, I.S. Harris, T.W. Mak, Regulation of cancer cell metabolism, nrc 11 (2011) 85–95. https://www.nature.com/articles/nrc2981.pdf.

[83] C.V. Dang, K.A. O'Donnell, K.I. Zeller, T. Nguyen, R.C. Osthus, F. Li, The c-Myc target gene network, Seminars in cancer biology 16 (2006) 253–264.

[84] E.S. Goetzman, E.V. Prochownik, The Role for Myc in Coordinating Glycolysis, Oxidative Phosphorylation, Glutaminolysis, and Fatty Acid Metabolism in Normal and Neoplastic Tissues, Frontiers in endocrinology 9 (2018) 129.

[85] L. Liu, J. Ulbrich, J. Müller, T. Wüstefeld, L. Aeberhard, T.R. Kress, N. Muthalagu, L. Rycak, R. Rudalska, R. Moll, S. Kempa, L. Zender, M. Eilers, D.J. Murphy, Deregulated MYC expression induces dependence upon AMPK-related kinase 5, Nature 483 (2012) 608–612.

[86] G.L. Semenza, Targeting HIF-1 for cancer therapy, Nature reviews. Cancer 3 (2003) 721–732.

[87] A. Okamoto, C. Sumi, H. Tanaka, M. Kusunoki, T. Iwai, K. Nishi, Y. Matsuo, H. Harada, K. Takenaga, H. Bono, K. Hirota, HIF-1-mediated suppression of mitochondria electron transport chain function confers resistance to lidocaine-induced cell death, Scientific reports 7 (2017) 3816.

[88] J.G. White, E. Southgate, J.N. Thomson, S. Brenner, The structure of the nervous system of the nematode Caenorhabditis elegans, Philosophical transactions of the Royal Society of London. Series B, Biological sciences 314 (1986) 1–340.

[89] E. Beale, G. Li, M.-W. Tan, K.P. Rumbaugh, Caenorhabditis elegans senses bacterial autoinducers, Applied and environmental microbiology 72 (2006) 5135–5137.

[90] J.E. Sulston, D.G. Albertson, J.N. Thomson, The Caenorhabditis elegans male: Postembryonic development of nongonadal structures, Developmental Biology 78 (1980) 542–576.

[91] M.M. Barr, L.R. García, D.S. Portman, Sexual Dimorphism and Sex Differences in Caenorhabditis elegans Neuronal Development and Behavior, Genetics 208 (2018) 909–935.

[92] R.A. Butcher, M. Fujita, F.C. Schroeder, J. Clardy, Small-molecule pheromones that control dauer development in Caenorhabditis elegans, Nature chemical biology 3 (2007) 420–422.

[93] T.W. Harris, N. Chen, F. Cunningham, M. Tello-Ruiz, I. Antoshechkin, C. Bastiani, T. Bieri, D. Blasiar, K. Bradnam, J. Chan, C.-K. Chen, W.J. Chen, P. Davis, E. Kenny, R. Kishore, D. Lawson, R. Lee, H.-M. Muller, C. Nakamura, P. Ozersky, A. Petcherski, A. Rogers, A. Sabo, E.M. Schwarz, K. van Auken, Q. Wang, R. Durbin, J. Spieth, P.W. Sternberg, L.D. Stein, WormBase: a multi-species resource for nematode biology and genomics, Nucleic Acids Research 32 (2004) D411-7.

[94] J. Feng, F. Bussière, S. Hekimi, Mitochondrial Electron Transport Is a Key Determinant of Life Span in Caenorhabditis elegans, Developmental Cell 1 (2001) 633–644. http://www.sciencedirect.com/science/article/pii/S1534580701000715.

[95] B. Lakowski, S. Hekimi, The genetics of caloric restriction in Caenorhabditis elegans, Proceedings of the National Academy of Sciences of the United States of America 95 (1998) 13091–13096.

[96] L. Avery, The genetics of feeding in Caenorhabditis elegans, Genetics 133 (1993) 897–917.

[97] J. Lemieux, B. Lakowski, A. Webb, Y. Meng, A. Ubach, F. Bussière, T. Barnes, S. Hekimi, Regulation of physiological rates in Caenorhabditis elegans by a tRNA-modifying enzyme in the mitochondria, Genetics 159 (2001) 147–157.

[98] K.D. Kimura, H.A. Tissenbaum, Y. Liu, G. Ruvkun, daf-2, an insulin receptor-like gene that regulates longevity and diapause in Caenorhabditis elegans, Science (New York, N.Y.) 277 (1997) 942–946.

[99] K. Lin, J.B. Dorman, A. Rodan, C. Kenyon, daf-16: An HNF-3/forkhead family member that can function to double the life-span of Caenorhabditis elegans, Science (New York, N.Y.) 278 (1997) 1319–1322.

[100] D. Gems, A.J. Sutton, M.L. Sundermeyer, P.S. Albert, K.V. King, M.L. Edgley, P.L. Larsen, D.L. Riddle, Two pleiotropic classes of daf-2 mutation affect larval arrest, adult behavior, reproduction and longevity in Caenorhabditis elegans, Genetics 150 (1998) 129–155.

[101] M.J. Muñoz, D.L. Riddle, Positive selection of Caenorhabditis elegans mutants with increased stress resistance and longevity, Genetics 163 (2003) 171–180.

[102] M. Akerfelt, R.I. Morimoto, L. Sistonen, Heat shock factors: integrators of cell stress, development and lifespan, Nature reviews. Molecular cell biology 11 (2010) 545–555.

[103] V. Prahlad, T. Cornelius, R.I. Morimoto, Regulation of the cellular heat shock response in Caenorhabditis elegans by thermosensory neurons, Science (New York, N.Y.) 320 (2008) 811–814.

[104] A.-L. Hsu, C.T. Murphy, C. Kenyon, Regulation of aging and age-related disease by DAF-16 and heat-shock factor, Science (New York, N.Y.) 300 (2003) 1142–1145.

[105] S.C. Zevian, J.L. Yanowitz, Methodological considerations for heat shock of the nematode Caenorhabditis elegans, Methods (San Diego, Calif.) 68 (2014) 450–457.

[106] M. Rodriguez, L.B. Snoek, M. de Bono, J.E. Kammenga, Worms under stress: C. elegans stress response and its relevance to complex human disease and aging, Trends in genetics : TIG 29 (2013) 367–374.

[107] J.M. Morán, M.A. Ortiz-Ortiz, L.M. Ruiz-Mesa, J.M. Fuentes, Nitric oxide in paraquat-mediated toxicity: A review, Journal of biochemical and molecular toxicology 24 (2010) 402–409.

[108] C.E. Schaar, D.J. Dues, K.K. Spielbauer, E. Machiela, J.F. Cooper, M. Senchuk, S. Hekimi, J.M. van Raamsdonk, Mitochondrial and cytoplasmic ROS have opposing effects on lifespan, PLoS genetics 11 (2015) e1004972.

[109] A.B. Hwang, E.-A. Ryu, M. Artan, H.-W. Chang, M.H. Kabir, H.-J. Nam, D. Lee, J.-S. Yang, S. Kim, W.B. Mair, C. Lee, S.S. Lee, S.-J. Lee, Feedback regulation via AMPK and HIF-1 mediates ROS-dependent longevity in Caenorhabditis elegans, Proceedings of the National Academy of Sciences of the United States of America 111 (2014) E4458-67.

[110] I. Mori, Y. Ohshima, Molecular neurogenetics of chemotaxis and thermotaxis in the nematode Caenorhabditis elegans, BioEssays : news and reviews in molecular, cellular and developmental biology 19 (1997) 1055–1064.

[111] C.I. Bargmann, E. Hartwieg, H.R. Horvitz, Odorant-selective genes and neurons mediate olfaction in C. elegans, Cell 74 (1993) 515–527.

[112] K. Brune, D. Bickel, B.A. Peskar, Gastro-protective effects by extracts of Petasites hybridus: the role of inhibition of peptido-leukotriene synthesis, Planta medica 59 (1993) 494–496.

[113] R.B. Lipton, H. Göbel, K.M. Einhäupl, K. Wilks, A. Mauskop, Petasites hybridus root (butterbur) is an effective preventive treatment for migraine, Neurology 63 (2004) 2240–2244.

[114] B.V. Lovell, M.J. Marmura, New therapeutic developments in chronic migraine, Current opinion in neurology 23 (2010) 254–258.

[115] P. Kälin, Gemeine Pestwurz (Petasites hybridus)--Portrait einer Arzneipflanze, Forschende Komplementarmedizin und klassische Naturheilkunde = Research in complementary and natural classical medicine 10 Suppl 1 (2003) 41–44.

[116] R. Hänsel, H. Rimpler, K. Keller, G. Schneider, G. Abel, G. Bader, T. Baumann, B. Bertram, G. Beyer, U. Bodesheim, N. Brand, M. Brautigam, R. Brenneisen, A. Burger, J. Burghart, N. Chaurasia, U. Eilert, D. Ennet, W. Ferstl, B. Frank, B. Gehrmann, C. Goez, K. Gomaa, P. Gorecki, R. Hansel, G. Harnischfeger, F. Hasler,

E. Hecker, J. Heni, G. Henkler, G. Heubl, A. Hiermann, K. Hiller, K. Hoffmann-Bohm, J. Holzl, K.-H. Horz, W.-D. Hubner, O. Isaac, W. Juretzek, M. Kampfer, C. Kletter, H. Koch, H. Koehler, G. Konig, J. Kraus, B. Kreher, L. Krenn, H. Kretschmer, S. Kudicke, P. Laux, B. Meier, M. Meier-Liebi, I. Merfort, S. Moeck, S. Mundt, G. Reher, A. Rehwald, J. Reichling, E. Roder, C. Rothe, H. Rzadkowska-Bodalska, W. Schilz, H. Schleinitz, G. Schneider, K. Schneider, T. Schollhorn, E. Scholz, T. Schopke, V. Schulz, B. Schwarz-Schulz, H. Schwarze, S. Schweins, R. Seitz, U. Sonnenborn, V. Ssymank, K. Staesche, E. Stahl-Biskup, A.-B. Stalder, H. Stuppner, E. Teuscher, G. Tewocht, A. Thomas, M. Veit, M. Wink, H. Wolf (Eds.), Hagers Handbuch der Pharmazeutischen Praxis. Drogen P-Z, 5th ed., Springer Berlin Heidelberg, Berlin, Heidelberg, s.l., 1994.

[117] A. Schapowal, Butterbur Ze 339 for the treatment of intermittent allergic rhinitis: dose-dependent efficacy in a prospective, randomized, double-blind, placebo-controlled study, Archives of otolaryngology--head & neck surgery 130 (2004) 1381–1386.

[118] O.A.R. Thomet, A. Schapowal, I.V.W.M. Heinisch, U.N. Wiesmann, H.-U. Simon, Anti-inflammatory activity of an extract of Petasites hybridus in allergic rhinitis, International immunopharmacology 2 (2002) 997–1006.

[119] S.A. Steiert, U.M. Zissler, A.M. Chaker, J. Esser-von-Bieren, D. Dittlein, F. Guerth, C.A. Jakwerth, G. Piontek, C. Zahner, J. Drewe, C. Traidl-Hoffmann, C.B. Schmidt-Weber, S. Gilles, Anti-inflammatory effects of the petasin phyto drug Ze 339 are mediated by inhibition of the STAT pathway, BioFactors (Oxford, England) 43 (2017) 388–399.

[120] A. Schenk, B. Siewert, S. Toff, J. Drewe, UPLC TOF MS for sensitive quantification of naturally occurring pyrrolizidine alkaloids in Petasites hybridus extract (Ze 339), Journal of chromatography. B, Analytical technologies in the biomedical and life sciences 997 (2015) 23–29.

[121] J. Suonpää, Treatment of Allergic Rhinitis, Annals of Medicine 28 (1996) 17–22.

[122] P.J. Barnes, Therapeutic strategies for allergic diseases, Nature 402 (1999) B31-8.

[123] E.O. Meltzer, Pharmacological treatment options for allergic rhinitis and asthma, Clinical and experimental allergy : journal of the British Society for Allergy and Clinical Immunology 28 Suppl 2 (1998) 27–36.

[124] O.A. Thomet, U.N. Wiesmann, A. Schapowal, C. Bizer, H.U. Simon, Role of petasin in the potential anti-inflammatory activity of a plant extract of petasites hybridus, Biochemical pharmacology 61 (2001) 1041–1047.

[125] C. Scheidegger, C. Dahinden, U. Wiesmann, Effects of extracts and of individual components from Petasites on prostaglandin synthesis in cultured skin fibroblasts and on leucotriene synthesis in isolated human peripheral leucocytes, Pharmaceutica acta Helvetiae 72 (1998) 376–378.

[126] D. Berger, W. Burkard, W. Schaffner, Influence of Petasites hybridus on dopamine-D2 and histamine-H1 receptors, Pharmaceutica acta Helvetiae 72 (1998) 373–375.

[127] H.S. Li, S.S. Watowich, Innate immune regulation by STAT-mediated transcriptional mechanisms, Immunological reviews 261 (2014) 84–101.

[128] C.M. Horvath, STAT proteins and transcriptional responses to extracellular signals, Trends in biochemical sciences 25 (2000) 496–502.

[129] O.A. Thomet, U.N. Wiesmann, K. Blaser, H.U. Simon, Differential inhibition of inflammatory effector functions by petasin, isopetasin and neopetasin in human eosinophils, Clinical and experimental allergy : journal of the British Society for Allergy and Clinical Immunology 31 (2001) 1310–1320.

[130] A.F. Dumitru, M. Shamji, M. Wagenmann, S. Hindersin, K. Scheckenbach, J. Greve, T. Klenzner, L. Hess, S. Nebel, C. Zimmermann, C. Zahner, C.B. Schmidt-Weber, A.M. Chaker, Petasol butenoate complex (Ze 339) relieves allergic rhinitis-induced nasal obstruction more effectively than desloratadine, The Journal of allergy and clinical immunology 127 (2011) 1515-21.e6.

[131] A. Schapowal, Randomised controlled trial of butterbur and cetirizine for treating seasonal allergic rhinitis, BMJ (Clinical research ed.) 324 (2002) 144–146.

[132] Q. Shi, Z. Lei, G. Cheng, D. Li, Q. Wang, S. Luo, H. Yang, H. Jia, Mitochondrial ROS activate interleukin-1β expression in allergic rhinitis, Oncology letters 16 (2018) 3193–3200.

[133] T. Finkel, Signal transduction by reactive oxygen species, The Journal of cell biology 194 (2011) 7–15.

[134] M. Schieber, N.S. Chandel, ROS function in redox signaling and oxidative stress, Current biology : CB 24 (2014) R453-62.

[135] M.P. Mattson, A. Cheng, Neurohormetic phytochemicals: Low-dose toxins that induce adaptive neuronal stress responses, Trends in neurosciences 29 (2006) 632–639.

[136] M.P. Mattson, Hormesis Defined, Ageing research reviews 7 (2007) 1–7.

[137] V. Calabrese, C. Cornelius, A. Trovato, M. Cavallaro, C. Mancuso, L. Di Rienzo, D. Condorelli, A. de Lorenzo, E.J. Calabrese, The hormetic role of dietary antioxidants in free radical-related diseases, Current pharmaceutical design 16 (2010) 877–883.

[138] P.B. Esparza-Moltó, C. Nuevo-Tapioles, J.M. Cuezva, Regulation of the H+-ATP synthase by IF1: a role in mitohormesis, Cellular and molecular life sciences : CMLS 74 (2017) 2151–2166.

[139] M. Ristow, Unraveling the truth about antioxidants: mitohormesis explains ROS-induced health benefits, Nature medicine 20 (2014) 709–711.

[140] B.H. Morimoto, D.E. Koshland, Excitatory amino acid uptake and N-methyl-D-aspartate-mediated secretion in a neural cell line, Proceedings of the National Academy of Sciences of the United States of America 87 (1990) 3518–3521.

[141] B.H. Morimoto, D.E. Koshland, Induction and expression of long- and short-term neurosecretory potentiation in a neural cell line, Neuron 5 (1990) 875–880.

[142] M. Rabenau, M. Unger, J. Drewe, C. Culmsee, Metabolic switch induced by Cimicifuga racemosa extract prevents mitochondrial damage and oxidative cell death, Phytomedicine : international journal of phytotherapy and phytopharmacology 52 (2019) 107–116.

[143] J.E. Burdette, S.-N. Chen, Z.-Z. Lu, H. Xu, B.E.P. White, D.S. Fabricant, J. Liu, H.H.S. Fong, N.R. Farnsworth, A.I. Constantinou, R.B. van Breemen, J.M. Pezzuto, J.L. Bolton, Black cohosh (Cimicifuga racemosa L.) protects against menadione-induced DNA damage through scavenging of reactive oxygen species: bioassay-directed isolation and characterization of active principles, Journal of agricultural and food chemistry 50 (2002) 7022–7028.

[144] S. Schmitt, C. Eberhagen, S. Weber, M. Aichler, H. Zischka, Isolation of mitochondria from cultured cells and liver tissue biopsies for molecular and biochemical analyses, Methods in molecular biology (Clifton, N.J.) 1295 (2015) 87–97.

[145] S. Schulz, J. Lichtmannegger, S. Schmitt, C. Leitzinger, C. Eberhagen, C. Einer, J. Kerth, M. Aichler, H. Zischka, A protocol for the parallel isolation of intact

mitochondria from rat liver, kidney, heart, and brain, Methods in molecular biology (Clifton, N.J.) 1295 (2015) 75–86.

[146] M.V. Berridge, A.S. Tan, Characterization of the cellular reduction of 3-(4,5-dimethylthiazol-2-yl)-2,5-diphenyltetrazolium bromide (MTT): subcellular localization, substrate dependence, and involvement of mitochondrial electron transport in MTT reduction, Archives of biochemistry and biophysics 303 (1993) 474–482.

[147] N.M.C. Connolly, P. Theurey, V. Adam-Vizi, N.G. Bazan, P. Bernardi, J.P. Bolaños, C. Culmsee, V.L. Dawson, M. Deshmukh, M.R. Duchen, H. Düssmann, G. Fiskum, M.F. Galindo, G.E. Hardingham, J.M. Hardwick, M.B. Jekabsons, E.A. Jonas, J. Jordán, S.A. Lipton, G. Manfredi, M.P. Mattson, B. McLaughlin, A. Methner, A.N. Murphy, M.P. Murphy, D.G. Nicholls, B.M. Polster, T. Pozzan, R. Rizzuto, J. Satrústegui, R.S. Slack, R.A. Swanson, R.H. Swerdlow, Y. Will, Z. Ying, A. Joselin, A. Gioran, C. Moreira Pinho, O. Watters, M. Salvucci, I. Llorente-Folch, D.S. Park, D. Bano, M. Ankarcrona, P. Pizzo, J.H.M. Prehn, Guidelines on experimental methods to assess mitochondrial dysfunction in cellular models of neurodegenerative diseases, Cell death and differentiation 25 (2018) 542–572.

[148] C. Zou, Y. Wang, Z. Shen, 2-NBDG as a fluorescent indicator for direct glucose uptake measurement, Journal of Biochemical and Biophysical Methods 64 (2005) 207–215.

[149] S. Diemert, A.M. Dolga, S. Tobaben, J. Grohm, S. Pfeifer, E. Oexler, C. Culmsee, Impedance measurement for real time detection of neuronal cell death, Journal of neuroscience methods 203 (2012) 69–77.

[150] S.S.V.P. Sakamuri, J.A. Sperling, V.N. Sure, M.H. Dholakia, N.R. Peterson, I. Rutkai, P.S. Mahalingam, R. Satou, P.V.G. Katakam, Measurement of respiratory function in isolated cardiac mitochondria using Seahorse XFe24 Analyzer: applications for aging research, GeroScience 40 (2018) 347–356.

[151] N. Zamzami, D. Métivier, G. Kroemer, Quantitation of Mitochondrial Transmembrane Potential in Cells and in Isolated Mitochondria, in: J.C. Reed (Ed.), Methods in Enzymology, v. 322, Apoptosis, Academic Press, San Diego, 2000, pp. 208–213.

[152] S. Brenner, The genetics of Caenorhabditis elegans, Genetics 77 (1974) 71–94.

[153] T. Stiernagle, Maintenance of C. elegans, WormBook, 2006.

[154] F.R.G. Amrit, R. Ratnappan, S.A. Keith, A. Ghazi, The C. elegans lifespan assay toolkit, Methods (San Diego, Calif.) 68 (2014) 465–475.

[155] E. Fitzenberger, D.J. Deusing, C. Marx, M. Boll, K. Lüersen, U. Wenzel, The polyphenol quercetin protects the mev-1 mutant of Caenorhabditis elegans from glucose-induced reduction of survival under heat-stress depending on SIR-2.1, DAF-12, and proteasomal activity, Molecular nutrition & food research 58 (2014) 984–994.

[156] O. Margie, C. Palmer, I. Chin-Sang, C. elegans chemotaxis assay, Journal of visualized experiments : JoVE (2013) e50069.

[157] S. Wullschleger, R. Loewith, M.N. Hall, TOR signaling in growth and metabolism, Cell 124 (2006) 471–484.

[158] K. Hara, Y. Maruki, X. Long, K.-i. Yoshino, N. Oshiro, S. Hidayat, C. Tokunaga, J. Avruch, K. Yonezawa, Raptor, a Binding Partner of Target of Rapamycin (TOR), Mediates TOR Action, Cell 110 (2002) 177–189.

[159] N.V. Iyer, L.E. Kotch, F. Agani, S.W. Leung, E. Laughner, R.H. Wenger, M. Gassmann, J.D. Gearhart, A.M. Lawler, A.Y. Yu, G.L. Semenza, Cellular and developmental control of O2 homeostasis by hypoxia-inducible factor 1 alpha, Genes & Development 12 (1998) 149–162.

[160] B.L. Krock, N. Skuli, M.C. Simon, Hypoxia-Induced Angiogenesis: Good and Evil, Genes & Cancer 2 (2011) 1117–1133.

[161] G. He, Y. Jiang, B. Zhang, G. Wu, The effect of HIF-1α on glucose metabolism, growth and apoptosis of pancreatic cancerous cells, Asia Pacific journal of clinical nutrition 23 (2014) 174–180.

[162] R.C. Osthus, H. Shim, S. Kim, Q. Li, R. Reddy, M. Mukherjee, Y. Xu, D. Wonsey, L.A. Lee, C.V. Dang, Deregulation of glucose transporter 1 and glycolytic gene expression by c-Myc, The Journal of biological chemistry 275 (2000) 21797–21800.

[163] L. Szablewski, Glucose Transporters in Brain: In Health and in Alzheimer's Disease, Journal of Alzheimer's disease : JAD 55 (2017) 1307–1320.

[164] J. Tao, R.K. Diaz, C.R.V. Teixeira, T.J. Hackmann, Transport of a Fluorescent Analogue of Glucose (2-NBDG) versus Radiolabeled Sugars by Rumen Bacteria and Escherichia coli, Biochemistry 55 (2016) 2578–2589.

[165] E. Sanchez-Rangel, S.E. Inzucchi, Metformin: clinical use in type 2 diabetes, Diabetologia 60 (2017) 1586–1593.

[166] O. Zierau, C. Bodinet, S. Kolba, M. Wulf, G. Vollmer, Antiestrogenic activities of Cimicifuga racemosa extracts, The Journal of steroid biochemistry and molecular biology 80 (2002) 125–130.

[167] W. Wuttke, H. Jarry, J. Haunschild, G. Stecher, M. Schuh, D. Seidlova-Wuttke, The non-estrogenic alternative for the treatment of climacteric complaints: Black cohosh (Cimicifuga or Actaea racemosa), The Journal of steroid biochemistry and molecular biology 139 (2014) 302–310.

[168] Y.-M. Da, K.-Y. Niu, S.-Y. Liu, K. Wang, W.-J. Wang, J. Jia, L.-H. Qin, W.-P. Bai, Does Cimicifuga racemosa have the effects like estrogen on the sublingual gland in ovariectomized rats?, Biological research 50 (2017) 11.

[169] M. Garita-Hernandez, M.A. Calzado, F.J. Caballero, A. Macho, E. Muñoz, B. Meier, A. Brattström, B.L. Fiebich, K. Appel, The growth inhibitory activity of the Cimicifuga racemosa extract Ze 450 is mediated through estrogen and progesterone receptors-independent pathways, Planta medica 72 (2006) 317–323.

[170] M. Mercado-Feliciano, M.C. Cora, K.L. Witt, C.A. Granville, M.R. Hejtmancik, L. Fomby, K.A. Knostman, M.J. Ryan, R. Newbold, C. Smith, P.M. Foster, M.K. Vallant, M.D. Stout, An ethanolic extract of black cohosh causes hematological changes but not estrogenic effects in female rodents, Toxicology and Applied Pharmacology 263 (2012) 138–147. http://www.sciencedirect.com/science/article/pii/S0041008X12002475.

[171] C. Culmsee, H. Vedder, A. Ravati, V. Junker, D. Otto, B. Ahlemeyer, J.C. Krieg, J. Krieglstein, Neuroprotection by estrogens in a mouse model of focal cerebral ischemia and in cultured neurons: evidence for a receptor-independent antioxidative mechanism, Journal of cerebral blood flow and metabolism : official journal of the International Society of Cerebral Blood Flow and Metabolism 19 (1999) 1263–1269.

[172] J. Morán, M. Perez-Basterrechea, P. Garrido, E. Díaz, A. Alonso, J. Otero, E. Colado, C. González, Effects of Estrogen and Phytoestrogen Treatment on an In Vitro Model of Recurrent Stroke on HT22 Neuronal Cell Line, Cellular and molecular neurobiology 37 (2017) 405–416.

[173] C. Behl, T. Skutella, F. Lezoualc'H, A. Post, M. Widmann, C.J. Newton, F. Holsboer, Neuroprotection against Oxidative Stress by Estrogens: Structure-Activity Relationship, Mol Pharmacol 51 (1997) 535–541.

[174] Shagufta, I. Ahmad, Tamoxifen a pioneering drug: An update on the therapeutic potential of tamoxifen derivatives, European journal of medicinal chemistry 143 (2018) 515–531.

[175] F. Cabreiro, C. Au, K.-Y. Leung, N. Vergara-Irigaray, H.M. Cochemé, T. Noori, D. Weinkove, E. Schuster, N.D.E. Greene, D. Gems, Metformin Retards Aging in C.

elegans by Altering Microbial Folate and Methionine Metabolism, Cell 153 (2013) 228–239.

[176] B. Onken, M. Driscoll, Metformin induces a dietary restriction-like state and the oxidative stress response to extend C. elegans Healthspan via AMPK, LKB1, and SKN-1, PLoS ONE 5 (2010) e8758.

[177] H. Doostdar, S.J. Duthie, M.D. Burke, W.T. Melvin, M.H. Grant, The influence of culture medium composition on drug metabolising enzyme activities of the human liver derived Hep G2 cell line, FEBS Letters 241 (1988) 15–18.

[178] W.S. Yang, R. SriRamaratnam, M.E. Welsch, K. Shimada, R. Skouta, V.S. Viswanathan, J.H. Cheah, P.A. Clemons, A.F. Shamji, C.B. Clish, L.M. Brown, A.W. Girotti, V.W. Cornish, S.L. Schreiber, B.R. Stockwell, Regulation of Ferroptotic Cancer Cell Death by GPX4, Cell 156 (2014) 317–331. http://www.sciencedirect.com/science/article/pii/S0092867413015444.

[179] W.B. Mattes, A.P. Li, Quantitative reverse transcriptase/PCR assay for the measurement of induction in cultured hepatocytes, Chemico-Biological Interactions 107 (1997) 47–61.

[180] H. Fujimura, N. Murakami, S. Miwa, C. Aruga, W. Toriumi, The suitability of rat hepatoma cell line H4IIE for evaluating the potentials of compounds to induce CYP3A23 expression, Experimental and toxicologic pathology : official journal of the Gesellschaft fur Toxikologische Pathologie 64 (2012) 527–533.

[181] E.L. Mills, B. Kelly, A. Logan, A.S.H. Costa, M. Varma, C.E. Bryant, P. Tourlomousis, J.H.M. Däbritz, E. Gottlieb, I. Latorre, S.C. Corr, G. McManus, D. Ryan, H.T. Jacobs, M. Szibor, R.J. Xavier, T. Braun, C. Frezza, M.P. Murphy, L.A. O'Neill, Succinate Dehydrogenase Supports Metabolic Repurposing of Mitochondria to Drive Inflammatory Macrophages, Cell 167 (2016) 457-470.e13.

[182] F. Scialò, D.J. Fernández-Ayala, A. Sanz, Role of Mitochondrial Reverse Electron Transport in ROS Signaling: Potential Roles in Health and Disease, Frontiers in physiology 8 (2017) 428.

[183] A.L. Orr, D. Ashok, M.R. Sarantos, T. Shi, R.E. Hughes, M.D. Brand, Inhibitors of ROS production by the ubiquinone-binding site of mitochondrial complex I identified by chemical screening, Free radical biology & medicine 65 (2013) 1047–1059.

[184] J.R. Treberg, C.L. Quinlan, M.D. Brand, Evidence for two sites of superoxide production by mitochondrial NADH-ubiquinone oxidoreductase (complex I), The Journal of biological chemistry 286 (2011) 27103–27110.

[185] C.-J. Hu, L.-Y. Wang, L.A. Chodosh, B. Keith, M.C. Simon, Differential roles of hypoxia-inducible factor 1alpha (HIF-1alpha) and HIF-2alpha in hypoxic gene regulation, Molecular and cellular biology 23 (2003) 9361–9374.

[186] J.-w. Kim, I. Tchernyshyov, G.L. Semenza, C.V. Dang, HIF-1-mediated expression of pyruvate dehydrogenase kinase: a metabolic switch required for cellular adaptation to hypoxia, Cell metabolism 3 (2006) 177–185.

[187] I. Papandreou, R.A. Cairns, L. Fontana, A.L. Lim, N.C. Denko, HIF-1 mediates adaptation to hypoxia by actively downregulating mitochondrial oxygen consumption, Cell metabolism 3 (2006) 187–197.

[188] R. Fukuda, H. Zhang, J.-w. Kim, L. Shimoda, C.V. Dang, G.L. Semenza, HIF-1 regulates cytochrome oxidase subunits to optimize efficiency of respiration in hypoxic cells, Cell 129 (2007) 111–122.

[189] J.D. Gordan, C.B. Thompson, M.C. Simon, HIF and c-Myc: sibling rivals for control of cancer cell metabolism and proliferation, Cancer cell 12 (2007) 108–113.

[190] P. Liu, M. Ge, J. Hu, X. Li, L. Che, K. Sun, L. Cheng, Y. Huang, M.G. Pilo, A. Cigliano, G.M. Pes, R.M. Pascale, S. Brozzetti, G. Vidili, A. Porcu, A. Cossu, G. Palmieri, M.C. Sini, S. Ribback, F. Dombrowski, J. Tao, D.F. Calvisi, L. Chen, X. Chen, A functional mammalian target of rapamycin complex 1 signaling is indispensable for c-Myc-driven hepatocarcinogenesis, Hepatology (Baltimore, Md.) 66 (2017) 167–181.

[191] S. Mori, S. Nada, H. Kimura, S. Tajima, Y. Takahashi, A. Kitamura, C. Oneyama, M. Okada, The mTOR pathway controls cell proliferation by regulating the FoxO3a transcription factor via SGK1 kinase, PLoS ONE 9 (2014) e88891.

[192] M. Laplante, D.M. Sabatini, mTOR signaling in growth control and disease, Cell 149 (2012) 274–293.

[193] J. Zhang, Teaching the basics of autophagy and mitophagy to redox biologists—Mechanisms and experimental approaches, Redox biology 4 (2015) 242–259.

[194] G. Jia, A.R. Aroor, L.A. Martinez-Lemus, J.R. Sowers, Overnutrition, mTOR signaling, and cardiovascular diseases, American journal of physiology. Regulatory, integrative and comparative physiology 307 (2014) R1198-206.

[195] G. C. Kennedy, The role of depot fat in the hypothalamic control of food intake in the rat, Proc. R. Soc. Lond. B 140 (1953) 578–592.

[196] A. Drougard, A. Fournel, P. Valet, C. Knauf, Impact of hypothalamic reactive oxygen species in the regulation of energy metabolism and food intake, Frontiers in neuroscience 9 (2015) 56.

[197] R.D. Cone, M.A. Cowley, A.A. Butler, W. Fan, D.L. Marks, M.J. Low, The arcuate nucleus as a conduit for diverse signals relevant to energy homeostasis, International journal of obesity and related metabolic disorders : journal of the International Association for the Study of Obesity 25 Suppl 5 (2001) S63-7.

[198] E. Roh, M.S. Kim, Brain Regulation of Energy Metabolism, Endocrinology and metabolism (Seoul, Korea) 31 (2016) 519–524.

[199] J.W. Olney, Brain lesions, obesity, and other disturbances in mice treated with monosodium glutamate, Science (New York, N.Y.) 164 (1969) 719–721.

[200] H.J. Forman, M. Maiorino, F. Ursini, Signaling functions of reactive oxygen species, Biochemistry 49 (2010) 835–842.

[201] M. Valko, D. Leibfritz, J. Moncol, M.T.D. Cronin, M. Mazur, J. Telser, Free radicals and antioxidants in normal physiological functions and human disease, The international journal of biochemistry & cell biology 39 (2007) 44–84.

[202] G. Liot, B. Bossy, S. Lubitz, Y. Kushnareva, N. Sejbuk, E. Bossy-Wetzel, Complex II inhibition by 3-NP causes mitochondrial fragmentation and neuronal cell death via an NMDA- and ROS-dependent pathway, Cell death and differentiation 16 (2009) 899–909.

[203] Y. Li, P. Maher, D. Schubert, A role for 12-lipoxygenase in nerve cell death caused by glutathione depletion, Neuron 19 (1997) 453–463.

[204] S. Tobaben, J. Grohm, A. Seiler, M. Conrad, N. Plesnila, C. Culmsee, Bid-mediated mitochondrial damage is a key mechanism in glutamate-induced oxidative stress and AIF-dependent cell death in immortalized HT-22 hippocampal neurons, Cell death and differentiation 18 (2011) 282–292.

[205] B. Halliwell, Oxidative stress and neurodegeneration: where are we now?, Journal of neurochemistry 97 (2006) 1634–1658.

[206] Y.-W. Wang, S.-J. He, X. Feng, J. Cheng, Y.-T. Luo, L. Tian, Q. Huang, Metformin: a review of its potential indications, Drug design, development and therapy 11 (2017) 2421–2429.

[207] M.R. Owen, E. Doran, A.P. Halestrap, Evidence that metformin exerts its anti-diabetic effects through inhibition of complex 1 of the mitochondrial respiratory chain, The Biochemical journal 348 Pt 3 (2000) 607–614.

[208] G. Rena, D.G. Hardie, E.R. Pearson, The mechanisms of action of metformin, Diabetologia 60 (2017) 1577–1585.

[209] X. Zhao, Z. Zeng, U. Gaur, J. Fang, T. Peng, S. Li, W. Zheng, Metformin protects PC12 cells and hippocampal neurons from H2 O 2 -induced oxidative damage through activation of AMPK pathway, Journal of cellular physiology (2019).

[210] B.I. Pérez-Revuelta, M.M. Hettich, A. Ciociaro, C. Rotermund, P.J. Kahle, S. Krauss, D.A. Di Monte, Metformin lowers Ser-129 phosphorylated α-synuclein levels via mTOR-dependent protein phosphatase 2A activation, Cell death & disease 5 (2014) e1209.

[211] V. Nair, S. Sreevalsan, R. Basha, M. Abdelrahim, A. Abudayyeh, A. Rodrigues Hoffman, S. Safe, Mechanism of metformin-dependent inhibition of mammalian target of rapamycin (mTOR) and Ras activity in pancreatic cancer: role of specificity protein (Sp) transcription factors, The Journal of biological chemistry 289 (2014) 27692–27701.

[212] A. Zhavoronkov, A.G. Swick, A. Moskalev, D. Karpinsky-Semper, A. Artemov, F. Cortese, L. Jellen, A. Aliper, Towards natural mimetics of metformin and rapamycin, Aging 9 (2017) 2245–2268. https://s3-us-west-1.amazonaws.com/paperchase-aging/pdf/CreFziTch9NfHnRyp.pdf.

[213] C. Behl, M. Widmann, T. Trapp, F. Holsboer, 17-beta estradiol protects neurons from oxidative stress-induced cell death in vitro, Biochemical and biophysical research communications 216 (1995) 473–482.

[214] A. Grimm, K. Schmitt, U.E. Lang, A.G. Mensah-Nyagan, A. Eckert, Improvement of neuronal bioenergetics by neurosteroids: implications for age-related neurodegenerative disorders, Biochimica et biophysica acta 1842 (2014) 2427–2438.

[215] E. Gursoy, A. Cardounel, T. Al-khlaiwi, A. Al-drees, M. Kalimi, Tamoxifen protects clonal mouse hippocampal (HT-22) cells against neurotoxins-induced cell death, Neurochemistry international 40 (2002) 405–412.

[216] J.M. Mates, Effects of antioxidant enzymes in the molecular control of reactive oxygen species toxicology, Toxicology 153 (2000) 83–104.

[217] S.B. Nimse, D. Pal, Free radicals, natural antioxidants, and their reaction mechanisms, RSC Adv. 5 (2015) 27986–28006.

[218] T. Low Dog, K.L. Powell, S.M. Weisman, Critical evaluation of the safety of Cimicifuga racemosa in menopause symptom relief, Menopause (New York, N.Y.) 10 (2003) 299–313.

[219] A. Huntley, E. Ernst, A systematic review of the safety of black cohosh, Menopause (New York, N.Y.) 10 (2003) 58–64.

[220] HMPC, ASSESSMENT OF CASE REPORTS CONNECTED TO HERBAL MEDICINAL PRODUCTS CONTAINING CIMICIFUGAE RACEMOSAE RHIZOMA (BLACK COHOSH, ROOT (2007).

[221] M. Thomsen, M. Schmidt, Hepatotoxicity from Cimicifuga racemosa? Recent Australian case report not sufficiently substantiated, Journal of alternative and complementary medicine (New York, N.Y.) 9 (2003) 337–340.

[222] S. Lüde, M. Török, S. Dieterle, A.C. Knapp, R. Kaeufeler, R. Jäggi, U. Spornitz, S. Krähenbühl, Hepatic effects of Cimicifuga racemosa extract in vivo and in vitro, Cellular and molecular life sciences : CMLS 64 (2007) 2848–2857.

[223] N. Barzilai, J.P. Crandall, S.B. Kritchevsky, M.A. Espeland, Metformin as a Tool to Target Aging, Cell metabolism 23 (2016) 1060–1065.

[224] R. Pryor, P. Norvaisas, G. Marinos, L. Best, L.B. Thingholm, L.M. Quintaneiro, W. de Haes, D. Esser, S. Waschina, C. Lujan, R.L. Smith, T.A. Scott, D. Martinez-Martinez, O. Woodward, K. Bryson, M. Laudes, W. Lieb, R.H. Houtkooper, A. Franke, L. Temmerman, I. Bjedov, H.M. Cochemé, C. Kaleta, F. Cabreiro, Host-Microbe-Drug-Nutrient Screen Identifies Bacterial Effectors of Metformin Therapy, Cell 178 (2019) 1299-1312.e29.

[225] F. Cabreiro, D. Gems, Worms need microbes too: microbiota, health and aging in Caenorhabditis elegans, EMBO molecular medicine 5 (2013) 1300–1310.

[226] J. Alcedo, C. Kenyon, Regulation of C. elegans Longevity by Specific Gustatory and Olfactory Neurons, Neuron 41 (2004) 45–55. http://www.sciencedirect.com/science/article/pii/S089662730300816X.

[227] R. Curtis, G. O'Connor, P.S. DiStefano, Aging networks in Caenorhabditis elegans: AMP-activated protein kinase (aak-2) links multiple aging and metabolism pathways, Aging cell 5 (2006) 119–126.

[228] C. Saier, I. Gommlich, V. Hiemann, S. Baier, K. Koch, G. Horn, T. Kowalewsky, J. Bartelt, M. Seemann, W. Wätjen, Agrimonia procera Wallr. Extract Increases Stress Resistance and Prolongs Life Span in Caenorhabditis elegans via

Transcription Factor DAF-16 (FoxO Orthologue), Antioxidants (Basel, Switzerland) 7 (2018).

[229] M. Viswanathan, S.K. Kim, A. Berdichevsky, L. Guarente, A role for SIR-2.1 regulation of ER stress response genes in determining C. elegans life span, Developmental Cell 9 (2005) 605–615.

[230] B. Dilberger, M. Passon, H. Asseburg, C.V. Silaidos, F. Schmitt, T. Schmiedl, A. Schieber, G.P. Eckert, Polyphenols and Metabolites Enhance Survival in Rodents and Nematodes-Impact of Mitochondria, Nutrients 11 (2019).

[231] J. Apfeld, G. O'Connor, T. McDonagh, P.S. DiStefano, R. Curtis, The AMP-activated protein kinase AAK-2 links energy levels and insulin-like signals to lifespan in C. elegans, Genes & Development 18 (2004) 3004–3009.

[232] J. Chen, Y. Ou, Y. Li, S. Hu, L.-W. Shao, Y. Liu, Metformin extends C. elegans lifespan through lysosomal pathway, eLife 6 (2017).

[233] R.P. Bowler, J.D. Crapo, Oxidative stress in allergic respiratory diseases, The Journal of allergy and clinical immunology 110 (2002) 349–356.

[234] R.P. Bowler, Oxidative stress in the pathogenesis of asthma, Current allergy and asthma reports 4 (2004) 116–122.

[235] A. Zimmermann, M.A. Bauer, G. Kroemer, F. Madeo, D. Carmona-Gutierrez, When less is more: hormesis against stress and disease, Microbial cell (Graz, Austria) 1 (2014) 150–153.

[236] E.J. Calabrese, M.P. Mattson, How does hormesis impact biology, toxicology, and medicine?, NPJ Aging and Mechanisms of Disease 3 (2017).

[237] S.A. Malik, I. Orhon, E. Morselli, A. Criollo, S. Shen, G. Mariño, A. BenYounes, P. Bénit, P. Rustin, M.C. Maiuri, G. Kroemer, BH3 mimetics activate multiple pro-autophagic pathways, Oncogene 30 (2011) 3918–3929.

[238] N.M. Held, R.H. Houtkooper, Mitochondrial quality control pathways as determinants of metabolic health, BioEssays : news and reviews in molecular, cellular and developmental biology 37 (2015) 867–876.

[239] R. Scherz-Shouval, E. Shvets, E. Fass, H. Shorer, L. Gil, Z. Elazar, Reactive oxygen species are essential for autophagy and specifically regulate the activity of Atg4, The EMBO journal 26 (2007) 1749–1760.

[240] J. Yun, T. Finkel, Mitohormesis, Cell metabolism 19 (2014) 757–766. http://www.sciencedirect.com/science/article/pii/S1550413114000175.

Publications

Rabenau, M., Unger, M., Drewe, J., and Culmsee, C. (2019) Metabolic switch induced by *Cimicifuga racemosa* extract prevents mitochondrial damage and oxidative cell death. Phytomedicine, 52, 107–116

Rabenau, M., Unger, M., Drewe, J., and Culmsee, C. (2018) Effects of *Cimicifuga racemosa* extract Ze 450 on mitochondria in models of oxidative stress in neuronal cells. Data in Brief, 21, 1872-1879

Lu, P., Bruno, B. J., Rabenau, M., and Lim, C. S. (2016) Delivery of drugs and macromolecules to the mitochondria for cancer therapy. Journal of controlled release: official journal of the Controlled Release Society 240, 38–51

Meetings and Conferences

10th World Congress on Targeting Mitochondria. Berlin, Germany. October 2019 (poster)

EMAS. 12th Congress of the European Menopause and Andropause Society. Berlin, Deutschland. June 2019 (oral presentation)

International Ph.D. Symposium: GRK2213 Membrane Plasticity in Tissue Development and Remodeling. Marburg, Germany. April 2019 (poster)

Gordon Research Conference. Mitochondria in Health and Disease: Mitochondrial Signaling and Dynamics. Ventura, USA. March 2019 (poster)

9th World Congress on Targeting Mitochondria. Berlin, Germany. October 2018 (poster)

Dynamics of the Nervous System in Health and Disease. Marburg, Germany. September 2018 (poster)

XXII International Congress Phytopharm 2018. Horgen, Switzerland. June 2018 (oral presentation)

Tetranationaler Phytotherapiekongress. Vienna, Austria. May-June 2018 (poster)

65th Annual Meeting of the Society for Medicinal Plant and Natural Product Research. Basel, Switzerland. August 2017 (oral presentation)

EUROMIT Cologne: International Meeting on Mitochondrial Pathology. Cologne, Germany. June 2017 (poster)

Pharmacon Schladming: 47. Internationale Pharmazeutische Fortbildungswoche der BAK. Schladming, Austria. January 2017

Acknowledgments

An dieser Stelle möchte ich mich bei allen bedanken, die mich während meiner Doktorandenzeit unterstützt haben.

Zuerst möchte ich mich bei meinem Dokotorvater, **Carsten Culmsee**, der meine Arbeit betreut und begutachtet hat, bedanken. Ebenso, bin ich sehr dankbar für die Möglichkeit meine Doktorarbeit in seiner Arbeitsgruppe anfertigen zu können. Besonders schätzte ich die Freiheiten bezüglich der Versuchsgestaltung und die Ermöglichung der Teilnahme an zahlreichen nationalen und internationalen Konferenzen, was mir weitreichende Einblicke in eine für mich zu Beginn neue Welt der Wissenschaft verschaffte.

Darüber hinaus schätzte ich die Kooperation mit allen Beteiligten der **Max Zeller Söhne AG**. Die regelmäßigen Meetings und projektbezogenen Diskussionen haben maßgeblich zur Entwicklung des Projekts beigetragen. Insbesondere bedanke ich mich bei **Samuel Hasler** für die experimentelle Unterstützung zur Fraktionierung des *Cimicifuga* Extrakts. Des Weiteren bin ich sehr dankbar für die hilfreichen Anregungen, die konstruktive Kritik und Förderung durch **Matthias Unger**, **Jürgen Drewe**, **Veronika Butterweck** und **Georg Boonen**.

Weiterhin ist durch die *C. elegans* Expertise, die **Gunter Eckert** und **Benjamin Dilberger** in das Projekt eingebracht haben, ein entscheidender Effekt von Ze 450 auf einen lebenden Organismus analysiert worden. Diesbezüglich bedanke ich mich für eine angenehme und fruchtvolle Kooperation bei allen Beteiligten der AG Eckert.

Ebenso möchte ich dem **AK Diedrich** für die gute Kooperation und die Synthese des RSL-3 danken. Insbesondere danke ich Dir, **Lukas**, für eine unkomplizierte Zusammenarbeit und Deine stetige Hilfsbereitschaft.

Darüber hinaus gilt mein Dank den Arbeitsgruppen des Instituts für einen Arbeitsplatz, an den ich gerne komme und für reges Feedback bei den Seminaren.

Lieber **Hauke**, vielen Dank für deine ausgesprochene Hilfsbereitschaft und sehr gute Kooperation bei den Versuchsplanungen, ebenso danke ich der gesamten **AG Kockskämper** für die gute Zusammenarbeit.

Liebe **Sylvia**, in Salt Lake City haben wir entschieden zu promovieren, glücklicherweise beide in Marburg und sogar im gleichen Gebäude. In allen Situationen hast du immer ein offenes Ohr und stehst stets mit Rat und Tat zur Seite, auch wenn du ebenso

eingespannt bist. Vielen Dank für Deine Hilfe innerhalb und außerhalb meines Projekts, insbesondere bei dem Glucose Assay und der Konfokalmikroskopie.

Meine lieben Kollegen der **AG Culmsee**, Euch danke ich ausdrücklich für ein Arbeitsumfeld, das sich so kein zweites Mal wiederfinden lässt. Ihr seid einzigartig.

Lena, **Ina**, **Susanne** und **Lukas,** Ihr seid für mich mehr als Kollegen. Ich bin sehr dankbar an der Arbeit so gute Freunde gefunden zu haben und freue mich auf weitere Wandertouren, Wiesnfeste und Weinproben.

Katharina, eine bessere TA zur Unterstützung, die immer mit einer helfenden Hand zur Seite steht und stets mit Köpfchen bei der Sache ist, kann ich mir nicht vorstellen. Vielen Dank unter anderem für Deine zuverlässige Arbeit in der Zellkultur.

Liebe **Emma**, vielen herzlichen Dank, Du bist immer eine unterstützende Anlaufstelle für Fragen jeglicher Art und ich freue mich, dass wir auch außerhalb der Arbeit viel Spaß zusammen haben.

Susen, du hast immer eine helfende Hand parat und bist mit Deiner aufgeschlossenen und freundlichen Art unverkennbar. Vielen Dank für Deine Unterstützung!

Thank you very much, **Chiara**, for joining the lab and supporting the ongoing experiments. I enjoyed working with you and besides work, I got a new friend.

Ebenso möchte ich mich bei den ehemaligen Doktorandinnen bedanken. **Julia**, **Anja** und **Birgit**, Ihr habt mich super in die Gruppe aufgenommen und ich bin auch dankbar für die gemeinsame Zeit außerhalb des Labors, zum Bespiel in München auf dem Oktoberfest zusammen mit **Lena**, **Ina** und **Susanne**.

Weiterhin bedanke ich mich bei meinen **Freunden** und meiner **Sportgruppe**, ihr habt mir den nötigen Ausgleich gegeben und mich immer unterstützt.

Last but not least, gilt mein ausdrücklicher und größter Dank meiner **Familie**, die alle Höhen und Tiefen während des Studiums und meiner Promotion miterlebt, mich zu jeder Zeit unterstützt und mich ermutigt haben, meine Ziele zu verfolgen. Vielen Dank!

Curriculum vitae